# Energy and Thermal Comfort Management Strategies for Battery Electric Vehicles

Anas Lahlou

Sorbonne Université

Ecole Mohammadia d'Ingénieurs

Ecole doctorale Sciences Mécaniques Acoustiques Electronique et Robotique de Paris

*Geeps*

# Energy and Thermal Comfort Management Strategies for Battery Electric Vehicles

Par Anas Lahlou

Thèse de doctorat en Energétique

Dirigée par Florence Ossart et Mohammed Maaroufi

Présentée et soutenue publiquement le 06 novembre 2020

Devant un jury composé de :

| | | |
|---|---|---|
| Olivier BETHOUX | Professeur à Sorbonne Université | *Président du jury* |
| Rochdi TRIGUI | Directeur de recherche à L'Université Gustave Eiffel | *Rapporteur* |
| Abdellatif TOUZANI | Professeur à l'Ecole Mohammadia d'Ingénieurs | *Rapporteur* |
| Nissrine KRAMI | Professeure à L'Université Ibn Tofail | *Rapporteur* |
| Francis ROY | Responsable scientifique à Groupe PSA | *Tuteur de thèse* |
| Florence OSSART | Professeure à Sorbonne Université | *Directrice de thèse* |
| Mohammed MAAROUFI | Professeur à l'Ecole Mohammadia d'Ingénieurs | *Directeur de thèse* |
| Mohamed BAKHOUYA | Professeur à l'Université Internationale de Rabat | *Co-directeur de thèse* |

# Acknowledgement

This work is performed under the collaborative framework OpenLab "PSA@Paris-Saclay - Electrical engineering for Mobility" and OpenLab "PSA@Morocco—Sustainable mobility for Africa". My gratitude goes to Groupe PSA, ANRT and CNRST for giving me the honor to be the first PhD candidate of the CIFRE France Maroc program. Thank you for your trust, for this enjoyable experience and the financial support. A special thanks to the HERE company who provided us with real time traffic and contextual data.

Undertaking this PhD has been a truly life-changing experience for me and it would not have been possible to do without the support and guidance that I received from many people.

I am extremely grateful to Pr. Rochdi Trigui, Pr. Nissrine Krami and Prof. Abdellatif Touzani for spending their valuable time on reviewing this manuscript and providing constructive feedback and insights. I am also thankful to Pr. Olivier Bethoux for accepting to be the president of the jury.

Next, I would like to express my sincere gratitude to my first supervisor Prof. Florence Ossart, who gave me the honor of leading this work under the best conditions. I am truly grateful for her precious guidance, her constructive advises and her availability during all this time. I would like to underline and appreciate her passion for research and especially her human qualities, her optimism, enthusiasm and generosity. Also, I would thank my second supervisor, Prof. Mohammed Bakhouya, for welcoming me to the LERMA lab, introducing me to his research team, and giving me computer resources to run my extensive simulations. Many thanks also to Prof. Mohammed Maaroufi, for his feedbacks and his help with administrative procedures.

The next person I would like to thank is Francis Roy. I cannot do him justice in a single paragraph. You were there from the first moment, and still there until the end. Thank you for convincing me to pursue a PhD within Group PSA, and always defending vigorously our project. Thank you for the pleasant human relationship we kept throughout the years. Thank you for you constant good mood, and for always be willing to lend a helping hand or a willing ear.

Many thanks also to all my colleagues of Groupe PSA, especially Sandrine Loze, Bernard Sahut, Anne Catherine Maisonneuve, Thierry Cheriot and Eric Lalliard for showing the best mood each time I spent the day at my PSA's office. A special thanks to Emmanuel Boudard, for providing us valuable input to our work. Thank you, Emmanuel, for always being supportive and available to discuss our scientific approach, and share your passion about HVAC systems and electric vehicles

Last but not least, words fail me to express my appreciation to my beloved fiancee, Rim Jebbar, whose dedication, love and persistent confidence in me, has taken the load off my shoulder. This dissertation would not have been possible without her warm love, continued patience, and endless support. Thank you Rim for always being there to gossip, to cry, to laugh and to party. I am the luckiest man for having you by my side. I love you.

My gratitude also goes to my family, who have been an unfailing source of support. Your encouragement, advice and constant presence have been crucial to the success of this thesis and I am deeply grateful for that.

To Rabii, Abdelali, Wail and Imane, for beings their wonderful selves and for understanding that best friends remains best friends even though Phds make you disappear.

**TABLE OF CONTENT**

# LIST OF FIGURES

# LIST OF TABLES

# Abstract

The HVAC system represents the main auxiliary load in battery-powered electric vehicles (BEVs) and requires efficient control approaches that balance energy saving and thermal comfort. On the one hand, passengers always demand more comfort, but on the other hand the HVAC system consumption strongly impacts the vehicle's driving range, which constitutes a major concern in BEVs. Both of these requirements should be satisfied by the control approach, by suggesting to the driver to adjust either the thermal comfort or the vehicle speed, in order to meet the energy constraints. Indeed, if there is not enough embedded energy for both traction and optimal thermal comfort for the planned trip, the thermal comfort should be diminished in order to save energy and allow the vehicle to reach its final destination or the next charging point. In some situations, it may be wiser to consider slowing down in order to allow a better thermal comfort.

In the present thesis, an optimal thermal comfort management approach that optimizes the thermal comfort while preserving the driving range during a trip is proposed. The electric vehicle is first modeled including the powertrain and the HVAC system. Secondly, the passengers' thermo-physiological behavior and thermal comfort indices are presented. Then, the thermal comfort management issue is formulated as an optimization problem and solved by dynamic programing algorithm. Two representative test-cases of hot climates and traffic situations are simulated. In the first one, the energetic cost and ratio of improved comfort is quantified for different meteorological and traffic conditions. The second one highlights the traffic situation in which a trade-off between the driving speed and thermal comfort is important. A large number of weather and traffic situations are simulated and results show the efficiency of the proposed optimal approach in minimizing energy consumption while maintaining a good comfort. A comparison between different thermal comfort indices is finally conducted, to assess the gains from using our model of human thermo-physiology.

While the results of the optimal approach were promising and validate the principle of thermal comfort and energy management, the computation cost of dynamic programing is still too high for an implementation in an on-board computer. A real-time energy management strategy was therefore developed, by using the results of the optimal approach, and a simplified but still precise and representative model of thermal comfort. Based on traffic and weather predictions for a given trip, the real time algorithm first estimates the energy required for the traction and the energy available for thermal comfort. Then, it determines the best thermal comfort that can be provided in these energetic conditions and controls the HVAC system accordingly. If the predictions are updated during the trip, the algorithm adjust the thermal comfort level to meet the energy constraint. The real-time algorithm is tested for a wide variety of meteorological and traffic scenarios. Results show that the energy estimators have a good accuracy. The absolute relative error is about 1.7% for the first one (traction), and almost 4.1% for the second one (thermal comfort). The effectiveness of the proposed thermal comfort management strategy is assessed by comparing it to an off-line optimal control approach based on dynamic programming. Simulation results show that the proposed approach is near-optimal, with a slight increase of discomfort by only 3%.

# Résumé

Le système HVAC représente la principale charge auxiliaire des véhicules électriques à batterie (VEB) et nécessite des approches de contrôle efficaces qui équilibrent entre consommation énergétique et confort thermique. D'une part, les passagers exigent toujours plus de confort, mais d'autre part la consommation du système HVAC impacte fortement l'autonomie du véhicule, ce qui constitue un enjeu majeur des VEB. Ces deux exigences doivent être satisfaites par la stratégie de gestion énergétique, en suggérant au conducteur d'ajuster soit le confort thermique, soit la vitesse du véhicule, afin de satisfaire la contrainte d'énergie disponible. En effet, s'il n'y a pas assez d'énergie embarquée pour la traction et pour un confort thermique idéal, ce dernier doit être diminué afin d'économiser de l'énergie et permettre au véhicule d'atteindre sa destination finale ou le prochain point de recharge. Dans certaines situations, il peut être plus judicieux de ralentir afin de permettre un meilleur confort thermique.

Dans la présente thèse, une approche de gestion optimale du confort thermique qui optimise le confort thermique tout en préservant l'autonomie lors d'un trajet est proposée. Le véhicule électrique est d'abord modélisé. Ensuite, le comportement thermo-physiologique du conducteurs/passagers ainsi que les indices de confort thermique des passagers sont présentés. Le problème de la gestion du confort thermique est formulé comme un problème d'optimisation et résolu par l'algorithme de programmation dynamique. Deux cas-tests représentatifs de climats chauds et de situations de trafic sont simulés. Dans le premier cas-test, le coût énergétique et le ratio de confort amélioré sont quantifiés pour différentes conditions météorologiques et de circulation. Le second cas-test met en évidence les situation de trafic dans lesquelles un compromis entre la vitesse du véhicule et le confort thermique est important. Un grand nombre de scénarios météorologiques et routiers sont simulées et les résultats montrent l'efficacité de l'approche optimale proposée pour minimiser la consommation d'énergie tout en maintenant un confort acceptable. Une comparaison entre différents indices de confort thermique est enfin réalisée, pour évaluer les gains de l'utilisation du modèle thermo-physiologique.

Si les résultats de l'approche optimale sont prometteurs et valident le principe du confort thermique et de la gestion énergétique, le coût de calcul de la programmation dynamique reste important pour une implémentation à bord dans un véhicule électrique. Une stratégie de gestion énergétique en temps réel a donc été développée, en utilisant les résultats de l'approche optimale, et un modèle simplifié mais toujours précis et représentatif du confort thermique. Sur la base des prévisions de trafic et de météo pour un trajet donné, l'algorithme temps réel estime d'abord l'énergie nécessaire à la traction et l'énergie disponible pour le confort thermique. Ensuite, il détermine le meilleur niveau de confort qui peut être fourni dans ces conditions énergétiques et contrôle le système HVAC en conséquence. Si les prévisions sont mises à jour pendant le trajet, l'algorithme ajuste le niveau de confort thermique pour satisfaire la contrainte d'énergie disponible. L'algorithme en temps réel est testé pour une grande variété de scénarios météorologiques et de trafic. Les résultats montrent que les estimateurs d'énergie ont une bonne précision. L'erreur relative absolue est d'environ 1,7% pour le premier (traction), et de près de 4,1% pour le second (confort thermique). L'efficacité de la stratégie de gestion du confort thermique proposée est évaluée en la comparant à une approche de contrôle optimal hors ligne basée sur une programmation dynamique. Les résultats de la simulation montrent que l'approche proposée est quasi optimale, avec une légère augmentation de l'inconfort de seulement 3%.

# Introduction

## 1. General context

Electric vehicles are today the main solution envisaged in the world to reduce greenhouse gas emissions from road transport, relying on a low-carbon electricity production. If electric vehicles are not the only solution to decarbonize the transport sector, their development is significantly more advanced than the other clean technologies like renewable energy or air purification. Although still modest at present, the market share of the electric vehicle is growing strongly in France but also worldwide. In fact, annual global sales of electric vehicles (EVs) increased by around 60% in 2017, reaching 1.2 million units worldwide, half of them were sold in China (Figure 1). With these sales volumes, china remains the world's largest electric car market, followed by Europe and the United States. Norway is the global leader in terms of electric car market share (46%)

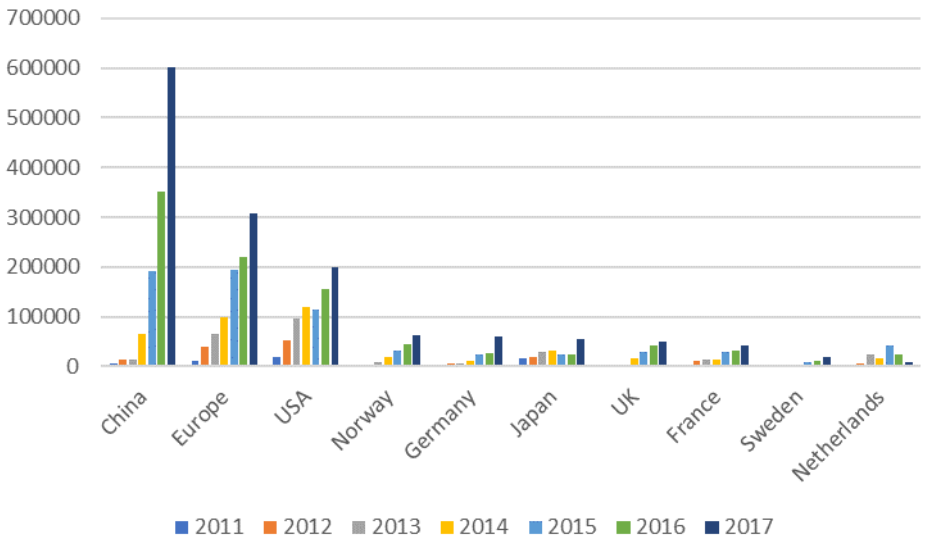


Figure 1.EVs worldwide sales per country, for the period 2011-2017

According to those statistics, it now seems very likely that electric vehicles should develop strongly over the next few years. This considerable development, results in particular from the various long-term objectives, which certain European countries, China and the United States have set themselves. In France and the UK, for example, vehicles emitting greenhouse gases will be banned from sale by 2040, which will significantly boost EV sales. The various projections of french manufacturers and public authorities expect a fleet of 3 to 4 million units over the next fifteen years The Groupe PSA, considered as the most important French and European manufacturer, undertakes to reduce the $CO_2$ emission rates by 55% compared to 2012, to electrify all brands and to produce a new generation of electric vehicle with a high range by 2035. To achieve this, Groupe PSA took actions since 2019 by proposing an electrified version of each new produced vehicle Groupe PSA has set important objectives for the next ten years, especially to produce 15 electrified vehicles between 2019 and 2021, and to electrify 80% of its brands by 2023 and 100% by 2025 (Figure 2). Similar national commitments have been made by other European countries. In the Netherlands, thermal vehicles will no longer have the right to circulate from 2030, unlike Norway which will still allow the sale of these vehicles, and will rely more on the profitability of battery electric vehicles (BEVs) and an inexpensive electrical energy.


Figure 2. Groupe PSA roadmap for electrification

The massive development of the electric vehicle constitutes a challenge and a structural development for the energy and transport sectors. The global fleet is expected to represent tens of millions of vehicles in 2030 and a market of several tens of billions of dollars each year. However, the success of this development requires that the national objectives mentioned in the previous paragraph be achieved. Different measures have been implemented by the concerned countries, and relate in particular to charging stations, research and development in the field of batteries and energy management, and public policies that aims to promote electric vehicle purchase. The first measure is the deployment of more charging stations. The objective set in France is to deploy, on a national average, a charging point for 5 to 6 vehicles. The second measure is to support R&D efforts, primarily in the field of batteries but also in the fields of new materials, digital and recycling. Recent advances in lithium batteries have permitted a decrease by half of their cost, which stimulated sales. Some manufacturers like Tesla, have placed on the market BEVs with autonomy of 400 km on the road and 250 on the highway, with a 60 kWh battery. Groupe PSA has also marketed a new generation of versatile and spacious electric vehicles (e-208, DS 3 Crossback E-Tense) equipped with a 50 kWh lithium-ion battery, a 100 kW electric motor, and a high-performance heat pump. These new electric vehicles can travel up to 350 km on a WLTP cycle, and save energy on air conditioning and heating systems. The third measure is to provide government incentives to compensate for the "utility" differential that exists today between an electric vehicle and its thermal equivalent. Among these incentives, we can cite:

- Increasing the price and penalty taxes of thermal vehicles due to the tightening of emission standards;
- Lowering electric vehicles costs as technology advances, sales volume increases and battery cost decreases.
- Providing direct financial incentives, which must be maintained as long as the cost of the electric vehicle is higher than that of the thermal vehicle. This aid could be adjusted according to the average income, as it is done in California. These incentives should be decreased gradually with the drop in production costs.
- Providing indirect financial incentives: free road tolls, tunnels and ferry crossings, possibility to use the bus lanes.
- Removing of regulatory and legal obstacles that hinder the development of the electric vehicle.

- Introducing paid traffic zones or zones reserved for electrified vehicles would give a visible advantage to EVs, as in Los Angeles, where electric vehicles can use the lanes reserved for carpooling.

- Imposing quotas sales of electrified vehicles on manufacturers such as in China and California. Until 2018, most European manufacturers choose to optimize their thermal vehicle instead of developing BEVs, unlike the German manufacturers who understood that the development of BEVs enabled them to reduce penalties. At the end of 2018, the European parliament's environment committee voted a series of environmental standard, and sales quotas of low/zeros emission vehicle. For each European car manufacturer, the sales of these vehicles must represent 20 % by 2025, and 40% by 2030.

For instance in France, subsidies for low-emission vehicles as well as the exemption from registration taxes and the relatively low electricity costs, significantly reduce the four-year vehicle expense of a privately owned BEV. Figure 3 shows a comparative analysis of ownership cost for a Golf TSI and its electrified equivalents. The 6,000 € French government subsidy helps to offset the higher cost of acquisition of the BEV version, making the e-Golf cost-competitive with gasoline, diesel autos and plug-in hybrid electric vehicle (PHEVs) versions. However, the gasoline car still has a slight cost advantage on acquisition over the BEV model, and remains more reliable in terms of driving range

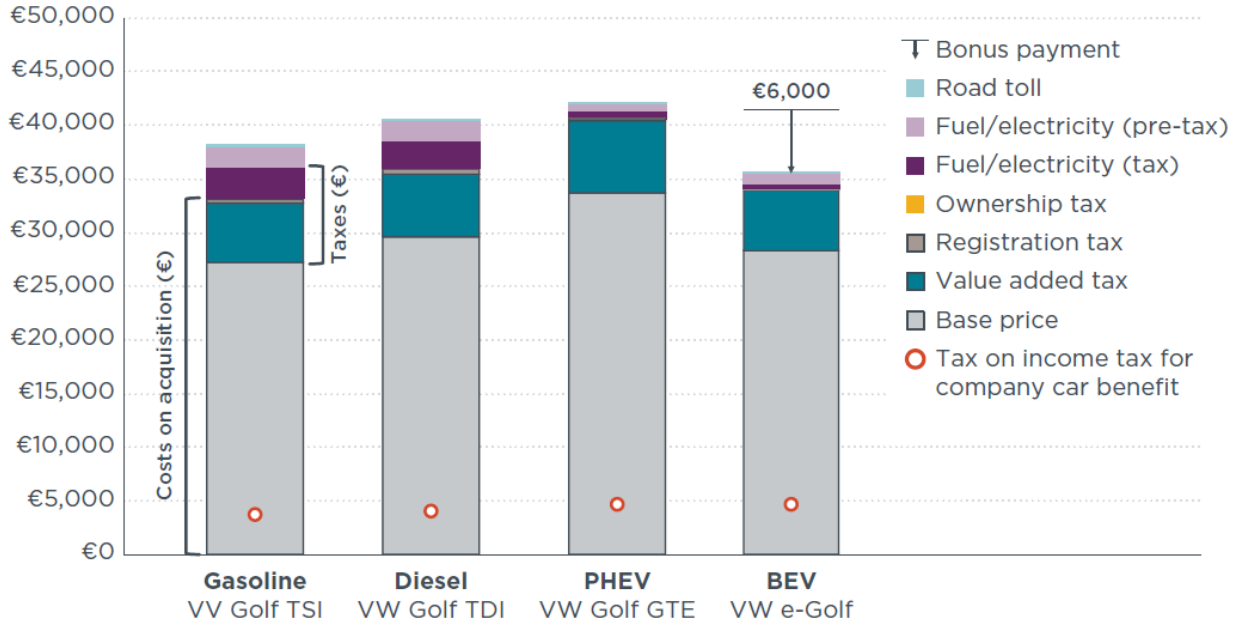


Figure 3.Four-year consumer ownership costs in France, including three-year tax on company car benefit.

## 2. Motivations

The electric vehicle will not take off until it is accessible to households with modest wages possessing an automobile, and when it offers a driving experience without dealing with range anxiety. On the one hand, this implies a marked reduction in the price of electric vehicles without compromising on the quality of the end product and the services offered by the vehicle. On the other hand, this involves overcoming the range anxiety of using a vehicle with limited autonomy, especially during long trips.

One of the solutions to comfort drivers and guarantee to arrive to their destination or to the next charging point in comfortable conditions, is to integrate a predictive energy management system. The objective of such a system is to manage the available energy in the battery until the end of the trip while ensuring the best possible comfort. This type of system is essentially based on optimization and

management tools for the vehicle's components. We can cite in particular the very famous BMS which manage the battery state of charge and temperature, but also other supervision tools for managing energy consumption and comfort, like BSI (Boîtier de Servitude Intelligent). These energy and comfort management systems use generally conventional controllers based on rules and look-up tables precalculated by car manufacturers. They can ensure one or more objectives, in particular the regulation of cabin temperature, battery temperature , vehicle speed,… etc. However, this type of system suffers from several problems, where the most important one is probably the absence of the predictive aspects. Indeed, an efficient and satisfactory energy and comfort management is correlated to the optimization's time horizon, which allows making decisions based on future environmental conditions.

Another important problem lies in ensuring comfort services, considered as a criteria of the brand's prestige, especially from the car manufacturer's point of view. The evaluation methods of comfort has been thoroughly studied in the literature, but they still not applied to the vehicular environment. A good comfort assessment permits to perform a correct diagnosis of driver and passengers comfort conditions. This suppose to fully characterize the ambiance and the occupants, and establish the physical interactions between both of them. This evaluation is crucial since the driver's performance and the safety of all occupants depends on its accuracy. According to a classification presented by Corbridge [1] comfort can be influenced by three factors: i) dynamic factors, related to vibration, shocks, and acceleration; and ii) spatial factors, dealing with the ergonomics of the passenger's position, and iii) ambient factors, where thermal comfort, air quality, noise, pressure gradients, etc, are considered. The first factor type deal with discomfort generated from seat vibrations and changes in longitudunal acceleration. Proper design of a seat contributes largely to attenuate vibration levels, generally below the biomechanical resonance frequency. Also, appropriate control of acceleration, braking and steering improves the driver stability and balance. The second type of factors concerns the ergonomics of the cabin. This requires a comfortable design of seat for the driver and passengers, a suitable pedal/steering wheel position, enough head/knee room, appropriate transmission type,... etc. The third type of factors focus on the ambience itself, through physical quantities like pollutant concentration, sound frequency, temperature and humidity. The first two quantities can be monitored by convenable air renewal system, filters, suspension system, ... etc. However, the "thermal comfort", based on quantities like temperature and humidity, may be trickier to control, since it involves a complex thermal distribution over the cabin, and more consumed energy. Also, the interaction between the human thermo-physiology, clothing, posture, aeraulic quantities and subjective considerations, add to the complexity of assessing thermal comfort in vehicle cabin. Unfortunately, until today, most of thermal comfort management systems bypass this interaction . For example, the conventional cabin temperature of 25 ° C does not correspond to the ideal thermal comfort in summer for a moderately dressed passenger, and may generate discomfort in a sunny day or at night.

These two problems, i.e. energy management and comfort assessment, will constitute the common thread of this thesis work. On the one hand, we will focus on two types control approach that minimize energy consumption and discomfort. Indeed, an electric vehicle has limited energy in the battery to power its various components, including the powertrain and the heating, ventilation and air conditioning (HVAC) system. This energy must be efficiently rationalized in such a way as to guarantee the arrival at destination, and ensure the best achievable thermal comfort. On the other hand, a particular interest will be paid to the complex notion of thermal comfort, especially its assessment methods and integration to energy management tools. Several objectives are targeted. Firstly, to meet the real thermal comfort needs in the vehicle cabin taking into account weather conditions and passenger's characteristics. Secondly, to better evaluate energetic needs for thermal comfort, and hence offer to car manufacturers valuable information to design suitable ventilation, heating and air conditioning components. Finally, to make best compromises between energy consumption and thermal comfort.

## 3. Thesis outline

In contrast to conventional and hybrid vehicles, electric vehicles have a limited range. In some situations, the energy shortage may be inevitable unless a wise management is conducted. One can imagine a management system that anticipate the energy needs over the whole trip and manage them according to the energy available in the battery. The powertrain is the primary energy consumer in EVs, but the heating, ventilating and air conditioning system (HVAC) represents also an important auxiliary load. The HVAC system is expected to provide good thermal comfort to the passengers, regardless of the surrounding context. In practice, its consumption depends on both the climatic conditions and the passengers' comfort requirements. It generally represents 20% of the total vehicle consumption, but it can reach up to 60% in urban areas and harsh conditions and can affect the vehicle driving range.

For example, Let us assume the following scenario: a 210 km highway trip in a hot and moderately humid weather. If we regulate the cabin temperature around 25°C, the powertrain and the HVAC systems may consume respectively 38 kWh and 2kWh. We can notice that the sum of these energies is greater than the battery capacity. Without an energy management, the vehicle will certainly run out of power in the middle of a highway. Effective control approaches are required in order to provide an acceptable balance between the passengers' comfort and the HVAC energy consumption, so as to preserve the vehicle autonomy range in given conditions.

Based on such approaches, one can imagine a driver assistance system that could use contextual data in order to forecast the energy needs for traction and thermal comfort, analyze them and subsequently suggest the driver to adjust either the thermal comfort or the vehicle speed in order to meet the energy constraints for the current trip. In the above mentioned scenario, such system has to better anticipate and manage the energy needs of the HVAC systems all over the trip. In other words, the destination arrival must be ensured by allocating 38 kWh to powertrain consumption, which leaves 1 kWh available energy for operating the HVAC. If ideal thermal comfort cannot be provided at an acceptable energy cost (i.e without violating the available energy condition), then thermal comfort is reduced, in order to stay within the available energy limits. This will ensure the driver to arrive safely to destination or to the next charging point. Another option, is to reduce the vehicle speed by some percent, which will decrease the consumption of powertrain and leave more available energy for thermal comfort. The sole drawback, will be to arrive late to destination. Another requirement for the assistance system is to be able to assess thermal comfort correctly, since a set point temperature of 25°C doesn't correspond to a comfortable state in many life situation. Based on the driver and passengers personal data, the assistance system must find the correct combination of thermodynamic quantities of the ambiance, that generate the best possible comfort state. Such a system require first to develop an appropriate energy management strategy, well suited to find the best compromises, and to integrate a sophisticated thermal comfort indices.

As it will be in the state of the art chapter, energy management strategies are subdivided into two categories: off-line and on-line ones. Off-line approaches assume a perfect knowledge of the upcoming surrounding conditions in order to find the best compromise between concurring objectives. They are used to evaluate the maximum gains that can be reached by a proper energy management. Such approaches require solving an optimization problem considering the whole trip, usually by dynamic programming (DP) [2] or by the Pontryagin minimum principle (PMP) [3]. In practice, these approaches are not suitable for implementation on board systems, since the future conditions are uncertain, and the solving algorithms are time consuming. Despite these drawbacks, off-line approaches are necessary in order to help developing on-line controllers and assessing their performance. On-line approaches are based either on real-time or predicted/forecasted data. Their main purpose is to be implemented on board systems. They have to be sufficiently rapid, apt to handle real-time data, and able to find near-optimal compromises. This type of approaches can be based on classical controllers such as rule based,

PIDs and fuzzy logic controllers, or optimal ones with short time horizon like model predictive control (MPC).

Both approaches will be developed and studied in this thesis. First, an off-line optimal control that minimizes discomfort under the constraint of limited energy will be formalized and solved by dynamic programming algorithm. Some weaknesses noticed in the rare papers that study the same optimization problem will be overcome, especially taking time horizons of one or two hours instead of few minutes. Also the bi-objective optimization will conducted without weighting comfort and consumption terms. Instead, an energy constraint will be set.

The goal of the off-line optimal management strategy is to show:

- The compromise between consumed energy and the resulted thermal comfort,
- The influence of traffic and weather conditions on the consumption of the air conditioning system and thermal comfort
- The advantage of reducing the speed of the vehicle in order to save energy without degrading thermal comfort.

This optimization will be studied through the prism of 3 different comfort criteria:

- A simple criterion based on a cabin temperature of 25 ° C and a relative humidity of 45%
- The thermal sensation criterion *PMV*, which will be defined in the next chapter
- The *equivalent temperature* index combined with the thermo-physiological model of the human body. Both models will be explored in the next chapter.

A comparison of thermal comfort at given energy obtained by these three indices will allow us to demonstrate the interest of using more representative sensation / comfort criterion of the vehicle occupants, than simpler ones.

In practice, this kind of algorithm cannot be deployed in a real on board system given the considerable computation time, and the a priori lack of knowledge of the driving conditions. A real-time control of the air conditioning system is then necessary. In the literature, studies that deal with real-time control of thermal comfort in vehicles are abundant, and often use a thermal comfort index based on a temperature set point, and MPC as an optimal online approaches or fuzzy logic as classical control. Given that the time horizons considered in the thesis are considerable, of the order of an hour, the MPC will not be entirely suitable as an optimal online management due to the prohibitive computation time that the resolution of the problem would require. Hence, we have thought, to develop a fast predictive algorithm, based on heuristic estimators, since this control is intended for an industrial application. The comfort index adopted is the *PMV*.

The real time approach is based on two energy estimation: the first one estimates the traction needs to reach the destination. Given an initil state of charge of the battery, the available energy for HVAC system is then deduced. The second estimation aims to determine the “energetically acceptable” thermal comfort, i.e, that doesn’t violate the available energy constraint. This thermal comfort level is then maintained at the lowest energy cost. The comfort level can be readjusted according to updated predictions of vehicle speed and weather. First, the energy needs for traction are re-evaluated, then a new available energy for HVAC system is deduced. Next, the best comfort level that respects the energy

constraint, is maintained during a control horizon. This re-evaluation process is repeated as long as prediction's updates occurs.

To test the validity and the robustness of the algorithm, a multitude of climate scenarios and driving conditions were simulated. The goal is to show:

- The validity of the estimated energies made by the algorithm
- The near-optimality of the real-time algorithm
- The real-time aspect of the algorithm when the predictions change during the trip

## 4. Contributions

The devlopped algorithms brings a fair amout of contributions, when compared to similar work in the litterature. Regarding the off-line algorithm, the following contributions can be stated:

- Development of an off-line optimization approach for long horizon thermal comfort management,
- Integration of a realistic model of the HVAC and the cabin,
- Integration of a thermo-physiological model of the driver,
- Integration of a thermal comfort index representative of human sensations in a vehicle cabin environment,
- Extensive simulations of the proposed approach for different climatic and traffic scenarios.

The results of the off-line approach serve as a basis for developing an embedded real time thermal comfort management algorithm. The related contributions can be summarized as follows:

- Estimation of the traction energy for a given planned trip modeled by macroscopic traffic indicators,
- Estimation of the HVAC energy for given weather conditions over the planned trip,
- Integration of the PMV as an estimator for passenger thermal comfort,
- Real-time predictive control approach for long horizon thermal comfort management,
- Extensive simulations of the proposed real-time control for different climate and traffic scenarios, and comparison with an optimal dynamic programming approach.

## 5. Memory plan

The thesis is organized into five chapters:

The first chapter is dedicated to the state of the art of energy management algorithms, and the assessment methods of thermal comfort. In the first part of the chapter, both off-line and on-line approaches used to manage thermal comfort in vehicle cabin, will be explored. In the second part, we will give an exhaustive survey of thermal comfort indices, including those which use thermo-

physiological model of human body. A critical conclusion will be then established, in order to justify our choices and highlight the originality of our work.

The second chapter will deal with the modeling of the vehicle powertrain and the HVAC system. For each component of the powertrain, the governing equations will be given and commented. An introductory section of some important thermodynamic concepts will be given in order to help the reader to fully understand the HVAC system model equations. The last section of this chapter, will determine the control, state and disturbance variables, which are necessary to formalize the optimization problem.

The third chapter concerns the modelling of human thermophysiology and thermal comfort. The first part, will establish the heat balance equations over the body part and body layers. The objective is to evaluate the skin temperature, which constitute an important ingredient to assess thermal comfort. In the second part of the chapter, the thermal comfort notion will be defined, and modelled through three indices: (i) temperature and humidity, (ii) PMV/PPD, (iii) equivalent temperature.

In the fourth chapter, the optimal online management of thermal comfort will be formalized mathematically, and solved by the algorithm of dynamic programming. The principle of this algorithm will be explained. Its implementation on Matlab software will be detailed. The results of simulation of different weather and traffic conditions, with equivalent temperature as thermal comfort index will then be presented and analyzed. This chapter will be concluded by a comparison between different thermal comfort index used in the literature.

The fifth chapter will focus on the long horizon real-time control developed in this thesis. The principle of the algorithm will be explained, by specifying the stages of the algorithm, the different tools developed to estimate the consumed energies. The simulation results of a large number of scenarios will then be presented, analyzed, and compared to what would give an optimal approach under the same conditions. Other results on the predictive aspect of real-time control will finally be analyzed

The thesis will be concluded by the presentation of the major findings and future works intended to improve the approaches

# Chapter I : State of the art

*On ne peut rien enseigner à autrui, on ne peut que*
*l'aider à le découvrir lui-même.*
Galileo Galilée

## Contents

In this chapter, we will define the complex notion of thermal comfort and give the state of the art of thermal comfort models and evaluation standards. This synthesis will allow us to choose the appropriate thermal comfort models to a vehicular environment, representative of drivers and passengers sensation. Next, we will present the state of the art of energy and thermal comfort management strategies. An overview of past and current managment approaches, and their future trends, will give us a basis to built suitable algorithms, with some enhancements and originalities regarding the litterature.

# 1. State of the art of thermal comfort modeling

## *1.1. Generalities*

Designers in the automotive industry became interested in comfortable mobility in last two decades. Their approach was initially based on the methods used in buildings. Works on thermal comfort in vehicles gained in importance later for various reasons. On the one hand, given the increase in the time people spend in vehicles (private or public transport) [4]. This is mainly due to the increase in the distance between home and the workplace [5]. On the other hand, due to the desire of car manufacturers to offer more wellness services and to transform the vehicle into a living space.

In addition, an uncomfortable environment can affect both a person's physical and psychological state and can be essentially unhealthy. In the case of the driver, a comfortable thermal environment can alleviate the feeling of fatigue and improve their mood, thus contributing to safe driving conditions. An example is given in the study by Tsutsumi et al. [6], which shows that an uncomfortable cabin environment can affect the driver's performance and fatigue level. In another study proposed by Danen et al. [7] it was found that driver performance was affected by the extreme conditions (both hot and cold) of the vehicle space. Thus, a moderate thermal environment of the vehicle cabin is important not only in terms of comfort state of the driver and the passengers but also for their safety.

Thermal comfort is generally defined as the state of a person who would express a sensation of well-being in relation to the thermal conditions in an occupied space. It has not to be confused with thermal sensation [8], which is as a physiological response associated with thermal information explored by skin sensors. Thermal comfort is generally considered to be a combination of thermal sensation and subjective perception of the environment. This distinction is common in neurophysiology, but it is not usual in the field of the interior environment quality. In this thesis, we will not make this distinction. Therefore, thermal sensation will be considered as a measure of thermal comfort level. However, this distinction proves that thermal comfort depends on the two inseparable components of the human being, his physical and psychological state. This explains why for the same environment, different individuals can provide different comments regarding their state of comfort. Thus, thermal comfort depends on individuals, and can in principle be customized according to the characteristics of each occupant. One of the important steps towards this customization is to develop quantitative models capable of estimating, predicting or classifying the state of thermal comfort in occupied spaces.

Almost all attempts to develop thermal comfort models focus on the physical / physiological component. Most of these attempts started with the assumption that the thermal comfort can only be achieved when the heat produced by the human body from its metabolic sources is dissipated in the external environment. In this case, we speak of thermal neutrality. However, Humphreys and Hancock [9] have shown that thermal neutrality does not necessarily correspond to a desired or preferred thermal comfort. As an example, we should cite the case where it is hot outside and people would prefer a cooler condition to the requirements of thermal neutrality, and vice versa.

Historically, three main directions to think the thermal comfort can be distinguished. A first category of concepts is represented by all models based on heat balance equations. These models propose relationships between thermodynamic and physiological parameters which can affect the thermal sensation of the human body. Some of these parameters have values commonly accepted in the literature, such as the metabolic rate, the work rate, the area of an average person, etc. [10]. The best known and most widely accepted model is the Fanger's "comfort equation" and the associated indexes called "predicted mean vote" PMV and "predicted percentage of dissatisfied" PPD [10].

The second category of concepts is represented by the so-called adaptive models which include a psychological component of thermal comfort. If the previously mentioned models linked the physical parameters of the environment to the physiological constants, the adaptive models also include the psychological component. The principle behind adaptive models is to add confidence intervals to the PMV for example, expressing human acceptability to the thermal conditions of the passenger compartment. The best known approaches have been proposed by Nicol and Humphreys [11] and by De Dear and Brager [12]. However, other influences of a psychological nature, such as emotions, stress, concentration, cultural characteristics, etc., have never been addressed, probably due to the complexity of these concepts.

The third category of concepts is represented by the thermo-physiological nodal models which take into account the heat and mass production of the human body, the heat transfers with the environment at the local level, as well as the thermoregulation mechanisms. The main purpose behind these models is to calculate local skin temperatures, necessary for the calculation of certain thermal comfort indexes.

The following sections will offer an exhaustive state of the art of the various comfort indexes that best represent these three categories.

### *1.2. Thermal comfort models based on thermal balances*

Haldane [13], at the beginning of the 20th century, was among the first researchers to tackle the question of thermal comfort. He suggested that the wet bulb-temperature could be used as an index to assess discomfort due to thermal stress of workers in high temperature industrial environments. Since then, a large number of thermal comfort indexes have been proposed in the literature. These indexes were generally only a combination of thermodynamic parameters of the air. One of them is the effective temperature (ET) [14], and was proposed in the late 1920s based on three physical quantities: air temperature, relative humidity and the air speed. Later, the metabolic rate and the thermal resistance of clothes were integrated by Gagge [15] through a heat balance equation, which gave rise to two supplementary indexes: the corrected effective temperature (ET *) and the standard effective temperature (SET *)). Fanger then developed the famous PMV and PPD, which represent a predicted vote of thermal sensation and environmental dissatisfaction, respectively. These models integrate thermal, aeraulic, physiological quantities, ... as well as an energy balance equation which describes the heat exchange between the human body and the environment.

The models cited above are currently the most used models for the evaluation of thermal comfort in indoor environments [16]. They are the basis of two international standards - European and American [17] [18] used to assess thermal comfort for all types of occupied enclosures, despite the fact that they were originally intended to be applied to buildings, in the conditions of a permanent regime. For example, PMV and PPD were obtained from a study of steady state laboratory controlled conditions, which in principle restricts the use of these indexes to this type of habitat and conditions.

Unlike the interior environment of buildings, the vehicle cabin is dominated by transient and highly non-uniform thermal conditions, high air speeds, and localized air flows. The interior of vehicles is also subject to solar radiation, radiation fluxes from cabin surfaces and much higher relative humidity

levels [19]. To all these parameters are added the physiological differences between the passengers in terms of age, gender, state of health, cultural differences which would result, for example, in different clothing approaches.

To take account of all of these parameters, a considerable number of research has focused on the concept of thermal comfort in vehicle cabin. One of the main standard methods for predicting and evaluating the thermal comfort in vehicle cabin is the equivalent temperature index presented in ISO 14505 [20] [21] [22] and the ASHRAE 55 standard [18]. The definition given indicates that the equivalent temperature represents "the uniform temperature of an imaginary atmosphere in which an occupant would exchange the same amount of heat by radiation and by convection as in the real non-uniform environment". The current definitions of equivalent temperature as well as the diagrams of the associated comfort zones are based essentially on the work of Nilsson and al. [23] [24] [25] [26], as well as the thesis of Nilsson [24]. We note that several other concepts of equivalent temperatures are discussed by the above standards such as: the equivalent temperature of the whole body defined over the entire surface of the body; and the equivalent local temperature related to a single body part or to a certain number of body parts. ISO 14505 is presumed to be usable for all categories of vehicles which include: cars, trucks, buses, passenger train compartments, aircraft cabins, ship compartments, etc.

### *1.3. Thermal comfort models based on thermo-physiological models*

In the comfort models based on thermal balances, the body is treated as a whole and the model is used to predict the comfort level at steady state, related to a certain environment. However, the environments in which humans perform their daily activities are often non-uniform and transient. Researches have shown that in this type of environment, the thermal sensation of local parts of the body strongly influences the thermal comfort of the whole body [27]. In response to these results, the development of thermo-physiological models has gained in importance.

Thermo-physiological models are mathematical descriptions of the thermoregulatory mechanisms and complex heat transfers of the human body [28]. The development of thermo-physiological models began at the National Aeronautics and Space Administration (NASA) and the United States military with the sole purpose of assessing the effect of extreme environmental conditions on the human body [29]. The first attempts began in 1911, where Lefevre modeled the human body as a sphere with a core that exchanges heat with the environment [30]. In 1934, Burton presented the first thermo-physiological model which included the anatomy of the human body and the mechanisms of thermoregulation [31]. Since then, many human thermo-physiological models have been developed. The most referenced include the models developed by Tanabe [32], Fiala [33] [34], the Berkeley Comfort Model [35] [36] and ThermoSEM [37] [38]. These models are capable in particular of predicting the temperature of the skin for different parts of the human body as well as the central temperature of the body [39] over a wide range of environmental conditions, even asymmetrical [28].

Thermo-physiological models can be classified as single node thermal models, two node thermal models, multiple node thermal models and multiple element thermal models [30]. Single-node models are empirical models that predict thermal responses based on formulas derived from experimental conditions. These models simulate a human body as a single unit and the thermoregulation system is not included in the model. For example, Givoni and Goldman developed a single-node model for application in hot environments in 1971.

In two-node models, the human body is represented as a sphere divided into two concentric layers composed of a central core and the skin. The Gagge model is a well-known example of two-node thermal models. It was developed in 1971 [40] and improved in 1986 [41]. The model includes a thermoregulation system responsible for maintaining the internal temperature at 37 ° C, and is able to simulate the temperatures of the skin and the central nucleus under uniform and transient

environmental conditions with moderate activity levels [31] [42]. Other examples of two-node models have been developed by Kingma et al. [43] Kohri and Mochida et al. [44], Foda and Siren et al. [41], Takada et al. [45] Kaynakli and Kilic [46] [47].

Multi-node human thermal models are extended and more complex versions of two-node models. The first multi-node model was developed by Crosbie [48]. Multi-node models are able to simulate local skin temperatures of different parts of the body. The most influential multi-node model that has laid the groundwork for many studies of human thermal modeling has been developed by Stolwijk [49]. This 25 nodes thermo-physiological model was developed for NASA as part of the Apollo program to create a mathematical model able of predicting the thermal responses of astronauts while performing their activities in space outside of a spatial ship. Stolwijk's model accurately predicts the dynamics of the average skin temperature of an "average" person in low activity conditions. Stolwijk's approach to modeling heat transfer and thermoregulatory mechanisms is still used in most recent advanced models, such as the Tanabe model and the Berkeley model. Other examples of multi-node models includes the ones developed by Tanabe [32], the Fiala [33] [34], the UC Berkeley [35] [36], ThermoSEM [37] [38], Salloum et al. [50], Al-Othmani et al. [51], Novieto [52], Zhou et al. [53], Lai and Chen [54] and Dongmei and al. [55].

Among the most important models developed on the basis of the Stolwijk model, two thermo-physiological models were developed by Tanabe; the 65 MN model, and the JOS (Jointed Circulation System) model [56]. The 65 node thermo-physiological model (65 MN) is capable of predicting the evolution of skin temperature for 16 different parts of the body [32], as well as calculating heat exchanges by convection and evaporation with the environment. The model takes into account on the one hand the environment via its thermodynamic quantities, in particular the air temperature and the relative humidity, and on the other hand, the human body via its physiological characteristics like the size, gender [57], the size of each part of the body, metabolism, blood flow, etc. Another very important multi-node model based on the Stolwijk model is the one developed by Fiala [58] [59] [33]. It is used in several 3D calculation software, such as in Theseus-FE commercial software [60], since to date it is considered to be one of the most complete and precise models of human thermo-physiology.

The last type of thermo-physiological models are multi-element models. These are 3D models which subdivide the human body into a higher number of nodes than multi-node models, with more complex heat exchange equations. The first model was developed by Wissler in 1985 [61]. Other examples of multi-element models have been developed by Ferreira et al. [62], Sun et al. [63], Schwarz et al. [64] and Tang et al. [65].

The thermo-physiological models presented so far allow in particular to calculate the skin temperature of the whole body or body parts with a more or less good precision, which essentially depends on the number of nodes in the model. Certain thermal comfort indexes are based on these skin temperatures. One of the most important, we cite the equivalent temperature [20] [21] [22] defined in the previous section which can be based either on Tanabe or Fiala model, the universal thermal index of the climate (UTCI) based on the thermo-physiological model of Fiala [34] Zhang index [66] [67] [68] [69] based on the UC Berkeley model.

## 2. State of the art of energy management and thermal comfort methods

The penetration of electric vehicles in road transport remains hampered by their limited autonomy and by the user's fear of running out of battery. A big research effort is put on the battery itself, but another area of improvement is to better anticipate the energy needs throughout the trip and manage them according to the available energy in the battery. For example, the heating, ventilation and air

conditioning (HVAC) system should maintain acceptable thermal comfort inside the cabin, regardless of the surrounding climatic conditions. However, in hot or cold weather, its electrical consumption can be quite significant and affect the range of the vehicle. Therefore, energy management strategies are required in order to provide an appropriate compromise between HVAC consumption and passenger comfort. Such strategies can take great advantage of communication and context information such as traffic and weather forecasting, or the map of charging stations.

The challenge is to minimize HVAC energy consumption, while ensuring passenger comfort. The methods proposed in the literature can be classified into two main categories: offline and online approaches. The main interest of off-line approaches is to find the best compromise between concurring objectives and to evaluate the reachable gains or losses. This kind of approaches requires a perfect knowledge of the surrounding conditions, and hence cannot be implemented on-line Also, solving the optimization problem are time consuming , especially because time horizons are generally considerable. Despite, these drawbacks, off-line approaches are necessary to develop on-line controllers and assess their near-optimality. The main objectives of these controllers is to be implementable in real systems, sufficiently rapid, apt to handle real-time data, and able to find a good comprise comparable to an off-line approach.

### *2.1. Off-line approaches*

Few studies have concentrated on offline approaches to manage thermal comfort in EVs, probably due to their complexity, the very high non-linearity of the HVAC models and the computing time required. For example, in [70], the authors use the theory of optimal control to regulate the temperature of the cabin around 22 ° C, while minimizing the energy consumption and the variation of the battery current, for a time horizon of 30 minutes. Usually, this type of problem is solved by the Dynamic Programming algorithm (DP) or the Minimum Principle of Pontryagin (PMP). The DP is used in [2, 71, 70] where optimal results are calculated to assess the best energy reduction or the best thermal comfort that can be achieved. These results can also be considered as a benchmark for building optimal online controllers and evaluating their effectiveness. PMP is used in [3], after linearization and simplification of the HVAC model. Although PMP is very efficient and does not consume computing resources, the initialization of the co-states can be difficult, especially if there are many state variables. In other types of vehicles than EVs, the offline management of thermal comfort has been studied in greater depth, in particular in conventional vehicles. In [72, 73, 74], the authors have developed an optimal offline approach which allows the best compromise between thermal comfort and fuel economy, over a time horizon of 1200 s. Other studies solve the problem of hybrid electric vehicles (HEV) over much longer time horizons, reaching 3000s [75], which may be more representative of realistic driving time.

Table 1 lists the studies that have looked at the management of thermal comfort and energy in the automotive field by an offline approach. For each article cited, the thermal comfort index, the objective function, the time horizon and the resolution algorithm are specified. It is noted that thermal comfort is most often modeled by a reference cabin temperature $T_{hab,sp}$ of 22 ° C, or a blown thermal power of reference $\dot{Q}_{sp}$. Other more advanced criteria such as PMV or $SET^*$ (introduced in section 1.2. ) are used in some studies. The optimization problem generally minimizes thermal discomfort and power consumption of HVAC, and is solved in most studies by the dynamic programming algorithm or the principle of Pontryagin minimum over a time horizon of 1200s. The objectives of the optimization problem are noted by:

1. Comfort
2. Consumption
3. Current stability
4. Vehicle speed
5. Battery temperature
6. Battery State Of Charge

7. Command variation
8. Air speed
9. $CO_2$
10. Battery State Of Health
11. Hybridation

| Vehicle | Reference | Comfort index | Cost function | Horizon | Algorithm |
|---|---|---|---|---|---|
| EV | [76] [77] | $PMV$ | 1-2 | 180 s | LQR[1] |
| | [78] | $SET^*$ | 1-2 | - | - |
| | [70] | $T_{cab,sp} = 22\ °C$ | 1-2-3 | 1800 s | DP |
| | [3] | $\dot{Q}_{sp}$ | 2 | 1200 s | PontryaginPontryagin |
| | [79] | $T_{cab,sp} = 22\ °C$ | 1-2-4 | 1200 s | HGA[2] |
| | [80] | $T_{cab,sp} = 22\ °C$ | 1-2-5 | 1800 s | LGR[3] |
| HEV | [75] | $\dot{Q}_{sp}$ | 2 | 3000 s | DP |
| | [81] | $\dot{Q}_{sp}$ | 1 | 500 s | LQR |
| | [80] | $T_{cab,sp} = 22\ °C$ | 1-2-5 | 1800 s | LGR |
| PHEV | [81] | $\dot{Q}_{sp}$ | 1 | 500 s | LQR |
| | [82] | $T_{cab,sp} = 22\ °C$ | 6 | 24 h | DP |
| | [80] | $T_{cab,sp} = 22\ °C$ | 1-2-5 | 1800 s | LGR |
| CV | [74] | $T_{b,sp}$ | 1-2-7 | 70 s | DP & Pontryagin |
| | [81] | $\dot{Q}_{sp}$ | 1 | 500 s | LQR |
| | [73] | $\dot{Q}_{sp}$ | 1-2 | 1200 s | Pontryagin |
| | [72] | $T_{cab,sp} = 25\ °C$ | 1-2 | 1200 s | Pontryagin |
| Other vehicles | [83] | $T_{cab,sp} \in [14,20]$ | 2 | 600 s | DP |

Table 1 Off-line approaches studies

### *2.2. Online approaches*

The second category of control approaches, namely online approaches, can be subdivided into conventional control methods and short-term optimal control methods. In the first category, fuzzy logic is the most used algorithm for controlling comfort through cabin temperature [84] [85, 86].

Fuzzy logic has been widely used by Khayyam to develop cabin temperature control for conventional vehicles [87] [88] [89] and plug-in hybrid vehicles [90]. In his early studies, he presented a "rule-based" controller [91] as well as a PID controller [92]. Subsequently, he developed an energy management system based on fuzzy logic, capable of predicting the slopes of roads and adjusting accordingly the speed of the vehicle [88], the thermal comfort and the quality of the air [87]. The use of fuzzy logic notably allowed to achieve energy savings of 12% and 3% compared to the "rule-based" controller and the PID controller respectively. Khayyam then improved his controller in [89] and [90] by replacing the fuzzy logic module, with a learning algorithm. This method permitted real-time adjustments of thermal comfort, taking into account the different geometries of the road, wind and meteorological conditions. Other studies have developed temperature and relative humidity controllers for BEVs, using a combination of a PID and a fuzzy controller [84] [93]. A more representative thermal comfort criterion was used by Frazaneh et al. in [94] [95].

Other conventional control approaches have also been used to control the temperature of the passenger compartment in a vehicle, in particular the PID [96], the energetic macroscopic representation (EMR) [97] and the rule-based control [98] [99]. In [96], the authors used the PID to control the cabin temperature and the $CO_2$ level in a metro. A simulation was carried out for more than a year and shows a possible energy saving of 47%, which correspond to an amount of energy of 325 MWh. In [97], the authors present an advanced energy management system that couples the traction and heating systems of a hybrid electric vehicle. In this work, the presented tool incorporates a mixed-integer predictive hierarchical HVAC controller which can be tuned to optimally use regenerative braking energy and

[1] LQR : Linear Quadratic Regulator
[2] HGA: Hybrid Genetic Algorithm
[3] LGR : Legendre-Gauss Radau collocation (GPOPS II solver)

obtain high passenger comfort. Huang and al. [99] developed a rule-based control that maintains the target temperature for each specified area in the vehicle cabin. This is achieved by controlling the ventilation angle, the air speed propelled into the cabin, and the air flow at the inlet of the HVAC.

In the second category of online methods, the model predictive control (MPC) is practically the only optimal algorithm that has been studied for the management of thermal comfort. One of the most important works in this field applying to BEV was carried out by Vatanparvar in a series of articles [100, 101, 102, 103, 104]. His idea was to combine HVAC control and battery management in a single optimization problem, which meets different objectives: minimize discomfort and energy consumption, extend battery life and control the battery temperature [103]. The results show a considerable reduction in energy of 39% compared to on / off and fuzzy logic controllers, and a 24% improvement in battery life. Later, Vatanparvar includes an eco-driving module which calculates the vehicle trip taking into account energy consumption and battery life [101, 102]. This improvement allowed an energy reduction of 17% compared to a route proposed by a usual navigation system with a slight increase in driving time. His latest work [104] concerns the integration of driving behavior in the optimization approach, in order to better predict the speed of the vehicle. Notable work has been done also by Hongwen et al, who developed a stochastic MPC in [2] [71] with a speed predictor based on a Markov chain, to minimize discomfort and HVAC energy consumption.

The same approach has been applied to HEVs, mainly by Amini, Wang et al [105, 106, 107, 108] with an additional complexity, namely the power distribution between the thermal and electric sources of propulsion. Amini and al developed a three-layer MPC controller, each layer solving an optimization problem over a certain time horizon. The envisaged objectives are: eco-driving, thermal comfort and energy reduction, and power distribution. The results showed on one hand that the HVAC efficiency depends on the speed of the vehicle. On the other hand, 18.8% of the energy savings were achieved compared to the rule-based controller. An improvement in the thermal comfort criterion has been studied by Wang et al. in [107, 108], the results shows that considering thermal comfort only as a temperature setpoint can lead in several situations to discomfort. The approach demonstrates its effectiveness by achieving energy savings of 7% compared to a PI controller. Other authors have succeeded to go further in modeling comfort and personalizing it for passengers, by integrating a learning module [109] [110].

Table 2 lists the studies that focuses on the management of thermal comfort and energy in the automotive field using an online approach. For each cited paper, the thermal comfort index, the cost function, the time horizon and the solving algorithm are specified. It should be noted that thermal comfort is most often modeled by a set-point cabin temperature $T_{hab,sp}$ of 25 ° C. The optimization problem generally minimizes thermal discomfort and power consumption of HVAC, and is solved in most studies by the MPC algorithm over an average time horizon of 300s. Other optimal online algorithms based on xxx have been used, such as SDP (Stochastic Dynamic Programming) [111]. The optimization objectives are noted in the same way as in Table 1.

| Vehicle | Reference | Comfort index | Cost function | Horizon | Algorithm |
|---|---|---|---|---|---|
| EV | [112] | $T_{cab,sp} \in [20,25]$ | 2 | 5 s | MPC |
| | [113] | $PMV\ et\ T$ | 1-2-8-9 | - | MPC with GA |
| | [2] | $T_{cab,sp} = 25\ °C$ | 1-2 | 800 s | MPC and DP |
| | [114] | $T_{cab,sp}$ | 1-2 | 100 s | MPC |
| | [115] | $T_{cab,sp} = 25\ °C$ | 1-2-5 | 10 s | MPC |
| | [71] | $T_{cab,sp}$ | 1-2 | 1300 s | MPC et DP |
| | [116] | $PMV$ | 2 | 600 s | MPC |
| | [103] [101] [102] [104] | $T_{cab,sp} = 24.5\ °C$ | 1-2-10 | 30 s | MPC |
| | [117] | $T_{cab,sp} \in [21,24.5]$ | 1 | 8 s | MPC |
| | [118] | $T_{cab,sp}$ | 1-2 | 1800 s | MPC |

| | | | | | |
|---|---|---|---|---|---|
| | [119] | $T_{cab,sp} = 25\,°C$ | 1 | 30 s | MPC |
| | [111] | $T_{cab,sp} = 25\,°C$ | 1-2 | 180 s | SDP |
| | [109] | $T_{cab,sp}$ | 1-2 | | Fuzzy logic |
| | [84] | $T_{cab,sp} = 25°C$<br>$HR_{cab} = 45\%$ | | | Fuzzy logic |
| | [85] | $T_{cab,sp} \in [18,24]$ | | | Fuzzy logic |
| | [93] | $T_{cab,sp} = 26\,°C$ | | | Fuzzy-PID |
| | [110] | $PMV$ | | | SLPTC[4] |
| HEV | [107] | $P_{s,sp}$ | 1-2 | 10 s | MPC |
| | [108] [120] | $PMV$ | 1-2 | 30 s | MPC |
| | [106] | $T_{cab,sp} = 26\,°C$ | 1-2-11 | 180 s | MPC |
| | [121] | $T_{cab,sp} = 26\,°C$ | 1-2-5 | 30 s | MPC |
| | [97] [122] | $T_{cab,sp} = 19\,°C$ | | | REM |
| PHEV | [90] | $T_{cab,sp} = 22{,}5$ | | | HAGA[5] |
| CV | [123] | $T_{cab,sp} = 16\,°C$ | 1-2-7 | 24 h | MPC |
| | [124] [125] | $T_{cab,sp} = 16\,°C$ | 1-2-7 | 50 s | MPC |
| | [87] | $T_{cab,sp} = 23\,°C$ | | | Fuzzy control |
| | [126] | $T_{cab,sp} = 25\,°C$ | | | PID |
| | [88] [89] | $T_{cab,sp} = 22{,}5\,°C$ | | | Fuzzy logic |
| | [95] | $PMV$ | | | Fuzzy logic |
| | [94] | $PMV$ | | | GA[6] |
| | [127] | $T_{cab,sp} = 25\,°C$ | | | PID |
| | [99] | $T_{seat}$ | | | |
| Other vehicles | [128] | $T_{cab,sp}$ | 1-7-9 | - | MPC |
| | [129] | $T_{cab,sp} = 23\,°C$ | 1-2 | 3600 s | SDP |
| | [130] | $T_{cab,sp} = 23\,°C$ | 1-2 | 3600 s | MPC |
| | [96] | $T_{cab,sp} = 19\,°C$ | | | PI |
| | [86] | $T_{cab,sp} \in \{22,23,24\}$ | | | Fuzzy logic |
| | [131] | $PMV$ | | | Neural network |
| | [98] | $T_{cab,sp} \in \{21,22,23\}$ | | | Rule based |

Table 2 On-line approaches studies

### *2.3. Comments about literature*

These approaches are interesting and effectively make it possible to find a compromise between the different objectives set. The near-optimality aspect of the MPC algorithm is generally demonstrated, by comparing their results to global optimization approaches (offline) solved by dynamic programming [70] [75] [82] or the minimum principle of Pontryagin [3]. However, the following limitations may be noted. First, they do not take into account the energy needs of EVs over the entire planned trip, which can lead to a shortage of energy before reaching the destination. This is due mainly to the chosen prediction horizon, which is generally a short one of the order of 1 to 30 s [101] [104]. In rare studies, it can reach 600 s [116], 20 min [132] or even 30 min [118], however, no study taken into account the whole trip horizon to adjust the thermal comfort of the passenger if necessary. Secondly, passenger thermal comfort is often modeled by a target temperature of 25 ° C. However, this criterion can lead to thermal discomfort, with hot or cold sensations, depending on the humidity and the radiation temperature in the cabin [116], hence the need for more advanced modeling of thermal comfort

[4] SLPTC : self learning passenger thermal comfort
[5] HAGA : Hybrid Anfis Genetic Algorithm
[6] GA : Genetic Algorithm

# Chapter II : Powertrain and HVAC system model

*The problem of creating something which is new, but which is consistent with everything which has been seen before, is one of extreme difficulty.*
Richard Feynman, Lectures II, page 20-10

## Contents

Each management strategy uses a system model to monitor a particular quantities, usually needed to evaluate a given criterion, or to constrain them according to the system's limitations. In this thesis, the system is composed from: (i) the vehicle cabin, (ii) the driver/ passengers, (iii) the powertrain, (iv) the heating, ventilation and air conditioning (HVAC) system. The first subsystem refers simply to the vehicle interior, including cabin air and the seats. The second subsystem considers the cabin occupants, especially from thermo-physiological point of view. Both subsystems are modelled in the present thesis in order to assess the thermal comfort, through some quantities like the air temperature and relative humidity, the wall cabin temperature, and the skin temperature. The energy consumption is considered through the main EV consumers: the powertrain and the HVAC system. The powertrain, is composed from a set of components that generates, converts and transmits power to move the vehicle. It is modelled by a forward approach, which determines the power needed to achieve a desired vehicle speed $v_{cycle}$. The main objective of this model is to evaluate the traction energy necessary to complete the trip. From there, one can deduce the available energy to operate the HVAC subsystem. The latter controls the cabin ambiance, by either heating, cooling, or air blowing functions, which makes it the most important part of our system, since it controls the thermal comfort level. The HVAC system modelling approach is based on evaluating dynamically the heat exchanges between its component and the inlet air. Finally, to complete the vehicle model, the battery needs to be considered in order to monitor the energy consumption.

First we will present the powertrain model. This will consist on a brief description of its components, followed by their governing mathematical equations. A special focus is put on the electric motor since it represents the main load of the powertrain system. In the next section, we will present both the cabin and HVAC system. Both are important for this thesis, because the first one holds the control variables while the second one holds the controlled variables. Their variations affect considerably the thermal comfort, and hence it is important to propose a precise and a complete dynamic model. We will begin first by presenting the cabin, the heat and mass transfers affecting the controlled variables, and then the governing equation. Next, as the HVAC system constitutes the controlled system, it will benefit from a thorough modelling. For each one of its components, the working principle and the governing equations are presented. Then the control variables are specified. However, before doing this, we give a review of some thermodynamic concepts, used in the HVAC system model. Finally, in the third section, the main energy source in a electric vehicle, namely the high voltage battery is presented. The management strategy consists as in the thesis outline, in minimizing the discomfort subject to finite available energy in the battery. For this reason, a simple model is sufficient to monitor the state of charge (SOC).

# 1. System overview

The complete vehicle system is depicted in Figure 4. As stated above, the powertrain has to track the desired driving cycle $v_{cycle}$. To do this, the electric motor (EM) and the braking system has to provide enough torque to overcome the external resistive force and meet the speed requirement. We assume that only the electrical motor consumes electrical power $P_{EM}$ in this process

For a given control vector $u$ and a given weather conditions $w$, the HVAC system blows a cooled air with a given thermodynamic characteristics. This air exchanges heat with the existent air in the cabin, which brings it to a new state, is mainly characterized by a temperature and a humidity. Moreover, since the air is cooled, an electrical power $P_{HVAC}$ is consumed by the HVAC system to perform this operation.

Both powertrain and HVAC system are fed by a high voltage battery, which constitues the main energy source in the electric vehicle. The battery state is monitored by its state of charge (SoC).

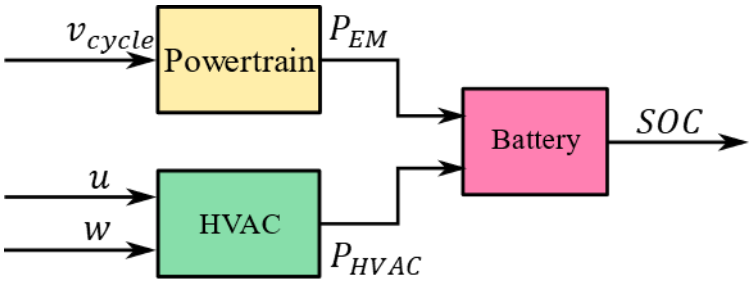


Figure 4. Block diagram of the overall system

## 2. Powertrain model

Powertrain refer to the set of components that generate the power required to move the vehicle and deliver it to the wheels. Figure shows the powertrain components and their most important physical quantities, which will be defined in the following sections.The electrical power is supplied by the high voltage battery to the electric motor which converts the electrical energy into a mechanical one. The latter play also a role of generator, recharging the battery during braking. The mechanical energy is finally delivered via the transmission to the wheel, which allows the vehicle to move forward.

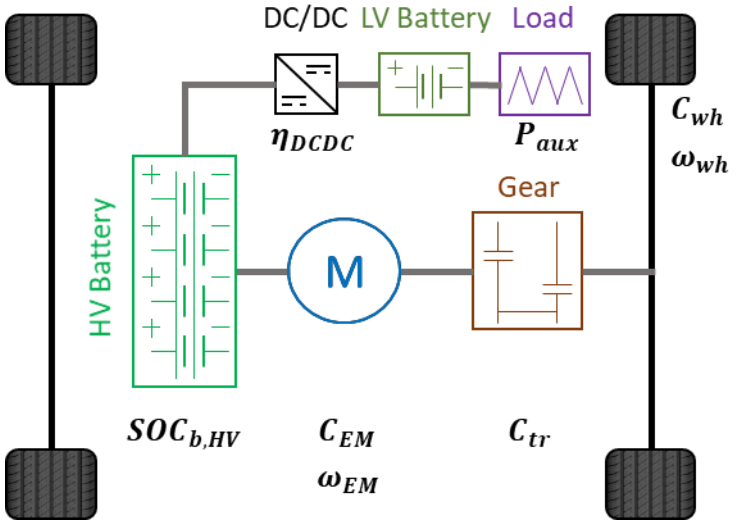


Figure 5. Schematic diagram of electric powertrain

Powertrain are usually modelled in the literature by the so called “backward facing” approaches [133]. They are a class of models, that do not require a driver model, as the vehicle speed is obtained directly from the driving cycle. In such models, the force required to accelerate the vehicle for a given time step, is calculated directly from the desired speed profile. The required force is then translated into a torque that must be provided by the component directly upstream, i.e. the transmission. Meanwhile, the vehicle’s linear speed is translated into a required rotational speed. Component by component, this calculation approach carries backward through the powertrain, against the tractive power flow direction, until electrical power necessary to perform the speed profile is computed. Since the transient characteristics are ignored in backward-facing models, they only need large time steps, resulting in quicker simulation times. However, due to this quasi-static nature, backward-facing models fail in some situations, to meet the desired speed due operational limitations, or to account for the vehicle inertia.

However, due to this quasi-static nature, backward-facing models fail to describe the actual behavior of the vehicle, as in several situation, the realized speed is different from the desired one. This is mainly due to operational limitations, and the vehicle inertia.

In contrast, the forward facing models takes into account the vehicle's dynamics, as well as the dynamics of its components. This is important for energy management approaches, since the consumption can be evaluated correctly, even in harsh situations. A forward-facing model provides insight into the vehicle model drivability, and it captures the limits of the physical system.

Forward-facing approaches also feature a driver model, which is typically modeled as a proportional-integral (PI) controller as shown in Figure 6. The objective is to meet the torque demand, with reference to the desired speed. The torque produced by the electric motor is transmitted through the transmission before ending up as torque applied at the wheels. This is then exerted on the vehicle mass via force on the tire contact patch. The vehicle speed that results from the applied force goes back through the drivetrain and returns to the electric motor as angular velocity at the primary shaft. The brake torque is split between the EM shaft and the wheels depending on the vehicle speed .The part allocated to the EM, follows the same path as the tractive force, whereas the second part is applied directly on the wheels.

Unlike backward-facing models, the driving cycle is not imposed on the vehicle, and, therefore, there will inevitably be a small difference between the actual vehicle's speed and the speed trace. It is the role of the driver model to minimize this error.

In next sections, we will present the powertrain model given by Groupe PSA for the thesis needs. Each powertrain component will first be described, then the governing equations will be given.

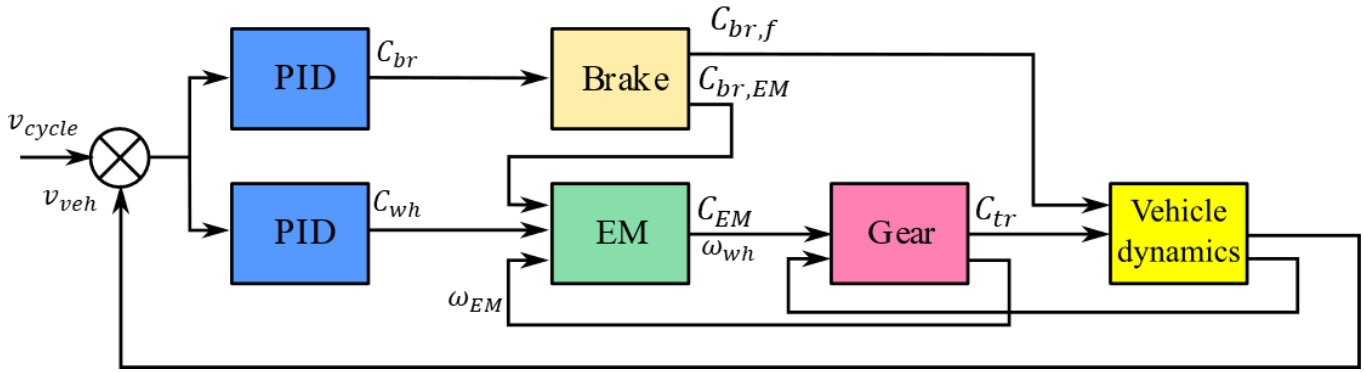


Figure 6. Block diagram of the powertrain model and the driver

## *2.1. Driver model*

A driver model in forward facing modelling approach simulates the behavior of a human driver. A driver decides whether to brake or accelerate the vehicle in order to follow the desired driving cycle. It is essentially a tracking controller that takes the speed profile as an input and generates the output in terms of acceleration and brake commands. In literature, many types of driver models are investigated, starting from simple PI controllers to advanced optimal control based models.

In the present work, the driver is modeled by two PIDs controllers. The first one is a proportional derivative controller that calculate the tractive torque applied to the wheel $C_{wh}$ while the second one computes the total braking torque $C_{br}$.

At first, the difference between the reference vehicle's speed $v_{cycle}$ and the actual speed $v_{veh}$ is fed to both controllers, which determine $C_{wh}$ and $C_{br}$. If the tractive torque can take positive or negative values, it is not the case for the braking torque. This quantity can only be positive, and takes strictly positive values when $v_{veh}$ is greater than $v_{cycle}$ and when their difference exceeds a certain threshold. These conditions are captured by the function $f_{br}$. The commands $C_{wh}$ and $C_{br}(t)$ are given by (1) and (2) where $k_p$ and $k_d$ are the controller coefficients.

$$C_{wh} = k_p * \left(v_{veh} - v_{cycle}\right) + k_d \frac{dv_{veh}}{dt} \quad (1)$$

$$C_{br} = \left(v_{veh} - v_{cycle}\right) * k_p * f_{br}\left(v_{veh}, v_{cycle}\right) \quad (2)$$

### *2.2. Brake model*

The total braking force of an EV is composed from a regenerative braking force of the electric motor, and a friction braking force of the wheels. Regenerative braking is an effective approach that improves vehicle efficiency, especially in heavy stop and go traffic [134]. It allows the vehicle to recover significant amounts of energy during braking and store it in the battery. Energy recovery through regenerative braking is accomplished by controlling the electric motor to operate as a generator and converting the kinetic or potential energy of the vehicle's mass into electric energy [135]. In this case, only the driven axle is effective during regenerative braking.

During most heavy braking situations, the required braking force to decelerate, or stop the vehicle, is much greater than the resistive force, which is produced by the electric motor. As a result, the majority of the braking energy must be absorbed by the friction brake system [136]. Therefore, in order to allow brake energy recovery while ensuring braking performance, both regenerative and friction braking have to coexist [137].

A major concern regarding EV brake system is the proper allocation of the braking force between the friction brakes and the electric motor used as a generator. In practice, regenerative braking should be applied to recapture as much energy as possible without compromising the vehicle stability.

When calculating the regenerative braking share $C_{br,EM}$, two main limitations should be considered. The first one is the maximum regenerative braking capability which is usually determined by the braking torque capability of the electric motor while operating as a generator [138]. This limits the energy recovery during harsh deceleration of the vehicle. The second limitation which plays an important role particularly when considering efficiency and energy consumption is the inability of the electric motor to operate as a generator and charge the vehicle battery at low speeds. During deceleration, regenerative braking employs the back electromotive force (EMF) [133] of the motor which can be considered as a voltage source to recharge the battery [139]. However, at low speeds due to the insufficient back EMF voltage generated by the electric motor, the regenerative braking process is no longer effective [137]. As a result, in an actual EV, when the vehicle speed is lower than a given threshold, braking is completely performed by the friction brakes . It worth noting that this threshold depends on the type and specifications of the electric motor and the battery. In order to model this, let us consider a weight function $w_{br}$ of vehicle speed that: (1) take null value when $v_{veh}$ is below a speed threshold $v_{veh,1}$, (2) increases linearly until a second speed threshold $v_{veh,2}$, where the function $w$ takes a value of 1, (3) remains constant beyond $v_{veh,2}$. The braking torque $C_{br}$ can be allocated according to the function $w$ into a torque for regenerative braking $C_{br,EM}$ and a torque for friction braking $C_{br,f}$. Both torques are given by (3) and (4):

$$C_{br,EM} = C_{br} \times w_{br}(v_{veh}) \quad (3)$$

$$C_{br,f} = C_{br} \times \left(1 - w_{br}(v_{veh})\right) \quad (4)$$

### *2.3. Electric motor model*

The electric motor is a key component in EVs. It is a reversible machine that converts the electrical power from the battery into a mechanical one to drive the vehicle. Furthermore, it recuperates the mechanical power from braking and convert it to electrical power to recharge the battery.

Electric motor torque/power characteristics differ from an internal combustion engine. The main difference is that the electric motor can provide the maximum torque from zero speed. The typical torque curve of an electric motor, as shown in Figure 7, is made up of a constant torque region, ranging from zero to base speed [140]. It is followed by a constant power region, where in a first approximation, the torque decreases as long as the motor speed increases, up to the maximum speed. Although in reality the torque reduces at a faster rate across the motors speed range reducing the power below a constant power.

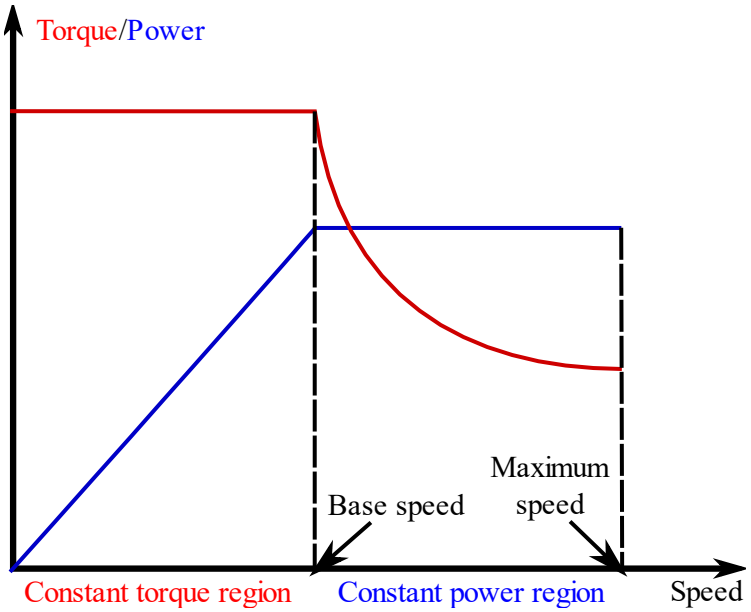


Figure 7. Electric motor torque and power curve

Electric motors basically can be organized into two main categories: direct current (DC) motors and alternating-current (AC) motors. All types of motors have a stationary part, called the stator, and a rotating part, called the rotor. Most electric motors operate through the interaction between the magnetic fields generated by the rotor and the stator. This interaction produces a torque applied on the motor's shaft. In the present work, the electrical machine is an AC synchronous motor with a nominal power of 125 kW.

In AC synchronous motor, windings are disposed in the stator, and are fed by three-phase alternating currents. A magnetic field is therefore generated, changing its orientation according to the sign of the current. Since this is continuously varying, the orientation of the magnetic field keeps varying also, which results in a rotating magnetic field. Concerning the rotor, a magnetic flux is created thanks to the permanent magnets or the windings placed on it. As the stator flux rotates, torque is generated to spin the rotor at the same speed as the stator magnetic field, hence the name “synchronous”.

The objective of the EM model is to evaluate the consumed electrical power when applying the command torques at a given wheel speed $\omega_{wh}$. The net command torque at the wheel, given by (5), is transmitted through the transmission (reprsesented by the gear ratio $k_{tr}$) , to become the reference torque $C_{EM,ref}$ to be applied on EM shaft. This quantity, given by (6), must respect the EM torque’s limitation $C_{min,EM}$ and $C_{max,EM}$. Usually, those limits are function of EM rotational speed $\omega_{EM}$, and are computed in practice through a look-up table.

$$C_{wh,net} = C_{wh} - C_{br,EM} \tag{5}$$

$$C_{EM,ref} = \frac{C_{wh,net}}{k_{tr}} \tag{6}$$

The net torque must be greater than a minimal value $C_{wh,min}$, which is a data given by Groupe PSA. Also, the reference torque is limited by a maximal value $C_{max,EM}$ when the EM operates as motor, and a minimal value $C_{min,EM}$ when it operates as a generator. Those extremal values are functions of the speed $\omega_{EM}$:

$$C_{wh,net} \geq C_{wh,min} \tag{7}$$

$$C_{min,EM} \leq C_{EM,ref} \leq C_{max,EM} \tag{8}$$

Hence, the reachable torque $C_{EM}$ is given by the set of equations (9-11)

$$C_{EM,m} = \min\left(C_{EM,ref}, C_{max,EM}(\omega_{EM})\right) \tag{9}$$

$$C_{EM,r} = \max\left(C_{EM,ref}, C_{min,EM}(\omega_{EM})\right) \tag{10}$$

$$C_{EM} = \begin{cases} C_{EM,m}\,, & C_{EM,ref} \times \omega_{EM} \geq 0 \\ C_{EM,r}\,, & C_{EM,ref} \times \omega_{EM} \leq 0 \end{cases} \tag{11}$$

The relationship between the mechanical power and $P_{EM}$ can be calculated without a detailed model of the system when a stationary loss map of the machine is available. This map, supplied by Groupe PSA, permits to evaluate power losses $P_{loss}$ as a function of torque and the vehicle's speed. A positive value of $P_{EM}$ means that the machine is operating as a motor, where a negative values means that the electrical machine is in a generator mode. In either situation, $P_{EM}$ is given by (12) :

$$P_{EM} = C_{EM} * \omega_{EM} + P_{loss}(C_{EM}, \omega_{EM}) \tag{12}$$

### *2.4. Transmission model*

Unlike conventional vehicle where the mechanical transmission is composed of numerous gears, battery electric vehicles utilize single-speed transmissions. The torque characteristics of the electric motor lend well to a single-speed transmission. The reason is that the zero speed torque region provides enough torque for pull-off and inclines, whilst the constant power region extends to a large speed range. However, recent research suggests that the performance and efficiency of an electric powertrain can be increased using a multiple-speed transmission [141].

In the present work, we assume that the transmission is represented by the gear ratio $k_{tr}$, and a loss map $C_{loss,tr}$. The gear ratio increases the torque $C_{EM}$ and reduces the rotational speed $\omega_{EM}$. The loss map evaluates the torque losses between the primary and secondary shaft, as a function of $C_{EM}$ and $\omega_{EM}$. The torque and speed at the secondary shaft are noted by $C_{tr}$ and $\omega_{tr}$ and are given by (13) and (14):

$$C_{tr} = \left(C_{EM} - C_{loss,tr}(|C_{EM}|, \omega_{EM})\right) * k_{tr} \tag{13}$$

$$\omega_{tr} = \frac{\omega_{EM}}{k_{tr}} \tag{14}$$

## *2.5. Wheel and vehicle dynamics*

The vehicle motion is completely determined by the forces acting on it. Besides the tractive force applied by electric motor to track the desired speed, the vehicle is subjected to three resistive forces. The first one is the gravitational force $F_g$, which applies only if the road has a slope $p$. The second one is the aerodynamic drag $F_a$, which represents the viscous friction forces with the surrounding air, acting on the opposite direction of vehicle motion. The third and final force is the rolling resistance $F_r$. The following subsection will detail each force and propose an adequate equation to model it. The speed evolution will be inferred by applying the fundamental dynamic principle.

### 2.5.1. Gravity resistance

The force induced by gravity when driving on a non-horizontal road is conservative and considerably influences the vehicle behavior. This force is defined by (15), where p is the road slope in[%], $m_{veh}$ the vehicle mass in [kg], and $g$ the gravitational acceleration:

$$F_g = \sin\left(\tanh^{-1}\left(\frac{p}{100}\right)\right) * m_{veh} * g \tag{15}$$

### 2.5.2. Aerodynamic resistance

The aerodynamic force have two components: the first one is in the direction of the air flow known as aerodynamic drag and the second one is in the perpendicular direction known as aerodynamic lift. In the present work, only the drag force is considered, since we model the vehicle longitudinal motion.

For a standard vehicle, the car body causes approximately 65% of the aerodynamic resistance. The rest is due to the wheel housings (20%), the exterior mirrors, eave gutters, window housings, antennas, etc. (around 10%) and the engine ventilation (approximately 5%) [142].

Usually, the aerodynamic drag force is approximated by considering the vehicle as prismatic body with a frontal area $S$.The force caused by the stagnation pressure is multiplied by an aerodynamic drag coefficient $C_d$, which represents the resistance to actual flow conditions. The value of $C_d$ depends on the smoothness and curvature of the surface. The aerodynamic drag force $F_a$ is given by (16)

$$F_a = \frac{1}{2}\rho S C_d (v_{veh} + v_{wind})^2 \tag{16}$$

where $C_d$ is the drag coefficient, $S$ is the projected area normal to the direction of air flow, $v_{veh}$ is the vehicle speed and $v_{wind}$ is the speed of the wind parallel to the motion of the vehicle. The term $v_{wind}$ has a negative or positive sign depending on whether the wind flows is the same or in the opposite direction of the vehicle motion. In the present work, $v_{wind}$ is assumed to be equal to zero.

### 2.5.3. Rolling resistance

The rolling resistance force is due to hysteresis effects of tyre deformation, shear of the tyre, and adhesion between surface and tyre. It is modelled by a rolling resistance coefficient $\mu_r$ which depends on the road type, tyre parameters [143] and the vehicle's speed $v_{veh}$. For instance, a wet road increases the coeficient $\mu_r$ by 10% [144], whereas driving in extreme conditions, such sand, can easily double that value [145]. Furthermore, the rolling resistance coefficient increases with the vehicle's speed above 60 km/h, and can be considered as constant below this threshold [146].

$$F_r = \mu_r(v_{veh}) m_{veh} g \quad (17)$$

### 2.5.4. Vehicle dynamics

The wheel dynamics is governed by newton's second law of motion. The law states that the angular acceleration of the wheel depends on one hand on the net torque $C_{wh}$ applied upon it. On the other hand, it depends on the equivalent moment of inertia $J_{e,wh}$, evaluated at the wheel. We will assume that the vehicle motion is performed only in longitudinal direction, and all outside forces are counted positive if they are resistive, and negative if they help the motion. Hence the net torque is given by (18):

$$C_{veh} = C_{tr} - C_{br,f} - \left(F_a + F_r + F_g\right) * R_t \quad (18)$$

Hence, the wheel dynamics is given by (19):

$$\frac{d\omega_{wh}}{dt} = \frac{C_{veh}}{J_{veh}} \quad (19)$$

Where $J_{e,wh}$ is the equivalent moment of inertia of the vehicle, calculated at the wheel. The expression of $J_{veh}$ can be derived from the definition of kinetic energy. Since the electric vehicle is composed from rotational components (i.e. EM, transmission and wheels), and static ones (i.e., chassis), one can infer the formula of an equivalent moment of inertia $J_{e,wh}$ of a theoretical rotational body by (20):

$$J_{e,wh} = J + m_{veh} * R_{pneu}^2 \quad (20)$$

The term $J$ is the sum of moment inertia of the rotational part calculated at the wheel, assumed constant and given by (21) :

$$J = (J_{EM} + J_{tr}) * k_{tr}^2 + J_{wh} \quad (21)$$

The linear velocity of the vehicle can be deduced by (22):

$$v_{veh} = \omega_{wh} * R_{pneu} \quad (22)$$

# 3. HVAC model

## *3.1. Working principle*

Figure 8 shows a schematic drawing of the HVAC system and the vehicle cabin. The HVAC sytem consists of three main components: one is the ventilation circuit (grey loop) that blows conditioned air in the cabin, and the two others are the cooling and heating systems (resp. blue and orange boxes) that exchange thermal power with the blown air in order to adjust its temperature and humidity.

As depicted in Figure 8, the cabin air exchanges thermal power with the outside by convection and radiation, and also with cabin walls and passengers. A certain amount of recirculated cabin air is then mixed with the outside air and blown by a fan into the ventilation system. The air is firstly cooled and dried up by yielding thermal energy to air conditioning system through the evaporator. This process is detailled in section 3.4. At this stage, it is too cold to be directly blown into the cabin and it needs to be warmed up in the heating system. This can be done at a zero energetic cost by exchanging with the cooling system of the traction motor.

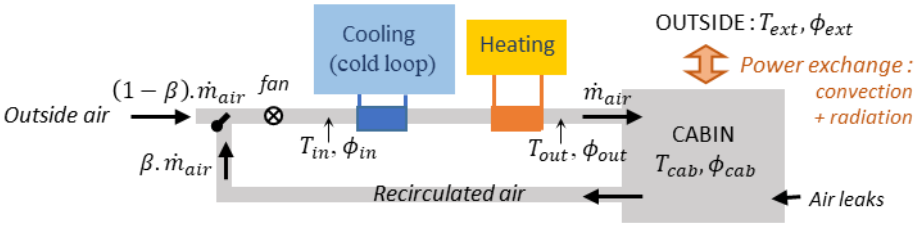


Figure 8. Schematic diagram of the HVAC system.

The next sections presents the mathematical model of the cabin and the HVAC system, supplied by Groupe PSA. The objective is firstly, to compute the thermodynamic properties of the cabin air that affect thermal comfort. Secondly, to evaluate the electrical consumption of the HVAC system. Before describing the system components, and giving the governing equations, a brief review of thermodynamic concepts is presented in section 3.2. The objective, is to clear up some thermodynamic notion used in the present work, and explain the modelling approach of heat exchangers. Next, in section 3.3. , we describe the cabin, and give the differential equations that govern the temperature and humidity. Thereafter, in section 3.4. , we explain the thermodynamic principles behind the refrigeration system and present the adopted modelling approach and its objectives. For each cooling system components, a brief description of its working principle will be given, followed by its governing equation. In section 3.5. and 3.6. , the heating and ventilation system model will be presented The last section, is dedicated to HVAC consumption model.

## *3.2. Thermodynamics concepts*

This section introduces some thermodynamic concepts that will be used extensively in the HVAC system and the cabin models. Firstly, we define thermodynamic properties such us enthalpy and specific humidity. Next, we present the calculation principles of air properties for given state of the air. In the same way, we present the calculation principles of the refrigerant properties. Finally, we describe heat exchangers, and detail the modelling approach that evaluate the heat flow rate between the refrigerant and external fluids.

### 3.2.1. Definitions of internal energy, enthalpy and entropy

- **The** Internal energy is the total energy that a thermodynamic system contains. It is the energy needed to create the system apart from energy related to external force fields (e.g. potential energy) or associated with movement (e.g. kinetic energy).

- The enthalpy is a property of a thermodynamic system, equal to the system's internal energy plus the product of its pressure and volume. This property can be defined for a unit mass. It is usually noted by $h$.

- The entropy is an extensive property of a thermodynamic system usually interpreted as the degree of disorder or randomness in the system. This property can be defined for a unit of mass. It is usually noted by $s$.

- The specific humidity is defined as the ratio of water vapor mass $m_{H_2O}$ to the total moist air parcel mass $m_{air}$. This quantity is noted by $\phi$ and given by (23):

$$\phi = \frac{m_{H_2O}}{m_{air}} \tag{23}$$

- The relative humidity is the ratio between the partial pressure of water vapor and the equilibrium vapor pressure of water at a given temperature; this quantity is noted by $RH$.

- The wet-bulb temperature is the temperature of an air parcel, if it is cooled adiabatically, by evaporation of water vapor, at constant pressure, until it reaches saturation.

### 3.2.2. Air properties

All thermodynamic properties of the air can be determined, if two of them are known. For instance, one can compute the air enthalpy as a function of its temperature and specific humidity. If the air is saturated, one thermodynamic property is sufficient. The calculation are based usually on tabulated data of the air, an uses linear interpolation to determine, for example, the air enthalpy at a given temperature and relative humidity. A graphical representation of these data, is available in the form of the psychometric chart of the air [147].

In the present work, we will use the following notations to refer to functions extracted from the tabulated data of the air:
$\hat{\phi}_{air}$: specific humidity, function of temperature $T$ and relative humidity $RH$

$\widehat{RH}_{air}$ : relative humidity, function of temperature $T$ and specific humidity $\phi$

$\hat{h}_{air}$: enthalpy, function of temperature $T$ and specific humidity $\phi$

$\hat{T}_{air}$: temperature, function of temperature $h$ and specific humidity $\phi$

$\hat{T}_{air,sat}$: temperature at saturation, function of enthalpy $h$

$\hat{\phi}_{air,sat}$: specific humidity at saturation, function of temperature $T$

$\hat{T}_{wet,air}$ : wet bulb temperature, function of temperature $T$ and relative humidity $RH$

### 3.2.3. Refrigerants properties

A refrigerant is a fluid used in refrigeration system to transfer heat from a zone to another. The main characteristic of refrigerants is that the boiling point is usually lower than most common liquids, which means that the refrigerant can evaporates at lower temperatures.

In refrigeration systems, the refrigerant undergoes a thermodynamic cycle where it receives compression work and exchanges heat with external fluids. The thermodynamic cycle is usually represented in Mollier diagram depicted in Figure 9. The blue curve represents the saturated state of the refrigerant, where the fluid is in equilibrium phase. It delimits the two phase region liquid-gas from the single phase region (i.e, either liquid or gaz). The green and the black curve refers to iso-lines of refrigerant density and quality (ratio between vapor and liquid mass). Using these curves helps to understand and evaluate qualitatively the effect of each transformation on the refrigerant. Nevertheless, we still need to evaluate numerically the refrigerant state through its thermodynamic properties.

For a given refrigerant state, all its thermodynamic properties can be determined if two of them are known. If the refrigerant is in a transition phase (evaporation or condensation), one thermodynamic quantity is sufficient. For example, the refrigerant entropy is a function of its temperature and pressure. However, if it undergoes a phase change, its entropy depends only on either its temperature or pressure. The calculation are based on tabulated thermodynamic data of the refrigerant R-1234yf [148]. In next sections, we will use the following notation to refer to the refrigerant look-up tables:
$\hat{h}_{ref}$ : enthalpy, function of temperature $T$ and pressure $P$

$\hat{s}_{ref}$: entropy, function of temperature $T$ and pressure $P$

$\hat{P}_{ref,sat}$: pressure at saturation, function of temperature $T$ and pressure $P$

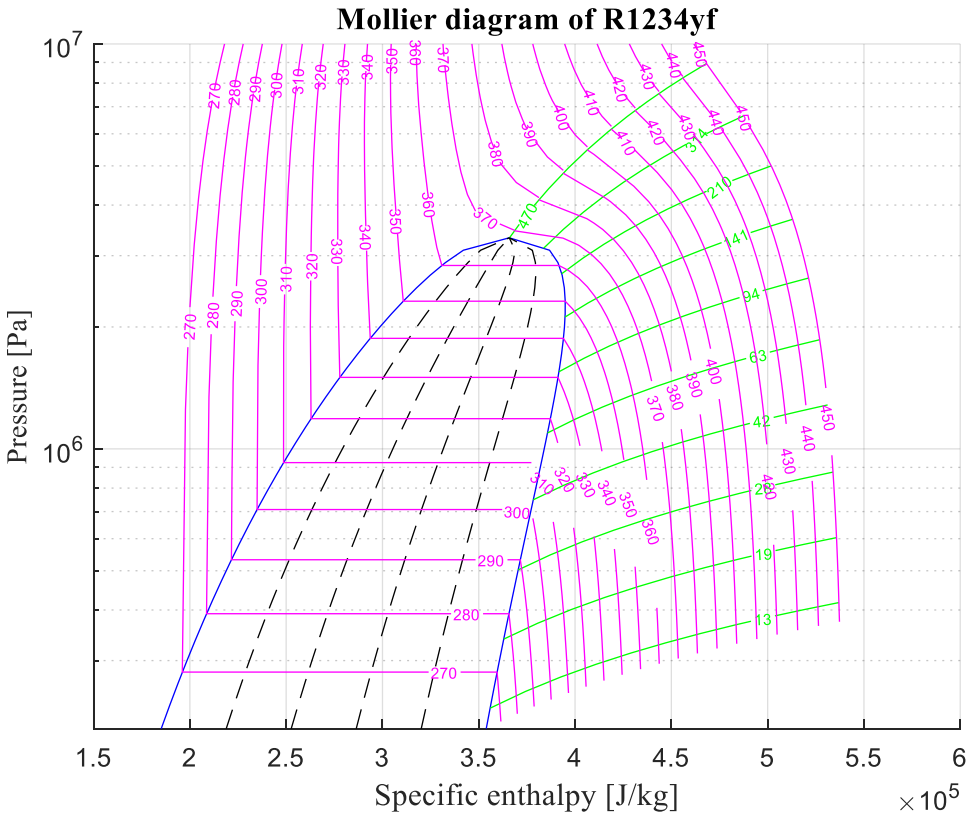


Figure 9. Mollier diagram of the refrigerant R1234yf

### 3.2.4. Heat exchangers

A heat exchanger is a device that transfers thermal energy between two fluids. Heat exchangers are normally classified depending on transfer process, number of fluids, construction type , flow arrangement, heat transfer surface area/volume ratio, …etc. [149]. The heat exchangers used in our HVAC system model are single pass tubular heat exchangers where the two fluids are in counter flow (Figure 10). This flow arrangement is considered as the most efficient.

In refrigeration systems, two heat exchangers are used: the *evaporator* which transfer the heat from the outside fluid to the refrigerant, and the *condenser* which performs the inverse function.

Among all modelling techniques of heat exchangers, the NTU (Number of Transfer Units) method was chosen for two reasons. The first one is that the temperature of both the refrigerant and the external fluid at the outlet of the heat exchanger is not known, which prevents from evaluating the heat exchange. The second reason is the relative simplicity of the method, compared to other modelling techniques in the literature [150]. The NTU method consists in determining the maximal heat flow rate exchanged between the two fluids, and multiplies it by a factor $\varepsilon$. This parameter is dimensionless, called the heat transfer effectiveness, and depends only on the heat exchangers geometry and flow arrangement. The effectiveness $\varepsilon$ is defined by (24):

$$\varepsilon = \frac{\dot{Q}}{\dot{Q}_{max}} = \frac{Actual\ heat\ transfer\ rate}{Maximum\ possible\ heat\ transfer\ rate} \tag{24}$$

The maximum possible heat flow rate $\dot{Q}_{max}$ occurs when the temperature difference between the air and the refrigerant is maximal as shown in Figure 10. Since the air temperature decreases through

the evaporator, and the refrigerant temperature is constant (due to phase transition), the maximal temperature difference between the two fluids, occurs at the inlet of the evaporator. At this moment, the air is the fluid which will experience the maximum heat flow rate, due to its lower heat capacity.

$$\dot{Q}_{max} = C_{air}\left(T_{air,in} - T_{ref,in}\right) \tag{25}$$

The effectiveness of a heat exchanger enables to determine the heat flow rate without knowing the outlet temperatures of the air. As stated before, the effectiveness of a heat exchanger depends on the geometry of the heat exchanger as well as the flow arrangement [151]. Therefore, different types of heat exchangers have different effectiveness relationship. In general, the effectiveness is a function of the number of transfer unit (NTU) [152]. This quantity is dimensionless, and depends on heat exchanger surface $A$, its overall heat transfer coefficient $U$ and the lowest heat capacity between the two fluids. The exact expression of $\varepsilon$ will be given in both heat exchangers sections.

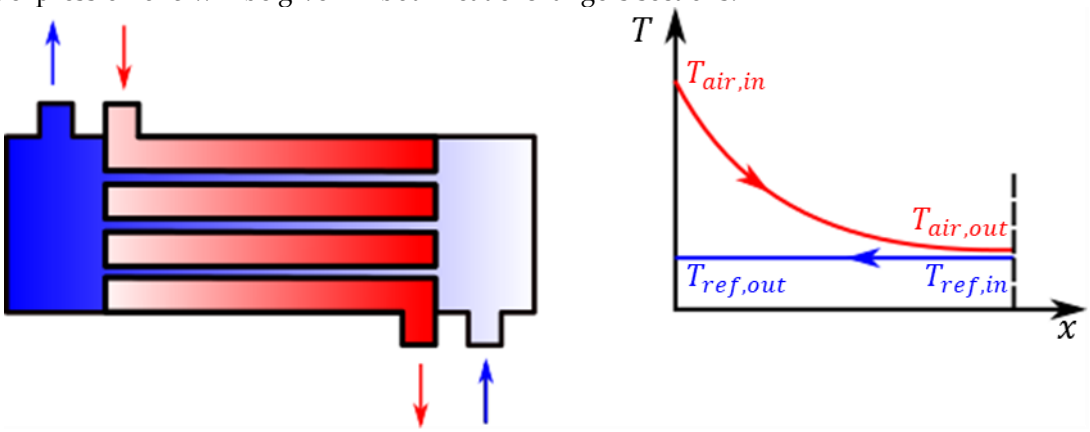


Figure 10. Counter flow heat exchanger

### *3.3. Cabin model*

As mentioned earlier, the present work uses a 1-D, lumped-parameter approach [153] to model the vehicle cabin, similar to those used by [154] [155] [156] [116]. A representation of the cabin is given in Figure 11. As shown in this figure, the air enters the vehicle cabin from vent outlets of the ventilation system and mixes with the existing cabin air. The latter is affected by the cabin walls, the number of passengers and the solar radiation. Then, the air exits the cabin and recirculate via the ventilation system. Three dynamic quantities characterize the cabin: the mean temperature of the cabin air $T_{cab}$, its relative humidity $RH_{cab}$, and the mean temperature of the interior walls, also called the mean radiant temperature $T_w$ [157].

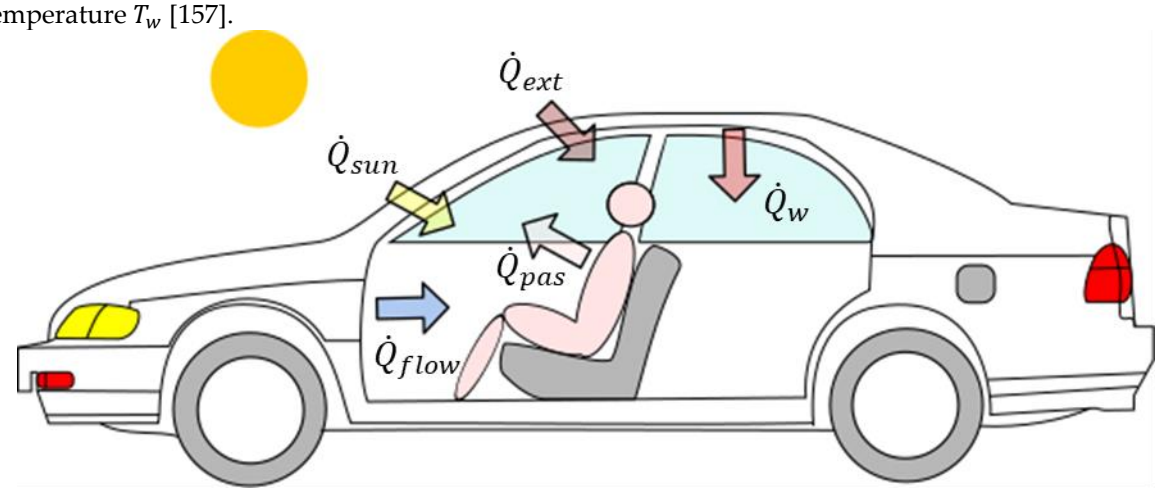


Figure 11. Heat exchanges in the vehicle cabin

The cabin model assumes that the three quantities are spatially uniform . The same assumption is applied to the heat capacity of the cabin wall $C_{wall}$ and the cabin air $C_{cab}$. In the flowing, the governing heat balances (26-30), and the mass balance (31) are presented and explained.

The cabin temperature evolution is governed by (26):

$$C_{cab}\frac{dT_{cab}}{dt}(t) = \dot{Q}_{ext}(t) + \dot{Q}_{flow}(t) + \dot{Q}_{w}(t) + \dot{Q}_{pas}(t) \tag{26}$$

where $C_{cab}$ is the cabin thermal capacitance (including walls and seats). $\dot{Q}_{pas}$ is the heat flow rate produced by the passengers by sweat evaporation and respiration. The exact formula of $\dot{Q}_{pas}$ is given by the thermo-physiological model, presented in the next chapter.

The heat flow rate $\dot{Q}_{flow}$ ,due to the air blown by the ventilation system, is quantified using the enthalpy difference between the ventilation outlet air $h_{out}$ and the cabin air $h_{cab}$. Both enthalpies are functions of the air temperature and the relative humidity, and can be computed through tabulated data of air thermodynamic properties. The heat flow rate $\dot{Q}_{flow}$ is expressed by (27) :

$$\dot{Q}_{flow} = \dot{m}_{air} \times \left(\hat{h}_{air}(T_{out}, RH_{out}) - \hat{h}_{air}(T_{cab}, RH_{cab})\right) \tag{27}$$

where $T_{out}$ and $RH_{out}$ are the air temperature and the relative humidity at the ventilation system outlet. These quantities are computed by the air conditioning and heating system model, which us presented in the following sections. The term $\dot{m}_{air}$ refer to the mass flow rate of the air.

$\dot{Q}_{w}$ represents the heat flow rate exchanged with the cabin walls windows and windshield , with a constant heat transfer coefficient $h_{c,w}$. We assume that the heat transfer is done only by convection. The term $\dot{Q}_{w}$ is expressed by (28):

$$\dot{Q}_{w} = h_{c,w} \times (T_{w} - T_{cab}) \tag{28}$$

$\dot{Q}_{ext}$ is the convective heat follow rate exchanged with the outside through vehicle body leakages. The heat transfer coefficient $h_{c,ext}$ is a logarithmic function of the vehicle's speed $v_{veh}$. The heat flow rate $\dot{Q}_{ext}$ is expressed by (29):

$$\dot{Q}_{ext} = h_{c,ext}(v_{veh}) \times (T_{ext} - T_{cab}) \tag{29}$$

The cabin wall, windows and windshield temperature $T_{w}$ evolves according to equation (30), where $C_{wall}$ is the cabin wall heat capacity and $\dot{Q}_{sun}$ is the solar radiation load. The heat flow rate $\dot{Q}_{sun}$ is the product of the solar irradiance $\dot{q}_{sun}$ and the overall surface of the vehicle.

$$C_{w}\frac{dT_{w}}{dt}(t) = \dot{Q}_{sun}(t) - \dot{Q}_{w}(t) \tag{30}$$

The water vapor mass evolves according to the mass balance equation (31), where $\dot{m}_{sw}$ denote the sweat mass flow rate produced by the passenger. This quantity is computed by the thermo-physiological model, which will be presented in the next chapter.

$$\frac{dm_{H_2O}}{dt} = \dot{m}_{air} \times \left[\hat{\phi}_{air}(T_{out}, RH_{out}) - \hat{\phi}_{air}(T_{cab}, RH_{cab})\right] + \dot{m}_{sw} \tag{31}$$

If we assume that the cabin air is an ideal gas, one can express the moist air mass as a function of its temperature $T_{cab}$ according to (32), where $M_{air}$ represents the molar mass of the air, $P_{air}$ its pressure, $V_{cab}$ the volume of the vehicle cabin and $R$ the ideal gaz constant.

$$m_{air} = \frac{M_{air} \times P_{air} \times V_{cab}}{R \times T_{cab}} \tag{32}$$

Moreover, resolving the mass balance lead to determine the mass of water vapor $m_{H_2O}$, and hence by using (23) and (32) one can compute the specific humidity of the cabin air $\phi_{cab}$. The relative humidity is then deduced by (33):

$$RH_{cab} = \widehat{RH}_{air}(T_{cab}, \phi_{cab}) \tag{33}$$

### *3.4. AC system model*

Let us now focus on the cooling system (or AC sytem), sketched in Figure 12. The cold loop is composed of four main entities: compressor (a), condenser (b), expansion valve (c) and evaporator (d). A refrigerant fluid circulates throughout these entities and undergoes a thermodynamic cycle during which it receives thermal energy from the ventilated air and yields it outside.

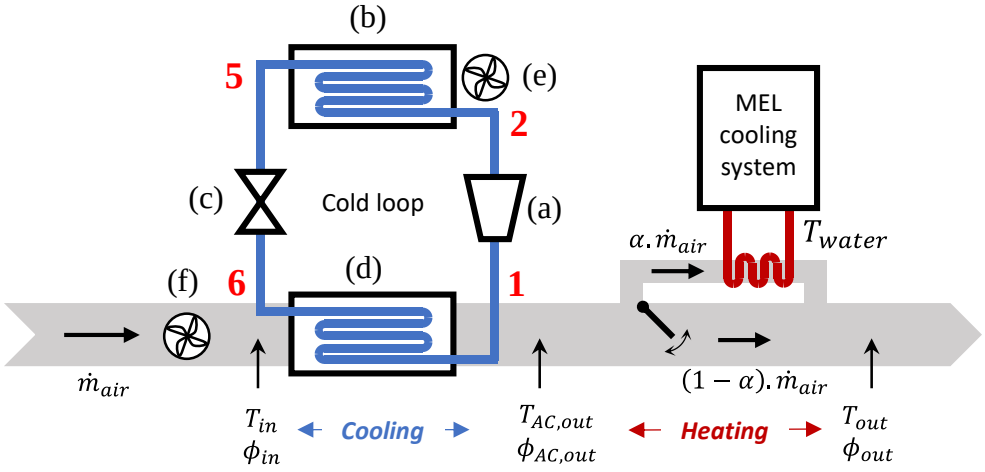


Figure 12. Schematic diagram of the air cooling and heating system: (a) compressor - (b) condenser – (c) expansion valve – (d) evaporator - (e) moto-ventilator group (MVG) – (f) ventilation fan. The points 1, 2, 5 & 6 correspond to different thermodynamic states of the refrigerant explained in Figure 13

The first stage of the thermodynamic cycle is the compression, throughout which the compressor brings the refrigerant from a low pressure, gaseous state to a higher pressure and temperature state (transformation 1 → 2). Then, during the condensation stage, the fluid releases the heat to the outside air, while turning into a high pressure saturated liquid state (transformation 2 → 5). The moto-ventilator group forces the circulation of the outside air in order to help evacuating heat from the refrigerant. Next, the saturated liquid undergoes an isenthalpic expansion through the expansion valve: its pressure and temperature decrease and it turns into a cold two-phase fluid (transformation 5 → 6). Finally, during the evaporation phase, this two-phase fluid absorbs heat from the ventilation circuit air. It evaporates and exits the evaporator at low-pressure gas state (transformation 6 → 1).

During these transformations, the refrigerant can increase its enthalpy beyond the saturated gas limit or decrease it more than the saturated liquid limit. The temperature differences between these points and the saturation temperatures are known as superheating (transformation 7 → 1), desuperheating (transformation 2 → 3) and subcooling (transformation 4 → 5).

A crucial point to note is that the whole cold loop is controlled by the compressor rotational speed, denoted by $N_{comp}$.

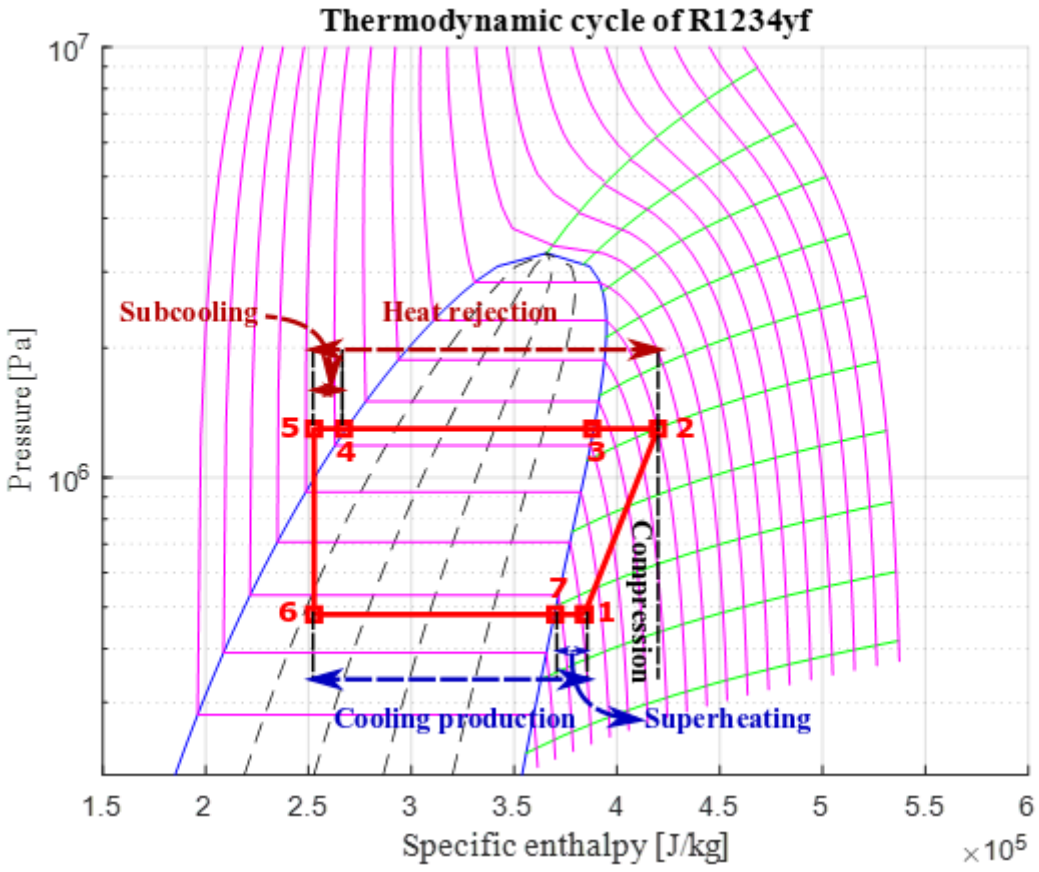


Figure 13. Refrigerating thermodynamic loop

### 3.4.1. Modelling approach

The cold loop model consists in evaluating at each time step, the refrigerant enthalpy at each point of the thermodynamic cycle (Figure 13), and then the heat exchanges with the air and the power consumed by the compressor. Practically, the model computes the refrigerant evaporating and condensing temperature $T_7$ (evaporator) and $T_4$ (condenser) by solving the heat balances (34) and (35). Then, it then deduces the refrigerant enthalpies for each point $i \in [\![1,7]\!]$. In equations (34) and (35), $\dot{Q}_{evap}$ and $\dot{Q}_{cond}$ are the heat exchange between the refrigerant and the air at the evaporator and condenser level. $C_{ref}$ is the heat capacity of the refrigerant (J/°K).

$$C_{ref}\frac{dT_7}{dt} = \dot{H}_6 - \dot{H}_1 + \dot{Q}_{evap} \tag{34}$$

$$C_{ref}\frac{dT_4}{dt} = \dot{H}_2 - \dot{H}_5 - \dot{Q}_{cond} \tag{35}$$

Where $\dot{H}_i$ is the enthalpy power, at a given point $i$ of the thermodynamic cycle depicted in Figure 9. It is defined by (36), where $h_i$ is the specific enthalpy (J/kg) at point $i$, calculated using the refrigerant temperature and pressure. If the refrigerant is in the two-phase region or in the saturated state, one thermodynamic property is sufficient to determine the enthalpy $h_i$. On the contrary, if the refrigerant is the gaseous or liquid state, two thermodynamic properties are necessary to compute $h$. In the present work, this computation is based on tabulated thermodynamic data defined in section 3.2.3. . The quantity $\dot{m}_{ref}$ is the mass flow rate of the refrigerant, controlled by the compressor rotational speed.

$$\dot{H}_i = \dot{m}_{ref} h_i \tag{36}$$

### 3.4.2. Compressor model

The compressor used in the AC model is a reciprocating compressor. A reciprocating compressor is, quite simply, a piston in a cylinder. It is, essentially, the opposite of the internal combustion engine. In an internal combustion engine, a petroleum-air vapor mixture is ignited to raise its temperature and pressure, which drives the piston downward causing the crankshaft to rotate. Thus, it is the expanding vapor that provides the power in the system. For reciprocating compressors, external power is used to drive the crankshaft, which pushes the piston upward in the cylinder, compressing the trapped refrigerant vapor. In this work, an electric motor is used to power the compressor. Figure 14 shows the compression cycle for a typical reciprocating compressor. The cycle begins with the piston at the top of the cylinder (step 1). The suction valve is on the left side while the discharge valve is on the right side in the cross-sections shown in Figure 14 The suction valve opens allowing the low pressure refrigerant vapor to flow into the cylinder. As the piston goes through its down stroke, the refrigerant vapor expands (step 2). Once the piston reaches its lowest point, the suction valve closes. The piston, which is connected to a motor driven crankshaft, is then driven upward. The trapped refrigerant vapor is then compressed as the piston goes through its upstroke. This volumetric reduction causes both the pressure and temperature of the refrigerant vapor to rise. Towards the end of the up stroke, the discharge valve is opened and most of the high pressure refrigerant escapes the cylinder (step 3). The volume of the cylinder at the completion of the upstroke is called the clearance volume. After the completion of the upstroke, there is some amount of high pressure refrigerant left in the cylinder. In order to allow the low pressure refrigerant in the suction valve to enter the cylinder and begin the next compression cycle, this high pressure refrigerant must be re-expanded until it is brought down to a low pressure (step 4).

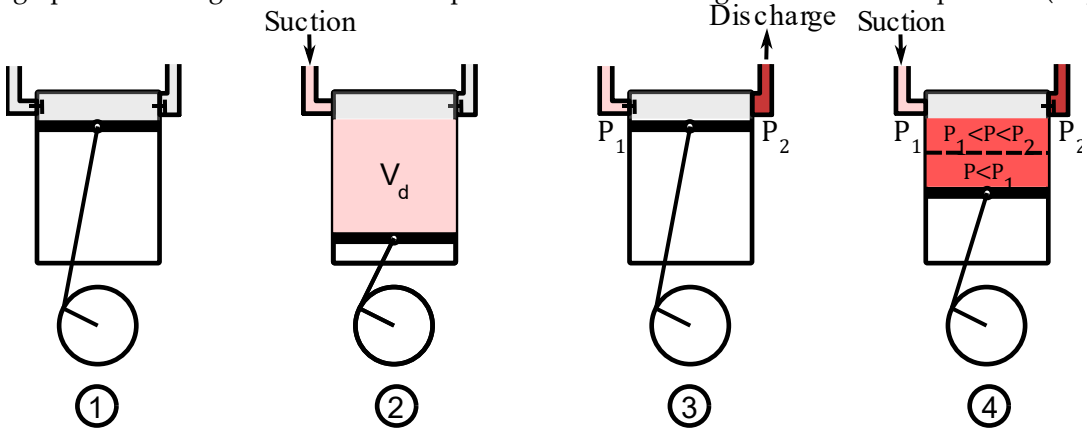


Figure 14. Compressor working principle

This re-expansion is a loss that limits the mass flow rate of the refrigerant $\dot{m}_{ref}$, and can be taken into account through the volumetric efficiency $\eta_{vol}$. The actual refrigerant mass flow rate is given by (37), $V_d$ refers to the refrigerant volume trapped in the cylinder per revolution (assumed to be constant) and $\rho_1$, its specific mass at the compressor inlet:

$$\dot{m}_{ref} = \rho_1 \frac{N_{comp}}{2\pi} . V_d . \eta_{vol} \tag{37}$$

The volumetric efficiency $\eta_{vol}$ is a function of the ratio of inlet and outlet pressure $P_1$ and $P_2$, the rotational speed $N_{comp}$, and the refrigerant trapped volume $V_d$. The coefficient $a$ and $b$ are assumed to be constant, and usually are given by the compressor designers. The coefficient $\gamma$ is called the adiabatic index [158], defined by the ratio of heat capacity at constant pressure $c_p$ and constant volume. $c_v$. The volumetric efficiency is given by (38):

$$\eta_{vol} = 1 - \frac{a\frac{N_{comp}}{2\pi} + b}{V_d}\left(\frac{P_2}{P_1}\right)^{\frac{1}{\gamma}} \tag{38}$$

The compressor raises the refrigerant enthalpy from $h_1$ to $h_2$ by applying a mechanical work $W_{comp}$ on the piston. This action compresses the inlet gas, which increases its pressure, and hence its enthalpy.

$$h_2 = h_1 + W_{comp} \tag{39}$$

The mechanical action applied to the refrigerant goes usually with irreversibilities, such as friction, turbulence and nonquasi-equilibrium compression. Those irreversibilities downgrade the compressor performance, and because of them, more work is required to compress the gas to a given pressure.

Such phenomenon, are taken into account when designing compressors by assigning an efficiency. If the compressor was ideal, it will be adiabatic, which means that no heat is exchanged with the exterior. Moreover, the refrigerant undergoes no irreverssibilities. In thermodynamics, this type of transformation is called isentropic transformation. In such process, the refrigerant entropy remains constant. Hence, the compressor efficiency is the ratio between the real actual work and the isentropic one $W_{is}$. The isentropic efficiency is given by (40):

$$\eta_{is} = \frac{W_{is}}{W_{comp}} \tag{40}$$

The isentropic work $W_{is}$ is defined by the refrigerant enthalpy difference at point 1 and 2, subjected to a constant entropy. Since the refrigerant enters the compressors with a pressure $P_1$ and an entropy $s_1$, it should exit with a pressure $P_2$ and the same entropy. The isentropic work can be then expressed as follows (41):

$$W_{is} = h_{2,is} - h_1 \tag{41}$$

where $h_1$ is the enthalpy of the refrigerant at the pressure $P_1$ and temperature $T_1$, and given by (42). From there, the entropy $s_1$ can be deduced by (43) thanks to refrigerant thermodynamic data.

$$h_1 = \hat{h}_{ref}(P_1, T_1) \tag{42}$$

$$s_1 = \hat{s}_{ref}(P_1, T_1) \tag{43}$$

The isentropic compression transformation raises the refrigerant pressure to $P_2$, but conserves its inlet entropy $s_1$. Therefore the isentropic enthalpy $h_{2,is}$ at outlet of the compressor is given by (44):

$$h_{2,is} = \hat{h}_{ref}(P_2, s_1) \tag{44}$$

By combining (39), (40) and (41), one can express the actual outlet enthalpy $h_2$ as a function of $h_1$, $h_{2,is}$ and the isentropic efficiency $\eta_{is}$. Usually, this efficiency is derived experimentally. In the present model, $\eta_{is}$ is given by an affine function (46) and depends on the refrigerant mass flow $\dot{m}_{ref}$, its inlet temperature $T_1$ and compressor rotational speed $N_{comp}$. The coefficient $a$,$b$, $c$ and $d$ are constant.

$$h_2 = h_1 + \frac{h_{2,is} - h_1}{\eta_{is}} \tag{45}$$

$$\eta_{is} = a\dot{m}_{ref} + bT_1 + cN_{comp} + d \tag{46}$$

The enthalpy flows $\dot{H}_1$ and $\dot{H}_2$ at the inlet and outlet of the compressor, can be finally deduced by (48) and (47):

$$\dot{H}_2 = \dot{m}_{ref} h_2 \tag{47}$$

$$\dot{H}_1 = \dot{m}_{ref} h_1 \tag{48}$$

### 3.4.3. Valve model

A thermal expansion valve is basically a small orifice, which throttles the flow of liquid refrigerant, being pumped from the condenser to the evaporator. The refrigerant experiences a rapid expansion through the valve, which brings it consequently to a low pressure continuous liquid-vapor stream state. Another purpose of the thermal expansion valves is to control the superheating at the outlet of the evaporator, in order to keep a good performance of the refrigerating cycle. In the mathematical model, this control function is not considered. However, we assume that the superheating is constant.

At the inlet of the expansion valve, the refrigerant is in liquid state, with a temperature $T_5$. The relationship (49) allows to determine the enthalpy of the refrigerant as a function of its temperature $T_5$ and the high pressure $P_4$. From there, the enthalpy flow can be calculated by (50)

$$h_5 = \hat{h}_{ref}(T_5, P_4) \tag{49}$$

$$\dot{H}_5 = \dot{m}_{ref} h_5 \tag{50}$$

The model of the expansion valve neglects heat losses, i.e., constant enthalpy is assumed throughout the expansion valve.

$$\dot{H}_6 = \dot{H}_5 \tag{51}$$

### 3.4.4. Evaporator model

As the working principle of heat exchanger is described in section 3.2.4. , we will directly present the governing equations of the evaporator.

The evaporator model is based on NTU method described in section 3.2.4. . The objective of this method, is to model the heat flow between the air and the refrigerant as a function of the maximal heat flow between the two fluids, and an efficiency factor. The maximal heat flow can be calculated in two different ways. As depicted in Figure 10, the maximal heat flow occurs at the inlet of the evaporator when the temperature difference is maximal. Also, it can be considered as an ideal hypothetical flow, where the outlet air is in perfect thermodynamic equilibrium with the refrigerant. That means, that the air temperature at the evaporator outlet is equal to $T_7$. Hence, for a dry air, the maximal heat flow $\dot{Q}_{e,d,max}$ is expressed by (52). For a humid air, one must take into account its relative humidity. In this situation, the maximal heat flow $\dot{Q}_{e,h,max}$ is given by (53).

$$\dot{Q}_{e,d,max} = \dot{m}_{air} C_{p,air} (T_{in} - T_7) \tag{52}$$

$$\dot{Q}_{e,h,max} = \dot{m}_{air} \left( \hat{h}_{air}(T_{in}, HR_{in}) - \hat{h}_{air}(T_7, 100\%) \right) \tag{53}$$

The actual heat flow is given by (54), where $\eta_{e,d}$ is the efficiency of the evaporator when the air is dry. The term $\eta_{e,d}$ is given by (55):

$$\dot{Q}_{e,d} = \dot{Q}_{e,d,max} \eta_{e,d} \tag{54}$$

$$\eta_{e,d} = 1 - \exp\left(-NTU_{e,d}\right) \tag{55}$$

where $NTU_{e,d}$ is a dimensionless quantity, equal to the ratio of the overall heat transfer coefficient $UA$ by the smallest heat capacity of the two fluids. During heat exchange, the refrigerant is in the transition phase, which means that its heat capacity tends to infinity. Hence, the air has the smallest heat capacity:

$$NTU_{e,d} = \frac{UA}{\dot{m}_{air} C_{p,air}} \tag{56}$$

It is worth noting that the overall heat transfer coefficient $UA$ depends on $\dot{m}_{air}$ and $\dot{m}_{ref}$

In the same manner, the actual heat flow when the air is humid, is given by the set of equations (57) to (59).

$$\dot{Q}_{e,w} = \dot{Q}_{e,w,max} \eta_{e,w} \tag{57}$$

$$\eta_{e,w} = 1 - \exp\left(-NTU_{e,w}\right) \tag{58}$$

$$NTU_{e,w} = \frac{UA}{\dot{m}_{air} C_{p,\mathrm{w},air}} \tag{59}$$

In this humidity conditions, the specific heat capacity $C_{p,\mathrm{w},air}$ depends on the thermodynamic properties of the air, and it is given by (60).

$$C_{p,\mathrm{w},air} = \frac{\hat{h}_{air}\left(\hat{T}_{wet,air}(T_{in}, RH_{in}), 1\right) - \hat{h}_{air}(T_7, 1)}{\hat{T}_{wet,air}(T_{in}, RH_{in}) - T_7} \tag{60}$$

Finally, the actual heat flow is given by taking the maximum between $\dot{Q}_{e,d}$ and $\dot{Q}_{e,w}$.

$$\dot{Q}_e = \max\left(\dot{Q}_{e,d}, \dot{Q}_{e,w}\right) \tag{61}$$

Computing the actual heat flow $\dot{Q}_e$ at the evaporator allows next to determine the temperature and the pressure of the refrigerant fluid, and more importantly, the thermodynamic properties of the outlet air. By combining (48),(51) and (61) one can resolve the heat balance equation (34), and calculate the saturation temperature of the refrigerant. Since it is in thermodynamic equilibrium, its pressure depends only on $T_7$.

$$P_7 = \hat{P}_{ref}(T_7) \tag{62}$$

For simplicity sakes, we assume that the refrigerant pressure at the outlet of the evaporator is equal to its saturated pressure:

$$P_1 = P_7 \tag{63}$$

The saturation of the refrigerant occurs usually before it exists the evaporator. That means that it continues to exchange heat flow with air, which causes an increase of its temperature, and a complete transition to superheated gas phase. The temperature difference is called the superheat $T_{sh}$, and it is usually controlled by the expansion valve.

$$T_1 = T_7 + T_{sh} \tag{64}$$

The existence of superheat is important in a refrigerating cycle, as it ensures that no liquid enters the compressor chamber.

The actual heat flow $\dot{Q}_e$ exchanged at the evaporator serves also to evaluate the thermodynamic properties of the outlet air. Its enthalpy $h_{AC}$ is governed by the heat balance (65) where $h_{in}$ is the enthalpy of the inlet air. This quantity depends on the inlet temperature $T_{in}$ and relative humidity $RH_{in}$ according to (66)

$$m\frac{dh_{AC}}{dt} = \dot{m}_{air}h_{in} - \dot{Q}_e - \dot{m}_{air}h_{AC} \tag{65}$$

$$h_{in} = \hat{h}_{air}(T_{in}, RH_{in}) \tag{66}$$

The process of air cooling can provoke water vapor condensation. In this case, the air is in saturated state, which means that its temperature and specific humidity are functions of only one thermodynamic property. These quantities are calculated by (67) and (68).

$$T_{AC,2} = \hat{T}_{air}(h_{AC}) \tag{67}$$

$$\phi_{AC,2} = \hat{\phi}_{air}(T_{AC,2}) \tag{68}$$

If the air cooling does not produce a water vapor phase transition, the specific humidity is constant, since the mass of water vapor does not change. Hence, the specific humidity at the outlet is a function of $T_{in}$ and $RH_{in}$, and it is given by (69). From there on can compute the air temperature at the outlet by (70).

$$\phi_{AC,1} = \hat{\phi}_{air}(T_{in}, RH_{in}) \tag{69}$$

$$T_{AC,1} = \hat{T}_{air}\left(h_{AC}, \phi_{AC,1}\right) \tag{70}$$

Both $\phi_{AC,1}$ and $T_{AC,1}$ represent the limits of temperature and humidity reachable by the air. On one side, the air cannot be cooled beyond $T_{AC,1}$, which means that $T_{AC,1}$ is the inferior limit of air temperature. On the other side, the air cannot store a mass of water vapor greater than $\phi_{AC,1}$. Hence, $\phi_{AC,1}$ is the upper limit of the outlet specific humidity :

$$T_{AC} = \max\left(T_{AC,1}, T_{AC,2}\right) \tag{71}$$

$$\phi_{AC} = \min\left(\phi_{AC,1}, \phi_{AC,2}\right) \tag{72}$$

Consequently, the relative humidity is given by (73):

$$RH_{AC} = \widehat{RH}_{air}(T_{AC}, \phi_{AC}) \tag{73}$$

### 3.4.5. Condenser

As the working principle of heat exchanger is described in section 3.2.4. , we will focus only on the governing equations of the condenser.

The condenser is modeled by using the same NTU method used to express the actual heat flow in the evaporator. The maximal heat flow in the condenser, given by (74), is a function of temperature difference between the outside air and the refrigerant at the inlet of the heat exchanger:

$$\dot{Q}_{c,max} = \dot{m}_{GMV}C_p(T_4 - T_{ext}) \tag{74}$$

The actual heat flow is deduced by multiplying $\dot{Q}_{c,max}$ by the condenser efficiency $\eta_c$ :

$$\dot{Q}_c = \dot{Q}_{c,max}\eta_c \tag{75}$$

As seen in the evaporator model, the efficiency is a function of the number of transfer unit NTU, which depends on the overall heat transfer coefficient $UA_c$, and the smallest heat capacity between the two fluids. It is worth noting that $UA_c$ depends on the air and the refrigerant mass flow. Hence, the efficiency $\eta_c$ of the condenser is given by (76-77)

$$\eta_c = 1 - \exp(-NTU_c) \tag{76}$$

$$NTU_c = \frac{UA_c}{\dot{m}_{GMV} C_{p,air}} \tag{77}$$

Computing the actual heat flow at the condenser allows next to determine the temperature and pressure of the refrigerant fluid. By combining (47),(50) and (75) one can resolve the heat balance equation (35), and calculate the saturation temperature of the refrigerant. Since it is in thermodynamic equilibrium, its pressure depends only on $T_4$.

$$P_4 = \hat{P}_{ref}(T_4) \tag{78}$$

For simplicity, we assume that the refrigerant pressure at the outlet and inlet of the condenser is equal to its saturated pressure:

$$P_2 = P_5 = P_4 \tag{79}$$

The saturation of the refrigerant usually occurs before it exits the condenser. It continues to evacuate heat to outside air until reaching the point 5 in the refrigeration cycle. From there, the refrigerant is totally liquid and can enter the expansion valve without causing damages. The temperature difference is called the subcooling, and allows to determine the refrigerant temperature at the exit of the condenser by (80):

$$T_5 = T_4 - T_{sc} \tag{80}$$

### *3.5. Heating*

When exiting the cooling system, the air is very dry and cold: only a few degrees Celsius. Hence, it needs to be warmed up before being blown into the cabin. The heating system consists of two heating resistors and an exchanger with the water cooling system of the electric machine. For the weather conditions, considered in the present thesis, the heating resistors are not needed and free heating is provided by the water cooling system of the electric machine.

Again, an important point to note is that the heating is controlled by the ratio of the air flow derived into the heat exchanger, denoted by $\alpha$.

The water cooling system is modeled as a heat exchanger, where the concerned fluids are the heating water and the cooled air. Again, the NTU method is used to evaluate the actual heat exchange $P_H$. The maximal heat flow is then the product of the temperature difference $T_{AC}$ and $T_{w,EM}$ at the inlet, and the smallest heat capacity of the two fluids $C_{H,min}$. The water temperature is assumed to be constant.

$$P_{H,max} = C_{H,min}(T_{w,EM} - T_{AC}) \tag{81}$$

Unlike the evaporator or the condenser, the working fluid (here is the water) does not undergoes a phase transition. Hence, its heat capacity $C_{p,water}$ is finite, and one must compute at each time step the smallest heat capacity by (82):

$$C_{H,min} = \min\left(\dot{m}_{w,EM} C_{p,\mathrm{w,EM}}, \dot{m}_H C_{p,air}\right) \tag{82}$$

Where $\dot{m}_{w,EM}$ is the water mass flow, assumed to be constant, $C_{p,w,EM}$ represents the heat capacity of the water expressed as a function of $T_{AC}$, the water temeprature $T_{w,EM}$. The term $\dot{m}_H$ refers to the fraction of air mass flow to be heated.

$$\dot{m}_H = \dot{m}_{air}\alpha \tag{83}$$

The actual heat flow is the product of $P_{H,max}$ and the efficiency $\eta_H$, given by (84):

$$P_H = C_{H,min}(T_{w,EM} - T_{AC})\eta_H \tag{84}$$

The mathematical expression of the efficiency in this heat exchangers differ from those used in the evaporator and the condenser. It is given by (85). The reason is that the working fluid does not undergo a phase transition. For more information in heat exchangers types and architectures and their respective efficiencies, we refer the reader to the following reference [159].

$$\eta_H = 1 - \exp\left(\frac{\exp\left(-{NTU_H}^{0.78}R_H\right) - 1}{R_H \times {NTU_H}^{-0.22}}\right) \tag{85}$$

where NTU is the number of transfer units expressed as the ratio of overall heat transfer coefficient $UA_H$ and the smallest heat capacity $C_{H,min}$. It's worth noting that $UA_H$depends on the mass flow of the water $\dot{m}_{EM}$, the water temperature $T_{w,EM}$, and the air mass flow $\dot{m}_H$.

$$NTU_H = \frac{UA_H}{C_{H,min}} \tag{86}$$

The term $R_H$ is the ratio between $C_{H,min}$ defined in (82) and $C_{H,max}$ which is the biggest heat capacity of the two fluids.

$$R_H = \frac{C_{H,min}}{C_{H,max}} \tag{87}$$

$$C_{H,max} = \max\left(\dot{m}_{w,EM}C_{p,\mathrm{w,EM}}, \dot{m}_H C_{p,air}\right) \tag{88}$$

The actual heat flow $P_H$ allows to evaluate the thermodynamic properties of the heated air. Its temperature $T_H$ at the outlet of the heating system, is governed by the heat balance (89)

$$C_p\frac{dT_H}{dt} = \dot{m}_H C_{p,air}T_{AC} + P_H - \dot{m}_H C_{p,air}T_H \tag{89}$$

Since the cooled air is mixed with the heated one, the temperature of the air at outlet of the HVAC system $T_{out}$, is weighted using to the ratio $\alpha$.The heated air passes through the ventilation duct before it is blown into the cabin

$$T_{out} = (1 - \alpha) \times T_{AC} + \alpha \times T_H \tag{90}$$

At this stage, we assume that specific humidity remains constant. That means, no water vapor evaporation occurs during the heating. Hence, one can deduce by (90-92), the relative humidity $RH_{out}$ as a function of $T_{out}$ and $\phi_{out}$, as follows:

$$\phi_{out} = \phi_{AC} \tag{91}$$

$$RH_{out} = \widehat{RH}_{air}(T_{out}, \phi_{out}) \tag{92}$$

### *3.6. Ventilation*

The ventilation system is mainly composed from ducts, fans and mixing valves at inlet of AC and the heating system. Besides duct and the recycling valve, the other component of ventilation were introduced in the previous sections. Both fans were characterized by the air mass flow $\dot{m}_{air}$ and $\dot{m}_H$. The second valve was represented by the mixing ratio $\alpha$ between the cooled and the heated air.

Now, the duct is usually modeled by a pressure and temperature drop, which are neglected in the present work. The first valve, at the inlet of AC system, can be represented by a mixing ratio between the outside and the recirculated air. Hence, after mixing, the temperature $T_{in}$ and the specific humidity $\phi_{in}$ of the air are given by (93) and (94).

$$T_{in} = \beta . T_{cab} + (1 - \beta) . T_{ext} \tag{93}$$

$$\phi_{in} = \beta . \phi_{cab} + (1 - \beta) . \phi_{ext} \tag{94}$$

### *3.7. HVAC consumption*

In the HVAC system, three components need power feeding: the compressor (a), the fan (e), and the moto-ventilator group MVG (f). The compressor consumption $P_{elec,comp}$ is given by (95), where $h_1$ and $h_2$ denote the refrigerant enthalpy at the points 1 and 2 of the thermodynamic cycle represented in Figure 13, $\dot{m}_{ref}$ is the refrigerant mass flow rate (linked to the compressor rotational speed), $\eta_{meca}$ and $\eta_{elec}$ are the mechanical and electrical efficiencies of the compressor.

$$P_{elec,comp} = \frac{(h_2 - h_1) . \dot{m}_{ref}}{\eta_{méca} \eta_{elec}} \tag{95}$$

The consumptions of the fan and the MVG depend on the external temperature according to tabulated data provided by Groupe PSA. The total electric consumption of the HVAC system $P_{HVAC}$ is the sum of the electric power consumed by the compressor, the fan and the MVG (96).

$$P_{HVAC} = P_{elec,comp} + P_{fan} + P_{MVG} \tag{96}$$

## 4. Battery pack model

The battery pack is composed from a high voltage battery, a 12-volts battery, and a DCDC converter. The first battery constitutes the main energy source of the electric vehicle, while the second one supplies energy for accessories such as lights and radio. The DCDC converter transfer the electrical power from the high voltage battery to the 12V battery.

### *4.1. HV battery*

In the present work, the main energy source is a Li-ion battery composed from 192 cells. The battery is characterized by high nominal electromotive force of 350 V.

All proposed battery models used in BEVs can be categorized into three categories: electrochemical experimental and electrical circuit models (ECM). The first category is based on solving coupled differential equations by control volume methods. Despites their accuracy, those models requires high computational resources, which makes them not suitable for management or control purposes. The second category, are based on experimental data. Usually, they are specific to a particular type of battery and operating conditions. The third category represents the battery as an electrical circuit that combines basic elements, such as voltage sources, resistors, and capacitors. Different combinations of these

elements give birth to different ECM models. The more straight-forward and conventional one represents the battery as an ideal source of voltage connected in series with a resistance. More complex and accurate representation can be developed by using Thevenin equivalent circuit model [160].

The main use of a battery model, at least in the present work, is to monitor the state of the charge (SOC). For this purpose, we choose to use the most basic ECM since it provides good results in most energy management studies [70, 132]. The model represents the battery as an ideal voltage source connected in series with an internal resistance. Those elements are characterized respectively by an equivalent open circuit voltage $E_{b,HV}$ and an equivalent resistance $R_{b,HV}$. The term equivalent is used because the battery is composed from $N_p$ parallel circuits of $N_s$ cells in series.

We assume that all cells are similar, and their resistance $R_{c,HV}$ and open circuit voltage $E_{c,HV}$ are only function of the state of charge of the battery $SOC_{b,HV}$. Actually, those quantities also depend on temperature, especially when dealing with hot weather conditions. This dependence is not taken into account in this thesis, but will be considered in future works.

$$R_{b,HV} = R_{c,HV}\left(SOC_{b,HV}\right) \times \frac{N_s}{N_p} \tag{97}$$

$$E_{b,HV} = E_{c,HV}\left(SOC_{b,HV}\right) \times N_s \tag{98}$$

According to the kirchhoff's voltage law, the terminal voltage $U_{b,HV}$ is given by (99):

$$U_{b,HV} = E_{b,HV} - R_{b,HV} I_{b,HV} \tag{99}$$

where $I_{b,HV}$ is the load current. This quantity takes a positive value when the battery is discharging and negative one when it is charging.

As explained before, the three consumers or loads in an electric vehicle are the electrical machine, the HVAC system and low voltage auxiliaries. Each one of them requires an electrical power to ensure their functions, such as tracking the speed cycle or meeting the comfort requirement. The total consumed power $P_{b,HV}$ is therefore given by (100):

$$P_{b,HV} = P_{EM} + P_{HVAC} + P_{DCDC,in} \tag{100}$$

After simple algebraic rearrangement, one can deduce the formula of the current $I_{b,HV}$ through the total load :

$$I_{b,HV} = \frac{U_{b,HV} - \sqrt{{U_{b,HV}}^2 - 4R_{b,HV}P_{b,HV}}}{2R_{b,HV}} \tag{101}$$

The battery state of charge is the accumulated current that flows in or out the battery during the charge or discharge process. It is given by (102), where $Q_{b,HV}$ is the nominal capacity of the high voltage battery

$$\frac{dSOC_{b,HV}}{dt} = \frac{I_{b,HV}}{Q_{b,HV}} \tag{102}$$

### *4.2. DCDC and LV battery*

The 12-volt battery supplies the electrical power for the vehicle's accessories, such as the radio, lights, wipers, steering pump… etc. Since the 12 V battery is powered by the high voltage battery, a converter is required to reduce the voltage and transfer the power. Usually, DCDC converters are used

to perform this task. These devices convert the direct current (DC) from one voltage level to another, by storing the input energy temporarily and then releasing that energy to the output at a different voltage. The storage may be in either magnetic field storage components (inductors, transformers) or electric field storage components (capacitors) [xx]. DCDC converters can be designed to transfer power in only one direction, from the input to the output, or in both directions.

The model of DCDC converter and the 12 volt battery is straightforward. Some assumptions are considered: (1) the output of the DCDC converter voltage $U_{DCDC,out}$ is equal to the voltage of 12-volt battery $U_{b,LV}$, (2) the current at the output of DCDC $I_{DCDC,out}$ is equal to the current flowing in the above mentioned accessories $I_{aux}$, (3) the power consumed by the accessories is constant and equal to 100W. With these assumptions, one can conclude that the output power of the DCDC converter is equal 100W.

$$P_{DCDC,out} = P_{aux} = 100W \tag{103}$$

The losses in a DCDC converter are the losses produced by the semiconductors switches (transistors and diodes) and the passive components (capacitors and inductors). These power losses are modeled by a constant efficiency $\eta_{DCDC}$. Therefore, the power at the input of DCDC $P_{DCDC,in}$ converter is given by (104):

$$P_{DCDC,in} = \frac{P_{DCDC,out}}{\eta_{DCDC}} \tag{104}$$

# 5. State and control variables

The energy management strategy studied in this thesis, aims to control the HVAC system in order to offer the best possible comfort within a finite available energy. Three types of variables has to be defined before formalizing the optimal control problem:

(i) State variables: or the controlled variables, are usually the quantities that evolves according to the system's differential equations

(ii) Control variables: are the system's input that can be controlled dynamically to keep the controlled variables at their set point value.

(iii) Disturbances variables : are the system's input that cannot be controlled. They usually cause the controlled variables to deviate from their set point value.

The overall system { Battery + HVAC + cabin } presents a considerable amount of differential equations. Since we are only interested in thermal comfort and energy consumption, we will choose the quantities that affect them directly. The air cabin temperature and specific humidity are characteristics of the ambiance, together with the wall temperature. They usually figure among the set of quantities that influence thermal comfort, as it will be seen in the next chapter. In the meantime, the HVAC energy consumption can be monitored through the state of charge of the battery SOC. Therefore, we will define the state variable's vector by $x = [SOC, T_{cab}, \phi_{cab}, T_{wall}]'$.

As stated in this chapter, the HVAC system has three actuators: the compressor, the air blower, the recycling valve and the heater. Each one of these component is controlled respectively by : the rotational speed, the air mass flow, the recycling ratio and the heating ratio. Hence, the control variable's vector is defined by $u = [N_{comp}, \dot{m}_{air}, \alpha, \beta]$.

The outside weather and the vehicle speed constitute finally the disturbance vector $w = [T_{ext}, \phi_{ext}, \dot{q}_{sun}, v_{veh}]'$. The three first quantities cannot be controlled by essence. Since the autonomous driving is not in the scope of this thesis, we assume that the vehicle speed is likewise not intended to be controlled.

# 6. Conclusions

In this chapter, we presented the powertrain and the HVAC system model of an electric vehicle. The model was provided by Groupe PSA for the sake of this thesis. Firstly, we presented the powertrain model approach, that consist on tracking the desired speed profile by two PID controllers. One can calculate the required wheel and braking torques , and then deduce the consumed power through the transmission and electric motor model. Secondly, we presented the cabin and HVAC system model. Before we jumped into the governing equations, we judged necessary to remind the definitions of some thermodynamic concept, and introduce some known modelling approaches of heat exchangers. The cabin consisted on three differential equation of air temperature, air specific humidity and wall temperature. The HVAC system model was more complex, since it held three components: the air conditioning (AC), the heating and the ventilation system. The HVAC model focused mainly on the AC system, since it performs the air cooling operations, and represent the biggest consumer. The AC model is based on solving heat balance equations of the refrigerant, evaluate the heat exchange between the refrigerant and the inlet air and the associated electrical consumption. Finally, the battery was modeled in a very classical way together with DCDC converter. The last section of this chapter gave a synthesis of the state, control and disturbance variables, which important for formalizing the energy management problem.

The next chapter will focus on thermo-physiological model of the human body, and the equivalent temperature as a thermal comfort index. Both models are important to evaluate the heat exchanges between the body and the ambiance, and to assess correctly the thermal comfort in a vehicular cabin

# Chapter III : thermo-physiological and thermal comfort model

*Quels que soient les jeux de mots et les acrobaties de la logique,*
*comprendre c'est avant tout unifier. [...]*
*Comprendre le monde pour un homme, c'est le réduire à l'humain,*
*le marquer de son sceau. [...]*
*Cette nostalgie d'unité, cet appétit d'absolu illustre*
*le mouvement essentiel du drame humain.*
Albert Camus, Le mythe de Sisyphe

## Contents

The thermal comfort management strategy needs, in addition to vehicle model, to assess correctly thermal comfort. In the previous chapter, the quantities that affect thermal comfort were monitored and controlled through a dynamic model of the vehicle cabin and the HVAC system. Based on these quantities, one can build a thermal comfort criterion, to formalize the optimization problem. As a reminder, our objective is to develop an energy management system that ensure to the driver to arrive to its destination, while having the best thermal comfort, within the available energy for HVAC. The first step to solve the problem, was to develop a model for the vehicle cabin, powertrain and HVAC system in order to account for energy consumption, and evaluate thermal quantities of the cabin. The second step will consist on evaluating the effect of these quantities on driver's/passenger's bodies, through a thermo-physiological model, then assessing the associated thermal comfort via a suitable index for vehicular applications. Various models of thermal comfort indices are available in the literature, from simple ones based on environmental physical quantities, to more representative ones which include the behaviour of the human thermal system.

Mathematical modelling of the human thermal system goes back 60 years. In the past three decades several multi-segmental models of human thermoregulation have been developed and have been valuable tools for contributing to a deeper understanding of regulatory processes. In this work, an enhanced Tanabe model will be presented. The choice was motivated by the moderate complexity of the model, and its ability to handle thermal comfort indices, that are suitable for vehicular environment. Besides the utility to predict human thermal response, a multi-segmental model of human thermoregulation like Tanabe model is also a valuable tool to include physiological mechanisms involved in the thermal comfort. Most of thermal comfort indices are based on environmental physical quantities, or on steady state heat balance with the surroundings. Mechanisms like sweating are neglected, which may alter thermal comfort evaluation. Furthermore, thermo-physiological model allows also to assess local (dis)comfort in arbitrary conditions.

The aim of this chapter is to present firstly a thermo-physiological model that predicts human thermal behavior, then a thermal comfort model. The objectives are as follows.

- In section I: To introduce general concept on human thermo-physiology, and thermal comfort
- In section II: To present the Tanabe model of the passive system including:(i) modelling the heat transfer in living tissues; and (ii) modelling the environmental heat exchange, i.e. surface convection, long wave radiation, skin evaporation, and respiration;
- In section III: To present the human thermoregulatory system (active system) developed by Tanabe including: (i) modelling individual thermoregulatory responses using the appropriate afferent signals; ie. to develop control equations for sweating, shivering, and cutaneous vasomotion (ie. constriction and dilatation)
- In section IV: To present three comfort models

# 1. Concepts of thermoregulation and thermal comfort

## *1.1. Homeothermy, thermoreceptors and thermoregulation*

Human beings are homeothermic organisms, able to regulate their internal temperature so that it remains constant over a wide range of environmental conditions. Homeothermy is defined as the ability of body to keep its core temperature constant against heat loss to the environment by internal heat production and by means of appropriate counter measures taken by the thermoregulatory system. Temperature regulation is made possible by specific central and peripheral nervous structures that continuously detect the organism's thermal state.

Human beings can perceive different levels of cold and warmth (including pain) through two types of sensory organs : cold and warmth receptors. These organs are better known as thermoreceptors, and are defined as the endings of nerve fibers. Thermoreceptors are located mainly in the skin and in the hypothalamus, but are also found in places such as the spinal cord, abdominal viscera, and in or around the great veins in the upper abdomen and thorax.

Cutaneous thermoreceptors play a major role in the perception of thermal comfort. Indeed, the relative degree of stimulation of the nerve endings determine the level of thermal sensation. This thermal sensation can be different from one region to another, since both thermoreceptors are distributed in a non-homogenous way over the skin surface. When a thermoreceptor is subjected to an abrupt change in temperature, it is strongly stimulated at first, sending impulses at a high frequency. But this stimulation fades rapidly during the first minute following the temperature change, and then progressively more slowly until it reaches a steady level. A person feels much colder or warmer when the temperature of the skin is actively falling or rising than when the temperature remains at the same level. This explains the stronger sensation of coolth or warmth felt upon entering a cold pool or a hot tub.

Cutaneous thermoreceptors are located beneath the skin surface, about 0.2 mm for cold, and 0.5 mm for warmth thermoreceptors. Also, the number of cold thermoreceptors far exceeds the number of warmth receptors. In general, there are about ten times more cold receptors than warmth receptors in skin. This preponderance of cold spots, and their shallower depth relative to the skin surface, suggest that humans are more sensitive to danger from cold than from heat.

Cutaneous thermoreceptors contribute significantly in the process of thermoregulation. They produce both positive and negative afferent signals into the human central thermal integrator, i.e; the posterior hypothalamus . The latter produces thermoregulatory signals: sweating, shivering, vasodilation and vasoconstriction, which are thereafter processed by the effectors.

It was observed that all of these thermoregulation mechanism are triggered when the mean skin temperature hit a given threshold [161]. Some of these mechanism can be influenced by the effect of local skin temperature. In the presence of a constant central signal, local skin temperature modifies the local sweating rate and the local skin blood flow [162]. From these observations, we can infer that thermoregulatory signals are a function of temperature signals from the body core and the body periphery. Assuming that the hypothalamus is proportional controller, additive relationships of the mean skin temperature $T_{sk,m}$ and internal temperature $T_c$ can be established. Some works developed equations involving the product of $T_{sk,m}$ and $T_c$ [163].

It is worth noting that in addition to autonomous thermoregulatory mechanism, man corrects disturbances of the body's thermal state by behavioural thermoregulation: changes in clothing insulation, changes in body posture, and seeking shade,…etc.

### *1.2. Thermal Comfort*

According to ASHRAE's definition, thermal comfort is "that condition of mind which expresses satisfaction with the thermal environment" [164]. Thermal comfort is defined also more objectively as: " the absence of punitive impulses from both (ie. cutaneous and hypothalamic) receptor fields" [165]. Only resting subjects can reach this state of ideal comfort when for instance they are exposed, unclothed, to an ambient temperature of 30°C [166] Under these thermoneutral conditions no regulatory adjustments occur.

For a steady state, the physiological conditions of thermal comfort (at low activity levels) have been described as follows [164]:

- Internal body temperature 36.6 to 37.1°C,
- Mean skin temperature 33 to 34.5°C for man and 32.5 to 35°C for women,
- Temperature regulation is completely accomplished by vasomotor control of blood flow to the skin (no sweating/shivering present).

Most applied work on thermal comfort has dealt with thermal sensation. Thermal comfort refers commonly to the subjective state of the subject that can be described using verbal scales (ASHRAE-scale [164]) for (dis)comfort or (un)pleasantness. It depends on the general thermal and regulatory state of the body. In contrast, thermal sensation refers to a rational and objective experience which can be characterized using terms in the ASHRAE-scale [164]. Thermal sensation seems to depend mainly on the activity of cutaneous thermoreceptors [166]. Under steady state, thermal sensation is related to the ambient temperatures, radiant temperature, humidity ,and air velocity.In many cases, however, the perception of thermal comfort and thermal sensation correlate with each other.

As for the thermoregulatory responses, there are local effects in the perception of comfort and temperature. Local discomfort can be perceived due to inhomogeneous environmental conditions such as asymmetric radiant fields, draughts, and vertical air temperature gradients.

The physiological mechanisms governing local thermal comfort are associated to local cutaneous thermoreceptors. Indeed, if the local temperature of the skin deviates too far from the mean skin temperature, local discomfort can be experienced in this area. From that, it appears that local (dis)comfort is highly dependent on the state of general comfort, which is better known as. *alliesthesia.* In contrast, local thermal sensation is governed by local skin temperature irrespective of the general thermal state of the body [167].

## 2. Modelling the passive system

The human organism model is separated into two interacting systems: the controlling active system and the controlled passive system. The passive system combines the physical human body and the heat transfer phenomena occurring in it and at its surface. Indeed, within the body, metabolic heat is produced. This heat is distributed over body regions by blood circulation and is carried by conduction to the body surface. Heat is then lost to the surrounding by convection, radiation, and evaporation. The active system is a closed loop controller predicting regulatory responses of the central nervous system. The latter plays the major role on regulating the internal temperature of human body, around 37°C for a resting man through four mechanisms: shivering, vasodilatation, vasoconstriction and sweating.

In the following sections, we will present the passive system of the Tanabe thermophysiological model, originally developped from Stolwijk works. Some refinements were injected, especially on the

modelling of convective and radiative heat exchanges. . These improvements are extracted from Fiala thermophysiological model, and are necessary for a better evaluation of thermal comfort indices. We will refer frequently to Tanabe, Fiala and Stolwijk works to justify some assumptions, and give insights on numerical data.

### *2.1. Body Construction*

The passive system is depicted in Figure 15. It consists of 15 cylinders representing trunk, arms, hands, legs, and feet. The head is represented as a sphere. The cylinders or segments, are each subdivided into four concentric layers or compartments, representing the core, muscle, fat, and skin layers. An additional central blood compartment, representing the large arteries and veins, exchanges heat with all other compartments via the convective heat transfer. Each 2-uplet (segment,layer) is reffered as a node, which brings the thermophysiological model to a 65 node model.

For each node, complete heat balance equations are developed to account for heat flow into and out of the compartment, via conduction and convection, and the metabolic heat production within the compartment. For those compartments in contact with the environment, appropriate equations express the heat exchanges by radiation, convection, and evaporation.

Numerical values for the system are based on a "standard" man with the following characteristics:

- body weight : 74.4 kg
- surface area : 1.89 $m^2$
- Height : 172 cm
- Volume: 74.4 x $10^{-3}$ m

To facilitate the notation of temperatures and heat exchanges in the various compartments and segments, the following convention will be used: segments will be noted by the index $i$ where $i$ belongs to [1,16]. The 16 segments are listed in Figure 15.

Each segment is subdivided into 4 layers, indexed by $j$. The central layer is the core ($j = 1$), followed by muscles ($j = 2$), then fat ($j = 3$), and finally the skin ($j = 4$).

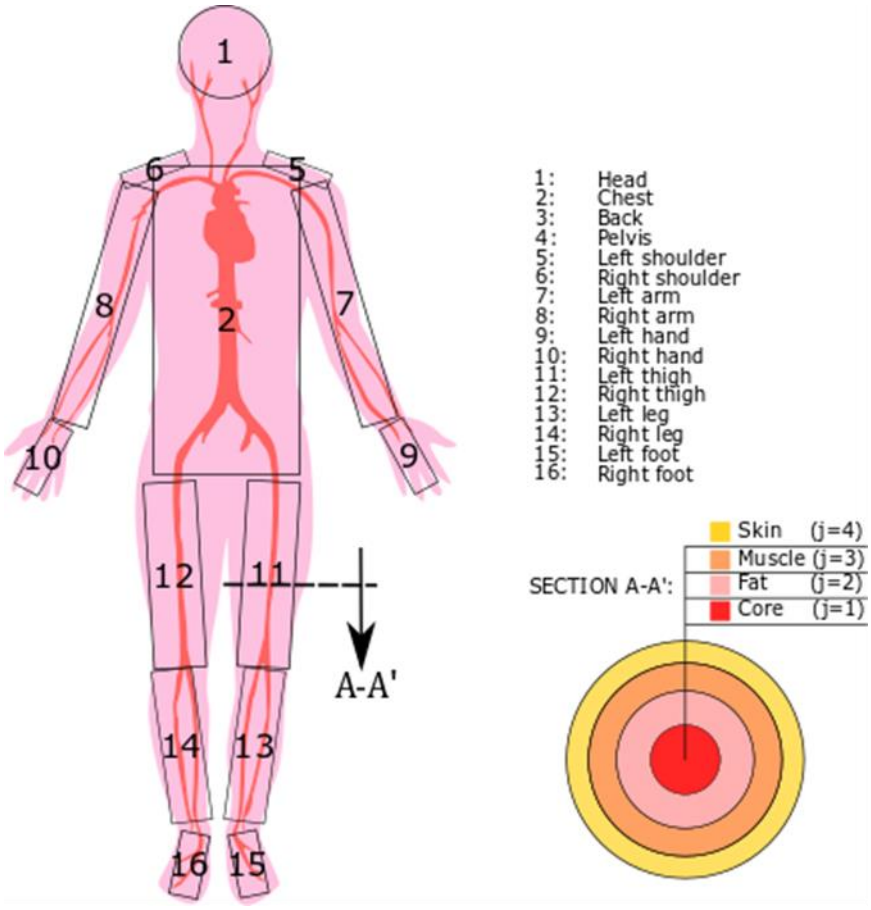


Figure 15. Passive system [58]

## *2.2. Heat balance*

The passive system model contains four heat balance equations (105)-(109), established for each node $(i,j)$ with $(i,j) \in [\![1,16]\!] \times [\![1,4]\!]$, and a fifth equation (109) representing the heat balance for the blood compartment. The produced metabolic heat flow $\dot{Q}_m$ is transferred through tissues by conduction $\dot{Q}_d$ and by the blood convection $\dot{Q}_b$. The heat exchange with the environment occurs by respiration $\dot{Q}_{res}$, which is considered only from chest core (segment 2), evaporation $\dot{Q}_e$, radiation $\dot{Q}_r$ and convection $\dot{Q}_c$. (Figure 16)

If a segment is in contact with the seat, the heat exchanges by convection radiation and evaporation are considered null, and should be replaced by the heat contact between the segment and the seat. Since the cabin model does not account for seats, the contact heat flux is not considered.

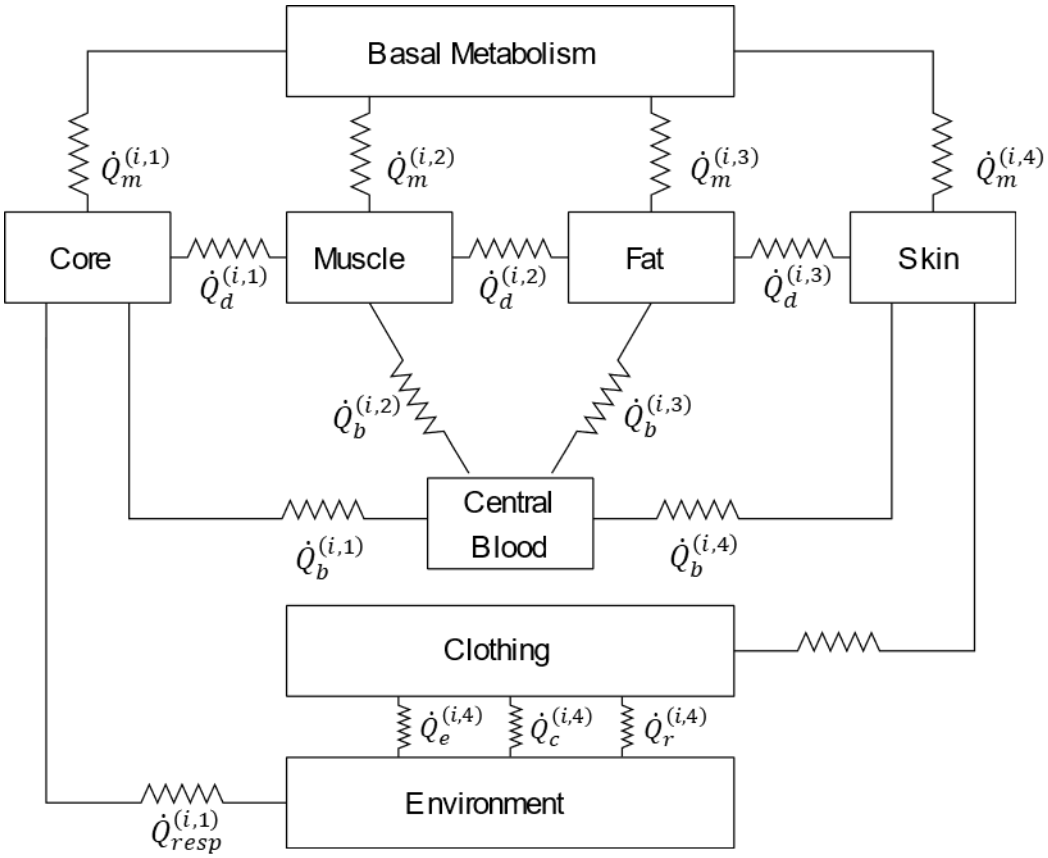


Figure 16. Heat exchanges within the human and with the environment

The heat balance equations in the four layers and central blood are the followings:

$$C^{(i,1)}\frac{dT^{(i,1)}}{dt} = \dot{Q}_m^{(i,1)} - \dot{Q}_b^{(i,1)} - \dot{Q}_d^{(i,1)} - \dot{Q}_{res}^{(i,1)}\delta_{2,i} \tag{105}$$

$$C^{(i,2)}\frac{dT^{(i,2)}}{dt} = \dot{Q}_m^{(i,2)} - \dot{Q}_b^{(i,2)} + \dot{Q}_d^{(i,1)} - \dot{Q}_d^{(i,2)} \tag{106}$$

$$C^{(i,3)}\frac{dT^{(i,3)}}{dt} = \dot{Q}_m^{(i,3)} - \dot{Q}_b^{(i,3)} + \dot{Q}_d^{(i,2)} - \dot{Q}_d^{(i,3)} \tag{107}$$

$$C^{(i,4)}\frac{dT^{(i,4)}}{dt} = \dot{Q}_m^{(i,4)} - \dot{Q}_b^{(i,4)} + \dot{Q}_d^{(i,3)} - \dot{Q}_c^{(i,4)} - \dot{Q}_r^{(i,4)} - \dot{Q}_e^{(i,4)} \tag{108}$$

$$C_b\frac{dT_b}{dt} = \sum_{j=1}^{16}\sum_{j=1}^{4}\dot{Q}_b^{(i,j)} \tag{109}$$

Where $T$, $T_b$, $C$ and $C_b$ denote repectively the temperature for the node $(i,j)$, the blood temperature, the heat capacity for the node $(i,j)$, and the heat capacity for the blood. The term $\delta_{2,i}$ refer to the Kronecker delta. This function takes a value of 1 when the segment is the chest $i = 2$.

The expression of the different heat exchange for each compartment will be detailed in the following sections.

### *2.3. Metabolism & heat production*

The metabolism is defined as the set of the life-sustaining chemical reactions in organisms. Its main purposes are: the conversion of food to energy, building up compound such as proteins, lipids, and some carbohydrates, and eliminating nitrogenous waste. The body processes necessary for life requires a minimum essential heat generation known as the basal metabolic rate $\dot{Q}_m$. It is measured on a resting, awake, fasting subject. For a standard man, it is estimated to be equal to 86.5 W, where 17% is consumed by the brain, 60% is consumed by the trunk core, 5% by the skeleton and connective tissue and 18% by muscles fat and skin.

For core compartment, the metabolic heat production $\dot{Q}_m^{(i,1)}$ is assumed to be constant, equal to the basal metabolic rate $\dot{Q}_{m,b}^{(i,1)}$:

$$\dot{Q}_m^{(i,1)} = \dot{Q}_{m,b}^{(i,1)} \tag{110}$$

The body heat production is increased during physical activities in proportion to exercise intensity. A part of the internal heat production is converted into external mechanical power The heat metabolic production is increased also in cold exposure, by shivering, ie. contraction of the muscle fibers This capacity to raise heat production extends the range of environment conditions over which homeothermy can be sustained. Since muscles are the effectors of mechanical work, the metabolic heat production in the muscle layer, noted by $\dot{Q}_m^{(i,2)}$, can be modeled therefore as the sum of the basal metabolic rate $\dot{Q}_{m,b}^{(i,2)}$, the heat production rates due to muscular work $\dot{Q}_{work}^{(i,2)}$ and shivering thermogenesis $\dot{Q}_{chill}^{(i,2)}$. The expression of $\dot{Q}_{chill}^{(i,2)}$ is given in section 3.3.2. :

$$\dot{Q}_m^{(i,2)} = \dot{Q}_{m,b}^{(i,2)} + \dot{Q}_{work}^{(i,2)} + \dot{Q}_{chill}^{(i,2)} \tag{111}$$

Where the term $\dot{Q}_{work}(i,2)$ is the total heat production due to muscular work, expressed as a function of the difference of the activity metabolic rate $M$ and the basal metabolic rate. This quantity represent the caloric equivalent of the performed external work . It is given by (112):

$$\dot{Q}_{work}^{(i,2)} = \left( M - \sum_{i=1}^{16} \sum_{j=1}^{4} \dot{Q}_{m,b}^{(i,j)} \right) \times A_b^{(i)} \times k_m^{(i)} \tag{112}$$

Where $A_b$ is the surface area of the segment $i$, and $k_m^{(i)}$ is the weighting coefficient of muscular heat production [32]. The quantity $M$ corresponds to the activity level and it is measured in $met$. The values of $M$ for various typical activities are tabulated in the standard literature [168].

Finally, for the subcutaneous fat and the skin compartments, the metabolic heat production is assumed constant, equal to the basal values:

$$\dot{Q}_m^{(i,3)} = \dot{Q}_{m,b}^{(i,3)} \tag{113}$$

$$\dot{Q}_m^{(i,4)} = \dot{Q}_{m,b}^{(i,4)} \tag{114}$$

## *2.4. Blood Circulation*

The heat exchange $\dot{Q}_b$ between a given node $(i,j)$ and the central blood compartment, i.e. the 65th node, is given by (115):

$$\dot{Q}_b^{(i,j)} = a \times \rho \times C \times \dot{m}_b^{(i,j)} \times \left( T^{(i,j)} - T^{(65)} \right) \tag{115}$$

where $a$ is the ratio of counter-current heat exchange, $\rho C$ is the volumetric specific heat of blood, $\dot{m}_b^{(i,j)}$ is the blood flow rate, and $T^{(65)}$ is the blood temperature.

In [169], Stolwijk assumes some simplifications to characterize the blood flow $\dot{m}_b^{(i,j)}$. Some of these simplifications are made because of a lack of applicable data. Others are justified by the fact that mass

flow inaccuracies have only a very small effect on heat transfer. For example, Stolwijk assumed that blood flow to the core compartment remains at the basal value $\dot{m}_{b,b}^{(i,1)}$. This assumption will produce only slight increases in thermal gradients between core nodes, and hence, convective heat transfer will not be affected. The brain receives for instance a constant blood flow of about 45 $l.h^{-1}$ while visceral organs in the trunk core are estimated to receive 210 $l.h^{-1}$. The blood mass flow at the core layer is given by (116):

$$\dot{m}_b^{(i,1)} = \dot{m}_{b,b}^{(i,1)} \tag{116}$$

The muscle compartments, can have widely varying metabolic rates depending on the activity and, consequently, substantial variations in blood flow. Blood flow measurements and measurements of arteriovenous oxygen differences across the working quadriceps muscle during exercise, provided insight of muscle blood flow as shown in [169]. Each liter of blood contains about 200 $ml$ $O_2$ which, if completely consumed, could produce about 1.16 $Wh$ of heat. It is thus, reasonable to assume that at least 1 liter of blood is required to produce 1.16 $Wh$ of heat. The heat production can be induced either by muscular work du to exercise or chilling. With these assumptions, the following equation (117) approximately describes the blood flow to the muscle compartments

$$\dot{m}_b^{(i,2)} = \dot{m}_{b,b}^{(i,2)} + \frac{\dot{Q}_{work}^{(i,2)} + \dot{Q}_{chill}^{(i,2)}}{1.16} \tag{117}$$

Blood flow in the subcutaneous fat is assumed to be equal to its basal value and does not depend on thermoregulatory adjustments

$$\dot{m}_b^{(i,3)} = \dot{m}_{b,b}^{(i,3)} \tag{118}$$

Finally for the skin layer, cutaneous blood flow is highly dependent on the thermoregulatory mechanism. The basal blood flow at thermal neutrality can be reduced to very low values through vasoconstriction $cs$, and increased through vasodilatation $\dot{m}_{dl}$. For instance, at an ambient temperature of 30°C, the total skin blood flow for a resting man is about 105 $ml.min^{-1}.m^{-2}$, while in hotter conditions, at ambient temperature of 35°C, the blood flow reaches 240 $ml.min^{-1}.m^{-2}$. Both vasodilatation and vasoconstriction are weighted by the coefficient $k_{dl}(i)$ and $k_{cs}(i)$ since each segment has its own vasomotion properties. The expression for local skin blood flow is given by (119)

$$\dot{m}_b^{(i,4)} = \frac{\dot{m}_{b,b}^{(i,4)} + (k_{dl}(i) \times \dot{m}_{dl})}{1 + (k_{cs}(i) \times cs)} \times \gamma_{sk}^{(i,4)} \tag{119}$$

The values of $k_{cs}$ are such that the body extremities (i.e. hands and feet) have a high vasoconstriction. They will be therefore more sensitive to cold. The trunk and thigh are characterized however by high vasodilatation, which favors heat rejection during exercise. The values of $k_{dl}$ tends to be higher in those regions.

The expressions of vasodilatation and vasoconstriction will be given in section 3.3.5. and 3.3.3.

The term $\gamma_{sk}(i,4)$ refers to local temperature effect. This effect has a substantial influence on the resistance of cutaneous veins [170]. Experiments show that this resistance is doubled for a 10°C drop in local temperature, and divided by 2 when the latter increases by 10°C. Tanabe proposed the following equation (120) to model the local temperature effect:

$$\gamma_{sk}^{(i,4)} = 2^{\frac{e(i,4)}{\Delta T_{sk}}} \tag{120}$$

Where $e(i,4)$ is the difference between cutaneous and reference temperature. This quantity will be discussed in the active system, in section 3.2. .

## 2.5. Heat Conduction

The heat transmitted by conduction $\dot{Q}_d^{(i,j)}$ to the neighboring layer within the same segment and is expressed by (121).

$$\dot{Q}_d^{(i,j)} = C_d^{(i,j)} \times \left(T^{(i,j)} - T^{(i,j+1)}\right) \tag{121}$$

Where $C_d^{(i,j)}$ is the thermal conductance for a given segment $i$ between the layer $j$ and its neighbor $j+1$.

## 2.6. Heat Exchange with the Environment

### 2.6.1. Convection

The convective heat exchange $\dot{Q}_c^{(i,4)}$ occurs between the surface of a segment and ambient air. If the segment is clothed, the surface temperature $T_{sf}$ is equal to the temperature of the clothed area. Whereas if the segment is nude, $T_{sf}$ is equal to skin temperature. The expression of $T_{sf}$ will be given in section 2.6.3. , when clothing insulation will be discussed.

In either case, the convective heat exchange, given by (122), is a function of the temperature difference between $T_{sf}$ and $T_{cab}$, and convection coefficient $h_{c,mix}$ [W m$^{-2}$K$^{-1}$], that combines both natural and forced convection. The quantity $f_{cl}^{(i)}$is the clothing factor, defined as the ratio of the clothing surface area to the body surface area $A_b^{(i)}$ for a given segment $i$:

$$\dot{Q}_c^{(i,4)} = h_{c,mix}^{(i,4)} \times f_{cl}^{(i)} \times A_b^{(i)} \times \left(T_{sf}^{(i,4)} - T_{cab}\right) \tag{122}$$

In the present model, the convection coefficient $h_{c,mix}$ is a function of the temperature difference between the surface and the air, and the effective air speed $v_{a,eff}$. The latter is a composite of the local room air speed and the relative air speed due to body motion.

The expression of $h_{c,mix}$ is given by (123):

$$h_{c,mix} = \sqrt{a_{nat}\sqrt{\left(T_{sf}^{(i,4)} - T_{cab}\right)} + a_{frc}v_{a,eff} + a_{mix}} \tag{123}$$

The basis for $h_{c,mix}$are the experiments of Wang [171] who measured local convective heat losses on a heated full-scale manikin with a realistic skin temperature distribution for both natural and forced convection. Coefficients $a_{nat}$, $a_{frc}$, $a_{mix}$ were then obtained by means of regression analysis, for each segment $i$. These coefficient are available in Fiala thesis [58].

### 2.6.2. Radiation

A given body segment exchanges heat also by long wave radiation. In an enclosure characterized by different surface temperatures, the radiative heat exchange $\dot{Q}_r^{(i,4)}$ is the sum of the partial radiative heat exchanges between the segment and the surrounding structures (walls, windows, etc.).

The heat exchanged by radiation for a given segment is a function of temperature difference between segment surface $T_{sf}$ and the mean radiant temperature $T_{mrt}$. The latter is defined as the temperature of a fictitious uniform black envelope 'seen' by a segment which causes the same radiative heat exchange with the segment as the actual (asymmetric) enclosure. This temperature requires the computation of view factors (which describe the influence of geometry on the radiative heat exchange) between the segment and each surface of the surrounding. This type of computation is generally done in 3D models, where the enclosure geometry is established, and spatial distribution of temperature is

studied. In the present work, we assumed that cabin walls have the same temperature $T_w$, which means that $T_{mrt}$ is equal to $T_w$. Therefore, the heat exchange by radiation is calculated by:

$$\dot{Q}_r^{(i,4)} = h_r^{(i,4)} \times f_{cl}^{(i)} \times A_b^{(i)} \times \left(T_{sf}^{(i,4)} - T_w\right) \tag{124}$$

The coefficient $h_r$[[W$m^{-2}K^{-1}$] is the local radiative heat exchange coefficient, defined by (125), for a given segment:

$$h_r^{(i,4)} = \sigma \varepsilon_w \varepsilon_{sf}^{(i,4)} \psi_{sf-w}^{(i,4)} \left({T_{sf}^{(i,4)}}^2 + {T_w}^2\right)\left(T_{sf}^{(i,4)} + T_w\right) \tag{125}$$

where $\sigma$ is the Stefan-Bolzmann constant, and $\varepsilon_w$ is the emission coefficient of the surrounding, typically equal to 0.93 in indoor spaces. The term $\varepsilon_{sf}^{(i,4)}$ refers to longwave emissivity of a given segments. The values of $\varepsilon_{sf}^{(i,4)}$ are obtained from [58].

The quantity $\psi_{sf-w}^{(i,4)}$ refers to the view factor between a given segment $i$ and the surroundings 'seen' by it. The view factors $\psi_{sf-w}^{(i,4)}$ of the cylindrical and spherical body elements were extracted also from [58]. They vary from 0.1 to unity depending on the degree to which individual skin sectors are 'hidden' by other body parts. It is worth noting that the values of view factors are given for standing and sitting postures. This distinction comes from the fact seated position is characterized by a decreased body radiation area.

### 2.6.3. Clothing Insulation

Because clothing represents the resistance to heat exchanges with the surroundings, the present enhanced model made efforts to model garments in some detail. Unfortunately, Tanabe model uses only overall clothing parameters, ie. the intrinsic clothing insulation $I_{cl}$, the clothing area factor $f_{cl}$ and the moisture permeability index $i_{cl}$ (for exact definitions see [172]). These do not reflect the real insulating properties of the garments but provide characteristics of a uniform (imaginary) clothing layer covering the entire body. Therefore, the real insulation values $I_{cl}^*$, $f_{cl}^*$, and $i_{cl}^*$ of trousers, shirts, underwear, socks, etc. are extracted from the database provided in [173]. These local values include the insulation effect provided by any layer of air trapped between the skin and the fabric.

The intrinsic insulation can be seen as a resistive coefficient for dry heat exchange between skin and the ambient air. At steady state, the heat exchange by convection and radiation as defined by (122) and (124), equals to heat exchange between skin and clothes. Figure 17 shows the heat exchanges at the boundary of a clothed segment.

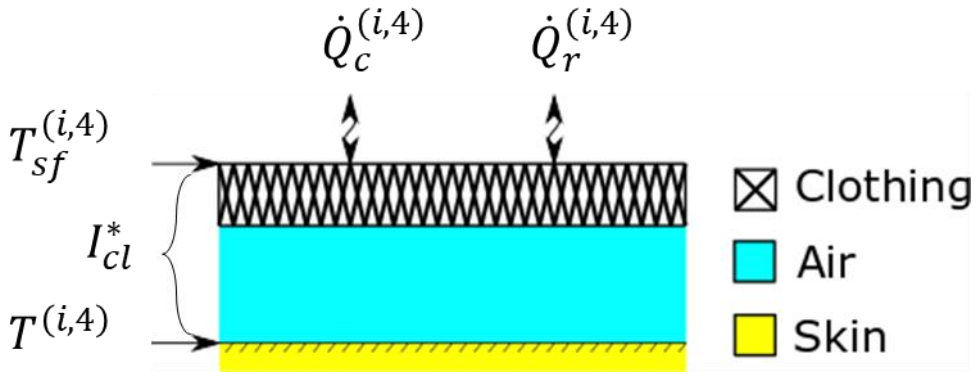


Figure 17. Heat exchanges on the boundary of clothing surface

Hence, the following equality can be stated for a given segment $i$:

$$\dot{Q}_c^{(i,4)} + \dot{Q}_r^{(i,4)} = \frac{T^{(i,4)} - T_{sf}^{(i,4)}}{I_{cl}^*} \tag{126}$$

It is worth noting that this equation is used practically to calculate the surface temperature $T_{sf}^{(i,4)}$. This quantity is important to evaluate thermal comfort.

Clothing insulation represents also a resistance towards evaporative heat exchange. The local evaporative coefficient $U_{e,cl}^{*}$ [W m$^{-2}$Pa$^{-1}$] is obtained using the local values of moisture permeability $i_{cl}^{*}$, thermal insulation $I_{cl}^{*}$ of individual clothing layers worn by a given body segment $i$, the clothing factor $f_{cl}^{*}$ of the outer clothing layer, the local convection coefficient $h_{c,mix}$ , and the Lewis constant $La$ for air (see definition in [174]):

$$U_{e,cl}^{*} = \frac{La}{\sum_{k=1}^{n}\left(\frac{I_{cl}^{*}}{i_{cl}^{*}}\right)_{k} + \frac{1}{f_{cl}^{*}h_{c,mix}}} \tag{127}$$

### 2.6.4. Evaporation

Evaporative heat loss occurs through the skin and the respiratory system. Under conditions of thermal neutrality, evaporation accounts for 10% to 25% of heat loss. In an environment where the air temperature is equal to or higher than the skin temperature, sweating is the only mechanism available for dissipation of heat that stems from metabolic production. In this situation, anything that limits evaporation, such as high ambient humidity or impermeable clothing, may easily lead to heat storage and a potentially fatal rise in body temperature. The driving force behind evaporation is the vapor pressure difference between the body surface and the environment. Since the water vapor at the skin is saturated, the pressure of water vapor corresponds to the saturated pressure. The rate of evaporative heat loss $\dot{Q}_e$ can be expressed by (128), in an almost similar way to that of non-evaporative heat loss.

$$\dot{Q}_e = U_{e,cl}^{*} \times A_{wet} \times \left(P_{sat}(T) - P(T_{cab})\right) \tag{128}$$

Where $U_{e,cl}^{*}$ is the evaporative heat transfer coefficient, $A_{wet}$ is the skin wetted area $P_{sat}$ is the saturated pressure of water vapor, and $P$ the partial pressure of water vapor. The formula of $P_{sat}$ and $P$ as a function of the temperature $T$ are given by (129) and (130):

$$P_{sat}(T) = e^{16.53 - \frac{4030.18}{T+235}} \tag{129}$$

$$P(T) = RH \times P_{sat}(T) \tag{130}$$

For a given segment $i$, the evaporative heat exchange is maximal when the wetted surface is equal to segment surface $A_b^{(i,4)}$. Hence, the following equation (131):

$$\dot{Q}_{e,max}^{(i,4)} = U_{e,cl}^{*} \times A_b^{(i,4)} \times \left(P_{sat}\left(T^{(i,4)}\right) - P(T_{cab})\right) \tag{131}$$

Evaporative heat loss from the skin is a combination of the evaporation heat loss $\dot{Q}_{sw}^{(i,4)}$ due to sweating, and the heat loss $\dot{Q}_{diff}^{(i,4)}$ due to natural diffusion of water through the skin.

$$\dot{Q}_e^{(i,4)} = \dot{Q}_{diff}^{(i,4)} + \dot{Q}_{sw}^{(i,4)} \tag{132}$$

The term $\dot{Q}_{sw}^{(i,4)}$ will be detailed in section 3.3.4. , since the sweating is part of the active system. With no regulatory sweating occurs, skin wettedness caused by diffusion represent approximately 6% of the evaporative heat exchange of the non-wetted area.

$$\dot{Q}_{diff}^{(i,4)} = 0.06 * \left(\dot{Q}_{e,max}^{(i,4)} - \dot{Q}_{sw}^{(i,4)}\right) \tag{133}$$

For large values of $\dot{Q}_{e,max}$ or long exposures to low humidities, the value of 6% may drop to 2%, because of dehydration of the outer skin layers alters its diffusive characteristics.

#### 2.6.5. Respiratory Heat Losses

Most heat is lost through the body surface; however, heat exchange with the environment also occurs by respiration. The model for respiratory heat loss was obtained from the work of Fanger [45] taking into account the loss by evaporation and convection. The latent heat exchange is a function of the whole body metabolism, and the difference between the temperature of the expired and inspired air. The latter is exactly equal the cabin air temperature, $T_{cab}$ while the expired air is assumed to have a temperature of 34°C The evaporative heat loss of respiration is given by (134).

$$\dot{Q}_{e,res}^{(2,1)} = 0.0014 \times (34 - T_{cab}) \times \sum_{i=1}^{16} \sum_{j=1}^{4} \dot{Q}_m^{(i,j)} \tag{134}$$

The dry heat loss of respiration due to the pressure difference between expired and inspired air can be expressed by (135), where $P_{cab}$ denote the partial air pressure in the cabin:

$$\dot{Q}_{d,res}^{(2,1)} = 0.017 \times \left(5.867 - P(T_{cab})\right) \times \sum_{i=1}^{16} \sum_{j=1}^{4} \dot{Q}_m^{(i,j)} \tag{135}$$

We assume that respiratory heat losses take place only in the chest segment.

Finally, the total respiratory heat loss is the sum of the dry and the evaporative heat losses.

$$\dot{Q}_{res}^{(2,1)} = \dot{Q}_{e,res}^{(2,1)} + \dot{Q}_{d,res}^{(2,1)} \tag{136}$$

# 3. Modelling the active system

## *3.1. Introduction*

Man maintains his internal temperature at a constant value by four essential responses: vasoconstriction, vasodilatation, shivering and sweating. Peripheral vasomotion, via vasoconstriction and vasodilatation of the skin blood flow, is activated to regulate internal temperature in moderate environments. These cardiovascular responses govern the transfer of heat from the body core to body surface (where it is lost to the environment). In cold conditions, vasoconstriction is accompanied by shivering thermogenesis. In hot conditions, vasodilatation is accompanied by the excretion of sweat.

One of the most well-known models of human thermoregulation (ie. the active system) was created by Stolwijk [49]. His feedback control system has been the source of motivation for various refinements and improvements [175]. The basic principles of Stolwijk's active system were also adopted in the present enhanced Tanabe model.

The passive system undergoes thermal disturbances at different body sites and these are represented as error-signals. Positive error-signals, ie. positive disturbances from the thermoneutral state of the body, where no regulation occurs, represent warm receptors. Negative error signals represent cold receptors. These local afferent signals are integrated in the *integrating system* (i.e. hypothalamus) which transmits appropriate commands to the effectors.

These commands are translated into the overall regulatory actions which are distributed over the body and may be weighted via local regulation (temperature local effect for instance) (Figure 18).

In the following section, we will present the enhanced Tanabe model for the integrating system, and thermoregulatory signals.

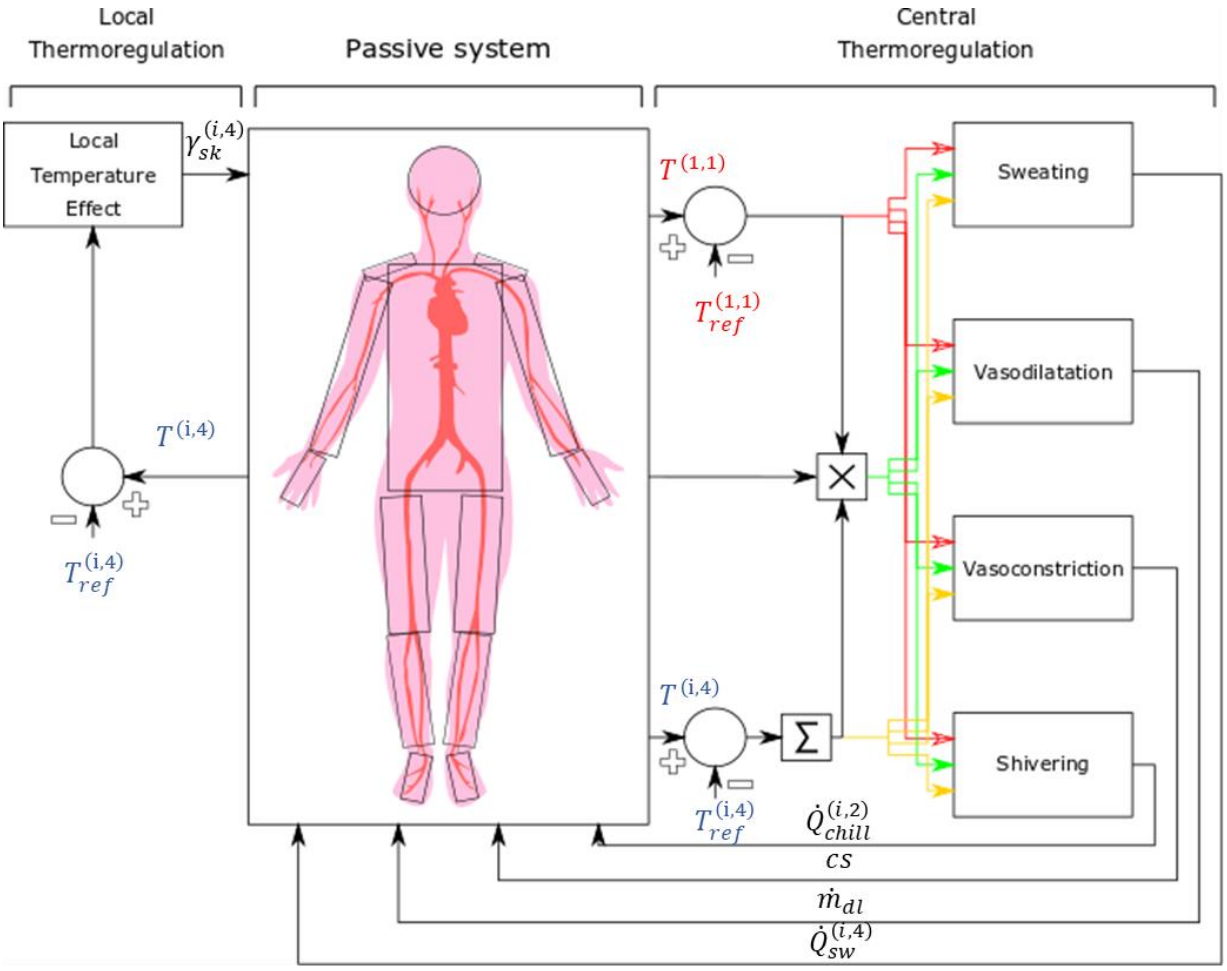


Figure 18. Active system [58]

### 3.2. *Integrating system*

We assume that thermoreceptors are present only in skin layer ($j = 4\,, i \in [1,16]$) and the head core (hypothalamus) ($j = 1\,, i = 1$). For a given node belonging to the aforementioned node set, the error signal is equal to the difference between the temperature $T^{(i,j)}$ and the set point temperature $T_{ref}^{(i,j)}$.

$$e^{(i,j)} = T^{(i,j)} - T_{ref}^{(i,j)} \tag{137}$$

Where $T^{(i,j)}$ is computed by the passive system, and $T_{ref}^{(i,j)}$ is supplied as constants.

The concept of set point in physiological thermoregulation was suggested in the 19th century to assess the description of temperature regulation during fever as "setting the physiological thermostat" to a higher level. This concept has also been used to explain the elevation of body temperature in exercise and even on exposure to heat. Different explanations have been given to how the physiological system provides itself with a function similar to a set point. One explanation states that the set point stems from a balance between the electrical activity of temperature insensitive and sensitive cells. Others explains that it stems from a balance between heat loss and heat conserving centers [169] in the anterior and posterior hypothalamic areas. Regardless of the origin of this concept, we will assume that the

thermo-physiological system admits set points for the skin layer and the hypothalamus. The values are available in [32].

We assume also that the warm and cold thermoreceptors, always generate positive error signal. This is conveniently accomplished by testing $e^{(i,j)}$ for its sign. If it is positive, we assume warmth receptors are effective. The warm signal $wrm^{(i,j)}$ can be then set to the value of $e^{(i,j)}$, and the cold signal to 0. If $e^{(i,j)}$ is negative, cold receptor is assumed to be effective. The cold signal $cld^{(i,j)}$ is then set to $-e(i,j)$, while the warmth signal $wrm^{(i,j)}$ is set to 0:

$$wrm^{(i,j)} = e^{(i,j)} \ \& \ cld^{(i,j)} = 0 \ \ if \ \ e^{(i,j)} > 0 \tag{138}$$

$$cld^{(i,j)} = -e^{(i,j)} \ \& \ wrm^{(i,j)} = 0 \ \ if \ \ e^{(i,j)} < 0 \tag{139}$$

The cutaneous warmth and cold signals are next integrated, according to distribution coefficients $k_{sk}^{(i)}$, available in [32]. The summation of these signals was not clear when Tanabe first developed his active system model. Instead, he proposed two integrated signals, $wrms$ and $colds$, respectively given by the weighted sums (140) and (141):

$$wrms = \sum_{i=1}^{16} k_{sk}^{(i)} \times wrm^{(i,4)} \tag{140}$$

$$clds = \sum_{i=1}^{16} k_{sk}^{(i)} \times cld^{(i,4)} \tag{141}$$

## *3.3. Thermoregulation mechanism*

### 3.3.1. Introduction

The controller equations $u_{AS}$ all have three terms. The first one consists of the product of a control coefficient $c$ and the head core error signal $e^{(1,1)}$. The second term consists of the product of a control coefficient $s$ and an integrated cutaneous signal. Finally, the third term is the product of control coefficient $p$, the cold/warm signal of the head core, and an integrated cutaneous signal. Controller equations $u_{AS}$ are expressed either by (142) or (143), depending of the nature of thermoregulation mechanism:

$$u_{AS} = c \times e^{(1,1)} + s \times (wrms - clds) + p \times cld^{(1,1)} \times clds \tag{142}$$

$$u_{AS} = c \times e^{(1,1)} + s \times (wrms - clds) + p \times wrm^{(1,1)} \times wrms \tag{143}$$

These expressions will become negative under certain circumstances. Since we assume that thermoregulatory mechanism are positive, it is necessary to make sure that the controller signals are set to 0 when they become negative.

The final part of the controller distributes the effector commands to the appropriate nodes and, if required, modifies them according to local conditions.

The next sections are concerned with the description of thermoregulation mechanism, and giving some insights on deriving the controller coefficients

### 3.3.2. Shivering

On exposure to cold, the thermoregulatory response of human beings is vasoconstriction and increased heat production through shivering. Shivering is usually intermittent and is under

considerable voluntary control. For this reasons, shivering is an area of uncertainty although some studies have indicated that both skin and internal temperatures must be lower than certain threshold values for shivering to occur. The shivering acts exclusively on muscle compartment to produce extra heat. It is modelled for a given segment $i$ by following relationship (144):

$$\dot{Q}_{chill}^{(i,2)} = \left\{-c_{chill} \times e^{(1,1)} - s_{chill} \times (wrms - clds) + p_{chill} \times cld^{(1,1)} \times clds\right\} \times k_{chill}^{(i)} \quad (144)$$

Where $c_{chill}$, $s_{chill}$, and $p_{chill}$ are the controller coefficients for shivering. They are evaluated by measuring the increases of metabolic rate at different internal and mean skin temperature [169]. The term $k_{chill}^{(i)}$ refers to the weighting coefficient of shivering of the segment $i$.

### 3.3.3. Vasoconstriction

In cold environments, skin blood flow decreases via cutaneous vasoconstriction. This produces less convective heat transfer from the core to the surface, and therefore a less heat dissipation from the skin. Vasoconstriction is sufficiently strong to reduce heat flow below 0.1 W.

Peripheral vasoconstriction occurs mainly in the body extremities, i.e hands and feet. The first consequence is the rapid decrease of skin temperature of fingers and toes, due the high surface to volume ratio, where the temperature of those part can reach the ambient temperature. The second consequence is the reduction of blood flow in favor of a central pooling of blood in the torse and deep body core. This mechanism allows to preserve the vital organs such as the heart and the brain at constant temperature.

In contrast to shivering, cutaneous vasoconstriction $cs$ remains active in moderate environments in which there are small disturbances from thermal neutrality.

The vasoconstriction control $cs$ is given by (145) :

$$cs = -c_{cs} \times e^{(1,1)} - s_{cs} \times (wrms - clds) + p_{cs} \times cld \times clds \quad (145)$$

Where $c_{cs}$, $s_{cs}$ and $p_{cs}$ represent the vasoconstriction control coefficients.

### 3.3.4. Sweating

Sweating, defined as production of fluid secreted by sweat glands, is a thermoregulation mechanism that allows a substantial heat rejection by evaporation. As high energy molecules evaporate from the skin, releasing energy absorbed from the body, the skin and superficial vessels decrease in temperature. Cooled venous blood then returns to the body's core and counteracts rising core temperatures.

The process of evaporation is more effective in dry ambient conditions. Indeed, high sweat rates can occur without causing an important skin wettedness, which avoids the obstruction of sweat gland opening. Nevertheless, an extended evaporation during prolonged heat exposures, may provoke an accumulation of NaCl on the skin. This accumulation reduce the sweat's vapor pressure and hence, the evaporative efficiency. In that situation, sweat glands reduces NaCl concentration in their secretions.

The sweating does not begin simultaneously all over the body. The first area is generally the forehead, followed in order by the upper arms, hands, thighs, feet, and back and abdomen

The expression of the sweating controller is given by (146)

$$\dot{Q}_{sw}^{(i,4)} = \left\{c_{sw} \times e^{(1,1)} + s_{sw} \times (wrms - clds) + p_{sw} \times wrm^{(1,1)} \times wrms\right\} \times k_{sw}^{(i)} \times \gamma_{sk}^{(i)} \quad (146)$$

Where $c_{sw}$, $s_{sw}$, and $p_{sw}$ represent the sweating control coefficient. The term $k_{sw}^{(i)}$ refers to distribution of sweat secretion, approximated by the distribution of sweat glands. The highest densities are observed in body parts like forehead, neck, back and the front of the trunk

The term $\gamma_{sk}^{(i)}$ refers to local temperature effect defined by the formula (120).

#### 3.3.5. Vasodilatation

Cutaneous vasodilation increases skin blood flow several times, which substantially increases cardiac output and convective heat transfer from the core to the periphery (heat rejection).

In thermoneutral environments, the skin blood flow is approximately 250 $ml/min$, which produces a heat dissipation of approximately 80 to 90 $Kcal/h$, for a resting subject. While in hot ambient conditions, skin blood flow can reach 6 to 8 $l/min$ corresponding to 60% of cardiac output. It is worth underlining that cutaneous vasodilatation is not active in thermal neutrality. It is activated only during increases in internal temperature, such as those that occur during exercise or heat exposure.

The cutaneaous dilatation $\dot{m}_{dl}$ is given by (147):

$$\dot{m}_{dl} = c_{dl} \times e^{(1,1)} + s_{dl} \times (wrms - clds) + p_{dl} \times wrm^{(1,1)} \times wrms \quad (147)$$

Where $c_{dl}$, $s_{dl}$, and $p_{dl}$ represent the vasodilatation control coefficient. These controller coefficients were derived through a series of conductance measurement for different mean skin and internal temperature [169]. Stolwijk assumed that blood flow is a linear function of conductance where an increase of 1.16 $Wm^{-2}{}^{\circ}C^{-1}$ corresponds to 1 $lm^{-2}h^{-1}$.

# 4. Modelling the thermal comfort

## *4.1. Introduction*

Over the past decades, several metrics and methods (more than 70) have been developed to assess human perception of the thermal environment and thermal response to different climatic conditions. Terms like comfort index have been commonly used in the scientific literature to identify those metrics, whose definition involves physiological, psychological, medical, climatological and engineering aspects. Depending on the context and the situation, some comfort indices may be more representative than others. For instance, in buildings, operative temperature, effective temperature and PMV/PPD index were extensively used. While for outdoor environment, indices such as WBGT [176] or UTCI [58] are more convenient.

In this section, we will present three comfort indices for vehicular environment, from the simplest to the more complex one. The first one is based on a temperature and relative humidity set point. The second one is the PMV/PPD indices developed by Fanger [10], where thermal sensation is evaluated according to thermal ambiance and clothing. The third one is the equivalent temperature, more convenient for vehicular environment, since it can take into account the ambiance, clothing, internal state of the human body, the subjective response of the person,… etc. We will assume that the equivalent temperature is the most representative index among the three.

The objective behind studying theses indices is to use them as a cost function of the optimization problem, and establish, for a given HVAC system consumption, the difference in thermal comfort. This comparison will prove the benefit to adopt the equivalent temperature as thermal comfort metric. Moreover, the comparison will give hints to modify the PMV model, and transform it in more representative index, suitable for a real time control.

### *4.2. Temperature and humidity set point*

ANSI/ASHRAE Standard 55-2004 [18] specified winter and summer comfort zones in term of a selection of physical quantities such us temperature, relative humidity, operative temperature [177] and effective temperature [177],…. Those comfort zones are constructed usually for a sedentary activity, typical to enclosures like building or vehicle cabin.

For either summer or winter, the relative humidity comfort zone is in the range of 30%-60%. When the indoor relative humidity is below 25%, the incidence of respiratory infections significantly increases. The temperature comfort zone depends however on the clothing insulation. For summer clothing (light slacks and short-sleeve shirt or comparable ensemble), in thermally uniform enclosure ($T_{ambient} = T_w$) with a relative humidity equals to 50%, Standard 55-1992 recommends a temperature comfort zone in the range of 23.5 – 26 °C. This range changes for winter clothing (heavy slacks, long-sleeve shirt, and sweater or jacket), where the comfort temperature lies in 20.5-23.5 °C

As mentioned before, this work focuses on developing thermal comfort and energy management, and studying it on hot summer conditions. Therefore, a thermal comfort criterion based on temperature and relative humidity, will take into account the following ranges for $T_{cab}$ and $RH_{cab}$ and set points $T_{cab,sp}$ and $RH_{cab,sp}$, recommanded by Groupe PSA for a good thermal comfort in vehicle cabin:

$$T_{cab,sp} = 25°C\ , T_{cab}[°C] \in [23.5\ , 26] \tag{148}$$

$$RH_{cab,sp} = 45\%\ , RH_{cab}[\%] \in [30\ , 60] \tag{149}$$

### *4.3. PMV*

One of the most known and used thermal comfort indexes is the Predicted Mean Vote (PMV), proposed by Fanger [10]. As stated in Fanger' work, the mean thermal sensation of a group of persons in a given indoor environment is quantified by an integer index ranging between -3 and +3, from the coldest feeling to the hottest one. The value zero reflects the best comfort (i.e., neither cold nor hot). (Figure 19)

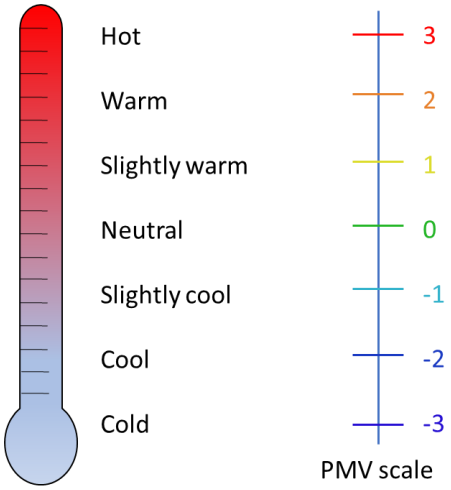


Figure 19. Thermal sensation scale

Fanger's PMV model establishes a relationship between the thermal load on the body and the average thermal sensation of individuals. The thermal load $\Delta\dot{Q}$ on the body is expressed as a simplified heat balance of the human body. It is a function of environment factors (temperature, humidity, air velocity, and mean radiant temperature) and individual factors (activity and clothing insulation). The expression of $PMV$ is given by (150):

$$PMV = A \times \Delta\dot{Q} \tag{150}$$

Where $A$ is an empirical coefficient that scales $\Delta\dot{Q}$ according to the thermal sensation scale (from -3 to +3). The term $A$ that was statistically determined from experimental studies, in climatic chambers, on nearly 1300 subjects. It is given by (151)

$$A = 0{,}303 \times \exp\left(-0.036\ \dot{Q}_m\right) + 0{,}028 \tag{151}$$

The heat balance $\Delta\dot{Q}$ is expressed by (152) :

$$\Delta\dot{Q} = \left(\dot{Q}_m - \dot{Q}_{work}\right) - \left(\dot{Q}_e + \dot{Q}_r + \dot{Q}_c + \dot{Q}_{resp}\right) \tag{152}$$

The PMV model assumes that the human body, is in steady state, and is not affected by heat exchanges with surroundings. For instance, for a sedentary person, the skin temperature has a value of 34 ° C while the sweating rate is null. Fanger has shown that in steady state, the skin temperature $T_{sk}$ and the sweating rate $\dot{Q}_{sw}$ depended solely on metabolic production according to (154):

$$T_{sk} = 35{,}7 - 0{,}0275 \times \left(\dot{Q}_m - \dot{Q}_{work}\right) \tag{153}$$

$$\dot{Q}_{sw} = 0{,}42 \times \left(\dot{Q}_m - \dot{Q}_{work} - 58{,}15\right) \tag{154}$$

Evaporative heat loss from the skin is a combination of the evaporation heat loss $\dot{Q}_{sw}$ due to sweating, and the heat loss $\dot{Q}_{diff}$ due to natural diffusion of water through the skin. The heat losses $\dot{Q}_{sw}$ and $\dot{Q}_e$ is given by (155) and (156):

$$\dot{Q}_{diff} = 3{,}05 \times 10^{-3} \times \left(P_{sat}(T_{cab}) - P(T_{cab})\right) \tag{155}$$

$$\dot{Q}_e = \dot{Q}_{sw} + \dot{Q}_{diff} \tag{156}$$

In the same way as Tanabe thermo-physiological model, the respiratory heat exchange is expressed by (157):

$$\dot{Q}_{resp} = 0{,}0014 \times \dot{Q}_m \times (34 - T_{cab}) + 0.017 \times \dot{Q}_m \times (5.867 - P(T_{cab})) \tag{157}$$

The heat exchanges by radiation $\dot{Q}_r$ and convection $\dot{Q}_c$ are a function of the surface temperature $T_{sf}$ and the mean radiant temperature $T_w$. Both $\dot{Q}_r$ and $\dot{Q}_c$ are given by (158) and (159):

$$\dot{Q}_r = 3{,}96 \times 10^{-8} \times f_{cl} \times \left[\left(T_{sf} + 273.15\right)^4 - (T_w + 273.15)^4\right] \tag{158}$$

$$\dot{Q}_c = f_{cl} \times h_c \times (T_{sf} - T_{cab}) \tag{159}$$

Where $f_{cl}$ is the clothing factor, defined as the ratio of the clothing surface area to the body surface area. The factor $f_{cl}$ is calculated according to the thermal insulation $I_{cl}$ $[m^2.°C/W]$:

$$f_{cl} = \begin{cases} 1.00 + 1.290 \times I_{cl} & if\ I_{cl} \leq 0.078 \\ 1.05 + 0.645 \times I_{cl} & if\ I_{cl} > 0.078 \end{cases} \tag{160}$$

At steady state, the heat exchange by convection and radiation, equals to heat exchange between skin and clothes. After algebraic rearrangement, this equality permits to compute the surface $T_{sf}$ by (161):

$$T_{sf} = T_{sk} - I_{cl} \times (\dot{Q}_c + \dot{Q}_r) \tag{161}$$

The convection coefficient $h_c$ depends on the flow regime. Convection can be either natural or forced. In the first case, the air is calm, and characterized by a convection coefficient that depends on temperature difference:

$$h_{c,n} = 2.38 \times (T_{cl} - T_{cab})^{0.25} \tag{162}$$

Convection can be also forced. The air is usually propelled by a ventilation system with a speed $v_{air}$. In this case, the convection coefficient is given by (163):

$$h_{c,f} = 12.1 \times \sqrt{v_{air}} \tag{163}$$

The convection coefficient $h_c$ is often taken as the maximum of $h_{c,n}$ and $h_{c,f}$

$$h_c = \max(h_{c,n}, h_{c,f}) \tag{164}$$

Based on the PMV, Fanger proposed a complementary index, called the predicted percentage of dissatisfied (PPD). The PPD represents the expected percentage of people who are thermally uncomfortable in an environment for a given PMV. Fanger. established experimentally that there is always a minimum of 5% dissatisfied even if the PMV equals to zero. The relationship between the PPD and the PMV is given by (165).

$$PPD = 100 - 95 \times \exp(-0.0335 \times PMV^4 - 0.2179 \times PMV^2) \tag{165}$$

### *4.4. Equivalent temperature*

The PMV thermal sensation index have been used extensively in the literature to evaluate thermal comfort, even in transient conditions and a small number of persons. Usually, the PMV index succeeds to evaluate correctly thermal comfort in uniform thermal conditions, in moderate climate. However, when hot and cold ambiances are considered, the PMV index tends to underestimate or overestimate thermal sensation depending on the situation. This stems from the fact that PMV model assumes that thermal comfort can be evaluated through the heat balance with the surroundings.

The equivalent temperature is a thermal comfort criterion, more suitable to vehicular environment, than the other above-mentioned thermal comfort indices.

The equivalent temperature is defined as the temperature of an imaginary enclosure (Figure 21) with the mean radiant temperature equal to air temperature and still air in which a person has the same heat exchange by convection and radiation as in the actual conditions. This definition concerns the whole body of a human being, but can be extended to local area or individual segments. Usually, we refer by global equivalent temperature when thermal comfort is evaluated for the whole body, and by local equivalent temperature when body segments are concerned.

The equivalent temperature can be seen as a measure of the effect of non-evaporative heat loss of the human body. This heat loss is correlated to a given thermal (dis)comfort level, evaluated according to the Mean Thermal Vote (MTV) scale [24] (Table 3):

| | |
|---|---|
| Much too hot | +3 |
| Too hot | +2 |

| | |
|---|---|
| Comfortable but hot | +1 |
| Neutral | 0 |
| Comfortable but cold | -1 |
| Too cold | -2 |
| Much too cold | -3 |

Table 3. MTV scale (Comfort scale)

Therefore, for a given set of thermal conditions, the resultant equivalent temperature correspond to a given thermal comfort. This relationship allows to determine the set of equivalent temperatures that belong to a given comfort zone. A graphical representation was proposed by Nilsson [24], where for each segment $i$, thermal comfort is plotted as a function of local equivalent temperature. Such a diagram, is composed from three zones. The green zone represents the range of the local equivalent temperatures $[T_{eq,min}^{(i)}, T_{eq,max}^{(i)}]$ that corresponds to the comfortable zone. The bold dash line represent equivalent temperature set points $T_{eq,sp}^{(i)}$ and corresponds to the ideal comfort. The red and blue zones represent the "hot comfortable" and "cold comfortable" zones, where the driver feels either hot or cold but in a comfortable way. The equivalent temperatures data $T_{eq,min}^{(i)}$, $T_{eq,max}^{(i)}$ and $T_{eq,sp}^{(i)}$ were extracted from Nilsson thesis [24], and corresponds to equivalent temperature collected from experiment on manikin dressed lightly, seated in experimental vehicle cabin, in summer conditions.

It is important to note that the diagram represented in Figure 20.b correspond to a given clothing, relative to a summer weather . Other diagrams exists in the literature for different clothing, worn for instance in spring and winter. Figure 20.a shows the comfort diagram for a subject dressed more lightly than the previous one. Distinguishing these diagrams according to thermal insulation, instead of temperature or relative humidity of the ambiance, stems probably from the fact that thermal properties of the ambiance are controllable. The clothing remains however a driver's choice.

In next chapters, two clothing levels will be studied. In the first one, the driver is dressed in an informal way (to do entertainment activities for instance) and wears a t-shirt, a short and shoes. In the second one, he adopts a formal dress code (to go the work space for instance) and wears a shirt, underpants, trousers, socks and shoes.

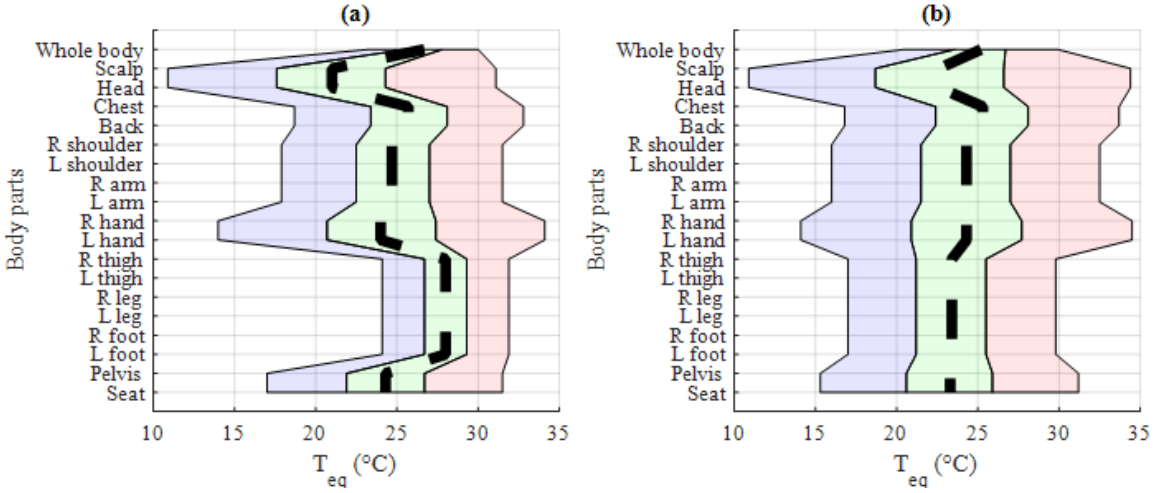


Figure 20. Comfort zone diagram for a driver dressed in a : (a) informal way, (b) formal way

In the following, we will model the equivalent temperature for a given segment $i$, according to its definition. In the Figure 21, the subject is exposed to two different environments. We assume that the posture, the activity level and the clothing are the same in both environments. The first one is the "real"

environment with a given $T_{cab}$,$T_w$ and $v_{air}$, where the thermal manikin exchanges $\dot{Q}_{real}$ with the surroundings by convection and radiation. The second environment satisfies the following conditions:

- Temperature is uniform: $T_{cab} = T_w = T_{eq}$
- Still air: $v_{air} = 0\ m/s$
- The heat exchange $\dot{Q}_{eq}$ is assumed to be only by convection and radiation. Also, it equals $\dot{Q}_{real}$.

One can formalize this definition mathematically, for a given segment $i$, by setting the local equivalent temperature $T_{eq}^{(i)}$ as the solution of the equation (166):

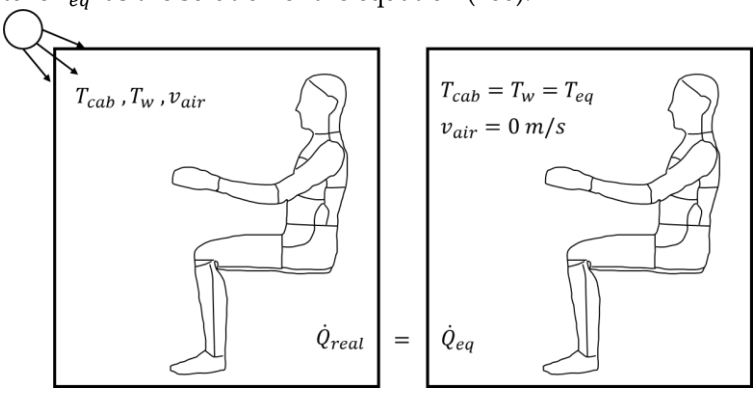


Figure 21.Definition of the equivalent temperature

$$\dot{Q}_{real}^{(i)} = \dot{Q}_{eq}^{(i)}\left(T_{eq}^{(i)}\right) \tag{166}$$

where $\dot{Q}_{real}^{(i)}$ is the sum of the heat exchange by convection $\dot{Q}_c^{(i,4)}$ and the radiation $\dot{Q}_r^{(i,4)}$, both calculated by the thermo-physiological model. The heat exchange $\dot{Q}_{real}^{(i)}$ is thus, given by (167) :

$$\dot{Q}_{real}^{(i)} = \dot{Q}_c^{(i,4)} + \dot{Q}_r^{(i,4)} \tag{167}$$

The term $\dot{Q}_{eq}^{(i)}$ is the equivalent heat exchange by convection and radiation for an air temperature and mean radiant temperature equal to $T_{eq}^{(i)}$, and a null air speed. $\dot{Q}_{eq}^{(i)}$ is expressed as the following (168):

$$\dot{Q}_{eq}^{(i)} = \dot{Q}_{c,eq}^{(i)} + \dot{Q}_{r,eq}^{(i)} = f_{cl}^{(i)} A_b^{(i)} h_c^{(i)}\left(T_{eq}^{(i)} - T_{sf}^{(i)}\right) + f_{cl}^{(i)} A_b^{(i)} h_r^{(i)}\left(T_{eq}^{(i)} - T_{sf}^{(i)}\right) \tag{168}$$

where $A_b[m^2]$ denotes the surface area of the segment $i$, $h_c^{(i)}[\mathrm{W}/(°C.m^2)]$ and $h_r^{(i)}[W/(°C.m^2)]$ refers to convection and radiation heat transfer coefficient, defined by (123) and (125), and evaluated at null air speed $v_{a,eff} = 0$. The term $T_{sf}^{(i)}[°C]$ is the surface temperature, related to skin temperature by means of intrinsic insulation $I_{cl}^*$ (eq (126)).

Considering these definitions of $\dot{Q}_{real}$ and $\dot{Q}_{eq}$, one could solve the equation (166) for $T_{eq}^{(i)}$ for each a given segment $i$.

The global equivalent temperature is deduced, by taking the weighted sum of local equivalent temperature by the segments area:

$$T_{eq} = \frac{\sum_{i=1}^{16} A_b^{(i)} \times T_{eq}^{(i)}}{\sum_{i=1}^{16} A_b^{(i)}} \tag{169}$$

# 5. Conclusions

This chapter presented an enhanced Tanabe thermo-physiological model of human body, together with three thermal comfort indices. The objective behind these models is to build a thermal comfort criterion for our energy management system.

Firstly, we presented the passive system, in which we detailled the body segments, the body layers, and the heat exchanges within the human body, and with the surrounfing environment. Indeed, we have seen that the metabolic heat is produced within the body. Then, it is distributed over body regions by blood circulation and is carried to the body surface by conduction. Heat is then lost to the surrounding by convection, radiation, and evaporation. For each heat exchange mode, we gave the governing equations developped by Tanabe himself, except for heat exchange by convection and radiation. The latters were extracted from Fiala model. Furthermore, the expression of surface temperature was added to the model, for thermal comfort assessment needs.

Secondly, we presented the active system, which is closed loop controller predicting regulatory responses of the central nervous system. The active system plays the major role on regulating the internal temperature of human body, around 37°C for a resting man through four mechanisms: shivering, vasodilatation, vasoconstriction and sweating. For each mechanism, the governing equation were expressed as function of head core error signal and an integrated cutaneous signal.

Finally, the thermal comfort was defined in the last section. Three comfort indices were introduced: temperature and relative humidity set point, the PMV/PPD index, and the equivalent temperature. Altough the first index was straightforward to present, since it is based on set point values and comfort intervals, the two others needed to be detailled and modelled. The PMV/PPD that combines a simplified model of the passive system, and empiric expression developed by Fanger. It assesses the thermal comfort by an integer, ranging from -3 to 3, where the value 0 corresponds to the ideal one. In contrast, the equivalent temperature index needs a multi-segmental model of human body, that computes at least the heat excahnges by convection and radiation, and the surface temperatures. The comfort level is evaluated by reporting the calculated equivalent temperature into the comfort zone diagram.

The next chapter will formalize the optimization problem of our energy management system and solve it by the dynamic programming algorithm. The study will focus first on a thermal comfort criterion based on equivalent temperature. An extensive simulations will be conducted for different weather and traffic scenarios. Then, the same optimization problem will be solved for criterions based on temperature and relative humidity set point, and the PMV/PPD index. A comparative study will be then performed.

# Chapter IV : Optimal energy management approach

*En un mot, pour tirer la loi de l'expérience, il faut généraliser ;*
*c'est une nécessité qui s'impose à l'observateur le plus circonspect.*
Henri Poincaré, La valeur de la science

## Contents

This chapter presents an optimal energy management approach, for the system presented in the previous chapters, which is composed from the powertrain, the HVAC system and the driver/passengers. As a reminder, the objectives are to ensure the driver to arrive to his destination, and to propose the best thermal comfort level within the available energy limitation. This can be formalized as an optimization problem subjected to energy constraint and to the system dynamics, in which the thermal comfort criterion is based on equivalent temperature index.

The optimization problem is solved by the dynamic programming algorithm, for a time horizon equal to the duration of the trip. We assume therefore a perfect knowledge of the traffic and weather conditions during the whole upcoming trip and we analyze which energetic gains or trade-off are possible. The idea is that, if there is not enough embedded energy for both traction and optimal thermal comfort for the planned trip, the thermal comfort should be diminished in order to save energy and allow the vehicle to reach its final destination or the next charging point. In some situations, it may be wiser to consider slowing down in order to allow a better thermal comfort.

The models presented in chapter II and III have been implemented in the dynamic programing optimization algorithm and simulations were run for a large number of scenarios corresponding to different weather and traffic conditions, from congested urban to highway. The multiplicity of test cases helps understanding the system behavior in different life conditions and allows to sketch an overview of the compromises that can be done between thermal comfort and consumption. As expected, the thermal comfort is found to have a stronger energetic impact in urban conditions. Possible trade-off between travel time and thermal comfort is also investigated. The study has been conducted for hot climates, but the proposed principles could be extended to cold conditions.

The remainder of this chapter is organized as follows. Section 1 presents the proposed thermal comfort management approach, formulated as an optimization problem and solved by dynamic programing. Section 2 presents results for a large number of weather and traffic scenarios. Two tests-cases are analyzed. The first one highlights the trade-offs between HVAC system consumption and comforts. The second one studies the effect of reducing vehicle speed on total consumption, while ensuring the ideal thermal comfort. A comparison between different thermal comfort index is conducted at the end of this section, to evaluate the gains of using the equivalent temperature index. Section 3 summarizes the conclusions of the chapter.

Optimal energy management

The objective of the HVAC management system is to control the cabin temperature, the relative humidity and the wall temperature, so that the driver feel comfortable at the lowest energy cost. On the other hand, the driver first priority is to reach his destination, and the battery state of charge may be too low in order to insure the ideal comfort during the whole trip. Hence, it may be necessary to limit the power provided to the air conditioning, in order to extend the vehicle driving range up to its final destination. This energy management problem can be described as an optimal control problem and we propose to use dynamic programing to solve it. In the rest of this section, we first introduce the cost function and then formulate the optimal energy management problem.

### *1.1. Cost function*

In this section, the local equivalent temperature is used to build a global thermal comfort criterion, since it is more accurate and suitable to vehicular environment than other thermal comfort indexes such as a set point temperature. We recall that the equivalent temperature is defined as the temperature of an imaginary enclosure with still air, and a wall temperature equal to the air temperature, in which a person has the same heat exchange by convection and radiation as in the actual conditions. The global

comfort criterion is built by comparing each local equivalent temperature to the local ideal comfort temperature $T_{eq,sp}^{(i)}$. As a first approximation, we propose to use a global quadratic discomfort criterion $L$, defined for the whole body by (170):

$$L = \sum_{i=1}^{16} A_{sf}^{(i)} \left( \frac{T_{eq}^{(i)} - T_{eq,sp}^{(i)}}{T_{eq,max}^{(i)} - T_{eq,min}^{(i)}} \right)^2 \tag{170}$$

where $T_{eq,sp}^{(i)}$ is the set point equivalent temperature for the body segment $i$, whereas $T_{eq,max}^{(i)}$ and $T_{eq,min}^{(i)}$ are the upper and lower limit values of the comfort zone. We use equivalent temperature data extracted from Nilsson thesis [24].

### *1.2. Problem formulation*

The role of the proposed energy management is to determine the best HVAC system control in order to reach the lowest thermal discomfort for a given trip. The trip is modeled by a driving cycle, which is known in advance. The powertrain model is used to calculate the instantaneous power required for the electric machine $P_{EM}(t)$, and then the total energy required for the traction over the considered trip. The difference between the energy embedded in the battery at the beginning of the trip and the energy needed for the traction gives the energy available for air conditioning, denoted by $E_{HVAC\ max}$.

The control model of the whole system is built by assembling the models of the four sub-systems previously described in section 3. Two state variables are defined: $x = [T_{cab}, \phi_{cab}, T_{wall}]'$, which corresponds to the thermodynamic quantities needed to estimate the passenger's thermal comfort, and $E_{HVAC}$ the energy consumed by the HVAC system. The four control variables are gathered in a vector, denoted by $u = \left[N_{comp}, \dot{m}_{air}, \alpha, \beta\right]'$ The outside weather and the vehicle speed constitute the disturbance vector $w = [T_{ext}, \phi_{ext}, \dot{q}_{sun}, v]'$.

Using these notations, the overall system model can be formalized by equation (171) and (172), where $f$ is the thermodynamic evolution equation of the system.

$$\dot{x}(t) = f\big(x(t), u(t), w(t)\big) \tag{171}$$

$$\dot{E}_{HVAC}(t) = \mathrm{P}_{HVAC}\big(x(t), u(t), w(t)\big) \tag{172}$$

Other operational constraints, such as the battery power and electrical current limitation, complete the model:

$$0 \leq P_{HVAC} \leq P_{HVAC,max} \tag{173}$$

$$0 \leq I_{HVAC} \leq I_{HVAC,max} \tag{174}$$

The optimization problem consists in determining the command $u^*$ that minimizes the global discomfort (175) for the considered trip.

$$u^* = \underset{u}{\operatorname{argmin}} J(u) \text{ where } J(u) = \int_0^{t_{fin}} L\left(x\big(u(t)\big)\right) dt \tag{175}$$

The finite energy constraint is an inequality end constraint (176).

$$E_{HVAC}\left(t_{fin}\right) \leq E_{HVAC\ max} \tag{176}$$

### *1.3. Problem solving by dynamic programing*

The optimization problem is discretized in time and energy and reformulated as a multi-stage decision-making process, which can be effectively solved by DP algorithms [178] [179]. The system state trajectory is discretized in the 2d-space $\{(t_k, \tilde{E}_{HVAC,i})\}_{k=0,N;i=0,M}$, where $t_k$ and $\tilde{E}_{HVAC,i}$ respectively denote the discrete values of time $t_k = t_0 + k.\Delta t$, and energy $\tilde{E}_{HVAC,i} = i.\Delta E_{HVAC}$. In the rest of this chapter, the subscript $k$ refers to the value of the corresponding quantity at time $t_k$. Using this notation, the command to look for is $u = \{u_k\}_{k=0,N-1}$ and equations (171)-(175) become (177)-(179).

$$J(u) = \sum_{k=0}^{N-1} L(x_k(u_k))) \times \Delta t \tag{177}$$

$$x_{k+1} = x_k + f(x_k, u_k, w_k) \times \Delta t \tag{178}$$

$$E_{HVAC,k+1} = E_{HVAC,k} + P_{HVAC}(x_k, u_k, w_k) \times \Delta t \tag{179}$$

Furthermore, since we work in the discretized space $(t_k, \tilde{E}_{HVAC,i})$, $u_k$ must be such that $E_{HVAC,k+1}$ is equal to one of the discrete values $\tilde{E}_{HVAC,i}$.

DP is usually implemented starting from a given final state, with a backward exploration phase, followed by a forward reconstruction phase. In our case, the final state of the system is not known: we work with an inequality constraint on the final battery state of energy and no constraint at all on the final thermal parameters in the cabin. Hence, dynamic programming must be applied starting from the initial state, with a forward exploration phase followed by a backward reconstruction phase. This does not change the algorithm principle and allows to study the influence of the HVAC energy consumption on the global comfort criterion $J$, simply by starting the backward reconstruction phase from any final energy state.

#### 1.3.1. Forward phase

Dynamic programming is based on the cost-to-go 2d-table $V_{k,i}$ defined by (180).

$$V_{k,i} = \min_{\{u_l\}_{l=0,k-1}} \sum_{l=0}^{k-1} L\big(x_l(u_l)\big) \times \Delta t \text{ with } 1 \leq k \leq N \text{ and } 0 \leq i \leq M \tag{180}$$

$V_{k,i}$ represents the lowest cost (cumulated thermal discomfort) to go from the initial state $(t_o, \tilde{E}_{HVAC,M})$ to the intermediate state $(t_k, \tilde{E}_{HVAC,i})$. At the final time step $t_N$, $V_{N,i}$ represents the lowest thermal discomfort from the initial state $(t_o, \tilde{E}_{HVAC,M})$ to any final state $(t_N, \tilde{E}_{HVAC,i})$.

The cost-to-go table and optimal command matrix $u^*_{k,i}$ are recursively constructed thanks to (181) and (182), where $u_{k,j,i}$ represents the command to go from $(t_k, \tilde{E}_{HVAC,j})$ to $(t_{k+1}, \tilde{E}_{HVAC,i})$ and $\Delta V_{k,i,j}$ the corresponding cost. An infinite cost is affected if the transition from $(t_k, \tilde{E}_{HVAC,j})$ to $(t_{k+1}, \tilde{E}_{HVAC,i})$ is impossible:

$$V_{k+1,i} = \min_{u_{k,j,i}} \left\{V_{k,j} + \Delta V_{k,j,i}\right\}, 1 \leq k \leq N-1 \tag{181}$$

$$u^*_{k,i} = \underset{u_{k,j,i}}{\operatorname{argmin}} \left\{V_{k,j} + \Delta V_{k,j,i}\right\}, 1 \leq k \leq N-1 \tag{182}$$

The determination of $u_{k,j,i}$ that leads to $\tilde{E}_{HVAC,i}$, involves inversing (178) to determine the compressor speed $N_{comp,k,j,i}$. It involves in the meantime, minimizing the thermal discomfort with respect to the other HVAC control variables $\dot{m}_{air,k,j,i}$, $\alpha_{k,j,i}$ and $\beta_{k,j,i}$.

Solving numerically the equation (178) for $u_{k,j,i}$, requires to: (i) discretize the control variable's intervals, (ii) build a relationship between the discrete control variables and $E_{HVAC,k+1}$, (iii) apply the relationship to $\tilde{E}_{HVAC,i}$ to find $u_{k,j,i}$. Let us formalize this mathematically.

At time $t_k$, we apply the discrete command vector $u_{k,j} = [N_{comp,k,j}, \dot{m}_{air,k,j}, \alpha_{k,j}, \beta_{k,j}]'$ to equation (178). The quantities $N_{comp,k,j}$, $\dot{m}_{air,k,j}$,$\alpha_{k,j}$ and $\beta_{k,j}$ refer to discrete values of the control variables, defined as multiples of a given discrete steps $\Delta N_{comp}$, $\Delta\dot{m}_{air}$, $\Delta\alpha$ and $\Delta\beta$.

Firstly, The equation (178) is used to numerically calculate the state vector $x_{k+1} = [E_{HVAC,k+1}, T_{hab,k+1}, \phi_{hab,k+1}, T_{wall,k+1}]'$ that stems from applying the command vector $u_{k,j}$. From there, we compute the corresponding thermal comfort criterion $L_{k+1}$ and the energy consumption $E_{HVAC,k+1}$ at time $t_{k+1}$. This can be formalized by the two functions $\Phi$ and $\Psi$ defined by (183) and (184).

$$L_{k+1} = \Phi(u_{k,j}) \tag{183}$$

$$E_{HVAC,k+1} = \Psi(u_{k,j}) \tag{184}$$

Secondly, we invert the relationship (184) with respect to $u_{k,j}$ and apply the inverse function to the tabulated $\tilde{E}_{HVAC,i}$. Doing this for a four variable's command vector, is computationally time consuming and may be a complex task. We decided then to invert $\Psi$ only with respect to one control variable. For a given $N_{comp,k,j}$, we choose the combination of $\dot{m}_{air,k,j}$, $\alpha_{k,j}$ and $\beta_{k,j}$ that lead to the least discomfort $L_{k+1}$. Next, the relation (184) is inverted with respect to $N_{comp,j}$.Let us denote heating and ventilation control's variables by $u_{HV,k,j} = [\dot{m}_{air,k,j}, \alpha_{k,j}, \beta_{k,j}] \in \mathbb{R}^3$. The optimal control $\mathrm{u}^*_{HV,k,j}$ and the corresponding consumed energy $E^*_{HVAC,k+1}$ for a given $N_{comp,k,j}$, are given respectively by (185) and (186).

$$\mathrm{u}^*_{HV,k,j}(N_{comp,k,j}) = \underset{u_{HV,k,j}\in\mathbb{R}^3}{argmin}\{\Phi(N_{comp,k,j}, u_{HV,k,j})\} \tag{185}$$

$$E^*_{HVAC,k+1} = \Psi(N_{comp,k,j}, \mathrm{u}^*_{HV,k,j}) \tag{186}$$

The function defined by (186) is strictly monotonic, and hence admit an inverse function $\Psi^{-1}$ with respect to $N_{comp,k,j}$. This inverse function is, finally, applied to $\tilde{E}_{HVAC,i}$ to get the control variable $N_{comp,k,j,i}$, and hence the command vector $u_{k,j,i}$ :

$$u_{k,j,i} = [N_{comp,k,j,i}, \mathrm{u}^*_{HV,k,j}(N_{comp,k,j,i})] \tag{187}$$

From there, equation (178) is used to compute the corresponding air cabin temperature and relative humidity, the wall temperature, and the corresponding cost function.

The function $\Psi$ cannot be directly obtained. Hence a mapping (look-up table) is built, based on numerical simulations performed for different $N_{comp,j}$ and $u_{HV,k,j}$. The computation of $N_{comp,k,j,i}$ is done by linear interpolation.

Of course, one needs to first calculate $V_{1,i}$ before starting the recursive algorithm. In addition, several 2d-tables are used in order to keep track of the intermediate optimal commands and corresponding thermal states.

### 1.3.2. Reconstruction phase

After completing the forward exploration phase, the optimal command matrix $u^*_{k,i}$ is used for the reconstruction phase and determining the optimal trajectories for any given consumed energy. The reconstruction phase is done backward, starting from a given energy at the final time $t_f$. For a given $(t_f, \tilde{E}_{HVAC,j})$, the optimal command matrix is used to determine optimal state at time $t_{f-1}$, and then at $t_{f-2}$, $t_{f-3}$ and so on, until reaching the initial time $t_0$. This process enables to reconstruct the optimal trajectories of $T_{cab}(t)$, $RH_{cab}(t)$ and $T_w(t)$ and other variables such as $P_{bat}(t)$, for any quantity of energy consumed by the HVAC over the whole trip.

# 2. Simulation results

This section presents the application of the proposed approach and shows its effectiveness in managing thermal comfort on a given trip, for a large number of meteorological and traffic conditions. The first test-case scenario highlights the tradeoffs that can be reached between the energy consumption of the HVAC system and the thermal comfort. Some preliminary results regarding the HVAC consumption for ideal comfort in different weather conditions will first be presented. In particular, the relationship between steady state cabin temperature and solar radiation will be studied. Thereafter, we illustrate the possible tradeoff for a given energy consumption, in different weather and traffic situations. Finally, we analyze the state variables, the commands, and the thermoregulation mechanisms trajectories. The second test-case illustrates how the speed profile can be adjusted to reduce the total consumption and preserve the ideal thermal comfort. This is done by applying a $k$-homothety on the speed profile, so that the driver travels the same distance at a lower speed. Results show how the traction and HVAC system's energy consumption evolve as a function of $k$. The results gives also, in some situations, the possible energy savings. At the end of this section, the same studied optimization problem is solved for other thermal comfort criterions. The objective is to assess the thermal comfort gains when using equivalent temperature index.

## *2.1. Simulation data and technical characteristics of the vehicle*

Each scenario corresponds to a trip completed in given weather and traffic conditions, with a certain type of clothing. As the HVAC system efficiency depends on the vehicle speed, four traffic conditions, representative of congested urban, fluid urban, road and highway environments are modeled, using the UL1, UF1, R2 and A2 INRETS driving cycles (Figure 22). The INRETS driving cycles are a set of ten driving cycles built with data logged around Lyon, France, in various driving environments. The main characteristics of these cycles are reported in Table 4. In order to build a trip with a duration around one hour, each type of cycle is repeated several times. When doing so, one obtains speed profiles with a duration of 1 hour 06 min.

| INRETS Cycles | Duration [s] | Distance [km] | $\overline{v}$ $[km/h]$ | $\sigma_v$ $[km/h]$ |
|---|---|---|---|---|
| UL1 | 806 | 0.85 | 3.81 | 4 |
| UL2 | 812 | 1.67 | 7.42 | 6.22 |
| UF1 | 681 | 1.88 | 9.92 | 9.74 |
| UF2 | 1055 | 5.61 | 19.14 | 12.97 |
| UF3 | 1068 | 7.23 | 24.36 | 16.43 |
| R1 | 889 | 7.79 | 31.55 | 21.94 |

Table 4. Characteristics of the UL1, UF1, R2 and A2 INRETS driving cycles

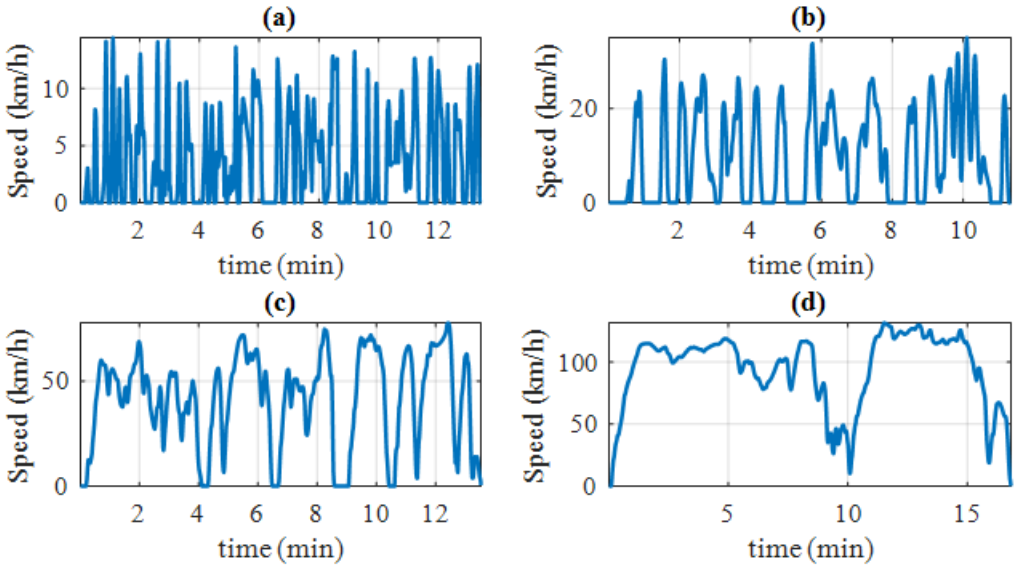


Figure 22. INRETS driving cycles : (a) UL1, (b) UF1, (c) R2 (d) A2

Weather scenarios with the same duration than the speed profiles have been defined. In these scenarios, the solar irradiance is kept constant, while the external temperature and humidity evolve, according to parametrized time profiles. The temperature profile $T_{ext}(t)$ is shown in Figure 23. The temperature rises from $T_{ext,0}$ at the beginning of the trip to $T_{ext,0} + 2°C$ at halfway, and then decreases back to $T_{ext,0}$. As for humidity, weather conditions are described in terms of relative humidity $RH$, whereas thermodynamic equation are written using the specific humidity $\phi$. The relationship between these two quantities is given by (188), where $P_{atm}$ is the atmospheric pressure and $P_{sat}$ denotes the saturated vapor pressure of water at the considered temperature.

$$RH_{ext}(t) = \frac{P_{atm} \times \phi_{ext}(t)}{P_{sat}\left(T_{ext}(t)\right) \times (\phi_{ext}(t) + 0.622)} \tag{188}$$

The chosen scenario assumes a linear increase of the specific humidity over the whole trip, from $\phi_{ext,0}$ to $\phi_{ext,0} + 0.05$, where $\phi_{ext,0}$ is calculated according to the values of the initial relative humidity $RH_{ext,0}$ and temperature $T_{ext,0}$. Figure 23 shows an example of the time evolution of the temperature, relative humidity and solar power for the following scenario parameters : $T_{ext,0} = 35\ °C$, $RH_{ext,0} = 55\%$ and $\dot{q}_{sun,0} = 1000\ W/m^2$.

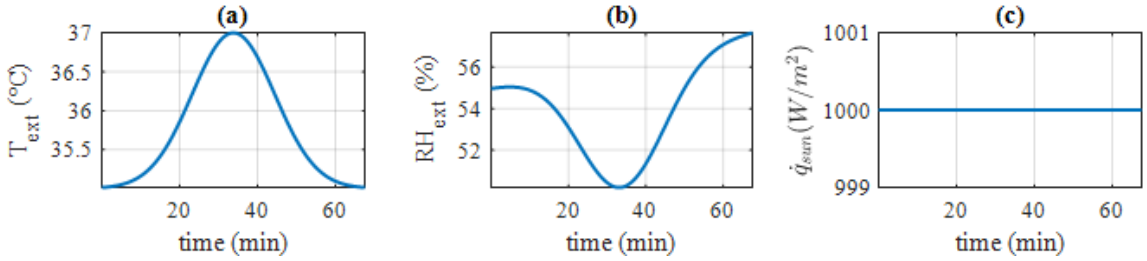


Figure 23. Weather scenario for the given parameters $T_{ext,0} = 35\ °C$, $RH_{ext,0} = 55\%$ and $\dot{q}_{sun,0} = 1000\ W$. (a) Temperature, (b) Relative humidity and (c) Solar irradiance

Different values of the parameters $T_{ext,0}$, $RH_{ext,0}$, and $\dot{q}_{sun,0}$ correspond to different weather conditions. In order to explore a wide range of weather conditions, without focusing on the weather profile itself, we have combined together the following values: $T_{ext,0}[°C] \in \{28\,;31\,;34\,;\,37\}$, $RH_{ext,0} \in \{0.35\ ;0.55\ ;0.75\}$, $\dot{q}_{sun,0}[W/m^2] \in \{0\,;500\,;1000\}$. This results in a total number of 36 weather scenarios.

Two clothing levels are considered. The first one corresponds to a driver dressed in an informal way (t-shirt, short and shoes), whereas the second one corresponds to a formal dress code (shirt, underpants, trousers, socks and shoes). The comfort zones corresponding to each dress code are depicted in Figure 20.

The initial temperature and relative humidity in the cabin are assumed the same as outside (vehicle parked in the shade). For all the tested scenarios, we consider that driver is at rest, seated.

In summary, the benchmark built from the abovementioned scenarios corresponds to four given trips carried out in 36 weather conditions and two clothing levels. This combination brings the total number of simulated test cases at $4 \times 36 \times 2 = 288$ .The vehicle is assumed to be a small size car, with a nominal power around 60 kW and a 40 kWh Li-ion battery. A summary of simulation data is reported in Table 5. The results are presented in the following sections.

| Data | Values |
|---|---|
| External temperature | $T_{ext,0}[°C] \in \{28\,;31\,;34\,;\,37\}$ |
| External relative humidity | $HR_{ext,0} \in \{0.35\;;0.55\;;0.75\}$ |
| Solar irradiance | $\dot{q}_{sun,0}[W/m^2] \in \{0\,;500\,;1000\}$ |
| Driving cycles | INRETS A2, R2, UF1, UL1 |
| Driver's clothing | Formal and informal clothing |
| Vehicle | Small size electric vehicle |
| Electric motor power | 60 kW |
| Battery capacity | 40 kWh |

Table 5. Summary of simulation data

## *2.2. Ideal comfort results*

This section reports some observations and analysis on three physical quantities : i) the HVAC system consumption $E^*_{HVAC}$ that provide ideal comfort, ii) the ratio $r^*_{HVAC}$ of $E^*_{HVAC}$ with respect to the total energy (sum of $E^*_{HVAC}$ and traction energy), iii) the steady state cabin temperature $T_{cab,steady}$. Figure 24 and Figure 25 summarize the results of $E^*_{HVAC}$ for a driver dressed in an informal and formal way, in a suburban traffic (i.e., INRETS R2 driving cycle). The graphs show the evolution of $E^*_{HVAC}$ as a function of solar irradiance for different $T_{ext,0}$ and $RH_{ext,0}$. We observe that $E^*_{HVAC}$ is an increasing function of the solar irradiance, outside temperature and relative humidity except in some situations. When the driver is dressed in an informal way, and that $\dot{q}_{sun} = 0$ and $T_{ext,0} \geq 32$°C, the energy consumed during the trip does not depend on the outside temperature, nor on the relative humidity. The reason is that at night, the comfort temperature is slightly less than 28 °C, as it will be explained later in this section. This temperature can be maintained by operating the compressor at the minimal rotational regime, using the other control variables. Since the compressor is by far the main consumer in the HVAC system, $E^*_{HVAC}$ is consequently almost the same for all scenarios where $\dot{q}_{sun} = 0$ and $T_{ext,0} \geq 32$°C. The same explanation applies to Figure 25.a.

In a typical hot summer day (i.e., $T_{ext,0} = 32°C$, $RH_{ext,0} = 55\%$, $\dot{q}_{sun} = 1000\ W/m^2$), with a driver dressed in an informal way, $E^*_{HVAC}$ reaches 1.3 kWh. This consumption increases if the driver is dressed in a formal way, and reaches 1.8 kWh for the weather conditions aforementioned.

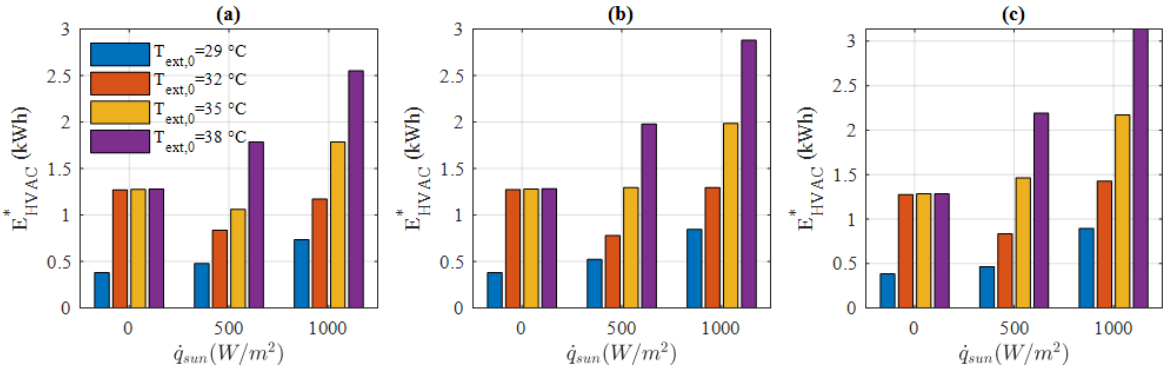


Figure 24. HVAC system consumption $E^*_{HVAC}$ for a driver dressed in an informal way, in suburban traffic (INRETS R2), for four $T_{ext}(t)$ and three $RH_{ext}(t)$ characterized by: (a) $RH_{ext,0} = 35\%$, (b) $RH_{ext,0} = 55\%$, and (c) $RH_{ext,0} = 75\%$

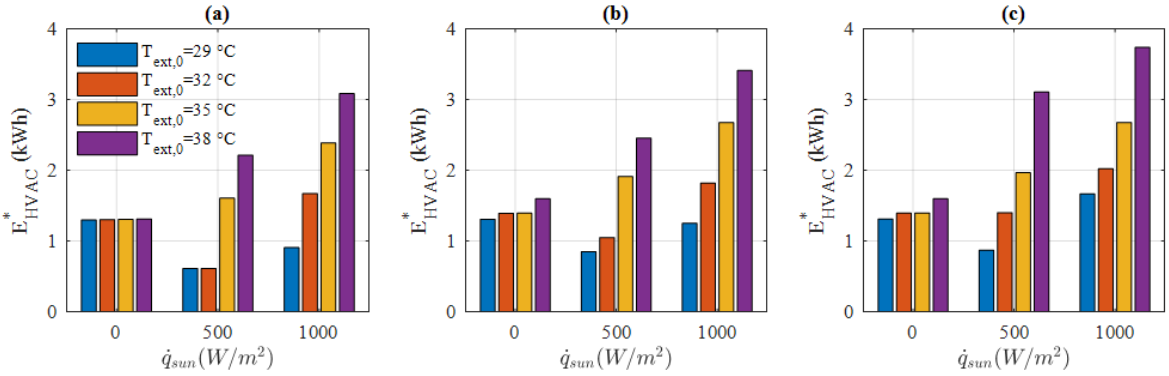


Figure 25. HVAC system consumption $E^*_{HVAC}$ for a driver dressed in a formal way, , in suburban traffic (INRETS R2), for four $T_{ext}(t)$ and three $RH_{ext}(t)$ characterized by: (a) $RH_{ext,0} = 35\%$, (b) $RH_{ext,0} = 55\%$, and (c) $RH_{ext,0} = 75\%$

Figure 26 and Figure 27 summarize the results of $r^*_{HVAC}$ for a driver dressed in the two ways presented in the previous section, in a moderate humid weather (i.e., $RH_{ext,0} = 55\%$). The graphs show the values of $r^*_{HVAC}$ with respect to four driving cycles: INRETS A2, R2, UF1 and UL1, for different $T_{ext,0}$ and $\dot{q}_{sun,0}$.The results illustrate the relative high value of $r^*_{HVAC}$ in congested and fluid urban conditions. This is mainly due to the low traction energy at low speed. For instance, in a typical hot summer day, in congested urban condition, this ratio reaches 80%. Results also show that for the same driving cycle, this ratio increases with outside temperature and solar irradiance.

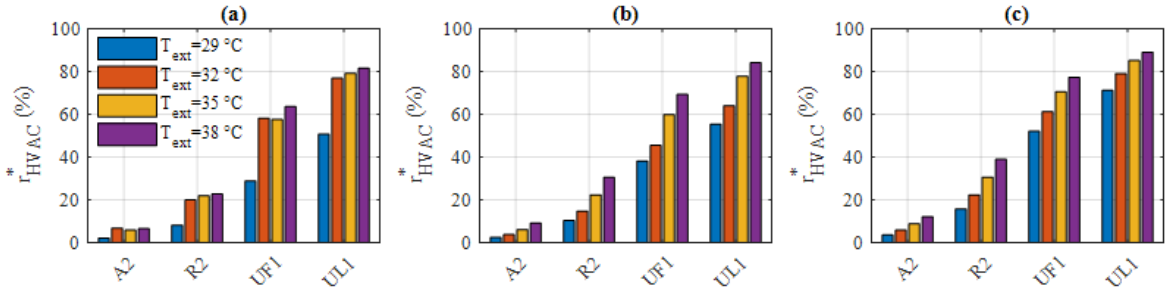


Figure 26. HVAC system consumption ratio $r^*_{HVAC}$ for a driver dressed in an informal way, in moderate humid weather ($RH_{ext,0} = 55\%$), for four $T_{ext}(t)$ and three $\dot{q}_{sun,0}$ characterized by: (a) $\dot{q}_{sun,0} = 0W$, (b) $\dot{q}_{sun,0} = 500W$, and (c) $\dot{q}_{sun,0} = 1000W$

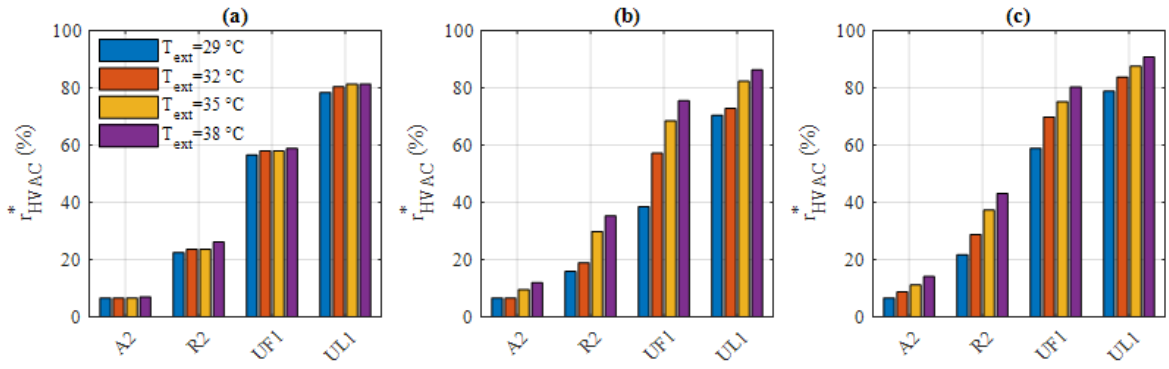


Figure 27. HVAC system consumption ratio $r^*_{HVAC}$ for a driver dressed in a formal way, in moderate humid weather ($RH_{ext,0}$ = 55%), for four $T_{ext}(t)$ and three $\dot{q}_{sun,0}$ characterized by: (a) $\dot{q}_{sun,0} = 0W$, (b) $\dot{q}_{sun,0} = 500W$, and (c) $\dot{q}_{sun,0} = 1000W$

It is worth underlining the capacity of the equivalent temperature model to account for the cabin wall radiant temperature. Figure 28 shows the optimal path of cabin temperature for an informal and formal clothing, for all 36 weather scenarios, for the driving cycle INRETS R2, when there is enough energy to ensure ideal comfort. We notice that the steady state temperature value is a function of solar irradiance. The same remark can be reported for the optimal path of wall temperature (Figure 29).

For a given clothing and solar irradiance, the steady state wall and cabin temperature are computed. Then, they are averaged over the number of outside temperatures and relative humidity profiles, characterized by $T_{ext,0}$ and $RH_{ext,0}$. As an illustrative example, we report results for different solar irradiance levels $\dot{q}_{sun} \in \{0\,;500\,;1000\}$ and two dress codes, for the INRETS R2 driving cycle. Table 6 reports the corresponding mean steady state cabin temperature $\bar{T}_{cab,steady}$, and the mean steady state wall temperature $\bar{T}_{wall,steady}$, for the same trip. In the absence of solar irradiance (at night), $\bar{T}_{wall,steady} = 28.3°C$, the ideal thermal comfort is obtained for $\bar{T}_{cab,steady} = 28.0°C$. In sunny conditions, all other parameters being equals, $\bar{T}_{wall,steady} = 40.0°C$ and ideal comfort requires a cooler ambient temperature $\bar{T}_{cab,steady} = 24.1°C$ and more energy. If the driver is dressed in a formal way, in sunny conditions, all other parameters being equal, $\bar{T}_{wall,steady} = 38.0°C$ and ideal comfort requires an even cooler ambient temperature $\bar{T}_{cab,steady} = 22.1°C$, and hence consumes more energy.

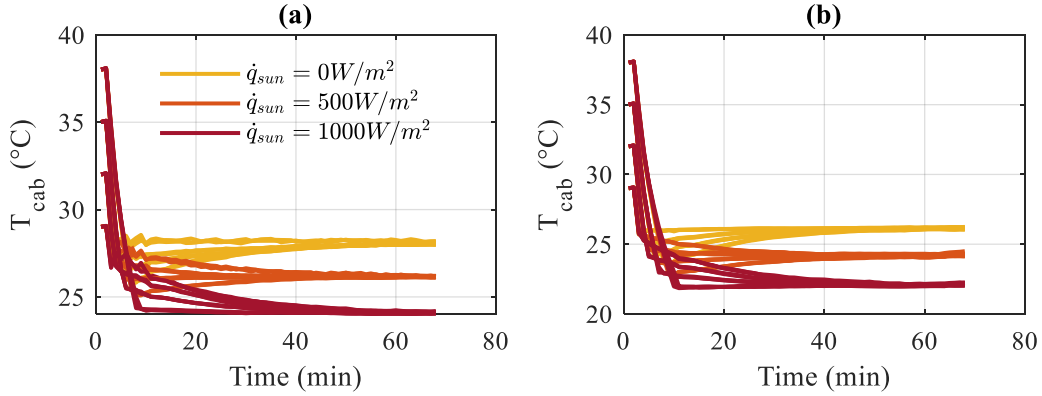


Figure 28. Cabin temperature trajectories for ideal comfort, for a driver dressed in (a) informal way, (b) formal way

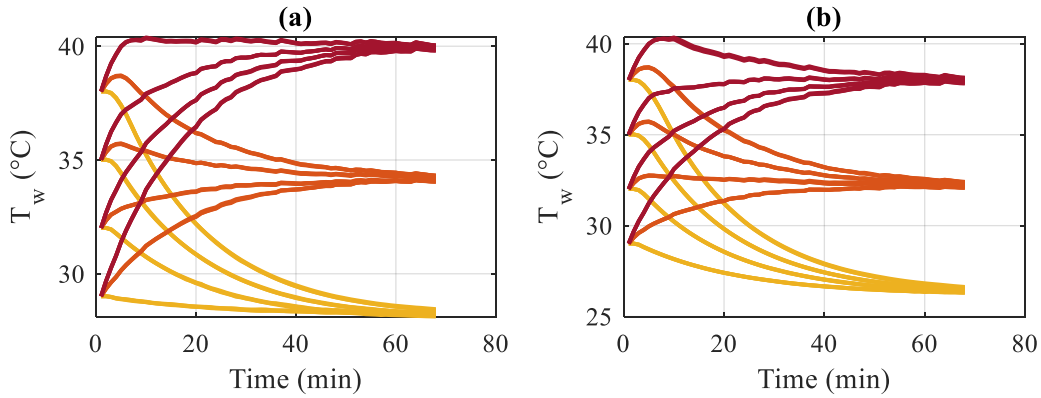


Figure 29. Wall temperature trajectories for ideal comfort, for a driver dressed in (a) informal way, (b) formal way

| *Clothing* | $\dot{q}_{sun}$ $[W/m^2]$ | $\overline{T}_{wall,steady}$ $[°C]$ | $\overline{T}_{cab,steady}$ $[°C]$ |
|---|---|---|---|
| Informal | 0 | 28.3 | 28.0 |
| | 500 | 34.2 | 26.2 |
| | 1000 | 40.0 | 24.1 |
| Formal | 0 | 26.4 | 26.1 |
| | 500 | 32.2 | 24.2 |
| | 1000 | 38.0 | 22.1 |

Table 6. Mean steady state cabin temperature and wall temperature for ideal comfort for different solar radiations and clothing ensembles

### *2.3. Test case 1: Thermal discomfort vs energy cost trade-off*

In this test-case, we investigate how the thermal comfort management algorithm adjusts thermal comfort according to the energy available for the HVAC system in different situations. The thermal comfort management algorithm computes the control actions that optimize the thermal comfort according to the energy available for the HVAC system. For the same available energy, these actions differ, depending on external conditions. In order to show that, we fix an available energy of 1.1 kWh, and analyze how thermal comfort is adjusted for different driving cycle and a given outside temperature. The same analysis will be done for different outside temperature profiles and a given driving cycle. All simulations have been performed for $RH_{ext,0} = 55\%$, $\dot{q}_{sun} = 1000\ W/m^2$ and two clothing ensembles.

The global thermal comfort is assessed by the cos t function L. Since the latter is a quadratic criterion, we prefer to present the optimization results in terms of mean global equivalent temperature $T_{eq,rms}$, which is a function of L, and defined by (189)

$$T_{eq,rms} = \frac{\sqrt{L} * \sum_{i=1}^{16}\left(T_{eq,max}^{(i)} - T_{eq,min}^{(i)}\right) + \sum_{i=1}^{16} T_{eq,sp}^{(i)}}{16} \tag{189}$$

Figure 30.a shows the optimal global equivalent temperature $T_{eq,rms}$ as a function of the HVAC system consumption $E_{HVAC}$ for four INRETS driving cycle : INRETS A2, R2, UF1 and UL1 , an outside temperature profile with $T_{ext,0} = 32°C$, and a driver dressed with an informal clothing. Those curves correspond to Pareto frontiers of the $\left(E_{HVAC}, T_{eq,rms}\right)$ bi-criteria optimization problem. For an available energy of 1.1 kWh, $T_{eq,rms}$ is deduced from the Pareto frontiers. The corresponding mean local equivalent temperatures $\overline{T}_{eq,i}$, over the last 15 min of the trip, are reported in Figure 30.b in the comfort

zones diagram. The same results are reported for a driver dressed with a formal clothing in Figure 30.c and Figure 30.d.

As expected, the optimal global equivalent temperature is a decreasing function of the HVAC system consumption. For example, in suburban conditions, $T_{eq,rms}$ is improved by 2°C at an additional energy cost of 430 Wh (1.1% of the battery capacity). We notice also that the thermal comfort consumes more energy in urban traffic (INRETS UL1 and UF1) than in highway (INRETS A2). This can be explained by two concomitant effects. The first one is due to a better efficiency of the HVAC at high vehicle speed $v_{veh}$. In other words, for the same power consumed by the compressor, the heat exchange at the evaporator is more important. This is mainly due to a better heat evacuation at the condenser, since the air flow generated by the moto-ventilator group is an increasing function of vehicle speed. The second effect is due to the important convection heat exchange between the vehicle's walls and the exterior at high $v_{veh}$. For the same cabin temperature, the wall temperature is lower, which induce less power consumption.

This vehicle speed effect, has consequences on thermal comfort management. For a given energy, the discomfort decreases with vehicle speed. This is shown in Figure 30.a, where the difference between optimal global equivalent temperatures in a INRETS A2 and UL1 driving cycle, is about 0.75°C, for the same consumed energy. Another representation of this effect is shown in Figure 30.b. The mean local equivalent temperatures lies in hot comfortable zone for an INRETS UF1 and UL1 driving cycle. However, almost all $\bar{T}_{eq,i}$ are close to the set point equivalent temperatures (comfortable zone), for an INRETS A2 for the same consumed energy of 1.1 kWh. The same conclusions can be formulated from the results depicted in Figure 30.c and Figure 30.d, where the driver is dressed in a formal way. However, we notice also that 1.1 kWh is not sufficient to achieve a good thermal comfort for a formal clothing, due to a higher thermal insulation. As consequence, the driver might feel discomfort in a INRETS A2 driving cycle, especially in lower body parts (Figure 30.d).

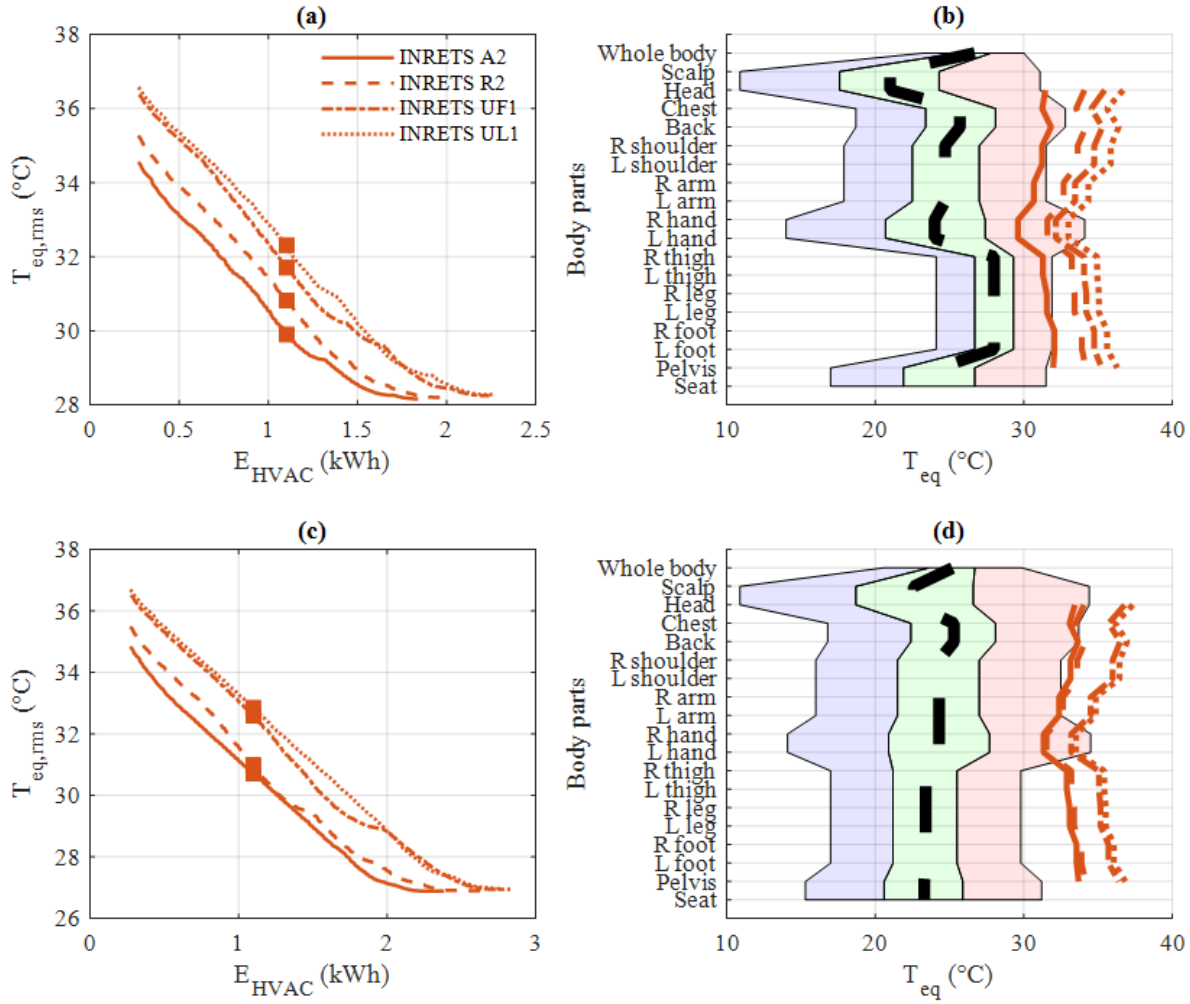


Figure 30. Pareto frontiers and the mean local equivalent temperatures for four INRETS cycles, in which $T_{ext,0} = 32°C$, $RH_{ext,0} = 55\%$, $\dot{q}_{sun} = 1000\ W/m^2$, and where the driver is dressed in: (a) & (b) informal way, (c) & (d) formal way.

Let us now do the same analysis for a given driving cycle, and different outside temperature profiles. Figure 31.a shows the Pareto frontiers for three outside temperature profiles characterized by $T_{ext,0}[°C] \in \{32\ ;35\ ;\ 38\}$, for an INRETS R2 driving cycle and a driver dressed with an informal clothing. For an available energy of 1.1 kWh, the optimal global equivalent temperature $T_{eq,rms}$ is deduced from the Pareto frontiers. The corresponding mean local equivalent temperatures $\bar{T}_{eq,i}$,, are reported in Figure 31.b in the comfort zone diagram. The same results are reported in Figure 31.c and Figure 31.d for a driver dressed with a formal clothing.

We notice that the outside temperature has a strong influence on thermal comfort, larger than the vehicle speed. For an available energy of 1.1 kWh, a good thermal comfort is achieved for an outside temperature of $T_{ext,0} = 29°C$. In this situation, the optimal global equivalent temperature is about 28°C and the corresponding local equivalent temperatures, are presented in Figure 31.b, all lie in the comfortable green zone. However, in hotter weather, $T_{eq,rms}$ increases significantly and it reaches 35°C for $T_{ext,0} = 38°C$ for the same available energy. In this harsh scenario, all $T_{eq,i}$ lie outside the comfort zone, which means that the driver experiences an uncomfortable hot thermal sensation in the last 15 min of the trip. The same conclusions can be formulated in the case of the driver dressed in a formal way (Figure 31.c and Figure 31.d).

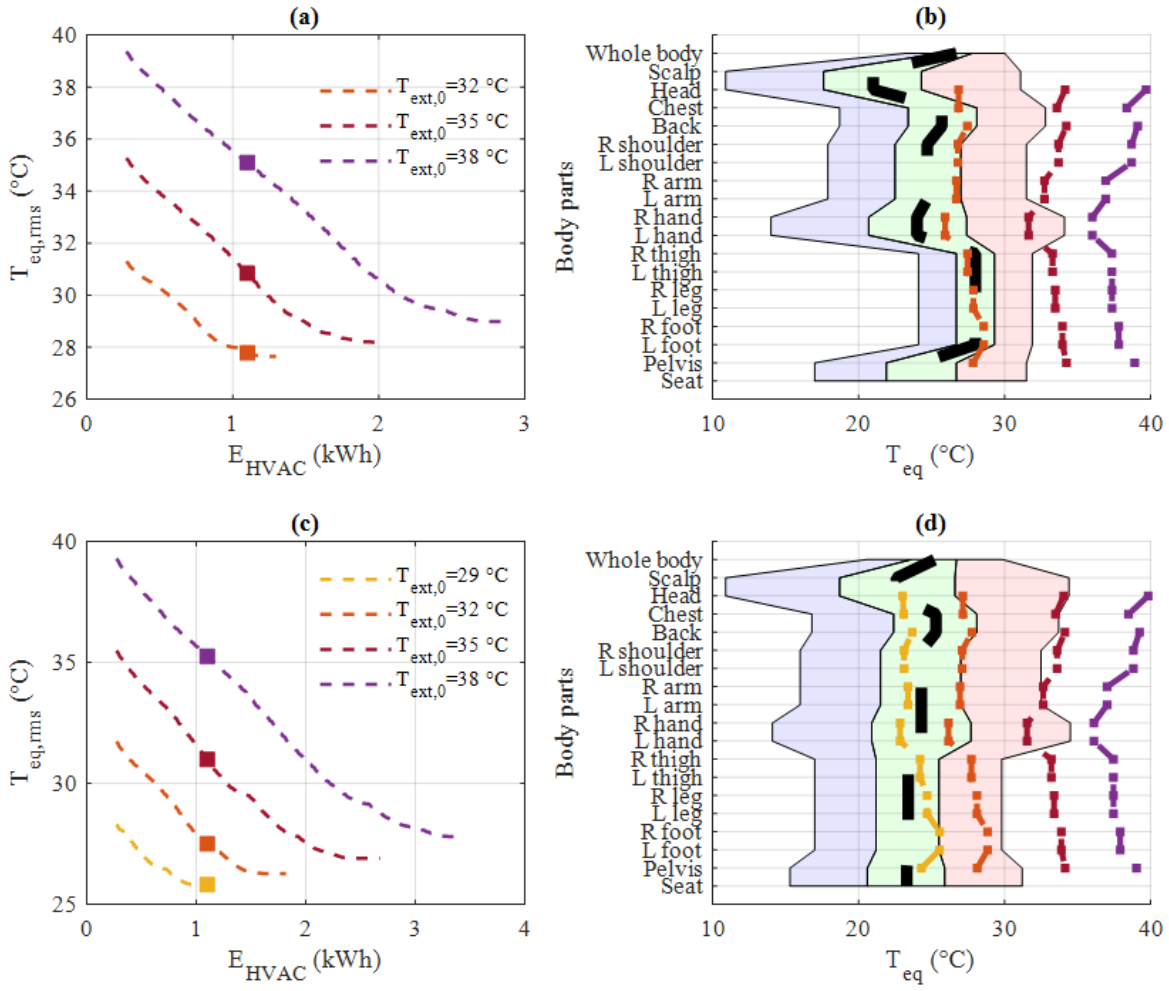


Figure 31. Pareto frontiers and the mean local equivalent temperatures for different outside temperature profiles, for a driver dressed in: (a) & (b) informal way, (c) & (d) formal way.

As stated before, the algorithm takes actions on the HVAC system in order to choose the optimal thermal comfort for a given available energy. Hence, it is worth analyzing these actions and their consequences on the cabin physical quantities and the driver's thermo-physiological responses.

Figure 32 shows the temporal evolution of cabin temperature and relative humidity that corresponds to colored squares plotted in Figure 31.c. The yellow cabin temperature profile has the ideal shape since it leads to an ideal comfort. First, the cabin temperature drops at the beginning of the trip, when the hot cabin needs to be cooled down. This phase cannot be reduced below a certain time due to thermal inertia and the maximum power of the HVAC system. The temperature decreases afterwards until reaching 22 °C, which is the comfort temperature at $\dot{q}_{sun} = 1000\ W/m^2$ (Table 6) For an outside temperature $T_{ext,0} = 32°C$, the available energy is not sufficient to maintain ideal comfort over the whole trip. In this situation, after the cooling phase, the cabin temperature is maintained around 23.7°C for 20 min, then it increases slowly until reaching 26°C at the end of the trip. For even higher $T_{ext,0}$, the temperature at final time can reach 34°C.

Figure 32 shows also the temporal evolution of two HVAC control variables: the compressor rotation speed (Figure 32.c) and the air flow (Figure 32.d). The compressor speed is set at its maximum value during the cooling phase, then it is adjusted according to the available energy, in order to provide the "reachable" thermal comfort. For instance, if the available energy cannot ensure the ideal comfort,

the compressor speed is set at the minimum regime before the end of the trip (red and purple curve). In this situation, the air flow and the heating ratio are slightly increased to adjust the thermal comfort.

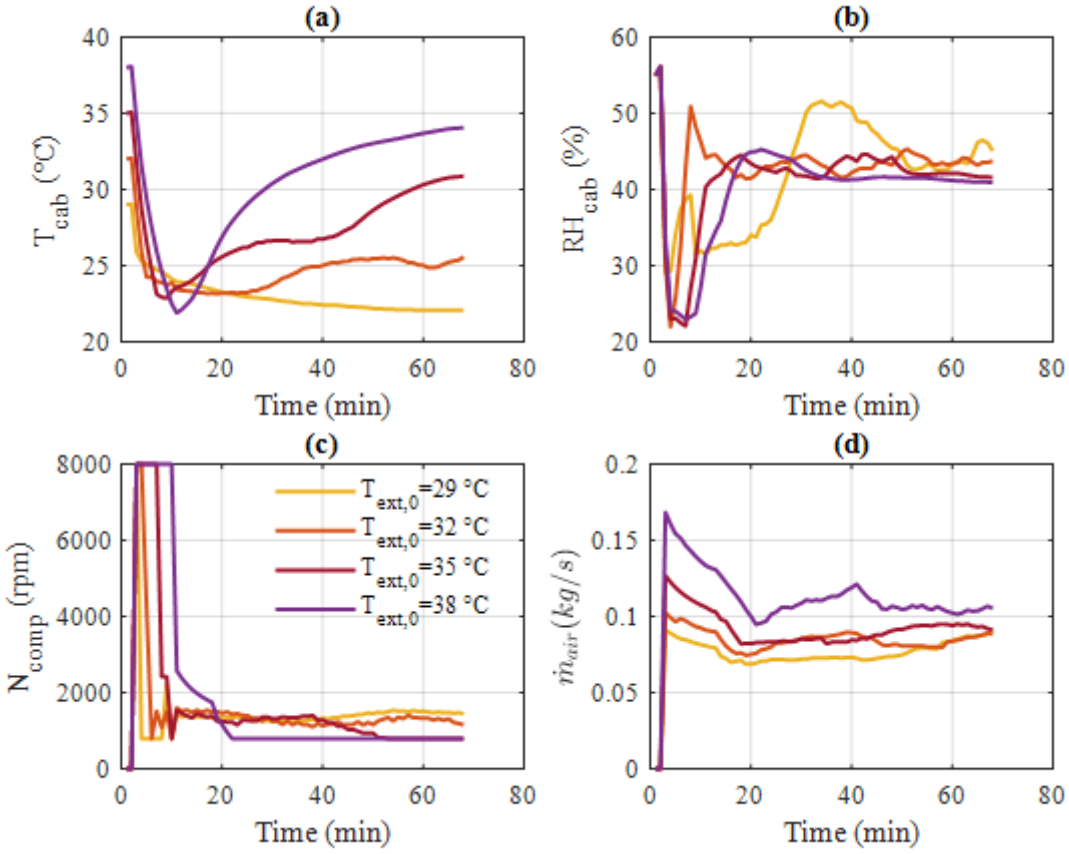


Figure 32. Cabin and command trajectories for a driver dressed in a formal way and for different outside temperature profiles: (a) Temperature, (b) Relative humidity, (c) Compressor rotational speed, (d) Air flow.

The driver thermo-physiological response is represented by four thermoregulation mechanisms: sweating, shivering, vasodilatation and vasoconstriction. Figure 33 shows the temporal evolution of these mechanisms, which correspond to the colored squares in Figure 31.c. Firstly, we observe in Figure 33.b that shivering is null for all outside temperatures. This result is expected since simulations are performed exclusively in hot weather. In such conditions, the human body regulates its internal temperature through sweating and vasodilatation. The first mechanism allows to evacuate metabolism heat production, through evaporation. The second one, increases the diameter of veins to improve the heat exchange between the skin and the ambient environment. In a comfortable state, both mechanism should be disabled, and the body is in thermal equilibrium. Figure 33.a and Figure 33.b illustrate these phenomena, especially when the outside temperature is $T_{ext,0} = 29°C$ and that all local equivalent temperatures lie in the comfort zone (Figure 31.d). This behavior of sweating and vasodilatation mechanism is also noticed at some extent for $T_{ext,0} = 32°C$. Although the sweating mechanism is negligible, the vasodilation is still activated in order to regulate internal temperature. This could be explained by the fact that the local equivalent temperatures of lower body parts, lies in "hot but comfortable zone" (red line in Figure 31.d). For higher outside temperature, the temporal evolution of both thermo-physiological mechanism is similar to the cabin temperature's one.

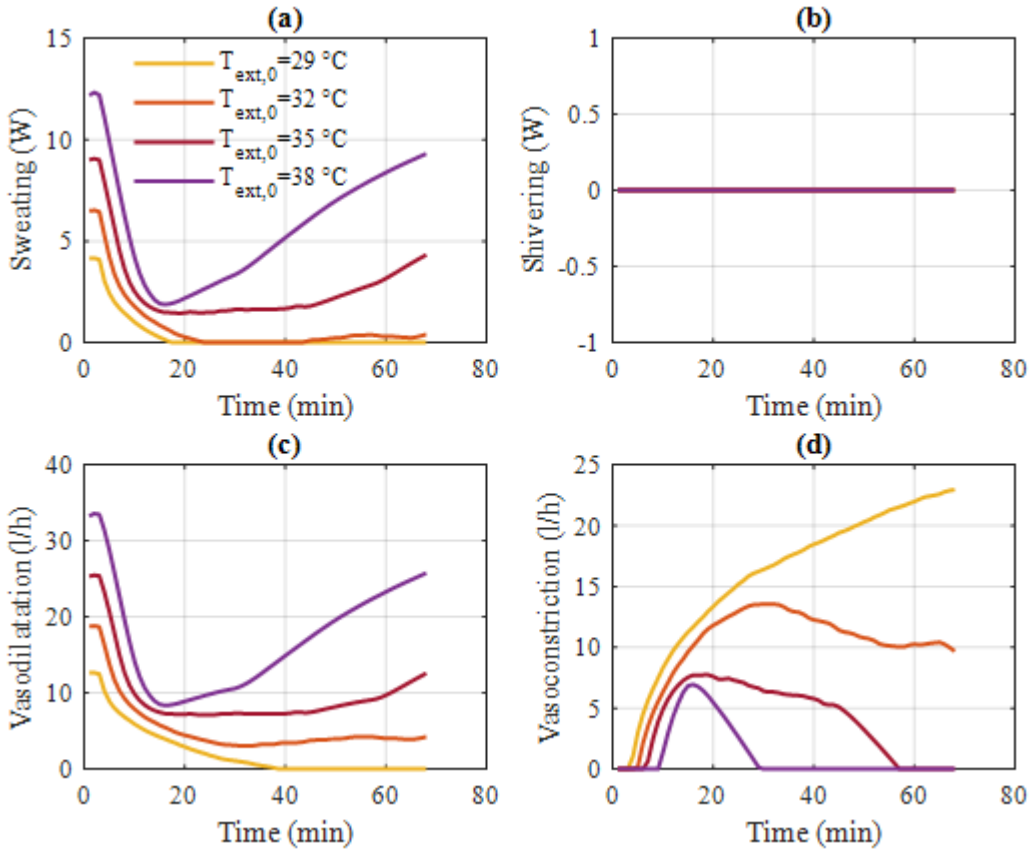


Figure 33. Thermoregulation mechanisms trajectories for a driver dressed in a formal way and different outside temperature profiles: (a) Sweating, (b) Shivering, (c) Vasodilatation, (d) Vasoconstriction.

The same Pareto frontier analysis can be done for different relative humidity and solar irradiance profiles, all other quantities being fixed. For this analysis, we assume an available energy of 1.1 kWh, an outside temperature profile characterized by $T_{ext,0} = 35°C$, and an R2 driving cycle. Figure 34 show the pareto frontiers for $\dot{q}_{sun,0}[W/m^2] \in \{0\ ;500\ ;1000\}$, $RH_{ext,0} = 55\%$ for a driver dressed in an informal (Figure 34.a) and formal way (Figure 34.c). For an available energy of 1.1 kWh, the optimal global equivalent temperature $T_{eq,rms}$ is deduced from the Pareto frontiers. The corresponding mean local equivalent temperatures $\bar{T}_{eq,i}$,, are reported in Figure 34.b and Figure 34.d in the comfort zone diagram. The same type of results is shown in Figure 35 for $RH_{ext,0}[\%] \in \{35\ ;55\ ;75\}$ and $\dot{q}_{sun,0} = 1000\ W/m^2$

We notice that the Pareto frontiers are far from each other when the humidity profile is fixed. This can be interpreted by the fact that solar radiation have a bigger influence on thermal comfort than the relative humidity. In this situation, if the driver is dressed in an informal way, a good thermal comfort can be achieved by consuming 1.1 kWh , especially at night or in cloudy conditions (i.e. $\dot{q}_{sun} = 0\ W/m^2$ or $\dot{q}_{sun} = 500\ W/m^2$). In both case, the optimal global equivalent temperature is about 28°C and the corresponding local equivalent temperatures, presented in Figure 34.b, all lie in the comfortable green zone. However, in sunny conditions, $T_{eq,rms}$ increases significantly and reaches 30.8°C for $\dot{q}_{sun} = 1000\ W/m^2$ for the same available energy. In this scenario, almost all $T_{eq,i}$ lie in the red zone, which means that the driver experiences a hot but comfortable thermal sensation in the last 15 min of the trip. If the driver is dressed in formal way, the same conclusions can be reported except when $\dot{q}_{sun} = 1000\ W/m^2$, in which the lower body parts experience a hot discomfortable sensation (Figure 34.d).

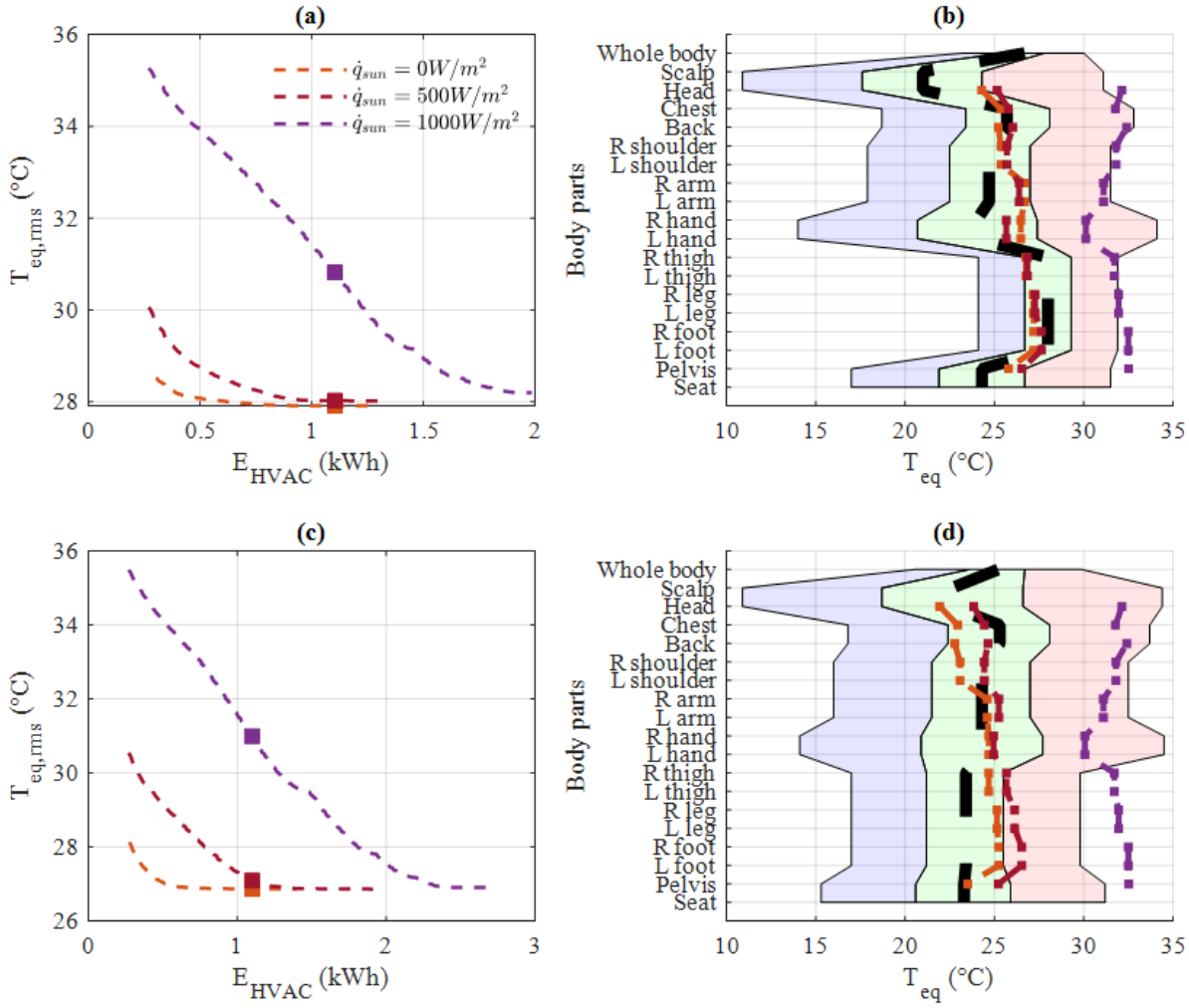


Figure 34. Pareto frontiers and the mean local equivalent temperatures for different solar irradiance, for a driver dressed in: (a) & (b) informal way, (c) & (d) formal way.

It is worth noting again the dependence between solar radiation and cabin temperature. Figure 35 and Figure 36 shows the cabin quantities results for the above mentionned scenario. For a driver dressed in an informal way, the cabin comfort temperature seems to tend respectively to 28°C and 26.2 °C when $\dot{q}_{sun,0} = 0\ W/m^2$ and $\dot{q}_{sun,0} = 500\ W/m^2$. These values corresponds to those reported in Table 6 for ideal comfort. However, in sunny conditions, the optimal temperature trajectory decreases to 25°C after the cooling phase, before increasing dramatically after the 40th minute. Similar observations can be stated in case of a driver dressed in a formal way.

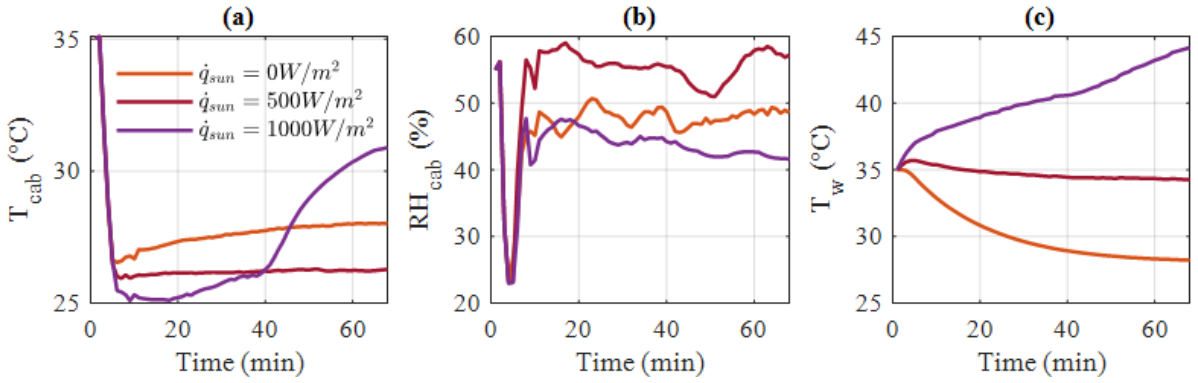


Figure 35.Cabin quantities trajectories for different solar irradiance, for a driver dressed in an informal way, and performing a R2 driving cycle in a hot and moderate humid weather ($RH_{ext,0} = 35°C$ and $RH_{ext,0} = 55\%$) : (a) Cabin temperature, (b) Cabin relative humidity, (c) wall temperature

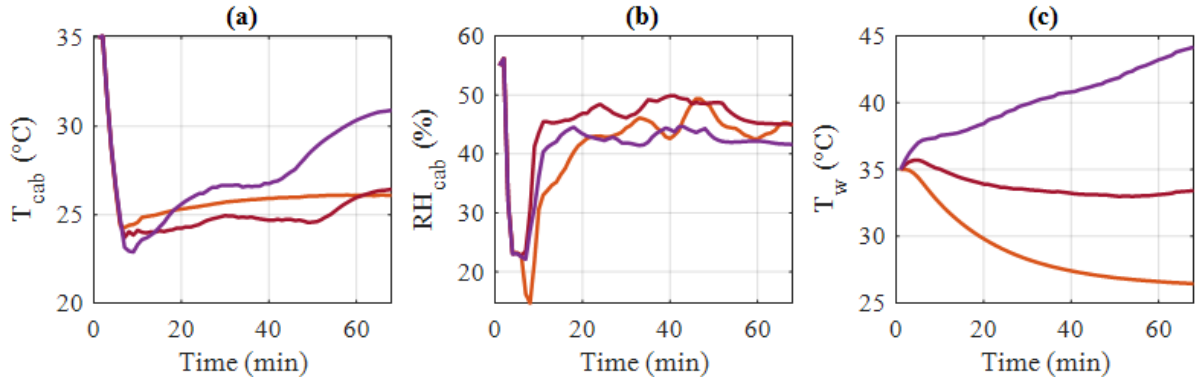


Figure 36.Cabin quantities trajectories for different solar irradiance, for a driver dressed in an formal way, and performing a R2 driving cycle in a hot and moderate humid weather ($RH_{ext,0} = 35°C$ and $RH_{ext,0} = 55\%$) : (a) Cabin temperature, (b) Cabin relative humidity, (c) wall temperature

The same type of Pareto frontier analysis can be conducted for a given solar radiation profile. Figure 37 shows that an available energy of 1.1 kWh is not sufficient to ensure a good thermal comfort. If the driver is dressed in an informal clothing, in a dry weather $RH_{ext,0} = 35\%$, the optimal global equivalent temperature is about 30°C and the corresponding local equivalent temperatures, presented in Figure 37.b, almost all lie outside the comfort zones. Whereas if the drived is dressed in a formal clothing, only the lower body part will feel a discomfortable sensation. This stems from the broad comfort zones that characterize this type of clothing.

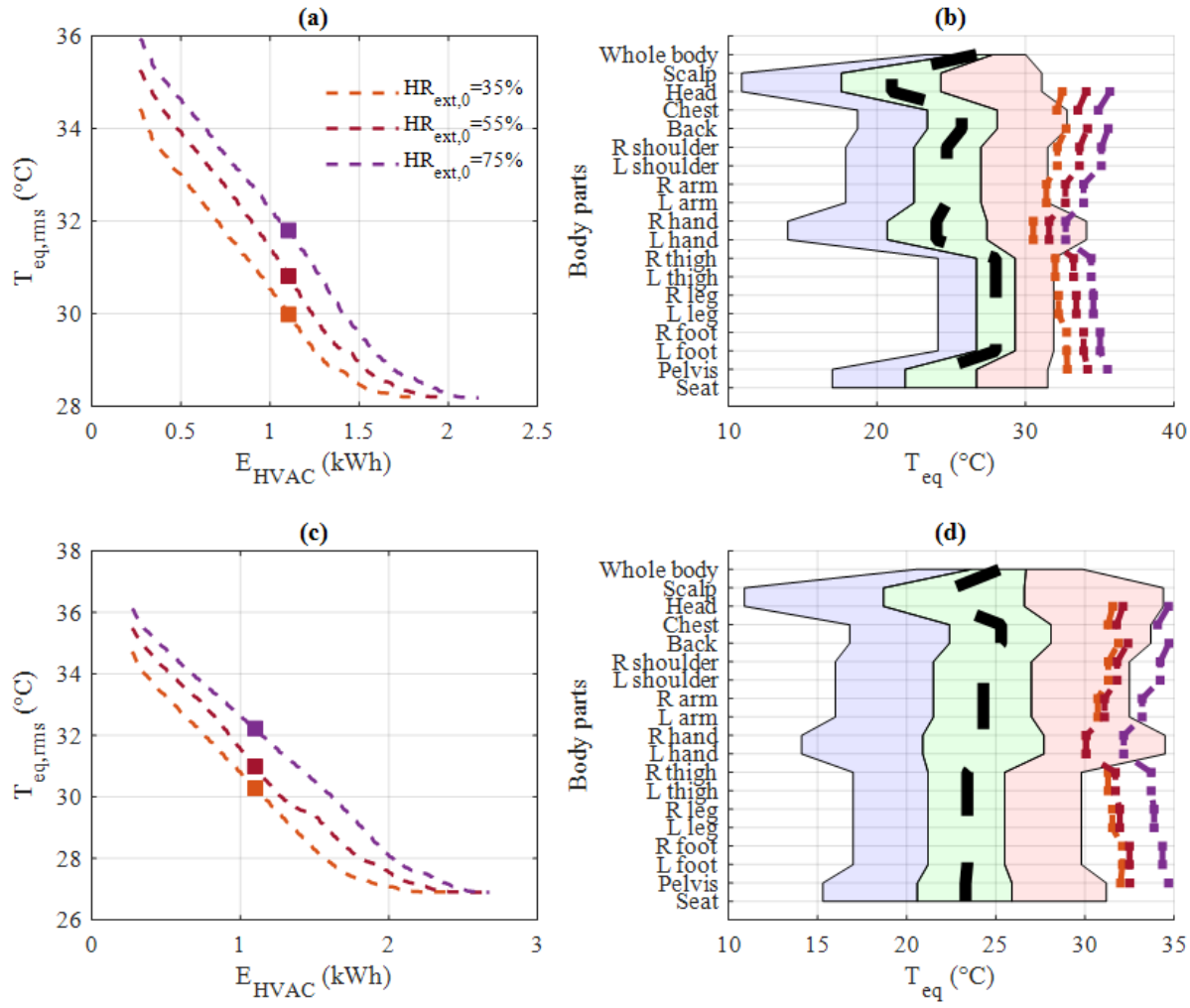


Figure 37. Pareto frontiers and the mean local equivalent temperatures for different outside temperature profiles, for a driver dressed in: (a) & (b) informal way, (c) & (d) formal way.

### *2.4. Test case 2: Vehicle speed vs thermal comfort trade-off*

In the second test case, the driving cycle is modified, so that the driver travels the same distance at a lower speed. Less energy is required for the traction, but more is needed for the ideal thermal comfort, since the trip lasts longer. The idea is to evaluate which effect is dominating, and if there is a possible compromise between the traction and the HVAC system consumption.

A scaling factor $k < 1$ is applied to the speed as follows:

$$v_{new,cycle}(t) = v_{cycle}(t).k \tag{190}$$

By decreasing the values of $k$, one reduces the energy needed for traction, but one also increases the HVAC system energy needed for the ideal thermal comfort. The total energy may be an increasing or a decreasing function of $k$, or a function that have a minimum. Simulations have been conducted on a combination of six INRETS driving cycles: A1, R3, R2, R1, UF3 and UF1, and the following range of outside temperature, relative humidity and solar radiation : $T_{ext}[°C] \in \{33\,,36\,,39\}$, $RH_{ext}[\%] \in \{30\,,50\,,80\}$ and $\dot{q}_{sun}[W/m^2] \in \{0\,,500\,,1000\}$. We assume that the driver is dressed in an informal way and for sake of simplicity, that the weather conditions are not time varying.

First, we will analyze the results for a specific weather condition, then an evaluation of potential energy gains will be assessed for all traffic and weather scenarios. Figure 38.a. shows the traction energy, the HVAC system energy for ideal comfort, and their sum, as a function of $k$ for the following scenario: INRETS R2 driving cycle, $T_{ext} = 36°C$, $RH_{ext} = 50\%$ and $\dot{q}_{sun} = 1000\ W/m^2$. We notice that the total energy presents a minimum for $k = 0.75$. The corresponding energy is 9 kWh, which represents a 0.45 kWh economy if the driver slows down by 25%. If the driver slows down only by 10% (i.e., $k = 0.9$), the energy saving is about 0.35 kWh. Figure 38.b shows the same type of results for the INRETS UF3 driving cycle. For this specific scenario, there is no substantial energy gain if the driver slows down, since the total energy is an increasing function of $k$.

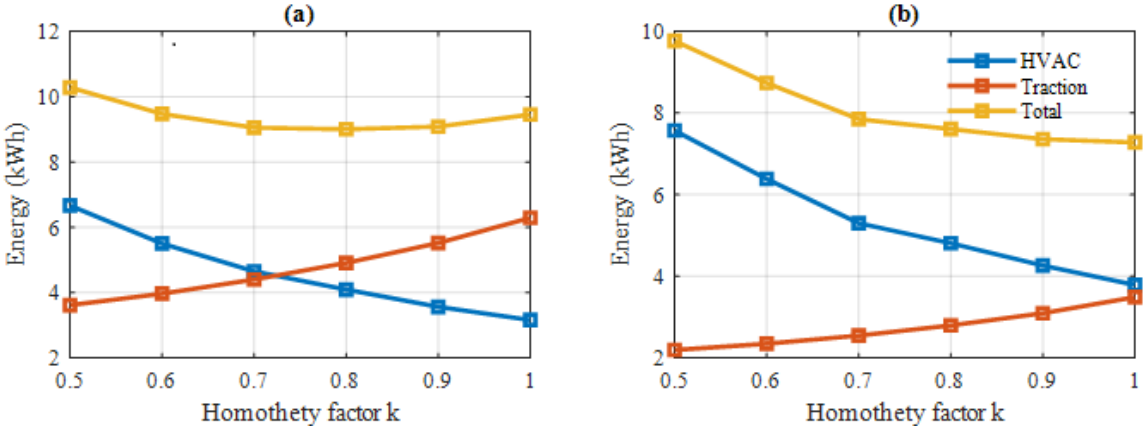


Figure 38. Traction, air conditioning and total energy consumed for a driver dressed in an informal way, for $T_{ext} = 36°C$, $RH_{ext} = 50\%$ $\dot{q}_{sun} = 1000\ W/m^2$, and: (a) INRETS R2, (b) INRETS UF3 driving cycle

Figure 39 shows the total energy as a function of $k$ factor, for the six driving cycles, and the aforementioned weather scenario. The obtained results indicate that for INRETS A2, R3 and R2, the dominant consumption is associated to the traction, and reducing the speed decreases the total consumption. On the contrary, for urban trips, the gain is not obvious, as a decrease of traction energy can be compensated by an increase of HVAC system consumption.

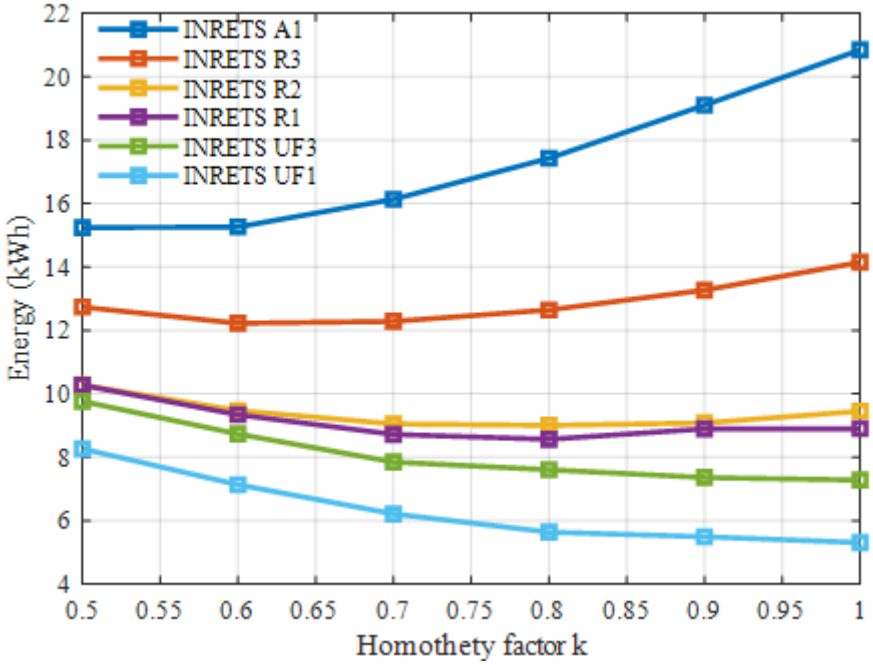


Figure 39 Total energy consumed for a driver dressed in an informal way, for $T_{ext} = 36°C$, $RH_{ext} = 50\%$ $\dot{q}_{sun} = 1000\ W/m^2$, and different driving cycle

Figure 40 reports the energy gain for $k = 0.9$ as a function of $T_{ext}$ in a moderate humid weather $RH_{ext}[\%] = 55\%$ for different solar irradiance $\dot{q}_{sun}[W/m^2] \in \{0\ ,500\ ,1000\}$. Depicted results show that this gain is significant for INRETS R3, R2 and R1 driving cycles, especially at night or in cloudy conditions, and can reach 2.2kWh for INRETS A1. However, it is negligible for urban driving cycles, an even null in sunny conditions.

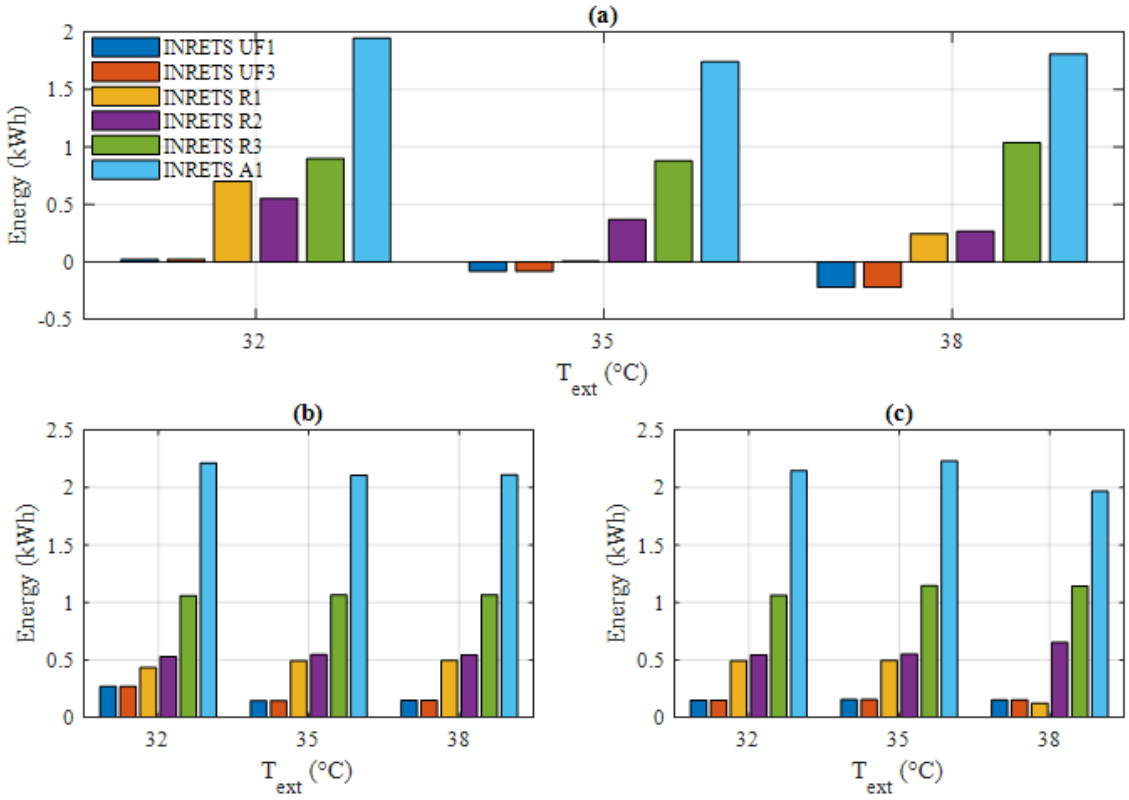


Figure 40. Energy gain at $k = 0.9$ for a driver dressed in an informal way, for different INRETS cycles, for $RH_{ext} = 55\%$, and for : (a) $\dot{q}_{sun} = 1000\ W/m^2$, (b) $\dot{q}_{sun} = 0\ W/m^2$, (c) $\dot{q}_{sun} = 500\ W/m^2$

## *2.5. Comparison between equivalent temperature and other thermal comfort indices*

The use of equivalent temperature as thermal comfort index, was justified by its suitability to vehicular environment, and its abitlity to handle the thermophysiological characteristcs of the human body. This was verified by the results shown in section 2.3. , where we noticed that thermoregularatory requirements for thermal comfort are met. The thermoregulatory mechanisms, especially sweatin, shivering and vasodilatation, were shutted off when all the local equivalant temperature lied on the green zone of the comfort zone diagram.

Nevertheless, one should assess the thermal comfort gains of using the equivalent temperature. This can be done by comparing it to other thermal comfort indices, such as temperature and relative humidity set point, and the predicted mean vote (PMV) index. The idea is to solve the optimization problem defined by (175), for the same set of constraints (171-174) & (176), with the following cost functions (191) and (192):

$$L_{T,RH} = 0.5 \times \left(\frac{T_{cab} - T_{cab,sp}}{T_{cab,sp,max} - T_{cab,sp,min}}\right)^2 + 0.5 \times \left(\frac{RH_{cab} - RH_{cab,sp}}{RH_{cab,sp,max} - RH_{cab,sp,min}}\right)^2 \quad (191)$$

$$L_{PMV} = PMV^2 \quad (192)$$

The optimization problem is solved exactly by the same manner described in section 1.3. . The simulations are conducted for the same weather and traffic scenarios presented in section 2.1. . Additional assumptions are required however when using the PMV index as cost function. We will assume a driver seated at rest, which correspond to a metabolism $M = 58.15\ W/m^2$ $(1\ met)$. We will assume also a driver dressed lightly in a formal way (i.e., a shirt, underpants, trousers, socks and shoes), which correponds sometimes in the litterature [76, 116, 108, 95] to a thermal insulation between 0.4 to 0.6 clo. Other works [180], more specialized in vehicular environment, estimates the global thermal insulation at 1.1 clo, taking into account the sitting position of the driver, and body parts in contact with the seat.

After solving the optimization problem with these new cost functions, the optimal trajectories of command variables (compressor speed, air mass flow, heating ratio, recycling ratio) are collected together with the driver personnal data (metabolsim and local thermal insulation). From there, one can compute the local surface temperature, and heat exchanges by convection and radiation through the coupled model of HVAC system and human thermophysiology. The next step is to the calculate the associated local equivalent temperature trajectories. Finally, for a given energy consumption, one can deduce the global equivalent temperature by (189). This relationship is the Pareto frontier of the considered optimization problem, represented in $(T_{eq,rms}, E_{HVAC})$ plane.

Figure 41 sumarizes the Pareto frontier results of four optimization problem, in which the thermal comfort criterions are based on: i) temperature and relative humidity set point, ii) PMV index with a thermal insulation of 0.5 clo, iii) PMV index with a thermal insulation of 1.1 clo and the equivalent temperature index. The Pareto frontiers correspond to a weather scenario defined by the following parameters: $T_{ext,0}[°C] \in \{31\,;34\,;\,37\}$, $RH_{ext,0} = 55\%$ and $\dot{q}_{sun,0} = 1000\ W/m^2$, and traffic scenario modeled by INRETS R2 driving cycle. Results show that the four pareto frontier are close to each other, when the available energy is not sufficient to maintain a good thermal comfort. Usually, in this situation, the compressor is set at its lowest speed regime. The thermal comfort is ajusted then by air mass flow, heating and recycling ratio which doesn't consume energy. However, when enough energy is allocated to HVAC system, the thermal comfort levels proposed by the four indices are different. From the equivalent temperature index point of view, only the PMV index with a thermal insulation of 1.1 gives almost the same results. The other indices generates discomfort, in which the driver feels an umpleasant hot sensation.

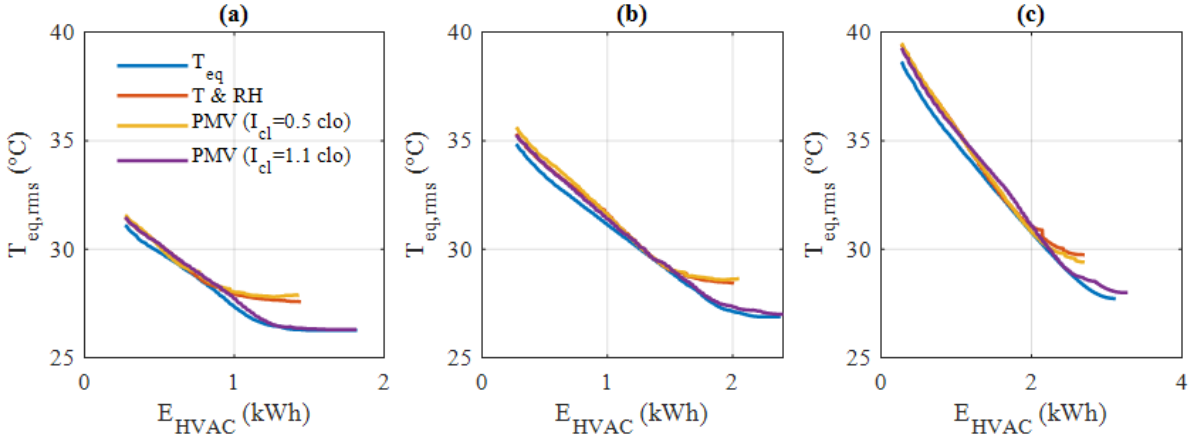


Figure 41.Pareto frontier for four thermal comfort criterion, for $RH_{ext,0} = 55\%$, $\dot{q}_{sun,0} = 1000\ W/m^2$, INRETS R2 driving cycle and (a) $T_{ext,0} = 31°C$, (b) $T_{ext,0} = 34°C$, (c) $T_{ext,0} = 37°C$

The comparison between equivalent temperature criterion and a given thermal comfort criterion, is performed by computing the average vertical distances between pareto frontier's points with the same consumed energy. Two comparison metrics were analyzed: the absolute error (vertical distance) in °C

denoted by $\Delta T_{eq,abs}$, and the relative error denoted by $\Delta T_{eq,rel}$ The smaller it is, the better thermal comfort is assessed by the considered index.

Figure 42 and Figure 43 summarize the results for the R2 driving cycles and a moderate humid weather $RH_{ext,0} = 55\%$. The curves show the evolution of $\Delta T_{eq,abs}$ and $\Delta T_{eq,rel}$ for each thermal comfort criterion, as a function of the external temperature, for different solar irradiances. We notice firstly that the PMV index with a thermal insulation of 1.1 clo gives the best results, where the average absolute and relative error is respectively 0.1 °C and 3.2%. Secondly, both other thermal comfort criterions, i.e. set point and PMV criterion, increase significantly thermal discomfort by respectively 19% and 42.4%,

Similar results are obtained for the other driving cycles, but we prefer not to present them here since they show same behavior

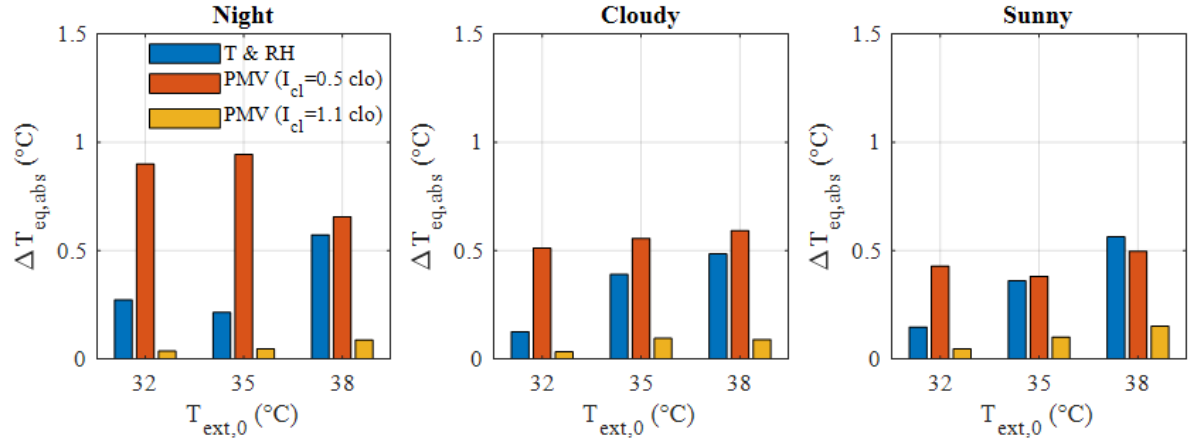


Figure 42. Mean absolute error [°C] between a thermal comfort criterion based on equivalent temperature, and three other indices

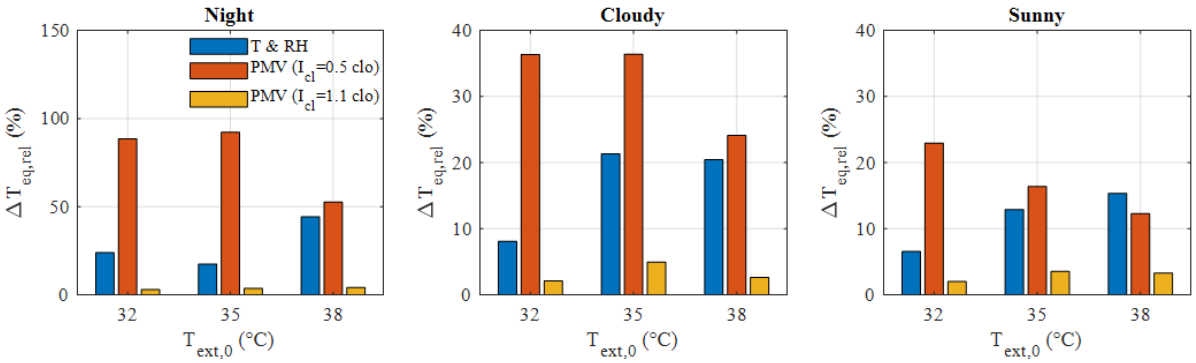


Figure 43. Mean relative error [%] between a thermal comfort criterion based on equivalent temperature, and three other indices

## 3. Conclusions and perspectives

This chapter introduced an optimal control approach, using dynamic programming principles, for thermal comfort and driving range management in BEVs. The passenger's thermal comfort was

modeled through the equivalent temperature index, estimated thanks to a model of human thermo-physiology. Simulations were conducted for different traffic and meteorological conditions. The main results are the following ones.

Using the equivalent temperature index and a detailed model of the HVAC permits to account for the influence of parameters such as the wall temperature, or the vehicle speed, on the comfort temperature and humidity in the cabin. Adjusting the four HVAC control variables enables to reach a given thermal comfort in the cabin at the lowest energetic cost.

A large number of simulation was performed and the energetic cost of thermal comfort in various conditions was quantified. Its strong impact in urban traffic conditions was underlined.

The results showed the usefulness of using DP for thermal comfort management. Indeed, when there is enough energy for ideal comfort, the algorithm drives all local equivalent temperatures to the green zone of the comfort diagram. The thermoregulation mechanism are disabled, which reflects a "comfortable" state. In contrast, when the available energy is low, the DP algorithm decreases the thermal comfort to meet the energy constraint, by putting the driver in a "hot but comfortable" state.

Furthermore, energy savings can be realized in some traffic conditions by decreasing the vehicle speed. For instance, when the driver slows down by 10% in highway, at night conditions, energy gains can reach 2.2 kWh for a one-hour trip.

The use of the equivalent temperature as thermal comfort index was justified by comparing it to other comfort indices, widely used in the field. The same optimization problem was solved for two additional criterions based on temperature and relative humidity set point, and the PMV index. Results show that when considering a global thermal insulation of 1.1 clo, the PMV index give quite the same results as equivalent temperature index, for all the simulated weather and traffic scenarios. However, the other indices showed their limitation, since they does not account for radiative effect, or for a correct assessment of clothing insulation. The thermal discomfort can be increased by 42% when using the consensual set point temperature and relative humidity of 25°C and 45%.

The next chapter will focus on developing a real-time management for thermal comfort in electric vehicles, based on the results of the present chapter. We will exploit as well some observations made on the optimal trajectories. Also, we will used the PMV index with a global thermal insulation of 1.1 clo, to assess the thermal comfort

# Chapter V : Real time management of thermal comfort

*Voici mon secret. Il est très simple : on ne voit bien qu'avec le cœur. L'essentiel est invisible pour les yeux.*
Antoine de Saint-Exupéry, Le Petit Prince

## Contents

The objective of the HVAC management system is to control the cabin temperature, relative humidity, and wall temperature, so that the passengers feel comfortable at the lowest energy cost. Yet, in some cases, the battery state of charge may be too low to insure ideal comfort during the whole trip, and it may be necessary to limit the power provided to air conditioning, in order to avoid power outage before reaching destination. If ideal thermal comfort cannot be provided at an acceptable energy cost, then it is reduced in order to allow the driver to arrive safely to the next charging point.

In the previous chapter, we have stated this energy management problem as an optimal control problem and solved it thanks to dynamic programing. The results have shown that it is indeed possible to adjust thermal comfort according to the amount of energy available for the trip, but the computation cost of dynamic programing is too high to consider implementing this method in an on-board controller.

In the present chapter, we propose a real-time thermal comfort management algorithm based on simplified estimations of the energy required for traction and thermal comfort. This approach assumes that the vehicle is equipped with a navigation aid system that provides traffic and weather prediction along the planned route. The estimators are built off-line and used on-line, first to determine the quantity of energy available for thermal comfort, and then to adjust the thermal comfort accordingly, in real time. An important point of this chapter is that we model the thermal comfort by the predicted mean vote criterion (PMV), instead of equivalent temperature. This choice is motivated by the fact that both criterions gives the same results for a given set of personal and environmental condition, provided that global thermal insulation is correctly adjusted.

The proposed approach was tested firstly for 4000 test-cases and compared to an optimal dynamic programming based approach [181]. The test-cases has been simulated for hot or moderate climates, but the proposed principles could also be extended to cold conditions. The results show that the proposed real-time management is able to adjust the thermal comfort in case of low battery state of charge, and provides a near optimal tradeoff between energy consumption and thermal discomfort. Next, The real time algorithm was tested for 800 test cases in which traffic predictions are updated periodically. The results show that the proposed approach can handle prediction change, and is able to reevaluate thermal comfort according to the updated available energy.

The remainder of this chapter is organized as follows. Section I presents the real time thermal comfort management approach. Firstly, an overview of the algorithm is presented together with the thermal comfort criterion. Then, the powertrain and the HVAC system power estimators are presented. Finally, the algorithm of the thermal comfort management strategy is given. Section II presents results for a large number of weather and traffic scenarios. The accuracy of the HVAC system consumption estimator is analyzed. The near-optimality of the proposed approach is assessed through comparison with an optimal dynamic programming approach. The real-time aspect of the approach is next established in changing traffic scenarios. Section III summarizes the conclusions of the present work and gives some perspectives for further works.

# 1. Real time energy management

The first subsection presents the general principles of the algorithm. Then, the models used to estimate the traction and HVAC energy consumptions are presented.

## *1.1. Principle of the proposed approach*

Figure 44 gives an overview of the proposed thermal comfort management strategy, which will be referred to as TCMS in the rest of the chapter. The idea is to cool down the cabin until a thermal comfort that can be maintained during the whole trip has been reached. This choice is based on previous results based on dynamic programing, that have shown that optimizing the thermal comfort over a given trip always starts with such a fast cooling phase. If there is enough energy in the battery, ideal comfort will be provided. Otherwise, thermal comfort will be less, but it will last until the end of the trip. This approach assumes that the vehicle is equipped with a navigation aid system that provides traffic and weather prediction along the planned route.

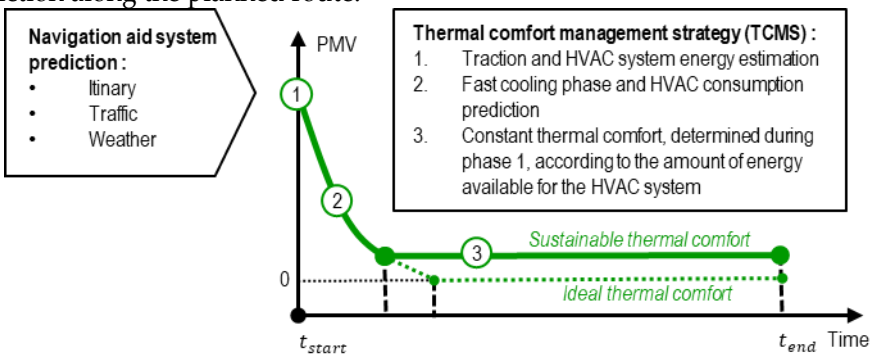


Figure 44. Schematic view of the proposed thermal comfort management strategy

The algorithm has three phases. Phase 1 consists in estimating the energy required for traction over the whole trip, based on information about the speed (average and standard deviation) and the slope profile. Since the initial state of charge of the battery is known, one can calculate the energy available for operating the HVAC system. Then, phase 2 starts: the HVAC system is operated at its maximum cooling capacity until an "energetically acceptable" thermal comfort is reached. All along this phase, the TCMS monitors the current thermal comfort and the HVAC consumption, and estimates the amount of energy required to maintain the current thermal comfort until the end of the trip. As long as the required energy is less than the available energy, and that ideal comfort has not been reached, the cooling phase goes on. As soon as ideal comfort has been reached or that an energy limit has been detected, phase 3 starts. It simply consists in maintaining the current comfort level at the lowest energy cost for a given control horizon.

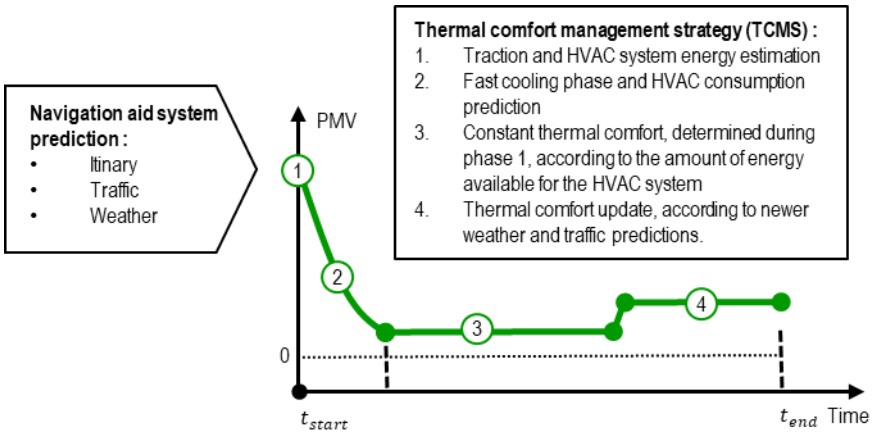

Figure 45. Schematic view of the thermal comfort management strategy, taking into account prediction's update

Figure 45 gives an overview of TCMS algorithm, when predictions are updated. The comfort level should be readjusted according to updated predictions of vehicle speed and weather. The algorithm approach with the three phases remains the same. When a change/update of predictions occurs in the third phase, the energy needs for traction are firstly re-evaluated, then a new available energy for HVAC system is deduced. Next, the best comfort level that respects the energy constraint, is maintained during a control horizon. This re-evaluation process is repeated as long as prediction's updates occurs.

### *1.2. Thermal comfort criterion*

The TCMS uses the PMV as a thermal comfort criterion. This choice was motivated by the moderate complexity of the PMV compared to the equivalent temperature index, in which a human thermo-physiological model is required. Furthermore, as shown in the previous chapter, the PMV index gives almost the same results as equivalent temperature provided that thermal insulation is adjusted. The PPD is also used to interpret the results. This index is more intuitive since it refers to the percentage of dissatisfied people towards an ambiance.

### *1.3. Phase 1 : traction energy estimation*

The dynamic model of the powertrain presented in chapter II cannot be used directly for the traction energy estimation, since it requires the knowledge of the exact speed profile in order to calculate the power along a given trip. In real life at the beginning of the trip, this information is not available, but the navigation aid system can provide statistics about the speed along the planned route. Based on numerous simulations using the dynamic model, we have developed an estimator that predicts the average traction power as a function of the expected average vehicle speed $\bar{v}$, its standard deviation $\sigma_v$ and the road slope $p$. The estimated traction power $\tilde{P}_{traction}$ is postulated as the sum of a bicubic function of $\bar{v}$ and $\sigma_v$, and a term to account for the slope $p$, as given by (193), where $a_{i,j}$ and $b$ are coefficients to be identified, $m_{veh}$ is the mass vehicle and $g$ is the gravitational acceleration.

$$\tilde{P}_{traction}(\bar{v},\sigma_v,p) = \sum_{i=0}^{3}\sum_{j=0}^{3} a_{i,j}.\bar{v}^i.{\sigma_v}^j + b.m_{veh}.g.\sin(\tan^{-1}(p)) \quad (193)$$

The coefficients of the model have been identified using 1200 speed cycles corresponding to various driving conditions [182]. The driving cycles were extracted from the National Renewable Energy Laboratory (NREL) data base. Those cycles were collected from real trips, which are performed in different cities and traffic situation. Each speed cycle has been characterized by its mean value and standard deviation $\bar{v}$ and $\sigma_v$, and simulated by the powertrain model for different fixed slopes $p$ ranging from $-10\%$ to $+10\%$. This gives a total number of 168000 scenarios. Then the average traction power over each cycle has been calculated, and linear regression has been used to compute the coefficients $a_{i,j}$ and $b$.

The accuracy of this estimation is assessed by analyzing the absolute and relative difference between $\tilde{P}_{traction}$, the average traction power estimated by (193), and $\overline{P_{traction}}$, the average traction power calculated by the dynamic powertrain model. These quantities, denoted respectively by $\Delta P_{abs}$ and $\Delta P_{rel}$, are defined by (194) and (195).

$$\Delta P_{abs}\ [\text{Wh}] = \left|\tilde{P}_{traction} - \overline{P_{traction}}\right| \quad (194)$$

$$\Delta P_{rel}\ [\%] = \left|\frac{\tilde{P}_{traction} - \overline{P_{traction}}}{\overline{P_{traction}}}\right| \quad (195)$$

Figure 46 summarizes the estimator accuracy through different mean values of $\Delta P_{abs}$ and $\Delta P_{rel}$. The plots (a) and (b) show the histograms of $\langle \Delta P_{abs,cycle} \rangle$ and $\langle \Delta P_{rel,cycle} \rangle$, the mean value of $\Delta P_{abs}$ and $\Delta P_{rel}$ averaged over the slope *for a given cycle*. The errors mainly lie in the ranges $[0W, 300W]$ and $[0\%, 5\%]$ respectively, with a mean value of $204\,W$ and 2.5%. Next, the curves (c) and (d) show the influence of the slope on $\langle \Delta P_{abs,slope} \rangle$ and $\langle \Delta P_{rel,slope} \rangle$, the mean value of $\Delta P_{abs}$ and $\Delta P_{rel}$ averaged over all the cycles, *for a given slope*. Although the absolute error increases with the slope, the relative error decreases because the traction power also increases with the slope (it reaches 100 kW for a 10% slope).

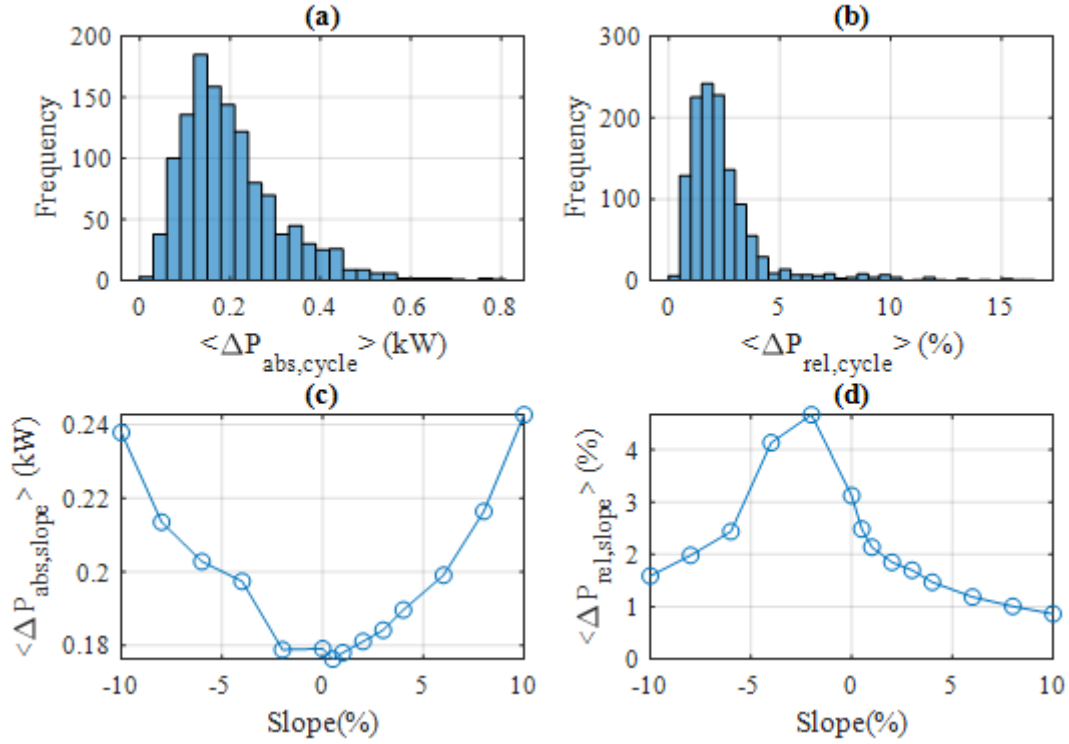


Figure 46. Assessment of the traction power estimator: (a) and (b) represent the histogram of $\langle \Delta P_{abs,c} \rangle$ and $\langle \Delta P_{rel,c} \rangle$, while (c) and (d) represent $\langle \Delta P_{abs,p} \rangle$ and $\langle \Delta P_{rel,p} \rangle$

A second series of tests was performed using INRETS driving cycles that were not used for the identification process. Figure 47 reports the results of the traction power estimator for the INRETS driving cycles. The plot (a) compares the estimated power $\tilde{P}_{traction}$ (dotted line) to $\overline{P_{traction}}$ (square), for different uniform slopes. The negative values obtained for $p = -10\%$ reflect regenerative braking. The plots (b) and (c) show the average relative error for a given cycle $\langle \Delta P_{rel,cycle} \rangle$ as a function of the speed average value $\overline{v}$ and standard deviation $\sigma_v$, whereas the plot (d) shows the average relative error for a given slope $\langle \Delta P_{rel,slope} \rangle$ as a function of the slope. The overall fit is good.

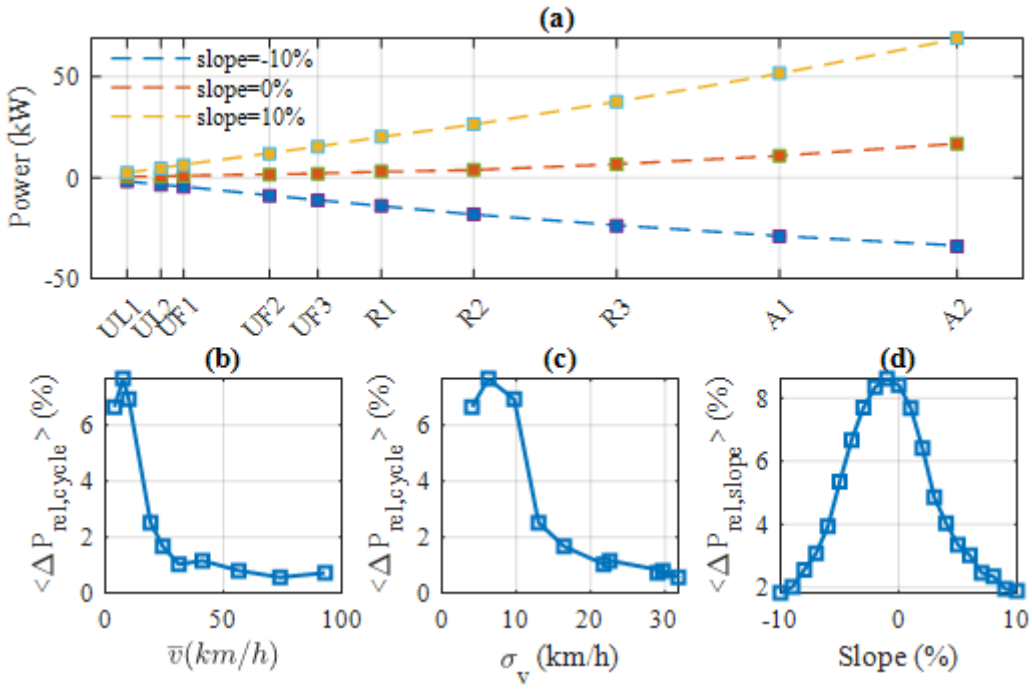


Figure 47. Power estimator assessment for the 10 INRETS driving cycles : (a) $\overline{P_{traction}}$ (squares) and $\tilde{P}_{traction}$ (dotted lines) versus cycle for three slopes, (b) $\langle \Delta P_{rel,cycle} \rangle$ versus $\overline{v}$, (c) $\langle \Delta P_{rel,cycle} \rangle$ versus $\sigma_v$, (d) $\langle \Delta P_{rel,slope} \rangle$ versus slope.

In real life conditions, the navigation aid system splits the planned route into a certain number of road sections of various length $l$ and provides the slope as well as traffic information for each of them. The total traction energy $E_{traction}$ should then be computed by summing up the traction energy corresponding to each road sections according to (196), where the subscript k refers to the kth section and $n$ denotes the number of sections.

$$\tilde{E}_{traction} = \sum_{k=1}^{n} \tilde{E}_{traction,k} = \sum_{k=1}^{n} \tilde{P}_{traction}(\bar{v}_k, \sigma_{v,k}, p_k) \times \frac{l_k}{\bar{v}_k} \tag{196}$$

We have tested this technique by splitting the INRETS cycles into 500 m sections. Figure 48 shows the results. The plot (a) represents the energy calculated using the dynamic model (red squares) and estimated by splitting the road into $k$ road sections, according to equation (196), for $p = 0\%$. The plots (b) and (c) show the average relative error for a given cycle $\langle \Delta E_{rel,cycle} \rangle$ as a function of the speed average value $\overline{v}$ and standard deviation $\sigma_v$, whereas the plot (d) shows the average relative error for a given slope $\langle \Delta E_{rel,slope} \rangle$ as a function of the slope. Again, the overall fit is good. The mean relative error $\langle \Delta E_{rel,slope} \rangle$ is around 4.8% for positive slopes, but can reach 10% for $p = -10\%$. We also notice that the mean relative error $\langle \Delta E_{rel,cycle} \rangle$ decreases according to INRETS average speed and INRETS speed standard deviation.

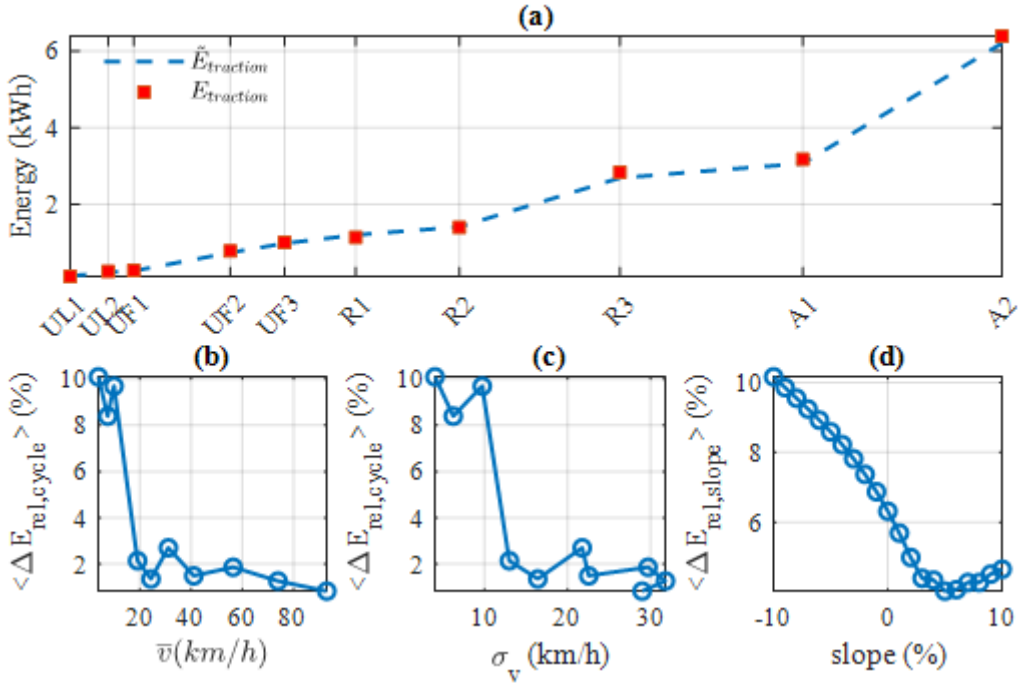


Figure 48. Energy estimator assessment for the 10 INRETS driving cycles : (a) $E_{traction}$ (squares) and $\tilde{E}_{traction}$ (dotted lines) versus cycle, (b) $\langle \Delta E_{rel,cycle} \rangle$ versus $\overline{v}$, (c) $\langle \Delta E_{rel,cycle} \rangle$ versus $\sigma_v$, (d) $\langle \Delta E_{rel,slope} \rangle$ versus slope.

### *1.4. Phase 2 : fast cooling and HVAC power estimation*

Once the energy available for operating the air conditioning system during the whole trip is known, the fast cooling phase starts. Its goal is to reach rapidly a thermal comfort that can be sustained until the end of the planned trip. The HVAC system is operated at its maximum cooling capacity, i.e. at maximum compressor rotational speed $N_{comp,max}$ and air flow rate $\dot{m}_{air,max}$. The heating system is disabled ($\alpha_{min} = 0$) and the recycled air ratio is set at its maximum value $\beta_{max} = 90\%$ (air quality issues require at least 10% air renewal).

The initial cabin temperature and humidity are assumed the same as outside (vehicle parked in the shade). For the considered warm weather situations, they correspond to a large positive value of PMV. As soon as the control vector $u_{cooling} = [N_{comp,max}, \dot{m}_{air,max}, \alpha_{min}, \beta_{max}]'$ is applied, the cabin temperature decreases and the thermal comfort starts to improve. All along the cooling phase, the TCMS monitors in real time the PMV. As it will be explained in the next paragraphs, it also estimates the amount of energy that the HVAC system would consume if the thermal comfort was kept constant at its current value until the end of the trip. As long as this energy is less than the energy available for the HVAC system and that ideal comfort has not been reached, the cooling phase goes on. The cooling phase stops when the system has reached a PMV that is either optimal ($PMV = 0$) or that cannot be improved, given the energy available for the HVAC system.

The prediction of the energy required to maintain the $PMV$ at a given value during the trip is based on the use of a look-up table $G$ that gives an estimate of the optimal power consumed by the HVAC system for maintaining a desired PMV in given conditions $w = [T_{ext}, \phi_{ext}, P_{sun}, v]$. This power is denoted by ${P_{HVAC}}^*(PMV, w)$ as formalized by equation (197).

$$ {P_{HVAC}}^*\left(PMV_{steady}, w\right) = G(PMV_{steady}, T_{ext}, \phi_{ext}, P_{sun}, v) \qquad (197) $$

This look-up table is built off-line, based on simulation results under static conditions, as explained in section 1.7. . It is used on-line, in real time dynamic conditions according to the following principle.

The predicted environment conditions along the trip are denoted by $\tilde{w}(t)$. At time $t_k$ of the cooling phase, the current PMV index is $PMV(t_k)$. The estimation of the energy required by the HVAC system in order to maintain this thermal comfort until the end of the trip, denoted by $\tilde{E}_{HVAC,maintain}(t_k)$, is obtained by integrating the estimated HVAC power, as stated by (198).

$$\tilde{E}_{HVAC,maintain}(t_k) = \int_{t_k}^{t_{end}} P^*_{HVAC}\big(PMV(t_k), \tilde{w}(t)\big)\,.\,dt \tag{198}$$

During the cooling phase, the TCMS also monitors the energy consumed by the HVAC system since the beginning of the trip, denoted by $E_{HVAC,cool}(t_k)$, and the energy available for the rest of the trip, denoted by $E_{HVAC,available}(t_k)$.

$$E_{HVAC,available}(t_k) = E_{HVAC,available}(t_0) - E_{HVAC,cool}(t_k) \tag{199}$$

As long as ideal thermal comfort has not been reached (i.e. $PMV > 0$) and there is enough energy available to improve the current thermal comfort (i.e. $E_{HVAC,available}(t_k) > E_{HVAC,maintain}(t_k)$), the cooling phase goes on. As soon as either ideal thermal comfort is reached or energy limitation is detected, the cooling stops and the phase 3 starts.

### *1.5. Phase 3 : thermal comfort maintaining*

Let us denote by $PMV_{set}$ the value of PMV reached at the end of the phase 2. We will assume that the weather and traffic prediction made at the beginning of the trip are not subjected to future updates. The phase 3 consists in maintaining the current $PMV$ at this setting value, at the lowest energy cost. At each time $t_k$, given the current external conditions $w(t_k)$, the TCMS algorithm determines the set of commands that lead to $PMV(t_{k+1}) = PMV_{set}$, and selects the one with the lowest energy cost.

### *1.6. Algorithm summary*

The main points of the thermal comfort TCMS algorithm, assuming no prediction updates, are summarized here after.

---

**Input :** battery initial state of charge; traffic prediction ($\overline{v}$ and $\sigma_v$ for each section of the planned road); weather prediction $w(t)$ along the planned road

**Phase 1 : Initialization**

Estimate energy required for traction for the whole planned trip

Calculate energy available for thermal comfort during the whole planned trip

Output : energy available for thermal comfort during the whole planned trip

**Phase 2 : Fast cooling**

While (current PMV > 0) :

Estimate $E_{HVAC,maintain}$, energy to maintain the current thermal comfort until the end of the trip

Calculate $E_{HVAC,available}$, energy left for the thermal comfort until the end of the trip

If ($E_{HVAC,available} > E_{HVAC,maintain}$ ) :

Apply maximum cooling command $u_{max}$

Else:

$PMV_{set} = current\ PMV$

Exit while loop

Output : Thermal comfort setting point for phase 3 $PMV_{set}$

**Phase 3 : Thermal comfort maintaining**

For the rest of the trip :

Apply command $u$ such that $PMV = PMV_{set}$ at the lowest energy cost

Output : Predicted and actual HVAC power profile, PMV profile

---

### *1.7. TCMS algorithm with prediction's update*

Weather and traffic forecast are subjected in real life to changes and updates. The TCMS algorithm should be able to handle these changes, and propose an updated thermal comfort level according to newer prediction. Indeed, The phase 3 will consists now on maintaining the $PMV$ reached at the end of phase 2 at the setting value $PMV_{set}$, for a given control horizon $\Delta t_c$, at the lowest energy cost.

At time $t_0 + \Delta t_c$, traffic and weather predictions are updated. If these predictions differ from those performed at the beginning of the trip, thermal comfort must be adjusted to a new level, in order to not violate the energy constraint. First, the traction energy needed to complete the trip is recalculated based on the updated traffic predictions and slope data. Next, a new available energy $\tilde{E}_{HVAC,av}$ for HVAC system is deduced. The update value of thermal comfort is the smallest $\widetilde{PMV}_{req} \in [0,3]$ that satisfies the following condition :

$$\tilde{E}_{HVAC,av}(t_0 + \Delta t_c) \geq E_{HVAC,maintain}\left(\widetilde{PMV}_{set}, t_0 + \Delta t_c\right) \quad (200)$$

Where $E_{HVAC,maintain}\left(\widetilde{PMV}_{req}, t_0 + \Delta t_c\right)$ is the energy consumed by the HVAC system to maintain the thermal comfort at $\widetilde{PMV}_{req}$, from $t_0 + \Delta t_c$ until the end f the trip. The quantity is given by (201) and (202):

$$E_{HVAC,maintain}\left(\widetilde{PMV}_{set}, t_0 + \Delta t_c\right) = \int_{t_0+\Delta t_c}^{t_{end}} P^*_{HVAC,maintain}\left(\widetilde{PMV}_{set}, t\right).dt \quad (201)$$

$$P^*_{HVAC,maintain}\left(\widetilde{PMV}_{set}, t\right) = G\left(T_{ext}(t), RH_{ext}(t), P_{sol}(t), V_{veh}(t), \widetilde{PMV}_{set}\right) \quad (202)$$

At all time $t_k \in [t_0 + \Delta t_c, t_0 + 2\Delta t_c]$, given the current external conditions $w(t_k)$, the TCMS algorithm determines the set of commands that lead to $PMV(t_{k+1}) = \widetilde{PMV}_{set}$, and selects the one with the lowest energy cost. The procedure of updating $\widetilde{PMV}_{set}$ and computing the command vector u is repeated at each time $t_0 + n\Delta t_c$ , $n \in \mathbb{N}$, until the end of the trip.

It is sometimes impossible to ensure correct thermal comfort, either because the weather conditions are very hot, or because there isn't enough energy for operating the HVAC system. In these situations, it is wiser to warn the driver. The thermal comfort will be greatly degraded ($PMV \geq 3$), and a correct thermal comfort cannot be maintained until the end of the trip. Recharging the battery or, reducing the vehicle speed is may be necessary to improve thermal comfort.

The main points of the thermal comfort TCMS algorithm, with prediction update are summarized here after.

---

**Input :** battery initial state of charge; traffic prediction ($\overline{v}$ and $\sigma_v$ for each section of the planned road); weather prediction $w(t)$ along the planned road

**Phase 1 : Initialization**

Estimate energy required for traction for the whole planned trip

Calculate energy available for thermal comfort during the whole planned trip

Output : energy available for thermal comfort during the whole planned trip

**Phase 2 : Fast cooling**

While (current PMV > 0) :

Estimate $E_{HVAC,maintain}$, energy to maintain the current thermal comfort until the end of the trip

Calculate $E_{HVAC,available}$, energy left for the thermal comfort until the end of the trip

If ($E_{HVAC,available} > E_{HVAC,maintain}$ ) :

Apply maximum cooling command $u_{max}$

Else:

$PMV_{set} = current\ PMV$

Exit while loop

Output : Thermal comfort setting point for phase 3 $PMV_{set}$

**Phase 3 : Thermal comfort maintaining**

For the rest of the trip :

If $t_k == t_{update}$

Estimate energy required for traction for the rest of the trip
Calculate energy available $E_{HVAC,av}(t_k)$ for thermal comfort for the rest of the trip
Determine the set $U = \{\text{PMV} \in [0\ 3] \mid E_{HVAC,av}(t_k) \geq E_{HVAC,maintain}(PMV, t_k)\}$
$PMV_{set} = \min U$
Apply command $u$ such that $PMV = PMV_{set}$ at the lowest energy cost
Output : Predicted and actual HVAC power profile, PMV profile

### *1.8. Construction of the look-up table G*

This section explains the process for constructing the look-up table $G$ that allows estimating ${P_{HVAC}}^*(PMV_{steady}, w)$, the optimal power needed by the HVAC system in order to maintain the PMV to a certain value $PMV_{steady}$, in given static external conditions $w = [T_{ext}, \phi_{ext}, P_{sun}, v]'$. For this given set of conditions $w$ and a given command vector $u = [N_{comp}, \dot{m}_{air}, \alpha, \beta]'$, equation (171) is used to numerically calculate the steady state vector $x_{steady} = [T_{hab,steady}, \phi_{hab,steady}, T_{wall,steady}]'$. From there, the corresponding $PMV_{steady}$ and the power consumed by the HVAC system in these conditions are calculated. This can be formalized by the two functions Φ and Ψ defined by (203) and (204).

$$PMV_{steady} = \Phi(u, w) \tag{203}$$

$$P_{HVAC,steady} = \Psi(u, w) \tag{204}$$

Our goal is to establish a relationship that allows determining $P_{HVAC,steady}$ as a function of $PMV_{steady}$, for a given vector $w$. This requires to invert the relationship (203) with respect to $u$, but this application is surjective: a given value of $PMV$ can be achieved by different combinations of temperature, humidity and radiation temperature, and hence by different control vector $u$. In practice, this multiplicity of combinations gives a degree of freedom to choose the command that provides a given $PMV_{steady}$ at the lowest energy cost.

In order to formalize this mathematically, let us denote by $U_{PMV,w}$ the set of control vectors able to provide a given value of $PMV$ for given external conditions $w$, as defined by (205).

$$U_{PMV,w} := \{u \in \mathbb{R}^4 \mid \Phi(u, w) = PMV\} \tag{205}$$

The optimal control $u^*$ and the corresponding power ${P_{HVAC}}^*$ are given respectively by (206) and (207).

$$u^*(PMV, w) = \underset{u \in U_{PMV,w}}{argmin}\{\Psi(u, w)\} \tag{206}$$

$${P_{HVAC}}^*(PMV, w) = \min_{u \in U_{PMV,w}}\{\Psi(u, w)\} = \Psi\big(u^*(\text{PMV}, \text{w})\big) \tag{207}$$

The function defined by (207) cannot be directly obtained. Hence a mapping (look-up table) is built, based on numerical simulations performed in the following ranges of target $PMV$ and external conditions: $0 \leq PMV \leq 3$ (in accordance with the ISO7730 norm [164]), $25\ °C \leq T_{ext} \leq 40\ °C$, $30\ \% \leq HR_{ext} \leq 80\ \%$, $0\ W \leq P_{sun} \leq 1000\ W$.

## 2. Results and discussion

In this section, the real-time comfort management algorithm is tested in simulation for a large number of scenarios with different weather conditions, traffics, and initial battery's state of charges. A

statistical analysis is conducted in order to assess the capacity of the proposed method to adjust the thermal comfort according to the amount of energy available for the HVAC system.

Firstly, we verify that the HVAC system consumption estimated during the cooling phase using the look-up table $G$ corresponds to its actual consumption, calculated afterwards using the system dynamic model. A good match justifies the relevance of using a precalculated static model in slowly varying conditions.

The next point is to evaluate the performance of the thermal comfort management algorithm. For this purpose, we formulate an optimization problem that consists into minimizing the global thermal comfort defined by (177) for a given amount of energy. Solving this problem using the dynamic programming approach presented in [183, 181] provides reference solutions against which the real-time algorithm efficiency can be assessed.

$$J(u) = \int_0^{t_{fin}} PMV^2\big(x(u(t), w(t))\big)\, dt \tag{208}$$

Finally, we assess the real-time aspect of the TCMS algorithm by simulating a large number of weather conditions and a specific traffic scenario, where the vehicle speed prediction is regularly updated. A good fit between estimated and realized energy, will prove that TCMS handles prediction changes and adjust the thermal comfort in real time.

## *2.1. TCMS without prediction update*

### 2.1.1. Test scenarios

In the following, we will present the weather and traffic scenarios simulated to assess the relevance of the look-up table G, and the efficiency of TCMS against optimal approach.

Each scenario corresponds to a trip completed in given weather and traffic conditions, with a given initial battery's state of charge. The construction of outside temperature, relative humidity and solar irradiance profiles, follows exactly the same methods reported in the previous chapter, section 2.1. Different values of the parameters $T_{ext,0}$, $HR_{ext,0}$, and $\dot{q}_{sun,0}$ correspond to different weather conditions. In order to explore a wide range of weather conditions, without focusing on the weather profile itself, we have combined together the following values: $T_{ext,0}[°C] \in \{25\,;26\,;\dots;38\}$, $RH_{ext,0} \in \{0.35\,;0.45\,;0.55\,;0.65\,;0.75\}$, $\dot{q}_{sun,0}[W/m^2] \in \{0\,;500\,;1000\}$. This results in a total number of 210 weather scenarios. As the HVAC system efficiency depends on the vehicle speed, the UL1, UF1, R2 and A2 INRETS driving cycles were used (Figure 22). In addition, a non-uniform slope is considered.

The initial temperature and relative humidity in the cabin are assumed the same as outside (vehicle parked in the shade). For all the tested scenarios, we consider that passengers are at rest, seated. We assume that passengers are lightly dressed, in a formal way, i.e. shirt, underpants, trousers, socks and shoes. As seen in the previous chapter section 2.5. , this type of clothing corresponds to a global thermal insulation of 1.1 clo.

Five initial SoC of the battery are tested, each one corresponding to a given amount of energy available for thermal comfort.

In summary, the benchmark built from the abovementioned scenarios corresponds to four given trips carried out in 210 weather conditions, with five different levels of available energy. The total number of test cases reaches 4200. This large number of situations allows assessing the capacity of the real-time algorithm to adjust the thermal comfort according to the available energy.

All 4200 scenarios were simulated. For each of them, the real-time thermal comfort management algorithm has been applied to the system model. The results are presented hereafter.

### 2.1.2. Qualitative observations for a specific scenario

The present section summarizes some qualitative observations made for a particular scenario, defined by $T_{ext,0} = 33\ °C$, $HR_{ext,0} = 45\%$, $P_{sun,0} = 500\ W$ and the R2 driving cycle. Similar trends are observed for all other scenarios [184].

Figure 49 shows the temporal evolution of the PMV, the temperature and the relative humidity in the cabin, for three initial battery state of charge. The PMV profile has the desired shape: it drops at the beginning of the trip, and then keeps constant at a PMV level that depends on the available energy. For an initial SOC of 27.7 %, the embedded energy is sufficient for almost reaching the ideal thermal comfort after a 6-minute cooling phase ($PMV = 0.03$). For an initial SOC of 26.5%, the cooling phase stops earlier at a PMV of 0.6, which remains acceptable for the passenger. For an initial SOC of 26.1 %, the cooling phase is even shorter and the PMV is 0.9. Figure 49.b and Figure 49.c display the corresponding temperature and humidity in the cabin. It is worth noting that both quantities evolve over time despite a constant value of PMV index, reflecting the fact that a given PMV can be obtained with different combinations of temperature and humidity.

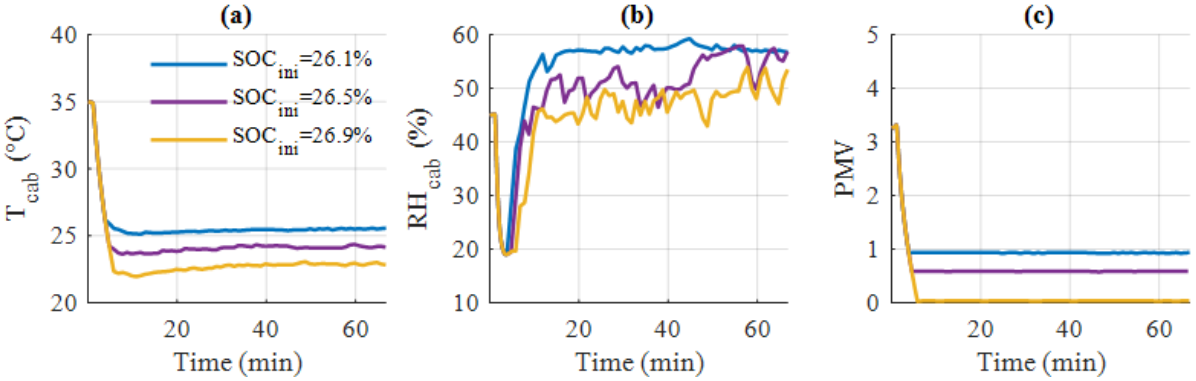


Figure 49. Cabin results for three initial SOCs: (a) PMV, (b) Temperature, (c) Relative humidity

Figure 50 focuses on the particular scenario with an initial SOC of 26.5%. The purple curves correspond to the results of the real time TCMS, whereas the blue curves represent results obtained by dynamic programing in order to serve as a reference. Two of the four HVAC control variables are plotted versus time: the compressor rotation speed (Figure 50.a) and the air flow (Figure 50.b). These commands are set at their maximum value during the cooling phase, and then adjusted in order to maintain the target PMV at the lowest energy cost. One notices that despite the temporal variations of the weather conditions, the control variables do not significantly change. Small oscillations reflect the search process of the control vector, which consists in minimizing the air conditioning power at all time. During the process, very close air conditioning powers are achieved with different combinations of $N_{comp}$, $\dot{m}_{air}$, $\alpha$ and $\beta$. Since the algorithm selects the combination that minimizes the HVAC power, the values of $\dot{m}_{air}$ can naturally differ from one step to the next. Figure 50.c reports the HVAC system power estimated during the cooling phase using the look-up table (black line), actually consumed during the trip (purple line). Both curves are very close to one another, indicating a good quality of the power prediction using the look-up table $G$.

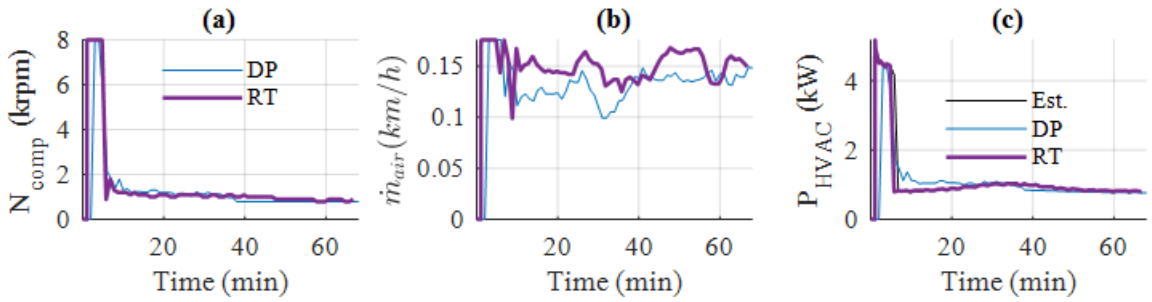


Figure 50. HVAC system results for $SOC_{ini} = 26.5\%$: (a) & (b) : compressor speed and air flow trajectories calculated by the real time control (red line) and DP (blue line) – (c) HVAC system power consumption estimated by the look-up table (black dots) and calculated (red : real time control, blue : DP)

It is worth underlining the capacity of the PMV model to account for the cabin wall radiant temperature. As an illustrative example, we have simulated an ideal thermal comfort ($PMV = 0$) obtained for given external temperature and humidity ($T_{ext,0} = 33\ °C$, $HR_{ext,0} = 45\%$) but different solar radiation levels $\dot{q}_{sun}$ (0, 500 and 1000 $W/m^2$). Figure 51 shows the results of theses simulations.

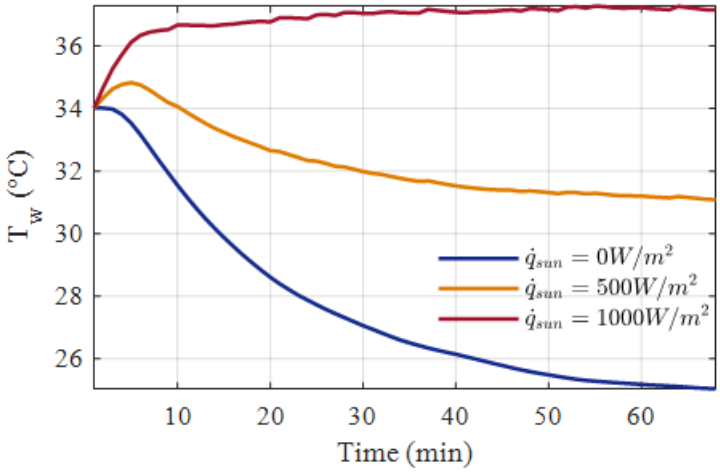


Figure 51. Wall temperature for three solar radiations

Table 7 reports the corresponding cabin wall radiant temperature $T_{wall}$, cabin ambiant temperature $T_{cab}$, and HVAC system energy consumption for the same trip. In the absence of solar radiation (at night), $T_{wall} = 25°C$, and ideal thermal comfort is obtained for $T_{cab} = 24.9°C$. In sunny conditions, other parameters being equals, $T_{wall} = 37.1°C$ and ideal comfort requires a cooler ambiant temperature $T_{cab} = 21.2°C$ and more energy.

| $P_{sun}\ [W/m^2]$ | $T_{wall}\ [°C]$ | $T_{cab}\ [°C]$ | $E_{HVAC}\ [kWh]$ |
|---|---|---|---|
| 0 | 25 | 24.9 | 1.64 |
| 500 | 31.1 | 22.9 | 1.69 |
| 1000 | 37.1 | 21.2 | 2.15 |

Table 7. Cabin temperature, mean radiant temperature and consumed energy for ideal comfort (PMV=0) for different solar radiations

### 2.1.3. Statistical analysis over all the scenarios

The present section reports the analysis of the results over a wide range of scenarios, necessary in order to assess the proposed real-time approach. Two aspects ought to be evaluated through relevant performance metrics: the power estimation accuracy on one hand, and the efficiency of the thermal comfort management on the other hand.

Firstly, the adequacy of using the static mapping $G$ in a dynamic context is quantified by looking at the absolute and relative differences between the HVAC energy estimated at the end of cooling phase, denoted by $E_{estimated}$, and the energy actually consumed during the trip, denoted by $E_{actual}$. The two metrics $\Delta E_{abs}$ and $\Delta E_{rel}$ are defined by equations (209) and (210).

$$\Delta E_{abs} = E_{actual} - E_{estimated} \tag{209}$$

$$\Delta E_{rel} = \frac{E_{actual} - E_{estimated}}{E_{actual}} \tag{210}$$

Figure 52.a and Figure 52.b represent the histograms of $\Delta E_{abs}$ and $\Delta E_{rel}$ calculated for each of the 1050 scenarios run for the driving cycle INRETS R2. Table 8 reports the mean value (subscript $mean$) and the standard deviation (subscript $rms$) of $\Delta E_{abs}$ and $\Delta E_{rel}$ for each of the four tested driving cycles. These metrics show that the estimation based on the look-up table G is quite reasonable and can be trusted.

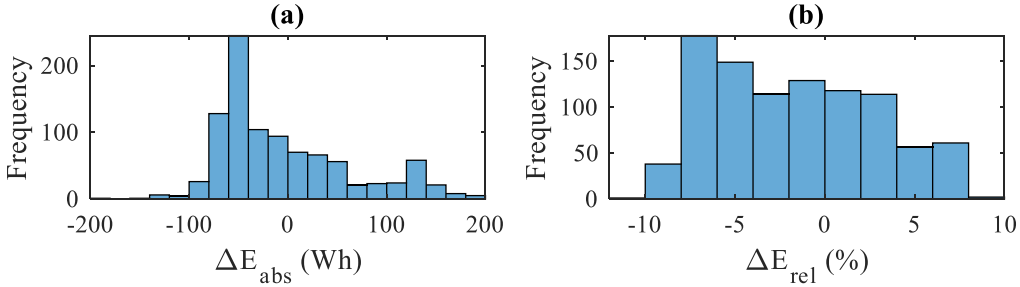


Figure 52. HVAC power estimation error : histograms of $\Delta E_{abs}$ (a) $\Delta E_{rel}$ (b).

| **INRETS Cycles** | $\Delta E_{abs,mean}$ $[Wh]$ | $\Delta E_{abs,rms}$ $[Wh]$ | $\Delta E_{rel,mean}$ [%] | $\Delta E_{rel,rms}$ [%] |
|---|---|---|---|---|
| A2 | -14.3 | 48.8 | -1.7 | 3.4 |
| R2 | -40.7 | 55.9 | -3.8 | 4.2 |
| UF1 | -32.5 | 55.3 | -3.2 | 4 |
| UL1 | -4.9 | 67.8 | -1.6 | 4.5 |

Table 8. Mean value and standard deviation of $\Delta E_{abs}$ and $\Delta E_{rel}$ for the four tested driving cycles

The comparison between the results of our real-time strategy and the optimal ones given by dynamic programming needs to account for two criteria: the total energy consumed by the HVAC system and the root mean square of the PMV, respectively denoted by $E_{HVAC}$ and $PMV_{rms}$. The different solutions obtained for a given weather and traffic scenario are reported in the $(E_{HVAC}, PMV_{rms})$ plane. Figure 53.a shows the results for the scenario defined by $T_{ext,0} = 33\,°C$, $RH_{ext,0} = 45\%$, $\dot{q}_{sun,0} = 500\,W$ and the R2 driving cycle. The black line corresponds to DP results and constitutes the Pareto frontier of the $(E_{HVAC}, PMV_{rms})$ bi-criteria optimization problem. The colored points correspond to the real-time control algorithm. As expected, they lie above the Pareto frontier, but at a small distance, indicating that the proposed algorithm gives near-optimal results for this particular scenario. Those results can be also reported in the $(E_{HVAC}, PPD_{rms})$ plane, where $PPD_{rms}$ refers the root mean square of PPD index (predicted percentage of dissatisfied people). This criterion has the advantage of being less abstract than the PMV.

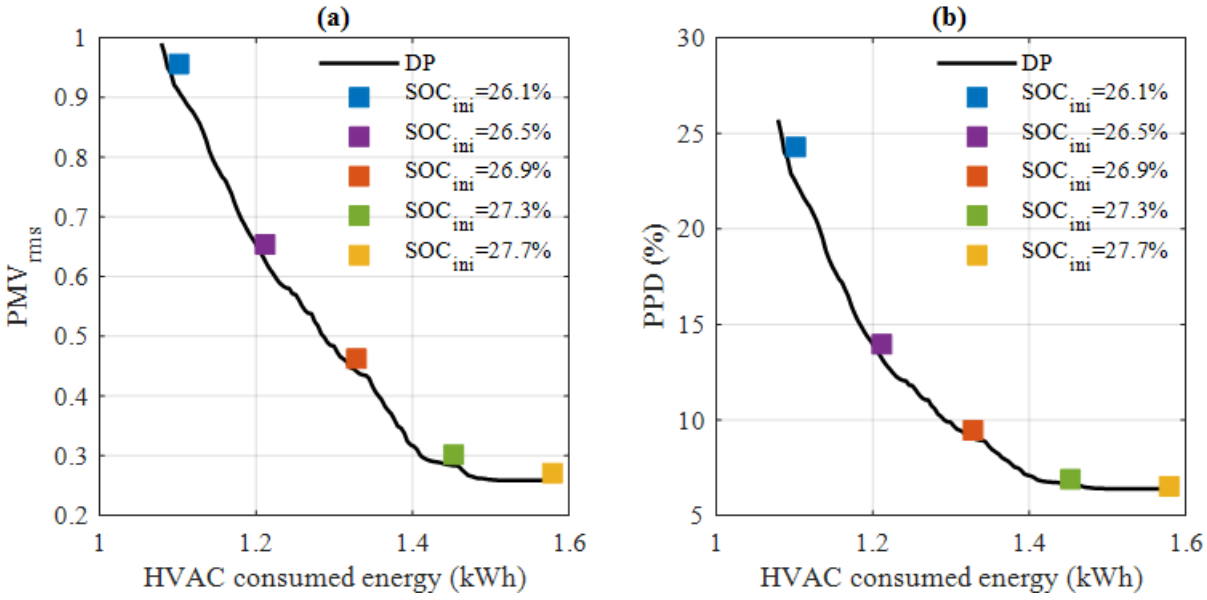


Figure 53. Thermal comfort versus HVAC consumed energy for DP (black line) and the real-time algorithm (colored points) – Results for $T_{ext,0} = 33\ °C$, $RH_{ext,0} = 45\%$, $\dot{q}_{sun,0} = 500\ W$ and the R2 driving cycle using (a) $PMV_{rms}$ and (b) $PPD$ as thermal comfort indices

Similar behaviors are observed when other profiles of solar radiation are taken. For $\dot{q}_{sun,0} = 0\ W$ and $\dot{q}_{sun,0} = 1000\ W$, other parameters beings equal, we notice also (Figure 54) that the colored dots lies just above the Pareto frontiers. Furthermore, for a given initial SoC, we remark that $PMV_{rms}$ is an increasing function of $\dot{q}_{sun,0}$. The reason is the available energy for operating the HVAC system may not be sufficient to overcome the high values of $T_w$, when $\dot{q}_{sun,0}$ reaches typically 1000 W/m².

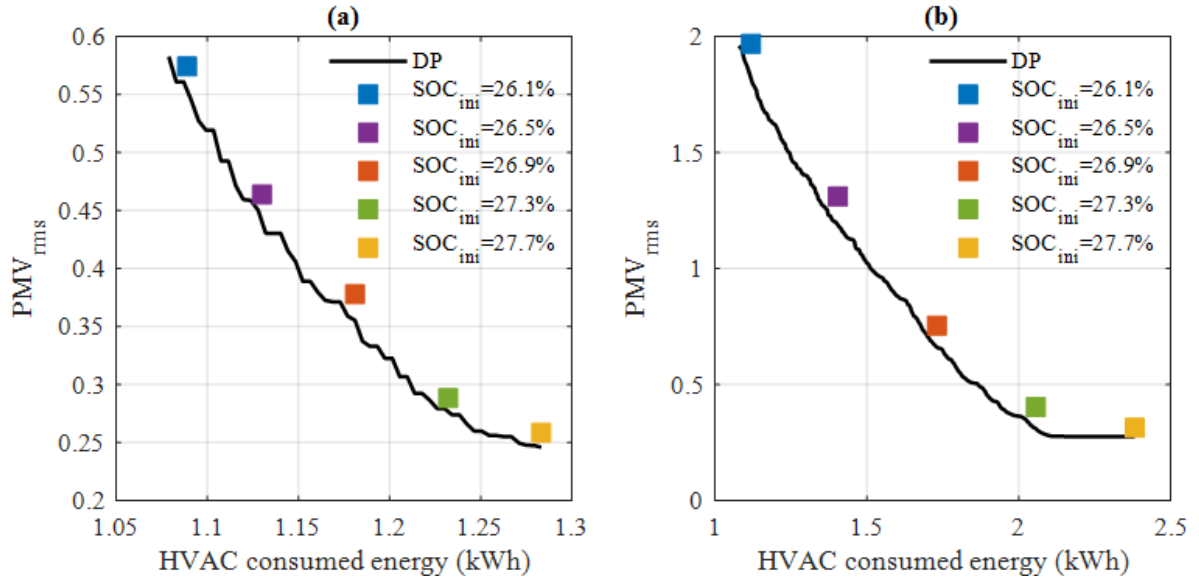


Figure 54. $PMV_{rms}$ versus HVAC consumed energy for DP (black line) and the real-time algorithm (colored points) – Results for $T_{ext,0} = 33\ °C$, $HR_{ext,0} = 45\%$, and the R2 driving cycle:
(a) $\dot{q}_{sun,0} = 0\ W/m^2$ & (b) $\dot{q}_{sun,0} = 1000\ W/m^2$

We have chosen to quantify the performance of the real-time TCMS by the average vertical distance between the colored points and the Pareto frontier. This distance is denoted by $\Delta PMV_{DP}$. The smaller it is, the better the real-time algorithm performs.

Figure 55 summarizes the results for the R2 driving cycles. The curves show the evolution of $\Delta PMV_{DP}$ as a function of the external temperature, for different conditions of humidity and solar radiation. The average value is 0.15, and we notice that this difference increases in warm and sunny conditions. Similar results are obtained for the other driving cycles. For instance, the $\Delta PMV_{DP}$ for INRETS A2 is reported in Figure 56, with an average value equal to 0.1.

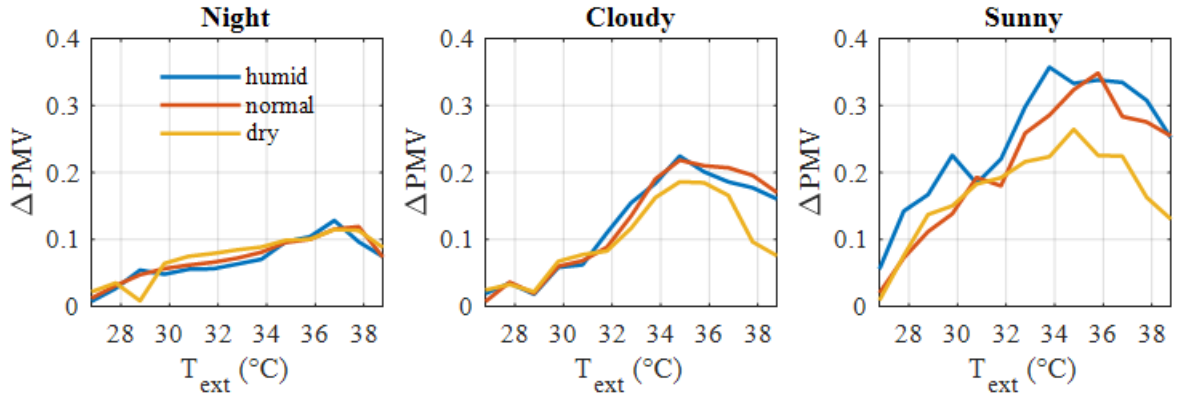


Figure 55. Mean PMV difference between DP and real-time control, for a given HVAC energy.

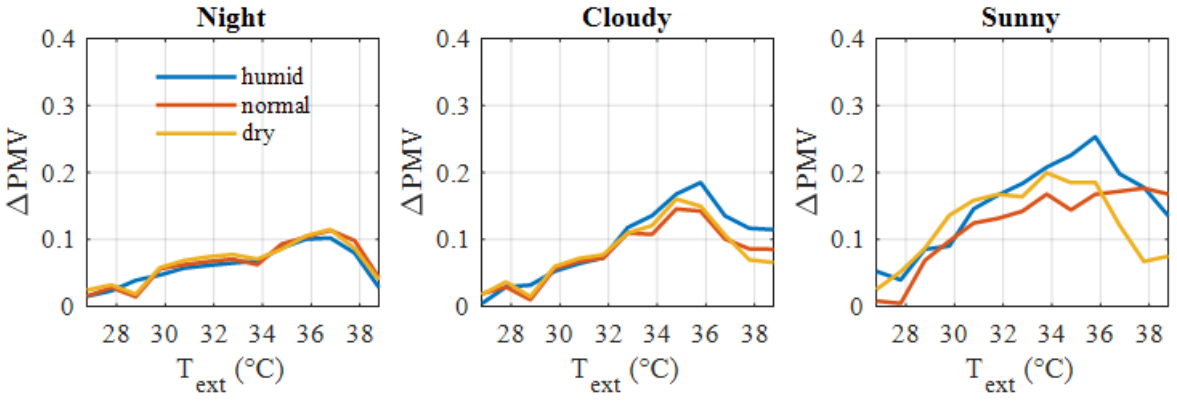


Figure 56. Mean PMV difference between DP and real-time control, for a given HVAC energy, for INRETS A2 driving cycle

The performance of the real-time TCMS can also be assessed using the PPD index (predicted percentage of dissatisfied people) for a given PMV. In a similar way than $\Delta PMV_{DP}$, we define the metrics $\Delta PPD_{DP}$ as the average difference between the root mean square value of the PPD obtained with the real-time algorithm, and the root mean square value of the PPD obtained by dynamic programming for the same HVAC energy. Figure 57 shows the $\Delta PMV_{DP}$ evolution as a function of temperature, for given humidity and solar irradiance conditions. The average $\Delta PPD_{DP}$ value is equal to 3%. Similar results are obtained for the other driving cycles, such as the INRETS A2 (Figure 58), where the average $\Delta PPD_{DP}$ is inferior than INRETS R2 cycle, equal to 2.6%.

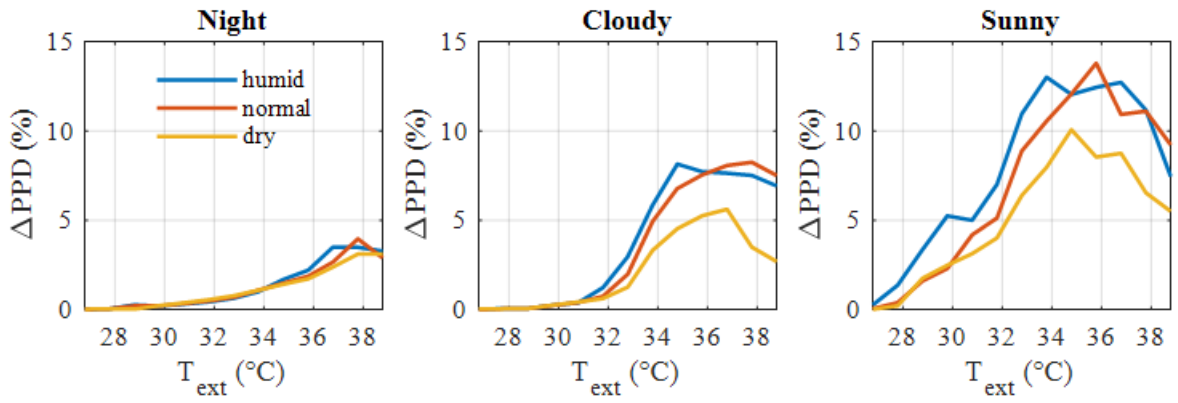


Figure 57. Mean PPD difference between DP and real-time control, for a given HVAC energy.

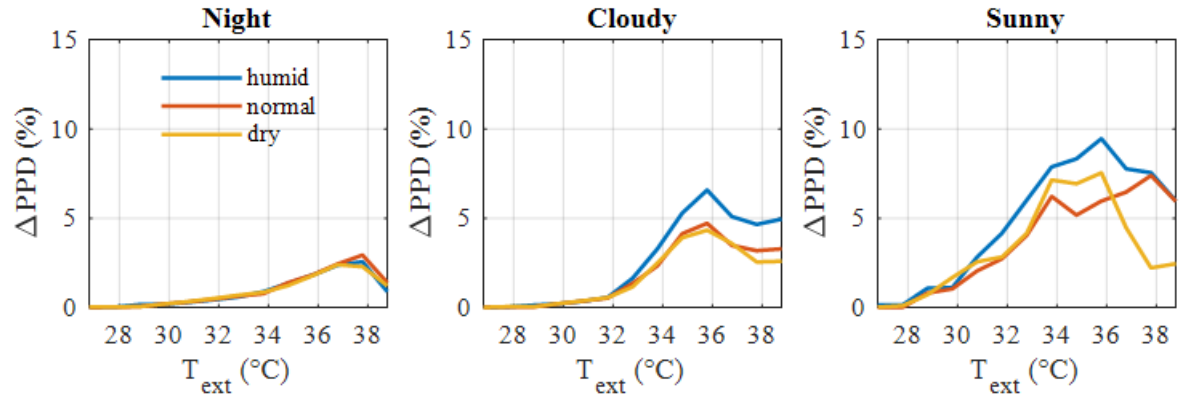


Figure 58.Mean PPD difference between DP and real-time control, for a given HVAC energy, for INRETS A2 driving cycle

## *2.2. TCMS with prediction update*

### 2.2.1. Test scenarios

One way to test the real time aspect of TCMS, is to push it to reevaluate periodically the available energy for HVAC, and compute the PMV that can be sustained until the end of the trip. To this end, we construct a test case that affect the available energy for HVAC system through a modification of the speed prediction. This prediction change can happen in real life, due for instance to unpredicted jams or accident. At each time period, a new thermal comfort level is determined, and maintained at the least energy cost until the next period.

In the following test case, we will assume a 1 hour trip during which the weather forecast made at time $t_0$, remains the same. However, we will assume that the speed profile, predicted at the beginning of the trip, is modified periodically, where for a given $n \in \mathbb{N}$, a fixed scaling factor $k < 1$ is applied to the speed as follows:

$$\begin{cases} v_{new,cycle}(t) = v_{cycle}(t).k \; ; \; \forall t \in [t_0 + n\Delta t_u, t_{fin}] \\ v_{new,cycle}(t) = v_{cycle}(t) \; ; \; \forall t \in [t_0, t_0 + n\Delta t_u[ \end{cases} \quad (211)$$

The scaling factor $k$ is applied to reduce the vehicle speed while traveling the same distance, hence the trip duration defined by (212) increases and becomes (213):

$$\Delta t_{cycle} = t_{fin} - t_0 \quad (212)$$

$$\Delta t_{new,cycle} = n\Delta t_u + \frac{t_{fin} - (t_0 + n\Delta t_u)}{k} \quad (213)$$

Since the trip lasts longer, less energy is required for the traction, but more is needed for thermal comfort. Figure 59.a shows the speed prediction made at time $t_0$. The depicted profile refers to the INRETS UF1, and correspond to a 1 hour trip in urban traffic. We will assume an updating period of 15 min, after which the vehicle speed prediction will be reduced by k=0.95, while travelling the same distance. Figure 59.b reports the new updated driving cycle, in which the blue curve represent the realized speed, and the red one represents the prediction of vehicle speed, made at the 15th min. This updating process is repeated at each time period. At arrival, the speed profile realized by the vehicle is depicted in Figure 59.c.

Simulations have been conducted on a combination of four INRETS driving cycles : A2,, R2, UF1, UL1, and the following range of outside temperature, relative humidity and solar radiation : $T_{ext,0}[°C] \in \{25\,;26\,;\ldots;38\}$, $RH_{ext,0} \in \{0.35\,;0.45\,;0.55\,;0.65\,;0.75\}$, $P_{sun,0}[W/m^2] \in \{0\,;500\,;1000\}$. We will assume for all scenarios that the available energy for HVAC system , at time $t_0$, is equal to 3 kWh. The initial battery SoC is fixed by adding this available energy, to the traction energy needed to perform the speed profile prediction made at time $t_0$.

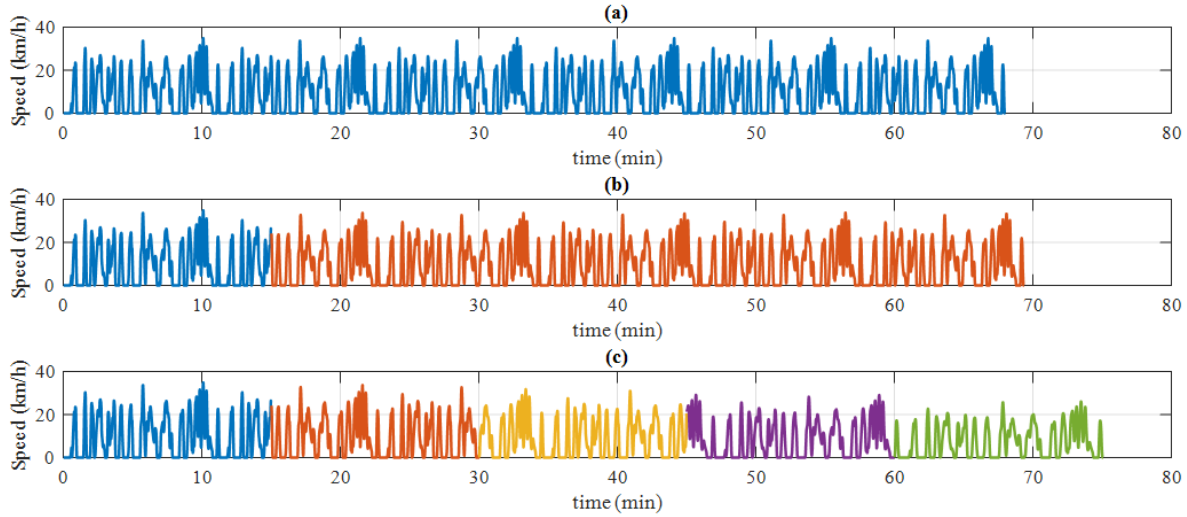


Figure 59. Prediction of vehicle speed profile in urban fluid traffic (INRETS UF1 driving cycle), made at time : (a) $t = t_0$, (b) $t = t_0 + \Delta t_u$, (c) $t = t_0 + 4\Delta t_u$

### 2.2.2. Statistical analysis over all scenarios

The present section reports the analysis of simulated scenarios, necessary to assess the real-time aspect of TCMS. Firstly, the estimation accuracy of the mapping $G$ in a dynamic context, with a periodically updated prediction, must be quantified.

This is done by evaluating the absolute and relative differences between the estimated HVAC energy, denoted by $E_{estimated}$, and the energy actually consumed during the trip, denoted by $E_{actual}$. It is important to note that the estimated HVAC energy, is re-evaluated at each time period, and hence, it is obtained when the trip is completed. Figure 60.a and Figure 60.b represent the histograms of $\Delta E_{abs}$ and $\Delta E_{rel}$ calculated for each of the 195 scenarios run for the driving cycle INRETS UF1 Table 9 reports the mean value (subscript $mean$) and the standard deviation (subscript $rms$) of $\Delta E_{abs}$ and $\Delta E_{rel}$ for each of the four tested driving cycles. These metrics show that the estimation based on the look-up table G is again quite reasonable and can be trusted, even in a context where speed predictions are updated.

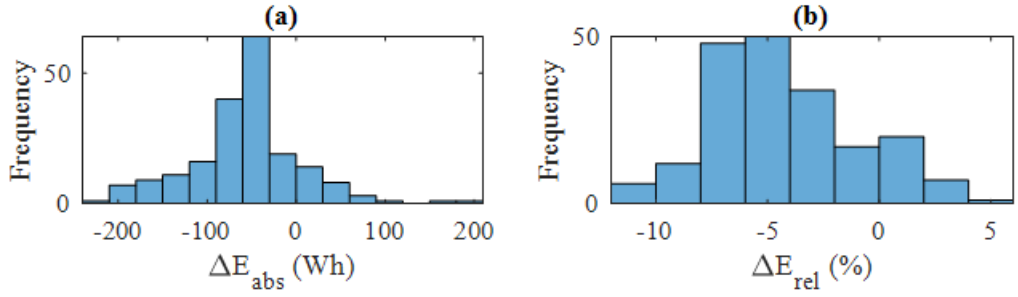


Figure 60. HVAC power estimation error : histograms of $\Delta E_{abs}$ (a) $\Delta E_{rel}$ (b).

| INRETS Cycles | $\Delta E_{abs,mean}$ $[Wh]$ | $\Delta E_{abs,std}$ $[Wh]$ | $\Delta E_{rel,mean}$ [%] | $\Delta E_{rel,std}$ [%] |
|---|---|---|---|---|
| A2 | -24 | 50.9 | -2.1 | 2.9 |
| R2 | -58.8 | 62.5 | -4.3 | 3.3 |
| UF1 | -92 | 70.7 | -5.3 | 2.6 |
| UL1 | -57.8 | 56.7 | -3.9 | 2.9 |

Table 9. Mean value and standard deviation of $\Delta E_{abs}$ and $\Delta E_{rel}$ for the four tested driving cycles

### 2.2.3. Qualitative observation for specific scenarios

In the following, we summarize some qualitative observations made for particular scenarios, defined by the following physical quantities; $T_{ext,0} = 38\,°C$, $RH_{ext,0} = 55\%$, $P_{sun,0} = 1000\,W$, and the four driving cycle: A2, R2, UF1 and UF2.

Figure 61 shows the temporal evolution of the PMV, the temperature and the relative humidity in the cabin, in fluid urban traffic (INRETS UF1). The PMV drops at the beginning of the trip, and then keeps constant at a $PMV = 1.5$ in the first 15 min. From there, The TCMS algorithm set the PMV to slightly lower value of 1.4 before increasing it drastically in the following periods.

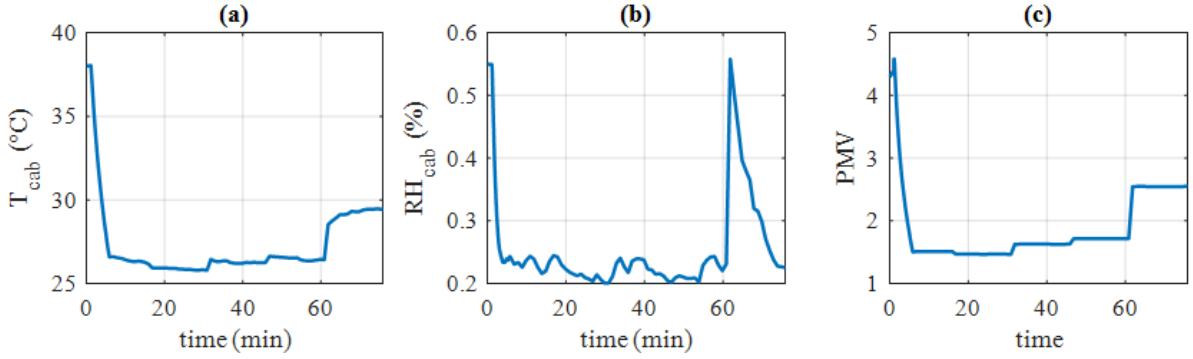


Figure 61. Cabin results for $T_{ext,0} = 38\,°C$, $RH_{ext,0} = 55\%$, $P_{sun,0} = 1000\,W$, and the speed profile depicted in Figure 59.: (a) PMV, (b) Temperature, (c) Relative humidity

This profile can be explained as follows: after the 15th min, the vehicle speed is reduced by 2.5% according the above mentioned traffic scenario, which provoke a decrease in traction power and hence the traction energy. After the first period, the thermal comfort is slightly improved, as the available energy becomes bigger, and allows to invest more cooling power into the cabin. However, in the second period, the reduction of vehicle speed by an additional 2.5% provokes an increase in traction energy needs. The reason is that in urban context, the surplus consumption due to an increased trip duration, predominates on consumption mitigation due to a reduced traction power. This rule is inversed in suburban traffic and highway as it will be seen later in this section. Furthermore, the extension of travel time jeopardize the quality of thermal comfort, since the energy needed to maintain $PMV = 1.4$ is no more available. The TCMS algorithm decides consequently to degrade thermal comfort in order to respect the energy constraint.

As the trip duration becomes bigger at each time period, the available energy for operating HVAC system becomes insufficient to maintain a $PMV = 1.4$, which translates in a periodical degradation of thermal comfort. This explains the increasing PMV setting values from 1.4 to a value of 2.5 at arrival. Figure 62 shows the repartition of estimated and realized HVAC system and traction energy, as a function of travel time increase. We notice that the traction energy needed to perform the trip (sum of estimated and realized energy) remains almost constant, which makes the available energy for thermal comfort not sufficient to maintain a PMV of 1.4. This also means that the thermal discomfort is caused mainly by the travel time extension.

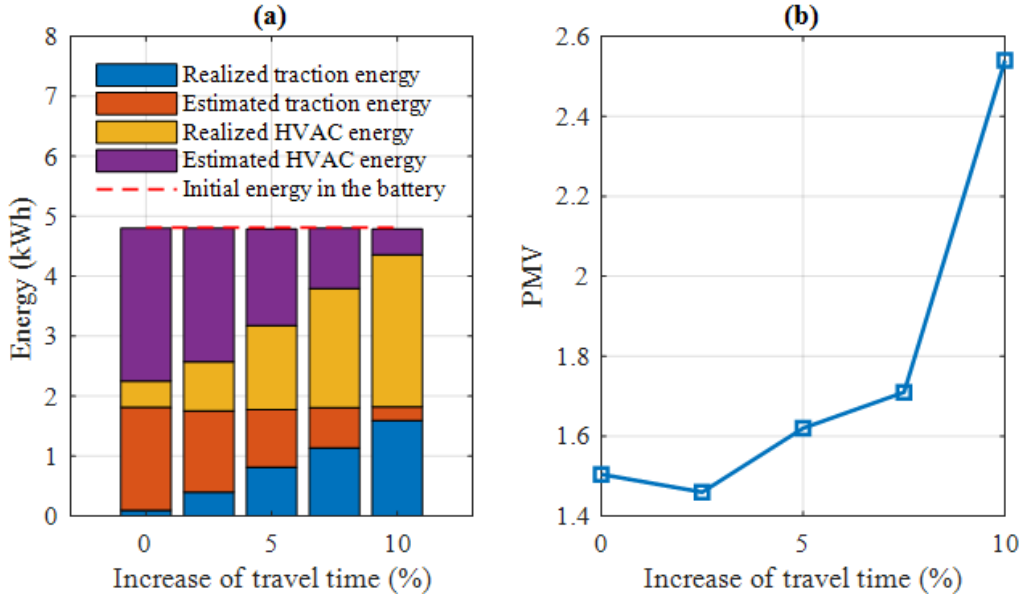


Figure 62. Evolution as a function of travel time increase of : (a) Realized and estimated energy of traction and HVAC system, (b) PMV index

Figure 61.b and Figure 61.c display the corresponding temperature and humidity in the cabin. It is worth noting that both quantities evolve over time despite the piecewise constant shape of $PMV(t)$, reflecting once again the fact that a given PMV can be obtained with different combinations of temperature and humidity.

In Figure 63, two of the four HVAC control variables are plotted versus time: the compressor rotation speed (Figure 63.a) and the air flow (Figure 63.b). These commands are set at their maximum value during the cooling phase, and then adjusted in order to maintain the targeted values of PMV (Figure 62.b) at the lowest energy cost. Small oscillations reflect the search process of the control vector, which consists in minimizing the air conditioning power at all time. Figure 63.c reports the estimation of HVAC system power using the look-up table (black line), actually consumed during the trip (blue line). This estimation is collected at the end of trip since the HVAC power updated periodically. Both curves are very close to one another, indicating a good quality of the estimation, using the look-up table $G$.

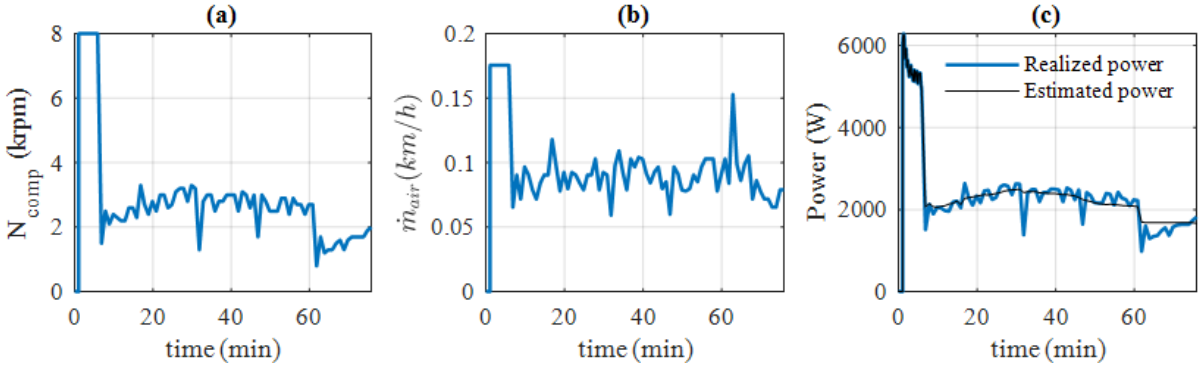

Figure 63. HVAC system results for $T_{ext,0} = 38\ °C$, $RH_{ext,0} = 55\%$, $P_{sun,0} = 1000\ W$, and the speed profile depicted in Figure 59. (a) & (b) : compressor speed and air flow trajectories calculated by the real time control – (c) HVAC system power consumption estimated by the look-up table (black line) and calculated by real time control (blue line)

The above analysis differs for other traffic scenarios. Figure 64.a shows the simulation results in highway, i.e. INRETS A2 driving cycle. The speed reduction improves highly the thermal comfort since it goes from PMV=0.8 to its ideal value PMV=0. The reason is that the available energy was increased by almost 1 kWh (Figure 65.a), which was sufficient to ensure ideal thermal comfort for the entire trip. Hence, the presence of a remaining energy in the battery at the following updating periods. The simulation results differs to a certain extent when a suburban traffic is considered (INRETS R2 driving cycle). Figure 64.b shows that the thermal comfort improved gradually at each speed reduction, where the PMV index went after the cooling phase, from a value of 1.2 to its ideal value PMV=0, at the fourth updating period. Nevertheless, in the last 15 min, thermal comfort was greatly degraded mainly because the available energy wasn't enough to maintain the ideal comfort. Indeed, the increased travel time pushed the TCMS algorithm to reset the PMV at the value of 1.2.

For a slow urban traffic (INRETS UL1), the results analysis are similar to those formulated for an urban fluid traffic (INRETS UF1).

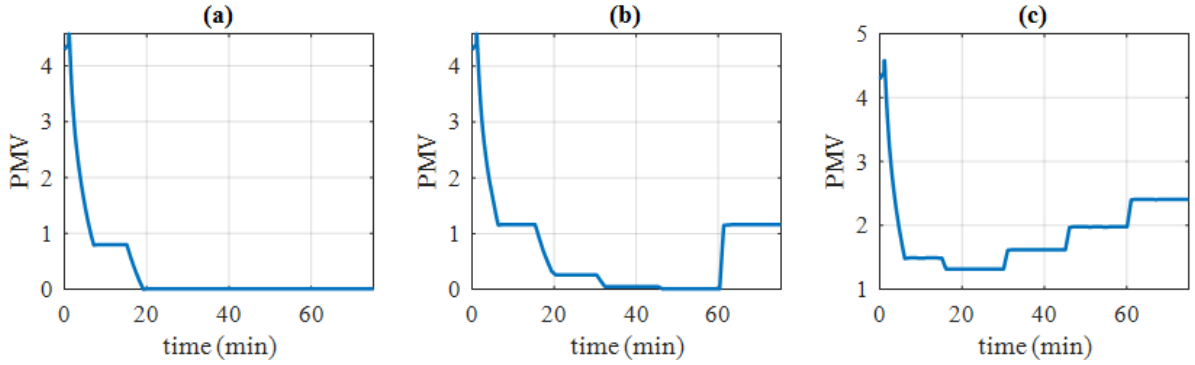


Figure 64. PMV results for $T_{ext,0} = 38\ °C$, $RH_{ext,0} = 55\%$, $P_{sun,0} = 1000\ W$ and (a) INRETS A2, (b) INRETS R2, (c) INRETS UL1 driving cycle

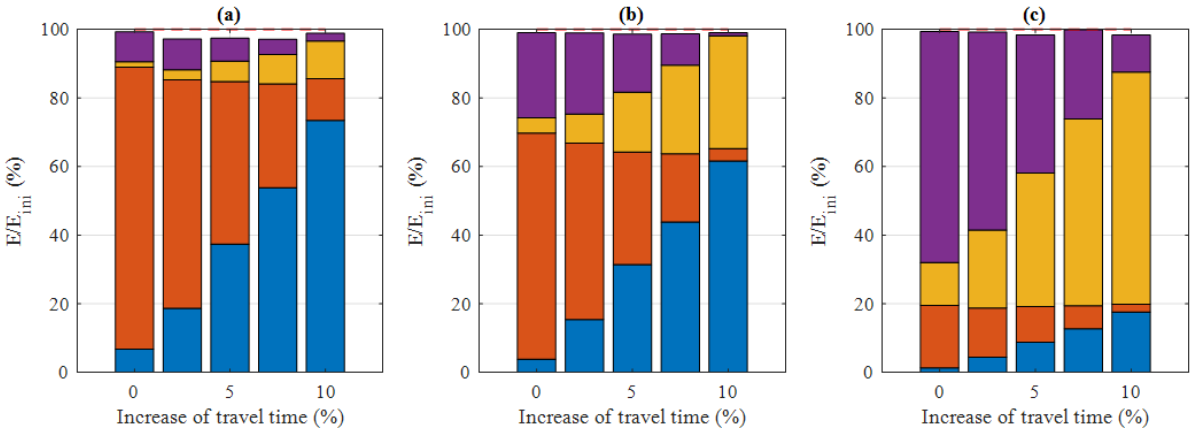


Figure 65. Repartition of estimated and realized energy for $T_{ext,0} = 38\ °C$, $RH_{ext,0} = 55\%$, $P_{sun,0} = 1000\ W$ and the following driving cycles: (a) INRETS A2, (b) INRETS R2, (c) INRETS UL1

## 3. Conclusions

This chapter presented a real time management approach of thermal comfort in BEVs, for given traffic and weather predictions provided by the navigation aid system. For this purpose, the PMV index

was used to assess thermal comfort, and adapted for vehicular application by taking a thermal insulation of 1.1 clo.

Two estimators were built. The first one estimates the traction power in given traffic conditions, that we propose to model by the average value and standard deviation of the speed. This estimator is used to calculate the traction energy necessary to complete the trip. Validation tests were run to assess its accuracy, for different driving cycles and slopes. Results showed that the average estimation error is about 3%.

The second estimator is needed to estimate the HVAC system power consumption for a given thermal comfort level, in given meteorological and speed conditions. It is built off-line and used on-line by the real-time algorithm in order to adapt the thermal comfort level according to the energy available for the coming trip. In order to prove its validity, simulations were conducted for different traffic and weather conditions scenarios, and different initial battery SOCs. Results showed a good fit between estimated and realized consumption.

The same scenarios were used to assess the near optimality of the overall approach, by comparing it to an optimal control approach. Results show that for the same consumed energy, the real-time algorithm increases discomfort by only 3%.

The validity of the second estimator was established also in scenarios, where speed profile is updated periodically. Results show again a good fit between estimated and realized consumption. Furthermore, they assess the algorithm's ability to reevaluate thermal comfort based on updated available energy.

# Conclusion

The present thesis presented a thermal comfort management strategy for occupants in an electric vehicle. The approach consist of finding the optimal balance between energy saving and thermal comfort, for a given embedded energy in the battery. The idea is that, if there is not enough embedded energy for both traction and optimal thermal comfort for the planned trip, the thermal comfort is diminished in order to save energy and allow the vehicle to reach its final destination. In some situations, it is wiser to slow down in order to allow a better thermal comfort.

This issue has been tackled in the literature, as a short-term horizon control problem, by using simplistic thermal comfort criterions, usually a set point temperature. Different strategies has been used, from methods of classical control theory, such as PID and fuzzy logic control, to methods from optimal control theory like the MPC (Model Predictive control). If these studies succeeded to control cabin temperature according to a short-term forecast of driving conditions, they lack to assess correctly the thermal comfort of the occupants, and manage the energy consumption all over the trip. Based on this literature review, we proposed better thermal comfort criterions, which are representative of the passenger's and driver's comfort state, and take into account their thermo-physiology. Furthermore, we develop an energy management strategy with time horizon that covers the overall trip, and which adjust the thermal comfort according to a finite available energy.

Firstly, we presented the powertrain, the HVAC system and the cabin model provided by the French car manufacturer Groupe PSA. The objective of the first model was to evaluate the traction energy needed to complete the trip. The model consisted on computing the motor and braking torque that performs the desired speed profile. Those torques are translated thereafter into a consumed power via the transmission and the electric motor model. The HVAC system has benefited from a great focus and a thorough modelling since it controls the thermal quantities of the vehicle cabin, and hence the thermal comfort level of the occupants. Four control variables were considered for the HVAC system: rotational speed of the compressor, the mass air flow, the heating and the recycling ratio. The HVAC model was based mainly on evaluating the thermodynamic quantities of the refrigerant, and deduce the temperature and relative humidity of the cooled air, at the outlet of the evaporator. These quantities evolves next according to the heating and the ventilation system dynamics. The vehicle cabin was represented by three heat balances, each one of them describes the temporal evolution of three state variables: cabin temperature, cabin relative humidity and wall temperature. Finally, in order to monitor the energy consumption, a simple model of the battery was considered to evaluate the fourth state variable: the battery state of charge.

Secondly, we presented an enhanced Tanabe model of human thermoregulation together with three thermal comfort indices. The objective was to take into account the thermo-physiological characteristics of the occupants and their subjective preferences when assessing the thermal comfort. After introducing some generalities about human homeothermy, thermoreceptors and thermoregulation mechanisms, we presented the passive system model. The latter consisted on expressing the heat exchanges within the human body, and with the surrounding environment. The passive model's improvement concerned mainly the convection and radiation heat exchanges, in which the governing equations were extracted from Fiala's work. The active system plays the role of a body thermostat, that regulate the internal temperature around 37°C, by meaning four thermoregulation mechanism: shivering, vasodilatation, vasoconstriction and sweating. Each mechanism was examined and expressed as function of head core signal and integrated cutaneous signal. Combining both passive and active system allowed to establish the heat balance equations for each node, which was important, in order to evaluate cutaneous temperatures, and subsequently assess the thermal comfort in a representative way. From there, we introduced and modelled the equivalent temperature index, which

is the most suitable metric for thermal comfort in vehicular environment, together with the PMV/PPD index and the conventional set point temperature and relative humidity.

After modelling the electric vehicle, the human thermo-physiology and thermal comfort, we introduced an optimal control approach, using dynamic programming principles, for energy and thermal comfort management. A thermal comfort criterion was built thanks to the equivalent temperature index. A large number of simulation was performed and the energetic cost of thermal comfort in various conditions was quantified. The results showed the strong impact of HVAC consumption in urban traffic conditions, compared to traction consumption. We noticed also the dependence between the ideal comfort temperature and solar irradiance. In sunny conditions for instance, the comfort temperature is 21°C whereas it equals to 26°C at night. Results showed also the usefulness of using DP for thermal comfort management. Indeed, when there is enough energy for ideal comfort, the algorithm drives all local equivalent temperatures to the green zone of the comfort diagram. The thermoregulation mechanism are disabled, which reflects a "comfortable" state. In contrast, when the available energy is low, the DP algorithm decreases the thermal comfort to meet the energy constraint, by putting the driver in a "hot but comfortable" state.

Furthermore, energy savings can be realized in some traffic conditions by decreasing the vehicle speed. For instance, when the driver slows down by 10% in highway, at night conditions, energy gains can reach 2.2 kWh for an one-hour trip.

The use of the equivalent temperature as thermal comfort index was justified by comparing it to other comfort indices, widely used in the field. The same optimization problem was solved for two additional criterions based on temperature and relative humidity set point, and the PMV index. Results show that when considering a global thermal insulation of 1.1 clo, the PMV index give quite the same results as equivalent temperature index, for all the simulated weather and traffic scenario. However, the temperature and relative humidity set point index showed its limitation, since it does not account for radiative effect, or clothing insulation. The thermal discomfort can be increased by 42% when using the consensual set point temperature and relative humidity of 25°C and 45%.

Although the results of the optimal approach were promising, and validate the energy management principle, still the computation cost were too high to consider implementing the algorithm on board controller. We proposed therefore a real time management approach of thermal comfort in BEVs, for given traffic and weather predictions, provided by the navigation aid system. For this purpose, the PMV index with a thermal insulation of 1.1 clo, was used to assess thermal comfort, since it was show that it is comparable to equivalent temperature.

Two estimators were built for the real time algorithm. The first one estimates the traction power in given traffic conditions, which are modeled by the average value and standard deviation of the speed. This estimator is used to calculate the traction energy needed to complete the trip. Validation tests were run to assess its accuracy, for different driving cycles and slopes. Results showed that the average estimation error is about 3%. The second estimator was built to estimate the HVAC system power consumption for a given thermal comfort level, in given meteorological and speed conditions. This estimator was constructed off-line and used on-line by the real-time algorithm in order to adapt the thermal comfort level according to the available energy for the upcoming trip. In order to prove its validity, simulations were conducted for different traffic and weather conditions scenarios, and different initial battery SOCs. Results showed a good fit between estimated and realized consumption.

The same scenarios were used to assess the near optimality of the real time approach, by comparing it to an optimal one. Results show that, for the same consumed energy, the real-time algorithm increases discomfort by only 3%. The real time aspect of the algorithm was established also, mainly in scenarios where speed profile is updated periodically. Results showed again a good fit between estimated and

realized consumption. Furthermore, they assess the algorithm's ability to reevaluate thermal comfort based on updated available energy.

This research has contributed to combine effective energy management approach with advanced thermal comfort assessment in electric vehicles. The developed optimal and real time algorithms have proved their validity in extensive test-case scenarios. However, we estimate that some improvements can be made in models and algorithms. In the following, we will list the future works:

- Taking into account the battery temperature and lifetime in the cost function.
- Improve the cabin and ventilation system model, by taking into account the air temperature gradients.
- Simplifying the HVAC and thermo-physiological model, by using machine learning techniques, in order to lighten the computation costs.
- Replacing the HVAC system model by a heat pump model, since this technology will be used in future brands of Groupe PSA vehicles.
- Testing the optimal and real-time algorithm in cold weather scenarios.
- Developing other control strategies based on Model Predictive control, provided that the system model is linearized.

# References


[1] C. Corbridge, «Vibration in vehicles: its effect on comfort,» University of Southampton, Southampton, 1987.

[2] H. He, W. Chen et J. Hui, «A Stochastic Model Predictive Controller Based on Combined Conditions of Air Conditioning System for Electric Vehicles,» chez *Joint International Conference on Energy, Ecology and Environment (ICEEE 2018) and International Conference on Electric and Intelligent Vehicles (ICEIV 2018)*, 2018.

[3] G. De Nunzio, A. Sciarretta, A. Steiner et A. Mladek, «Thermal Management Optimization of a Heat-Pump-Based HVAC System for Cabin Conditioning in Electric Vehicles,» chez *Thirteenth International Conference on Ecological Vehicles and Renewable Energies (EVER)*, 2018.

[4] C. Croitoru, I. Nastase, F. Bode, A. Meslem et A. Dogeanu, «Thermal comfort models for indoor spaces and vehicles – current capabilities and future perspectives,» *Renewable & Sustainable Energy Reviews,* 2015..

[5] J. Cheng et . L. Bertolini, «Measuring urban job accessibility with distance decay, competition and diversity,» *Journal of Transport geography,* 2013.

[6] H. Tsutsumi, Y. Hoda, S.-i. Tanabe et A. Arishiro, «Effect of Car Cabin Environment on Driver's Comfort and Fatigue,» *SAE,* 2007.

[7] H. A. Daanen, E. Van De Vliert et X. Huang, «Driving performance in cold, warm, and thermoneutral environments,» *Applied Ergonomics,* vol. 34, 2003.

[8] H. Hensel, Thermoreception and Temperature Regulation, L. Academic Press, 1981.

[9] Hot environments – estimation of the heat stress on working man,based on the WBGT-index (wet bulb globe temperature), Geneva: ISO 7243 , 1989.

[10] P. O. Fanger, Thermal Comfort-Analysis and Applications in Environmental Engineering, Copenhagen Danish Technical Press., 1970.

[11] M. Humphreys et F. Nicol, «Understanding the adaptive approach to thermal comfort,» *ASHRAE Transactions,* vol. 104, 1998.

[12] R. De Dear, G. S. Brager et D. Cooper, «Developing an Adaptive Model of Thermal Comfort and Preference,» ASHRAE Transactions, Sydney, 1997.

[13] J. S. Haldane, «The Influence of High Air Temperatures,» *The Journal of Hygiene,* 1905.

[14] F. C. Houghten, «Determining lines of equal comfort,» *ASHVE Transactions,* 1923.

[15] A. P. Gagge, A. P. Fobelets et L. G. Berglund, «A standard predictive index of human response to the thermal environment,» *ASHRAE Transactions,* 1986.

[16] J. Van Hoof, «Forty years of Fanger's model of thermal comfort: Comfort for all?,» *Indoor Air,* vol. 18.

[17] Ergonomics of the thermal environment - Analytical determination and interpretation of thermal comfort using calculation of the PMV and PPD indices and local thermal comfort criteria, ISO 7730, 2005.

[18] «Thermal environmental conditions for human occupancy,» chez *ANSI/ASHRAE Standard 55-2004*, Atlanta, GA, American Society of Heating, Refrigerating and Air-Conditioning Engineers, 2004.

[19] L. Fang, G. Clausen et P. O. Fanger, «Impact of temperature and humidity on the perception of indoor air quality,» *Indoor air,* 1998.

[20] , Ergonomics of the thermal environment -Evaluation of thermal environments in vehicles Part 3: Evaluation of thermal comfort using human subjects, ISO 14505-3:2006., 2006.

[21] Ergonomics of the thermal environment -Evaluation of thermal environments in vehicles Part 2: Determination of Equivalent Temperature, ISO 14505-3:2006., 2006.

[22] Ergonomics of the thermal environment - Evaluation of thermal environments in vehicles Part 1: Principles and methods for assessment of thermal stress, ISO 14505-1:2007, 2007.

[23] H. Nilsson, I. Holmér, S. Holmberg et M. Sandberg, «Thermal climate assessment in office environment - CFD calculations and thermal manikin measurements,» *7th International Conference on air distribution in rooms,* vol. 2, 2000.

[24] H. Nilsson, «Comfort Climate Evaluation with Thermal Manikin Methods and Computer Simulation Models,» Royal Institute Of Technology, 2004.

[25] H. O. Nilsson, «Thermal comfort evaluation with virtual manikin methods,» *Building and Environment,* vol. 42, 2007.

[26] H. Nilsson, I. Holmér, M. Bohm et O. Norén, «Equivalent Temperature and Thermal Sensation - Comparison with Subjective Responses,» *Comfort in the automotive industry. Recent development and achievements,* 1997.

[27] H. Zhang, E. Arens, C. Huizenga et T. Han, «Thermal sensation and comfort models for non-uniform and transient environments, part II: local comfort of individual body parts,» *Building and Environment,* vol. 45, 2010.

[28] L. Schellen, M. G. Loomans, B. R. Kingma, M. H. De Wit, A. J. Frijns et W. D. Van Marken Lichtenbelt, «The use of a thermophysiological model in the built environment to predict thermal sensation: Coupling with the indoor environment and thermal sensation,» *Building and Environment,* vol. 59, 2013.

[29] J. A. Stolwijk et J. D. Hardy, «Temperature regulation in man — A theoretical study,» *Pflüger's Archiv für die gesamte Physiologie des Menschen und der Tiere,* vol. 291, 1966.

[30] L. Yi, L. Fengzhi, L. Yingxi et L. Zhongxuan, «An integrated model for simulatinginteractive thermal processes in humaneclothing system,» *Journal of Thermal Biology,* vol. 29, 2004.

[31] R. Holopainen , «A Human Thermal Model for Improved Thermal Comfort,» Aalto University, 2012.

[32] S.-i. Tanabe, K. Kobayashi, J. Nakano, Y. Ozeki et M. Konishi, «Evaluation of thermal comfort using combined multi-node thermoregulation (65MN) and radiation models and computational fluid dynamics (CFD),» *Energy and Buildings,* vol. 34, 2002.

[33] D. Fiala, K. J. Lomas et M. Stohrer, «Computer prediction of human thermoregulatory and temperature response to a wide range of environmental conditions,» *International Journal of Biometeorology,* vol. 45, 2001.

[34] D. Fiala, G. Havenith, P. Bröde, B. Kampmann et G. Jendritzky, «UTCI-Fiala multi-node model of human heat transfer and temperature regulation,» *International Journal of Biometeorology,* vol. 56, 2011.

[35] H. Zhang, C. Huizenga, E. Arens et T. Yu, «Considering individual physiological differences in a human thermal model,» *Journal of Thermal Biology,* vol. 25, 2001.

[36] C. Huizenga, Z. Hui et E. Arens, «A model of human physiology and comfort for assessing complex thermal environments,» *Building and Environment,* vol. 36, 2001.

[37] B. Kingma, «Human Thermoregulation e A Synergy between Physiology and Mathematical Modelling,» Maastricht University, 2012.

[38] B. R. Kingma, L. Schellen, J. H. Frijns et W. D. Van Marken Lichtenbelt, «Thermal sensation: a mathematical model based on neurophysiology,» *Indoor Air,* 2012.

[39] E. Foda, I. Almesri, H. B. Awbi et K. Sirén, «Models of human thermoregulation and the prediction of local and overall thermal sensations,» *Building and Environment,* vol. 46, 2011.

[40] A. P. Gagge, J. A. Stolwijk et Y. Nishi, «An effective temperature scale based on a simple model of human physiological regulatory response,» *ASHRAE Transactions,* 1970.

[41] E. Foda et K. Sirén, «A new approach using the Pierce two-node model for different body parts,» *International Journal of Biometeorology,* vol. 55, 2010.

[42] A. Zolfaghari et M. Maerefat, «A new simplified thermoregulatory bioheat model for evaluating thermal response of the human body to transient environments,» *Building and Environment,* vol. 45, 2010.

[43] B. R. Kingma, A. J. Frijns, L. Schellen et W. D. Van Marken Lichtenbelt, «Beyond the classic thermoneutral zone, including thermal comfort,» *Temperature,* vol. 1, 2014.

[44] I. Kohri et T. Mochida, «Evaluation Method of Thermal Comfort in a Vehicle with a Dispersed Two-Node Model Part 1—Development of Dispersed Two-Node Model,» *Journal of the Human-Environment System,* vol. 6, 2002.

[45] S. Takada, H. Kobayashi et T. Matsushita, «Thermal model of human body fitted with individual characteristics of body temperature regulation,» *Building and Environment,* vol. 44, 2009.

[46] O. Kaynakli, U. Unver et M. Kilic, «Evaluating thermal environments for sitting and standing posture,» *International Communications in Heat and Mass Transfer,* vol. 30, 2003.

[47] O. Kaynakli et M. Kilic, «Investigation of indoor thermal comfort under transient conditions,» *Building and Environment,* vol. 40, 2005.

[48] R. J. Crosbie, J. D. HARDY et E. Fessenden, «Electrical Analog Simulation of Temperature Regulation in Man,» *IRE Transactions on Bio-Medical Electronics,* vol. 8, 1961.

[49] J. Stolwijk, «A Mathematical Model of Physiological Temperature Regulation (NASA Contractor Report),» New Heaven, Connecticut, 1971.

[50] M. Salloum, N. Ghaddar et K. Ghali, «A new transient bioheat model of the human body and its integration to clothing models,» *International Journal of Thermal Sciences,* vol. 46, 2007.

[51] M. Al-Othmani, N. Ghaddar et K. Ghali, «A multi-segmented human bioheat model for transient and asymmetric radiative environments,» *International Journal of Heat and Mass Transfer,* vol. 51, 2008.

[52] D. T. Novieto, «Adapting a Human Thermoregulation Model for Predicting the Thermal Response of Older Persons,» De Montfort University, Leicester UK, 2013.

[53] X. Zhou, Z. Lian et L. Lan, «X. Zhou, Z. Lian, L. Lan, An individualized human thermoregulation model for Chinese adults,» *Building and Environment,* vol. 70, 2013.

[54] D. Lai et Q. Chen, «A two-dimensional model for calculating heat transfer in the human body in a transient and non-uniform thermal environment,» *Energy Build,* vol. 118, 2016.

[55] P. Dongmei, C. Mingyin, D. Shiming et Q. Minglu, «A four-node thermoregulation model for predicting the thermal physiological responses of a sleeping person,» *Building and Environment,* vol. 52, 2012.

[56] Y. Kobayashi et S. Tanabe, «Development of JOS-2 human thermoregulation model with detailed vascular system,» *Building and Environment,* vol. 66, 2013.

[57] L. Schellen, M. G. Loomans, M. H. De Wit, B. W. Olesen et W. D. Van Marken Lichtenbelt, «The influence of local effects on thermal sensation under non-uniform environmental conditions - Gender differences in thermophysiology, thermal comfort and productivity during convective and radiant cooling,» *Physiology & Behavior,* vol. 107, 2012.

[58] D. Fiala, «Dynamic simulation of human heat transfer and thermal comfort,» De Monfort University, 1998.

[59] D. Fiala, K. J. Lomas et M. Stohrer, «A computer model of human thermoregulation for a wide range of environmental conditions: The passive system,» *Journal of Applied Physiology,* 1999.

[60] S. Paulke, D. Köster, R. Hass, V. Bader, S. Menzel et A. Gubalke, «Thermal simulation of a complete vehicle using manikin models,» *SIMVEC – Simulation und Erprobung in der Fahrzeugentwicklung,* 2014.

[61] E. H. Wissler, «Mathematical simulation of human thermal behavior using whole body models,» *Heat transfer in medicine and biology,* vol. 1, 1985.

[62] M. S. Ferreira et J. I. Yanagihara, «A transient three-dimensional heat transfer model of the human body,» *International Communications in Heat and Mass Transfer,* vol. 36, 2009.

[63] X. Sun, S. Eckels et C. Z. Zhongquan, «X. Sun, S. Eckels, Z.C. Zheng, An improved thermal model of the human body,» *HVAC & R Research,* vol. 18, 2012.

[64] M. Schwarz, M. W. Krueger, H.-J. Busch, C. Benk et C. Heilmann, «Model-Based Assessment of Tissue Perfusion and Temperature in Deep Hypothermic Patients,» *IEEE Transactions on Biomedical Engineering,* vol. 57.

[65] Y. Tang, Y. He, H. Shao et C. Ji, «Assessment of comfortable clothing thermal resistance using a multi-scale human thermoregulatory model,» *International Journal of Heat and Mass Transfer,* vol. 98, 2016.

[66] H. Zhang, «Human thermal sensation and comfort in transient and non-uniform thermal environments,» University of California Berkeley, 2003.

[67] E. Arens, H. Zhang et C. Huizenga, «Partial- and whole-body thermal sensation and comfort, part I: uniform environmental conditions,» *Journal of Thermal Biology,* vol. 31, 2006.

[68] H. Zhang, E. Arens et C. Huizenga, «Thermal sensation and comfort models for non-uniform and transient environments: Part Ⅱ: local comfort of individual body parts,» *Building and Environment,* vol. 45, 2010.

[69] H. Zhang, E. Arens, C. Huizenga et T. Han, «Thermal sensation and comfort models for non-uniform and transient environments: part III: whole-body sensation and comfort,» *Building and Environment,* vol. 45, 2010.

[70] B. Sakhdari et N. L. Azad, «An Optimal Energy Management System For Battery Electric Vehicles,» *IFAC-PapersOnLine,* Vols. %1 sur %248-15, 2015.

[71] H. He, H. Jia, C. Sun et F. Sun, «Stochastic Model Predictive Control of Air Conditioning System for Electric Vehicles: Sensitivity Study, Comparison and Improvement,» *IEEE Transactions on Industrial Informatics,* 2018.

[72] E. A. Müller, C. H. Onder, L. Guzzella et K. Mann, «Optimal Control of a Block Heater for an Improved Vehicle Warm-Up,» *IFAC Proceedings Volumes,* vol. 37, 2004.

[73] E. A. Müller, C. H. Onder, L. Guzzella et M. Kneifel, «Optimal control of a fuel-fired auxiliary heater for an improved passenger vehicle warm-up,» *Control Engineering Practice,* vol. 17, 2009.

[74] Q. Zhang et M. Canova, «Modeling air conditioning system with storage evaporator for vehicle energy management,» *Applied Thermal Engineering,* vol. 87, 2015.

[75] C. Mansour, W. Bou Nader, F. Breque, M. Haddad et M. Nemer, «Assessing additional fuel consumption from cabin thermal comfort and auxiliary needs on the worldwide harmonized light vehicles test cycle,» *Transportation Research Part D,* vol. 62, 2018.

[76] C.-C. Chiu, N.-C. Tsai et C.-C. Lin, «Near-optimal order-reduced control for A/C (air-conditioning) system of EVs (electric vehicles),» *Energy,* vol. 66, 2014.

[77] C.-C. Chiu, N.-C. Tsai et C.-C. Lin, «Construction of thermodynamic model and temperature regulation by near-LQR for electric vehicle,» *International Journal of Thermal Sciences,* vol. 81, 2014.

[78] T. Kubota et R. Watanabe, «Model-based Optimization of a Multi-zone HVAC System for Cooling,» chez *7th IFAC Symposium on Advances in Automotive Control. The International Federation of Automatic Control*, Tokyo, Japan, 2013.

[79] K. Minnerup, T. Herrmann, M. Steinsträter et M. Lienkamp, «Concept for a Holistic Energy Management System for Battery Electric Vehicles Using Hybrid Genetic Algorithms,» chez *2018 IEEE 88th Vehicular Technology Conference (VTC-Fall)*, 2018.

[80] P. Fussey, C. Rouaud et P. Martin, «xEV Thermal system control - solving the multi-variable constrained control challenge -,» chez *JSAE Annual Congress*, 2019.

[81] Q. Zhang et M. Canova, «Output Feedback Control of Automotive Air Conditioning System using H1 Technique,» *International Journal of Refrigeration,* vol. 58, 2015.

[82] S. Shojaei, «Application Of Key-Off Cooling And Partial Charging In Plug-in Electric Vehicles,» University of Warwick, 2018.

[83] M. Liebers, R. Kloß et B. Bäker, «Combined power train and thermal management optimization using an extended dynamic programming,» chez *Internationales Stuttgarter Symposium*, 2016.

[84] I. B.S.K.K, M. A. N.Aziah, A. S, R. Akmeliawati, N. H.M.I, M. A.G.A, T. S.F et H. M.K, «Fuzzy-based Temperature and Humidity Control for HVAC of Electric Vehicle,» *Procedia Engineering,* vol. 41, 2012.

[85] I. Beinarts, «Fuzzy Logic Control Method of HVAC Equipment for Optimization of Passengers' Thermal Comfort in Public Electric Transport Vehicles,» chez *Eurocon*, Zagreb, 2013.

[86] H. Nasution, «Development of fuzzy logic control for vehicle air conditioning system,» 2008.

[87] H. Khayyam, S. Nahavandi, E. Hu, A. Kouzani, A. Chonka, J. Abawajy, V. Marano et S. Davis, «Intelligent energy management control of vehicle air conditioning via look-ahead system,» *Applied Thermal Engineering,* vol. 31, 2011.

[88] H. Khayyam, J. Abawajy et R. N. Jazar, «Intelligent energy management control of vehicle air conditioning system coupled with engine,» *Applied Thermal Engineering,* vol. 48, 2012.

[89] H. Khayyam, «Adaptive intelligent control of vehicle air conditioning system,» *Applied Thermal Engineering,* vol. 51, 2013.

[90] H. Khayyam et A. Bab-Hadiashar, «Adaptive intelligent energy management system of plug-in hybrid electric vehicle,» *Energy,* vol. 69, 2014.

[91] H. Khayyam, A. Z. Kouzani et E. J. Hu, «Reducing Energy Consumption of Vehicle Air Conditioning System,» chez *Intelligent Vehicles Symposium*, 2009.

[92] H. Khayyam, A. Z. Kouzani, E. J. Hu et S. Nahavandi, «Coordinated energy management of vehicle air conditioning system,» *Applied Thermal Engineering,* vol. 31, 2011.

[93] J. Nan et Z. Zhou, «Control Algorithm Optimization of Electric Air Conditioning Based on ADVISOR,» *Advanced Materials Research,* Vols. %1 sur %2756-759, 2013.

[94] Y. Farzaneh et A. A. Tootoonchi, «Intelligent Control of Thermal Comfort in Automobile,» chez *IEEE Conference on Cybernetics and Intelligent Systems*, Chengdu, 2008.

[95] Y. Farzaneh et A. A. Tootoonchi, «Controlling automobile thermal comfort using optimized fuzzy controller,» *Applied Thermal Engineering,* vol. 28, 2008.

[96] H. Amri, R. N. Hofstädter et M. Kozek, «Energy Efficient Design and Simulation of a Demand Controlled Heating and Ventilation Unit in a Metro Vehicle,» chez *IEEE Forum on Integrated and*, Vienna, Austria, 2011.

[97] L. Horrein, A. Bouscayrol, Y. Cheng, C. Dumand, G. Colin et Y. Chamaillard, «Influence of the heating system on the fuel consumption of a hybrid electric vehicle,» *Energy Conversion and Management,* vol. 129, 2016.

[98] M. K. Mansour, M. N. Musa, H. Mat Nawi Wan et K. M. Saqr, «Development of novel control strategy for multiple circuit, roof top bus air conditioning system in hot humid countries,» *Energy Conversion and Management,* vol. 49, 2008.

[99] K. D. Huang, S.-C. Tzeng, T.-M. Jeng et W.-D. Chiang, «Air-conditioning system of an intelligent vehicle-cabin,» *Applied Energy,* vol. 83, 2006.

[100] K. VATANPARVAR et M. A. AL FARUQUE, «Design and Analysis of Battery-Aware Automotive Climate Control for Electric Vehicles,» *ACM Transactions on Embedded Computing Systems,* vol. 17, 2018.

[101] K. Vatanparvar et A. M. Al Faruque, «Eco-Friendly Automotive Climate Control and Navigation System for Electric Vehicles,» chez *ACM/IEEE 7th International Conference on Cyber-Physical Systems (ICCPS)*, 2016.

[102] K. Vatanparvar et M. A. Al Faruque, «Path to Eco-Driving: Electric Vehicle HVAC and Route Joint Optimization,» *IEEE Design and Test,* 2017.

[103] K. Vatanparvar et M. A. Al Faruque, «Battery Lifetime-Aware Automotive Climate Control for Electric Vehicles,» chez *52nd ACM/EDAC/IEEE Design Automation Conference (DAC)*, San Francisco, 2015.

[104] K. Vatanparvar, I. Burago et M. A. Al Faruque, «Extended Range Electric Vehicle with Driving Behavior Estimation in Energy Management,» *IEEE TRANSACTION ON SMART GRID,* vol. 14, 2018.

[105] A. Alahmer, M. A. Omar, A. R. Mayyas et A. Qattawi, «Analysis of vehicular cabins' thermal sensation and comfort state, under relative humidity and temperature control, using Berkeley and Fanger models.,» *Building and Environment,* 2012.

[106] M. R. Amini, X. Gong, Y. Feng, H. Wang, I. Kolmanovsky et J. Sun, «Sequential Optimization of Speed, Thermal Load, and Power Split in Connected HEVs,» *Annual American Control Conference (ACC),* 2019.

[107] H. Wang, Y. Meng, Q. Zhang, M. R. Amini, I. Kolmanovsky, J. Sun et M. Jennings, «MPC-based Precision Cooling Strategy (PCS) for Efficient Thermal Management of Automotive Air Conditioning System,» chez *The 3rd IEEE Conference on Control Technology and Applications (CCTA)*, Hong Kong, China, 2019.

[108] H. Wang, M. R. Amini, Z. Song, J. Sun et I. Kolmanovsky, «Combined Energy And Comfort Optimization Of Air Conditioning System In Connected And Automated Vehicles,» chez *ASME 2019 Dynamic Systems and Control Conference (DSCC)*, Park City, Utah, USA, 2019.

[109] M. Fayaz, I. Ullah, A. S. Shah et D. Kim, «An efficient energy consumption and user comfort maximization methodology based on learning to optimization and learning to control algorithms,» *Journal of Intelligent & Fuzzy Systems,* vol. 37, 2019.

[110] Y. Xie, Z. Liu, J. Liu, K. Li, Y. Zhang, C. Wu, P. Wang et X. Wang, «A Self-learning intelligent passenger vehicle comfort cooling system control strategy,» *Applied Thermal Engineering,* 2019.

[111] H. He, H. Jia, W. Huo et M. Yan, «Stochastic Dynamic Programming of Air Conditioning System for Electric Vehicles,» *Energy Procedia,* vol. 105, 2017.

[112] H. Wang, I. Kolmanovsky, M. R. Amini et J. Sun, «Model Predictive Climate Control of Connected and Automated Vehicles for Improved Energy Efficiency,» chez *Annual American Control Conference (ACC)*, Milwaukee, 2018.

[113] M. Busl, «Design of an Energy-Efficient Climate Control Algorithm for Electric Cars,» Lund University, 2011.

[114] S. Schaut, F. Hepperle et O. Sawodny, «Intelligent Air Conditioning System Activation in Passenger Cars with Electrified Powertrains,» chez *IEEE Conference on Control Technology and Applications (CCTA)*, Hong Kong, China, 2019.

[115] K. Vatanparvar et M. A. Al Faruque, «Design and Analysis of Battery-Aware Automotive Climate Control for Electric Vehicles,» *ACM Transactions on Embedded Computing Systems,* vol. 17, 2018.

[116] S. Schaut et O. Sawodny, «Thermal Management for the Cabin of a Battery Electric Vehicle Considering Passengers' Comfort,» *IEEE Transactions on Control Systems Technology,* 2019.

[117] B. Chiang Ng, I. Z. Mat Darus, H. Jamaluddin et H. M. Kamar, «Application of adaptive neural predictive control for an automotive air conditioning system,» *Applied Thermal Engineering,* vol. 73, 2014.

[118] D. Esqueda Merino, A. Dubray Demol, S. Olaru, E. Godoy et D. Dumur, «Energetic Optimization of Automotive Thermal Systems using Mixed-Integer Programming and Model Predictive Control,» chez *IEEE International Conference on Control Applications (CCA)*, Hyderabad, India, 2013.

[119] T. Fischer, T. Kraus, C. Kirches et F. Gauterin, «Demonstration of a Nonlinear Model Predictive Control of a Thermal Management System for Electric Vehicles in Real-Time,» chez *IEEE Conference on Control Technology and Applications (CCTA)*, Copenhagen, Denmark, 2018.

[120] H. Wang, «Model Predictive Climate Control for Connected and Automated Vehicles,» University of Michigan, 2019.

[121] M. R. Amini, H. Wang, X. Gong, D. Liao-McPherson, I. Kolmanovsky et J. Sun, «Cabin and Battery Thermal Management of Connected and Automated HEVs for Improved Energy Efficiency Using

Hierarchical Model Predictive Control,» chez *IEEE Transactions on Control Systems Technology*, 2019.

[122] L. Horrein, «Gestion d'énergie décompé d'un véhicule hybride integrant les aspects thermiques via la représentation énergétique macroscopique,» Université de Lille - Sciences et Technologies, 2015.

[123] Y. Huang, A. Khajepour, F. Bagheri et M. Bahrami, «Optimal energy-efficient predictive controllers in automotive air-conditioning/refrigeration systems,» *Applied Energy,* vol. 184, 2016.

[124] Y. Huang, A. Khajepour, F. Bagheri et M. Bahrami, «Modelling and optimal energy-saving control of automotive air-conditioning and refrigeration systems,» *Proceedings of the Institution of Mechanical Engineers Part D Journal of Automobile Engineering,* vol. 231, 2016.

[125] Y. Huang, A. Khajepour, M. Khazraee et M. Bahrami, «A Comparative Study of the Energy-Saving Controllers for Automotive Air-Conditioning/Refrigeration Systems,» *Journal of Dynamic Systems Measurement and Control,* vol. 139, 2016.

[126] X. Yan, J. Fleming et R. Lot, «A/C Energy Management and Vehicle Cabin Thermal Comfort Control,» *IEEE Transactions on Vehicular Technology,* 2018.

[127] F. Bjurling, «TRANSIENT THERMAL MODEL OF A MINIBUS' CABIN AND OPTIMIZATION OF THE AIR-CONDITIONING CONTROL STRATEGIES,» Royal Institute of Technology, Stockholm, Sweden, 2013.

[128] R. N. Hofstadter, J. Amaya et M. Kozek, «Energy optimal control of thermal comfort in trams,» *Applied Thermal Engineering,* vol. 143, 2018.

[129] M. Yan, H. He, C. Sun, H. Jia et M. Li, «Stochastic Dynamic Programming of Air Conditioning System under Time-varying Passenger Condition for Electric Bus,» *Energy Procedia,* vol. 105, 2016.

[130] H. He, M. Yan, C. Sun, J. Peng, M. Li et H. Jia, «Predictive air-conditioner control for electric buses with passenger amount variation forecast,» *Applied Energy,* vol. 227, 2018.

[131] L. Hongmin et T. Shuping, «Energy-saving analysis of neural network control based on PMV in a ship air conditioning system,» chez *International Conference on Mechatronic Science, Electric Engineering and Computer*, Jilin, China, 2011.

[132] T. Bächle, K. Graichen, M. Buchholz et K. Dietmayer, «Model Predictive Heating Control for Electric Vehicles Using Load Prediction and Switched Actuators,» *IFAC-PapersOnLine,* Vols. %1 sur %249-11, 2016.

[133] D. W. Gao, C. Mi et A. Emadi, «Modeling and Simulation of Electric and Hybrid Vehicles,» *Proceedings of the IEEE,* vol. 95, n° %14, pp. 729-745, 2007.

[134] Y. Hoon, K. Donghyun, H. Sungho et K. Hyunsoo, «Regenerative Braking Algorithm for a HEV with CVT Ratio Control During Deceleration,» *SAE international,* 2004.

[135] M. Ehsani, Y. Gao, S. E. Gay et A. Emadi, Modern Electric, Hybrid Electric, and Fuel Cell Vehicles: Fundamentals, Theory, and Design, CRC PRESS, 2014.

[136] Y. Gao, L. Chen et M. Ehsani, «Investigation of the effectiveness of regenerative braking for EV and HEV,» *SAE International,* 1999.

[137] P. Suntharalingam, «Kinetic energy recovery and power management for hybrid electric vehicles,» CRANFIELD UNIVERSITY, 2011.

[138] L. Chu, L. Yao, J. Chen, L. Chao, J. Guo, Y. Zhang et M. Liu, «Integrative braking control system for electric vehicles,» chez *Vehicle Power and Propulsion Conference*, Chicago, 2011.

[139] M. J. Yang, H. L. Jhou, B. Y. Ma et K. K. Shyu, «A cost-effective method of electric brake with energy regeneration for electric vehicles,» *IEEE Transactions on Industrial Electronics,* vol. 56, 2009.

[140] M. Zeraoulia, M. Benbouzid et D. Diallo, «Electric motor drive selection issues for HEV propulsion systems: A comparative study,» *IEEE TRANSACTIONS ON VEHICULAR TECHNOLOGY,* vol. 55, 2006.

[141] A. Sorniotti, M. Boscolo, A. Turner et C. Cavallino, «Optimisation of a multi-speed electric axles as a function of the electric motor properties,» chez *IEEE Vehicle Power and Propulsion Conference*, Lille, 2010.

[142] L. Guzzella et A. Sciarretta, Vehicle Propulsion Systems: Introduction to Modeling and Optimization, Heidelberg, Germany: Springer-Verlag Berlin Heidelberg, 2005.

[143] F. Grappe, R. Candau, B. Barbier, M. Hoffman, A. Belli et J. D. Rouillon, «Influence of tyre pressure and vertical load on coefficient of rolling resistance and simulated cycling performance,» *Ergonomics,* vol. 10, 1999.

[144] J. Y. Wong, Theory of ground vehicles, 1993.

[145] J. Ejsmont, L. Sjögren, B. Swieczko Zurek et G. Ronowski, «Influence of Road Wetness on Tire-Pavement Rolling Resistance,» *Journal of Civil Engineering and Architecture,* 2015.

[146] J. Páscoa, F. Brojo, F. C. Santos et P. M. O. Fael, «An innovative experimental on-road testing method and its demonstration on a prototype vehicle,» *Journal of Mechanical Science and Technology,* vol. 6, 2012.

[147] E. G. Pita, Air Conditioning Principles and Systems: An Energy Approach, London, England: Pearson, 2001.

[148] C. Zilio, J. S. Brown, G. Schiochet et A. Cavallini, «The refrigerant R1234yf in air conditioning systems,» *Energy,* vol. 36, pp. 6110-6120, 2011.

[149] R. K. Shah et D. P. Sekulić, Fundamentals of Heat Exchanger Design, John Wiley & Sons, 2003.

[150] A. Fakheri, «Heat Exchanger Efficiency,» *ASME. J. Heat Transfer,* vol. 129, p. 1268–1276, 2007.

[151] K. S. Ramesh et P. S. Dusan, Fundamentals of Heat Exchanger Design, Hoboken, USA: John Wiley & Sons, 2003.

[152] H. Jaber et R. L. Webb, «Design of Cooling Towers by the Effectiveness-NTU Method,» *ASMR J. Heat Transfer,* vol. 111, pp. 837-843, 1989.

[153] B. Torregrosa-Jaime, F. Bjurling, J. M. Corberán, F. Di Sciullo et J. Payá, «Transient thermal model of a vehicle's cabin validated under variable ambient conditions,» *Applied Thermal Engineering,* vol. 75, pp. 45-53, 2015.

[154] D. Marcos, F. J. Pino, C. Bordons et J. J. Guerra, «The Development and Validation of a Thermal Model for the Cabin of a Vehicle,» *Applied Thermal,* vol. 66.

[155] H. Lee, Y. Hwang, I. Song et K. Jang, «Transient thermal model of passenger car's cabin and implementation to saturation cycle with alternative working fluids,» *Energy,* vol. 90, 2015.

[156] B. Torregrosa-Jaime, F. Bjurling, J. M. Corberán, F. Di Sciullo et J. Payá, «Transient thermal model of a vehicle's cabin validated under variable ambient conditions,» *Applied Thermal Engineering,* vol. 75, 2015.

[157] ISO 7726, «Ergonomics of the thermal environment - Instrument for measuring physical quantities,» International Organization for Standardization, Geneva, Switzerland, 1998.

[158] F. White, Fluid Mechanics, New York, USA: McGraw Hill, 2015.

[159] Y. Cengel, M. Boles et M. Kanoglu, Thermodynamics: An Engineering Approach, New York, USA: McGraw-Hill, 2018.

[160] B. Chen, H. Ma, H. Fang, H. Fan, K. Luo et B. Fan, «An approach for state of charge estimation of Li-ion battery based on Thevenin equivalent circuit model,» chez *Prognostics and System Health Management Conference*, Zhangiiaijie, 2014.

[161] P. Tikuisis, D. G. Bell et I. Jacobs, «Shivering Onset, Metabolic Response, and Convective Heat Transfer During Cold Air Exposure,» *Journal of Applied Physiology,* vol. 70, 1991.

[162] E. R. Nadel, R. W. Bullard et J. A. Stolwijk, «Importance of skin temperature in the,» *Journal of Applied Physiology,* vol. 31, 1971.

[163] J. S. Hayward, J. D. Eckerson et M. L. Collis, «Thermoregulatory heat production in man: prediction equation based on skin and core temperatures,» *Journal of Applied Physiology,* vol. 42, 1977.

[164] «Thermal environmental conditions for human occupancy,» chez *ANSI/ASHRAE Standard 55-2013*, Atlanta, GA, American Society of Heating, Refrigerating and Air-Conditioning Engineers, 2013.

[165] T. H. Benzinger, «The physiological basis for thermal comfort,» *Indoor climate,* 1979.

[166] A. P. Gagge, J. A. Stolwijk et J. D. Hardy, «Comfort and thermal sensation and associated physiological responses at various ambient temperatures,» *Environmental Research,* vol. 1, 1967.

[167] G. D. Mower, «Perceived intensity of peripheral thermal stimuli is independent of internal body temperature,» *Journal of Comparative and Physiological Psychology,* vol. 90, 1976.

[168] ASHRAE Handbook Fundamentals, ASHRAE, 1989.

[169] J. A. Stolwijk et J. D. Hardy, «Control of Body Temperature,» *Comprehensive Physiology,* 2011.

[170] W. F. Taylor, J. M. Johnson, D. O'Leary et M. K. Park, «Effect of High Local Temperature on Reflex Cutaneous Vasodilation,» *Journal of Applied Physiology,* vol. 57, 1984.

[171] X. L. Wang, «Convective heat transfer coefficients from head and arms,» *Climate and Buildings,* vol. 2, 1990.

[172] E. A. McCullough, B. W. Jones et J. Huck, «A comprehensive data base for A comprehensive data base for,» *ASHRAE Transaction,* vol. 91, 1985.

[173] T. FE, Theory Manual, P+Z Engeneering.

[174] T. L. Bergman, F. P. Incropera, D. P. DeWitt et A. S. Lavine, Fundamentals of heat and mass transfer, John Wiley & Sons, 2011.

[175] K. Katić, R. Li et W. Zeiler, «Thermophysiological models and their applications: A review,» *Building and Environment,* vol. 106, 2016.

[176] G. M. Budd, «Wet-bulb globe temperature (WBGT)—its history and its limitations,» *Journal of Science and Medicine in Sport,* vol. 11, 2008.

[177] S. K. Wang, Handbook Of Air Conditionning And Refrigeration, McGraw-Hill, 2001.

[178] R. Bellman, Dynamic Programing, New Jersey, USA: Princeton University, 1957.

[179] D. P. Bertsekas, Dynamic programming and optimal control, Belmont: Athena Scientific, 2002.

[180] J. H. Lee, Y. K. Kim, K. S. Kim et S. Kim, «Estimating Clothing Thermal Insulation Using an Infrared Camera,» *Sensors,* vol. 16, 2016.

[181] A. Lahlou, F. Ossart, E. Boudard, F. Roy et M. Bakhouya, «Optimal Management of Thermal Comfort and Driving Range in Electric Vehicles,» *Energies,* 2020.

[182] «NREL Transportation Research,» [En ligne]. Available: https://www.nrel.gov/transportation/secure-transportation-data/tsdc-drive-cycle-data.htmlISO 7730:2005(en).

[183] A. Lahlou, F. Ossart, E. Boudard, F. Roy et M. Bakhouya, «A dynamic programming approach for thermal comfort control in electric vehicles,» chez *Vehicle Power and Propulsion Conference*, Chicago, Illinois, USA, 2018.

[184] A. Lahlou, F. Ossart, F. Roy, E. Boudard et M. Bakhouya, «A Real-Time Approach For Thermal Comfort Management In Electric,» *Energies,* 2020.

# Résumé

Le système de climatisation et de chauffage (HVAC) représente la principale charge auxiliaire des véhicules électriques à batterie (BEV) et nécessite des approches de contrôle efficaces qui équilibrent entre consommation énergétique et confort thermique. D'une part, les passagers exigent toujours plus de confort, mais d'autre part la consommation du système HVAC impacte fortement l'autonomie du véhicule, ce qui constitue l'enjeu majeur des BEV. Ces deux exigences doivent être satisfaites par la stratégie de gestion énergétique, en suggérant au conducteur d'ajuster soit le confort thermique, soit la vitesse du véhicule. En effet, s'il n'y a pas assez d'énergie embarquée pour la traction et pour un confort thermique idéal, ce dernier doit être diminué afin d'économiser de l'énergie et permettre au véhicule d'atteindre sa destination. Dans certaines situations, il est plus judicieux de ralentir afin de permettre un meilleur confort thermique.

Dans la présente thèse, deux approches de gestion énergétique ont été étudiées. La première est une stratégie optimale qui minimise l'inconfort thermique sous contrainte de l'énergie disponible. Le problème de la gestion énergétique est formulé sous forme d'un problème d'optimisation et résolu par l'algorithme de programmation dynamique. Comme le coût de calcul de ce dernier reste important pour une implémentation à bord, une seconde stratégie temps réel est développée. La performance des deux approches a été comparée pour une grande variété de scénarios météorologiques et de trafic. En particulier, il a été montré que l'approche en temps réel est quasi optimale, avec une légère augmentation de l'inconfort de seulement 3%.

**Mots-clés** : Véhicules électriques, système HVAC, Confort thermique, Thermophysiologie humaine, Gestion énergétique, Contrôle optimal, Programmation dynamique, Contrôle temps-réel.

# Abstract

The heating, ventilation and air conditioning (HVAC) system represents the main auxiliary load in battery-powered electric vehicles (BEVs) and requires efficient control approaches that balance energy saving and thermal comfort. On the one hand, passengers always demand more comfort, but on the other hand the HVAC system consumption strongly impacts the vehicle's driving range, which constitutes a major concern in BEVs. Both of these requirements should be satisfied by the control approach, by suggesting to the driver to adjust either the thermal comfort or the vehicle speed, in order to meet the energy constraints. Indeed, if there is not enough embedded energy for both traction and optimal thermal comfort for the planned trip, the thermal comfort should be diminished in order to save energy and allow the vehicle to reach its final destination. In some situations, it may be wiser to consider slowing down in order to allow a better thermal comfort.

In the present thesis, two energy management approaches have been studied. Firstly, an optimal strategy that minimizes thermal discomfort within the limits of available energy. The energy management problem was formulated as an optimization problem and solved by the dynamic programming algorithm. As the computation cost of the latter can be considerable for an on-board implementation, a real-time strategy was therefore developed. The performance of both approaches has been compared for a wide variety of weather and traffic scenarios. In particular, the real-time approach has been shown to be near optimal, with a slight increase in discomfort of only 3%.

**Keywords** : Electric Vehicles, HVAC systems, Thermal comfort, Human thermo-physiology, Energy Management, Optimal control, Dynamic programming, Real-time control.